



Deformation in foreland basins of the western Alps (Pelvoux massif, SE France); significance for the development of the Alpine ARC

Judith Bürgisser

► To cite this version:

Judith Bürgisser. Deformation in foreland basins of the western Alps (Pelvoux massif, SE France); significance for the development of the Alpine ARC. Tectonics. Eidgenössische Technische Hochschule Zürich (ETHZ), 1998. English. NNT: . tel-00799859

HAL Id: tel-00799859

<https://theses.hal.science/tel-00799859>

Submitted on 12 Mar 2013

HAL is a multi-disciplinary open access archive for the deposit and dissemination of scientific research documents, whether they are published or not. The documents may come from teaching and research institutions in France or abroad, or from public or private research centers.

L'archive ouverte pluridisciplinaire **HAL**, est destinée au dépôt et à la diffusion de documents scientifiques de niveau recherche, publiés ou non, émanant des établissements d'enseignement et de recherche français ou étrangers, des laboratoires publics ou privés.

Diss. ETH Nr. 12766

Pierre TRICART
Directeur UFR Géologie
INSTITUT DOLOMIEU
15, Rue Maurice Gignoux
38031 GRENOBLE Cedex

DEFORMATION IN FORELAND BASINS OF THE WESTERN ALPS
(PELVOUX MASSIF, SE FRANCE);
SIGNIFICANCE FOR THE DEVELOPMENT OF THE ALPINE ARC

Judith Bürgisser

— 1998 —

Diss. ETH Nr. 12766

DEFORMATION IN FORELAND BASINS OF THE WESTERN ALPS

(PELVOUX MASSIF, SE FRANCE);

SIGNIFICANCE FOR THE DEVELOPMENT OF THE ALPINE ARC

Judith Bürgisser

Diss. ETH Nr. 12766

**DEFORMATION IN FORELAND BASINS OF THE WESTERN ALPS
(PELVOUX MASSIF, SE FRANCE);
SIGNIFICANCE FOR THE DEVELOPMENT OF THE ALPINE ARC**

A dissertation submitted to the
SWISS FEDERAL INSTITUTE OF TECHNOLOGY ZÜRICH

for the degree of
Doctor of Natural Sciences

presented by
Judith Bürgisser
Dipl. Natw. ETH

born 11.8.1969
citizen of Oberlunkhofen AG

accepted on the recommendation of

Prof. Dr. J.-P. Burg	ETH Zürich	examiner
Dr. M. Ford	ETH Zürich	1. co-examiner
Dr. R.W.H. Butler	University of Leeds, UK	2. co-examiner
Prof. Dr. D. Bernoulli	ETH Zürich	3. co-examiner

1998

Acknowledgements

Many people at ETH and outside helped and supported me throughout the four years of my dissertation.

In the first place I would like to thank Mary Ford as my primary supervisor. She gave me all the freedom I needed and applied pressure when it was necessary. I am deeply grateful for everything I learned and for continuing enthusiasm and encouragement. I am much indebted to the Professors Jean-Pierre Burg and Daniel Bernoulli who never lost interest in and always supported the progress of my thesis. I also thank Rob Butler devoting his time to be my external co-referent.

There are many other people who were important for the progress of my thesis. Henry Lickorish supported me strongly to plan and carry out the analogue experiments. I appreciated his way of question raising and the critical feedback he gave. The rectification of field photographs for the construction of the Fournel profile was greatly improved with the help of the experts at the Institut für Geodäsie und Photogrammetrie, especially André Streilein. A special thank goes to Diane Seward who analysed the fission track samples which is a very time-consuming job. Furthermore, I acknowledge fruitful discussions with Martin Casey, Dorothee Dietrich, Bernhard Fügenschuh, Joelle Lazarre, Trey Meckel, Stefan Schmid, Ed Williams and many other friends and colleagues at ETH and outside which helped me and supported me during the last four years.

The experimental work for this thesis was undertaken at the Laboratoire de Modelisation at the University of Rennes in collaboration with Philippe Davy and Peter Cobbold. Jean-Jacques Kermarrec provided extensive technical assistance in the laboratory and with the deformation apparatus.

I thank the office of the 'Parc National des Ecrins' for authorisation to work in the national park. I was surprised by the hospitality of many 'Gîtes d'étape' in my field area and I appreciated much their care; especially family Engilberge from 'Le Baouti' at Vallouise. A special thank goes to my field assistants Christian Rosenkranz, Gabi Klaus, Marianne Landtwing, Nicole Bolliger and Reto Murer who accompanied me each for one or two weeks in the field.

My most warmly felt thanks, however, go to Stephan, for company during beautiful, adventurous and sometimes extremely strenuous days in the field, including camping and late-autumn trips, and for his continued encouragement. Last, but not least I owe a lot to my parents supporting me over the years and giving me the chance to study geology.

**Trust in the Lord with all your heart and lean not on your own understanding;
in all your ways acknowledge him, and he will make your paths straight.**

Proverbs 3, 5-6

Table of contents

Abstract	4
Kurzfassung	6
1. Introduction	9
1.1 The western Alpine arc: the problem	9
1.1.2 The geologic units of the Alps	9
1.1.3 The western Alpine arc: previous models	11
1.1.3 Objectives and aims of this study	18
1.1.4 Methods	18
1.2 Geological overview of the western Alps and the Pelvoux area	19
2. The Champsaur-Prapic fold zone:	
overthrust shear deformation of a foreland basin	25
2.1 Introduction	25
2.1.1 Geological setting and previous work	25
2.1.2 Overthrust shear and development of folds in simple shear	27
2.2 The Champsaur fold zone	29
2.2.1 The northern domain	31
2.2.2 The central domain: the Fournel profile	31
2.2.3 The southern domain	35
2.3 The Prapic fold zone	36
2.4 The basal shear zone: progressive shearing of the Nummulitic Limestone and Globigerina Marl	37
2.4.1 The main foliation (B1)	37
2.4.2 Folding of the main foliation (B2)	40
2.4.3 Sub-horizontal shear zones (B3)	45
2.4.4 West-dipping cleavage (B4)	45
2.4.5 Chambran: transition to WNW-directed deformation	46
2.4.6 A model of progressive shear	47
2.5 Selle-Fault	49
2.6 Burial and exhumation history of the Champsaur-Prapic fold zone	50
2.7 Interpretation and discussion	52
2.7.1 Overthrust shear model	52
2.7.2 Curvature of axial trends and late Alpine transport directions	55
2.7.3 The problem of the hangingwall	56
2.7.4 Summary	57

3. The Soleil Boeuf area northwest of the Selle-Fault zone:	
NW-directed folding and thrusting	59
3.1 Introduction	59
3.1.1 Geological setting	59
3.1.2 Previous work	61
3.2 Folding and thrusting in the autochthon	64
3.2.1 Queyrel Thrust	64
3.2.2 Palastre Thrust	66
3.2.3 Estang Syncline and Thrust	67
3.2.4 Méollion Syncline	69
3.2.5 Discussion	70
3.3 Geometry of the allochthonous units	70
3.3.1 The allochthonous sandstone sheets	72
3.3.2 Imbricated overturned sequences	76
3.3.3 Imbricated upright sequences	81
3.4 Burial and exhumation history of the Soleil Boeuf area	85
3.5 Interpretation and discussion	85
3.5.1 Interpretation of the Pousterle profile	85
3.5.2 Applicability of model to the whole Soleil Boeuf area	89
3.5.3 Discussion of previous work	91
3.5.4 Summary	91
4. Significance of new data for the evolution of the western Alpine arc	93
4.1 The relationship between the Soleil Boeuf area and the Champsaur-Prapic fold zone	93
4.1.1 Spatial relationship	93
4.1.2 Influence of variable substrate to deformational style	95
4.1.3 Relative timing of NW motion in Soleil Boeuf and SW transport in Champsaur-Prapic	96
4.2 Correlation with the kinematics of the surrounding region	100
4.2.1 Timing and relation of NW and SW-directed deformation on a regional scale	100
4.2.2 Models to explain simultaneous thrusting	102
4.3 Kinematics and geodynamics of the western Alpine arc	106

5. Analogue modelling of obstacles and oblique indentation	111
5.1 Introduction	111
5.1.1 Aim of this study	111
5.1.2 Previous models	112
5.1.3 Materials and scaling	114
5.1.3 Experimental setup	117
5.2 Obstacle experiments	118
5.2.1 Experiments with a low obstacle	118
5.2.2 Experiment with a high obstacle	125
5.3 Indentation experiments	128
5.3.1 Oblique straight translation path	128
5.3.2 Elliptical translation path	131
5.4 Interpretation and significance	135
5.4.1 Discussion of obstacle experiments	135
5.4.2 Discussion of indentation experiments	137
5.4.3 Summary	139
6. General conclusions	141
References	144
Curriculum vitae	

Abstract

This thesis documents the Late Tertiary structural evolution of the Champsaur-Prapic area and Soleil Boeuf area to the southeast and south of the Pelvoux basement massif in the western Alps (Hautes-Alpes, southeastern France). These remnants of the Alpine foreland basin are located at a critical zone in the kinematic pattern of the external Alpine arc, between the northern Subalpine chains with predominant WNW-NW-directed deformation and the WSW-SW-directed deformation in the southern Subalpine chains. The investigated areas record the transition between the northern and southern Subalpine chains. The data will be discussed in the context of the formation of the external Alpine arc and a new mechanism for arc formation is proposed based on analogue sand-box experiments.

The Champsaur-Prapic fold zone lies in the footwall of the Frontal Pennine Thrust. The 0.8 - 1.3 km thick Upper Eocene - Oligocene foreland basin succession lies directly on crystalline basement and was deformed by WSW-directed shear below the overthrusting internal Alpine units on the Frontal Pennine Thrust. To the north deformation changes to WNW-directed, partly post-dating the WSW-SW-directed deformation further south. The deformed strata are detached from the basement in the basal shear zone. Above, the turbidite sequence (Champsaur Sandstone) is folded in chevron-like folds. A 12 km long continuous profile across the Champsaur fold zone documents variations in chevron fold shape, axial plane dips and zonal distribution of folding which indicate progressively higher shear strains towards the Frontal Pennine Thrust in the east. Chevron fold axes trend generally NNW-SSE except close to the Pelvoux massif where fold axes curve to N-S possibly due to lateral drag against the basement massif. In the western part of the investigated area SW-directed thrusting on the Champsaur Thrust almost doubles the Tertiary stratigraphy. The Champsaur Thrust and chevron folding in its footwall deform the overlying internal thrust sheets. The Champsaur-Prapic fold zone is a particular example of overthrust shear deformation in the footwall of internal alpine nappes in which deformation is concentrated in diffuse ramp zones.

In the Soleil Boeuf area the Tertiary foreland basin sediments unconformably overlie folded basement to the north and Mesozoic rocks to the south. On top of the 0.6 - 0.7 km thick autochthonous Tertiary sequence lie several klippen of Mesozoic and Tertiary sediments which were emplaced towards the NW. The deformation in Soleil Boeuf is characterised by fault-propagation folding and thrusting which probably roots down into basement. Transect mapping across the most complete Pousterle klippe documents progressive deformation which accommodates at least 6.8 km shortening: post-mid-Oligocene thrusting (probably NW-directed) which carries Mesozoic sediments over Champsaur Sandstone; the formation of a large NW-vergent fold-propagation fold pair

with an amplitude of 1 - 2 km; and low-angle NW-directed breakthrough thrusts cutting through the common limb of the fault-propagation fold pair. Later N-S extension along the E-W Bonnets Fault and late displacements on the Selle-Fault zone drop the upper normal limb of the fault-propagation fold pair down towards south.

In the core of the external western Alpine arc two sub-perpendicular transport directions which barely overlap can therefore be distinguished. The 5 km WSW-directed shortening recorded in Champsaur-Prapic form the northern termination of the southern Subalpine chains, whereas the deformation in Soleil Boeuf is interpreted to detach from a deep satellite fault (in basement) to the NW-directed deformation in the northern Subalpine chains. Regional considerations demonstrate that in the core of the arc both systems were active at the same time, but at different levels. This implies that the external western Alpine arc is not a radial forming arc, but rather that it formed due to two main transport directions (NW and SW). NW shortening is the major deformation (~ 150 km shortening) while SW shortening is relatively minor (~ 22 km).

Analogue modelling experiments with sand-silicone suggest that the main features of the external Alpine arc can be best explained by oblique indentation along an elliptical translation path. In such experiments two sub-perpendicular thrust systems evolve at the same time with different amounts of shortening. Wrench shear deformation is restricted to the inner part of the model close to the indenter. Additional experiments with high and low obstacles in the foreland were carried out. They showed that the influence of such obstacles on the development of a fold and thrust belt is restricted to the peripheral area of the obstacle which indicates that obstacles (e.g. the Pelvoux massif) do not affect the regional transport direction.

Kurzfassung

Vorliegende Arbeit dokumentiert die spät-tertiäre Entwicklung der Champsaur-Prapic und Soleil Boeuf Gebiete am Südostrand des Pelvoux Massivs in den Westalpen (Hautes-Alpes, Südostfrankreich). Diese Reste des alpinen Vorlandbeckens liegen in der kritischen Kernzone des externen Alpenbogens, zwischen den nördlichen voralpinen Ketten (mit vorwiegend WNW-NW-Verkürzung) und den südlichen voralpinen Ketten (mit vorwiegend WSW-SW-Verkürzung). Die untersuchten Gebiete dokumentieren den Übergang von den nördlichen zu den südlichen voralpinen Ketten. Die kinematischen Daten werden unter dem Aspekt der Entwicklung dieses externen Alpenbogens diskutiert. Basierend auf Analogmodellen mit Sand und Silikon wird ein neuer Mechanismus für die Bogenbildung vorgeschlagen.

Das Champsaur-Prapic Gebiet umfasst eine 0.8 - 1.3 km dicke Vorlandbeckenabfolge (oberes Eozän - Oligozän), die diskordant auf kristallinem Grundgebirge liegt. Diese Abfolge verformte sich im Liegenden der penninischen Front durch WSW-gerichtete Scherung während des Überfahrens durch die internen alpinen Einheiten. Im Norden richtet sich die Verformung nach WNW aus und ist dort mindestens teilweise später als die WSW-SW-gerichtete Verformung im Süden. Die Verformung ist charakterisiert durch Abscherung in der basalen Scherzone über dem Grundgebirge und durch chevronartige Faltung der darüberliegenden Turbiditabfolge (Champsaur Sandstein). Ein 12 km langes Profil durch die Champsaur Faltenzone dokumentiert die Veränderungen der Faltenform, des Fallwinkels der Achsenebene und der zonalen Verteilung der Faltung. Diese Veränderungen zeigen, wie die Scherverformung mit abnehmender Entfernung von der penninischen Front im Osten immer grösser wird. Die Richtung der Chevronfaltenachsen ist NNW-SSE, ausgenommen nahe am Pelvoux Massiv, wo sie durch den seitlichen Widerstand des Grundgebirges auf N-S drehen. Die SW-gerichtete Champsaur Überschiebung im Westen verdoppelt beinahe die tertiäre Stratigraphie und verformt die darüberliegenden internen Überschiebungsdecken. Das Champsaur-Prapic Gebiet ist ein besonderes Beispiel für eine Überschiebungs-Scherung (overthrust shear) im Liegenden der internen Einheiten, bei der sich die Verformung in diffusen Rampenzonen konzentriert.

Im Soleil Boeuf Gebiet liegen die 0.6 - 0.7 km mächtigen tertiären Vorlandbeckensedimente diskordant auf verfaltetem Grundgebirge und verfalteten mesozoischen Sedimenten. Auf der autochthonen Tertiärabfolge liegen mehrere Klippen aus mesozoischen und tertiären Gesteinen, die nach NW aufgeschoben wurden. Die Verformung im Soleil Boeuf ist charakterisiert durch frontale Knickung (fault-propagation folding) und mehrere Überschiebungen, die vermutlich von einem tiefen Abscherhorizont im Grundgebirge aufsteigen. Die am besten erhaltene Pousterle Klippe dokumentiert eine progressive Verformung mit einer Minimalverkürzung von 6.8 km:

Überschiebungen, die mesozoische Sedimente (vermutlich nach NW) auf Champsaur Sandstein tragen; grosse NW-vergente frontale Faltung (Amplitude 1 - 2 km) vor einer progressiv wachsenden Überschiebung; und flache NW-gerichtete Vorderschenkelüberschiebungen. Später führen eine N-S Dehnung entlang der Bonnets Abschiebung und Bewegungen auf der subvertikalen Selle-Störungszone zur Absenkung des südlichen Teils.

Im Kern des externen westlichen Alpenbogens können deshalb zwei annähernd senkrechte Transportrichtungen unterschieden werden: die 5 km WSW-gerichtete Verkürzung von Champsaur-Prapic am nördlichen Ende der südlichen voralpinen Ketten und die NW-gerichtete Verformung im Soleil Boeuf, die als eine Zweigüberschiebung am Rand der WNW-NW-gerichteten Hauptüberschiebung in den nördlichen voralpinen Ketten interpretiert wird. Regionale Betrachtungen zeigen auf, dass beide Verkürzungssysteme im Zentrum des Alpenbogens gleichzeitig, aber auf verschiedenen Niveaus aktiv waren. Daraus ergibt sich, dass der externe westliche Alpenbogen nicht durch ein radiales kinematisches Muster entstanden ist, sondern durch zwei Haupttransportrichtungen (NW und SW). Die dominante Verformung ist die NW-gerichtete mit ~ 150 km Verkürzung während die SW-Verkürzung mit ~ 22 km viel geringer ist.

Analogexperimente mit Sand und Silikon deuten darauf hin, dass die Hauptmerkmale des externen Alpenbogens am besten mit einer schrägen Kollision entlang einer elliptischen Bahn erklärt werden können. In solchen Experimenten entstehen gleichzeitig zwei annähernd senkrechte Überschiebungssysteme mit unterschiedlichen Verkürzungsbeträgen. Weitere Analogexperimente mit hohen und niedrigen Hindernissen im Vorland zeigen auf, dass sich ihr Einfluss auf einen vorrückenden Überschiebungsgürtel auf die Randzone des Hindernisses beschränkt. Folglich haben Hindernisse (z.B. das Pelvoux Massiv) keinen Einfluss auf die regionale Verkürzungsrichtung.

1. Introduction

Tectonic arcs are either oroclines in which segments of the orogen change strike during the evolution of the bend or syntaxes in which segments of the orogen do not change strike during development of the bend. Both are observed in collisional orogens, e.g. the Alps, the Himalayas, the Variscides, the Apennines and in subduction-related orogens, in island arcs. Arcuate structural systems present geologists and geophysicists with fundamental kinematic and mechanical problems. These can be distilled in two essential questions: what are the large-scale plate tectonic parameters which cause the development of an arcuate system and what are the deformational processes and kinematic systems which accommodate the development of structural arcs?

This study concentrates on the western Alpine arc for two reasons: 1) the geology of the Alps is well known including a detailed kinematic data set, and 2) some very different geodynamic models have been proposed for the development of the Alpine arc which can be tested. The study concentrates on the external (younger) part of the arc because here foreland basin deposits provide stratigraphic control on the age of observed structures.

1.1 The western Alpine arc: the problem

1.1.2 The geologic units of the Alps

The Alps resulted from the closure of the Tethys ocean which started at the beginning of Late Cretaceous (around 92 Ma) with the onset of north-directed motion of Africa relative to Europe (Dewey *et al.*, 1989). The Alps are classically divided into three major structural zones which more or less coincide with Mesozoic paleogeographic domains of the Tethys ocean (Ramsay, 1963; Debelmas and Lemoine, 1970; Debelmas and Kerckhove, 1980; Trümpy, 1980). These are from north to south the Helvetic or Dauphinois (northern continental margin), the Penninic (oceanic basins and thinned continental crust) and the Austro- or South-Alpine domains (southern continental margin). The Southern Alps are derived from the same facies belt as the Austro-Alpine nappes, but their structure is different and they are separated from the Alps proper by the Insubric Line (Fig. 1.1). Underthrusting of the southward-facing Tethyan passive margin and ocean basin below the overriding Adria plate formed the Austro-Alpine and the Penninic nappes (Fig. 1.1). These thrust sheets and large nappes with basement cores are metamorphosed to high pressures and/or high temperatures. The two units are separated by slivers of ophiolitic material, representing Mesozoic oceanic crust (e.g. Laubscher, 1969). To the west and northwest this internal zone is limited by the Frontal Pennine Thrust (FPT) which thrusts internal Pennine units over the external zone (Fig. 1.1). Outside the FPT, the Prealps at the French-Swiss boundary and the Embrunais-Ubaye

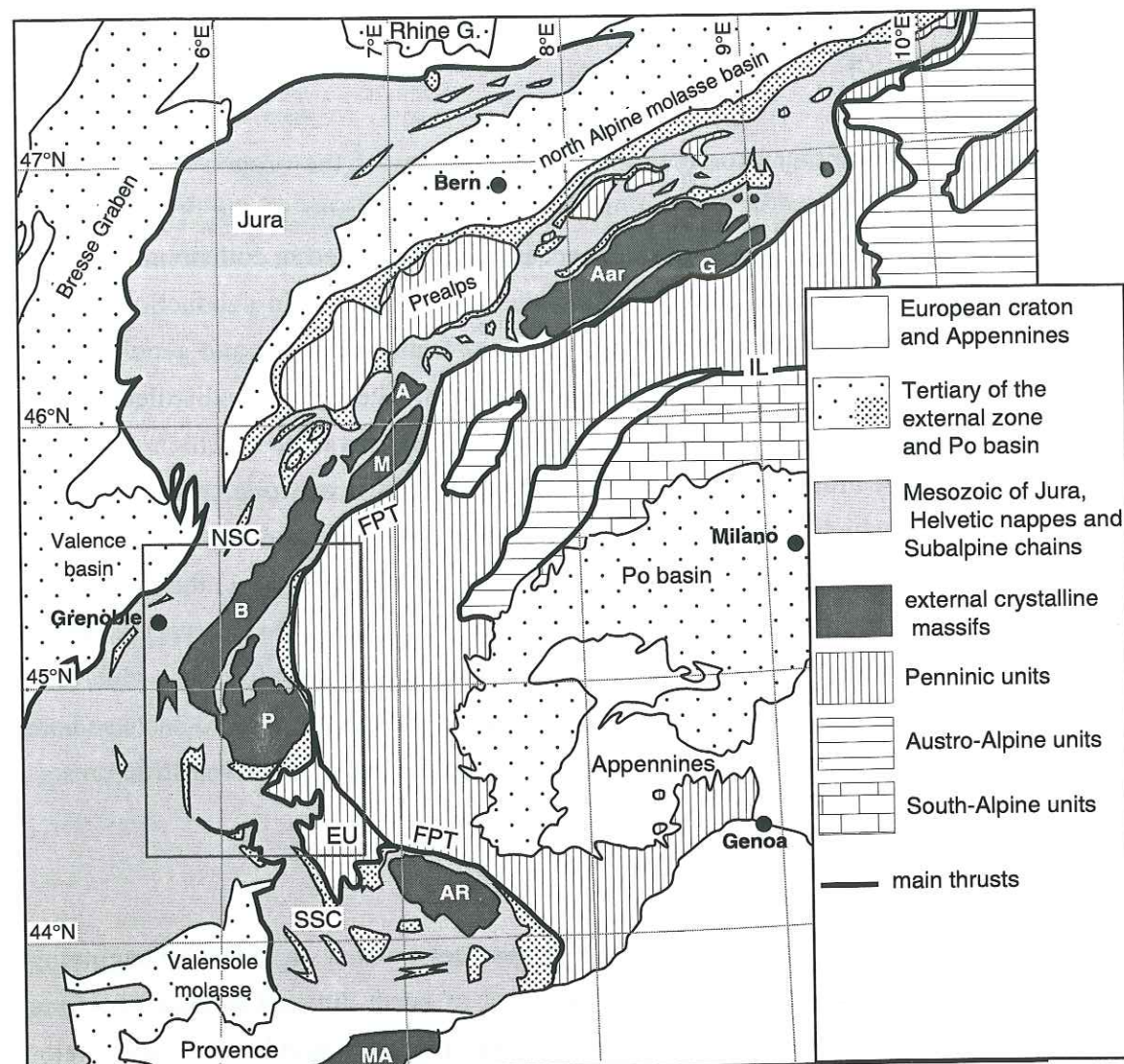


Fig. 1.1: Simplified geologic map of the Alps. A = Aiguilles Rouges, AR = Argentera, B = Belledonne, EU = Embrunais Ubaye nappes, FPT = Frontal Pennine Thrust, G = Gotthard, IL = Insubric Line, M = Mont Blanc, MA = Maures, NSC = northern Subalpine chains, P = Pelvoux, SSC = southern Subalpine chains. Outline of Fig. 1.6 is shown.

nappes in southeastern France are independent units which derive from the internal Pennine domain (Debelmas and Lemoine, 1970; Trümpy, 1980). They were completely stripped off their substratum and overrode onto the external zone.

The external zone forms the Helvetic Alps, the Subalpine chains, the molasse basins, and the Jura mountains. They consist dominantly of not only weakly metamorphosed sediments of the European plate. Along their internal margin there are large uplifted basement 'massifs', the Aar, Gotthard, Aiguilles Rouges, Mont-Blanc, Belledonne, Pelvoux, and Argentera massifs (Fig. 1.1). The European craton west and north of the external Alps remained relatively undeformed by Alpine orogenesis.

1.1.3 The western Alpine arc: previous models

The arc of the external western Alps, delineated by the external basement massifs and structures in the sedimentary cover, is roughly semi-circular and has a radius of approximately 150 km (Fig. 1.1). The northern arm of the arc, the northern Subalpine chains (NSC), trends NE-SW. It extends approximately 200 km from the Prealps to the south end of the Belledonne massif. The southern arm of the arc, the southern Subalpine chains (SSC) trends NW-SE and extends approximately 175 km from the Pelvoux massif to the south of the Argentera massif. The late Alpine (Oligocene to Pliocene) tectonic transport diverges dramatically around the arc (Fig. 1.2).

The timing and nature of the development of this arc is not well understood and several different models have been proposed to explain its genesis. They can be roughly organised in two groups: the 'radial hypotheses', invoking a smooth radial change of the

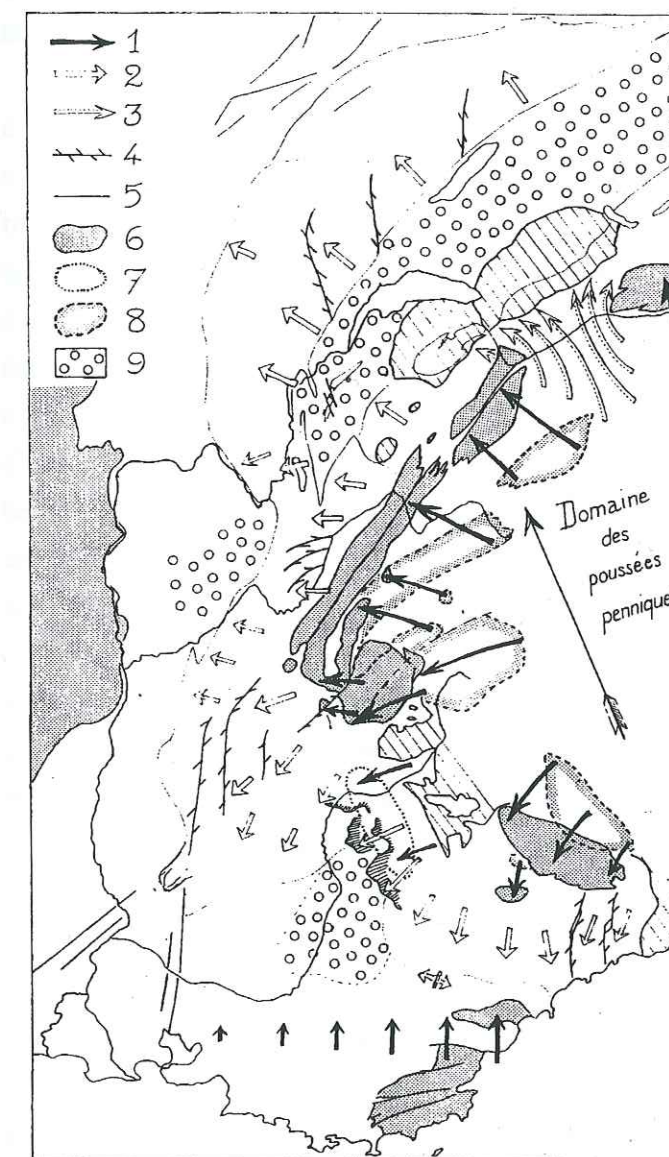


Fig. 1.2

Early reconstruction of the development of the curved western Alps, from Goguel (1963). The arc developed due to lateral 'recoiling' along the southwestern border of the main N to NW-directed compression. The rotation and translation of the basement massifs caused the divergent external cover motion

- 1) basement motion
- 2) independent cover motion
- 3) emplacement of the Helvetic nappes and Prealps
- 4) dextral strike-slip fault
- 5) fault
- 6) external crystalline massifs
- 7) basement massif, not unroofed by erosion
- 8) initial position of basement massifs
- 9) molasse basin

transport direction around the external arc and the 'corner hypotheses' invoking only two main, roughly perpendicular, transport directions.

The 'radial hypotheses'

In his interpretation of the western Alpine arc Goguel (1963) recognised that similar models for the western and central Alps, implying large westward displacements and large northward displacements respectively provoke a space problem. Restoring the internal nappes back along the proposed trajectories perpendicular to the Alpine chain, locates them simultaneously in the same region. Trying to avoid this problem he proposed a new model for the evolution of the divergent displacement pattern of the western Alps. The main features of this model are (Fig. 1.2) N-NW compression from Vienna to the French border combined with 'lateral recoiling' (contrecoup latéral) along its southwestern rim. Goguel argues that this lateral effect causes W and SW-directed thrusting along the Briançonnais front and translation and rotation of the external crystalline massifs which push ahead the sedimentary cover.

Vialon *et al.* (1989) came up with a similar model. They proposed that there is a change in displacement directions in time and space along the curvature of the western Alpine arc. The oldest directions are in the internal zones with a present orientation of displacement directions that is fairly regularly E-W. Vialon *et al.* (1989) argue that probably since the Miocene (25 Ma) directions became divergent in the outer zones accompanied by principal dextral strike-slip faults (Fig. 1.3a). They explain this pattern of roughly helicitic movement directions in the Subalpine chains by local rotation of a block belonging to the European margin, dragged along the western sidewall of the Adria indenter moving northwestwards (Fig. 1.4a & b). This laterally displaced block produced an anticlockwise helical shear about a pole of rotation within it. With such a model, the deformation process corresponds to lateral rotation-expulsion of a deformed unit belonging to the European plate margin, jammed against its stable foreland.

Platt *et al.* (1989) proposed radial thrusting ahead of a curved indenter. They proposed a model where the interaction between the plate motion of the indenter and the motion driven by gravitational force acting normal to the trend of the mountain chain (i.e. normal to the edge of the indenter) produced a divergent displacement pattern which lies within $\pm 90^\circ$ of the plate motion direction (Fig. 1.4c). According to their compilation, the kinematic data from the Alps range between N (eastern Jura and central Alps) through W to SW (southern Subalpine chains and Nice arc) from 40 - 0 Ma and between NNW to W from 80 - 40 Ma (Fig. 1.3b). Platt *et al.* (1989) argue that this pattern is best explained by a roughly WNW-directed Adria-Europe motion independent of Africa since about Late Cretaceous (70 Ma) or at least since Late Eocene (40 Ma) combined with radial thrusting.

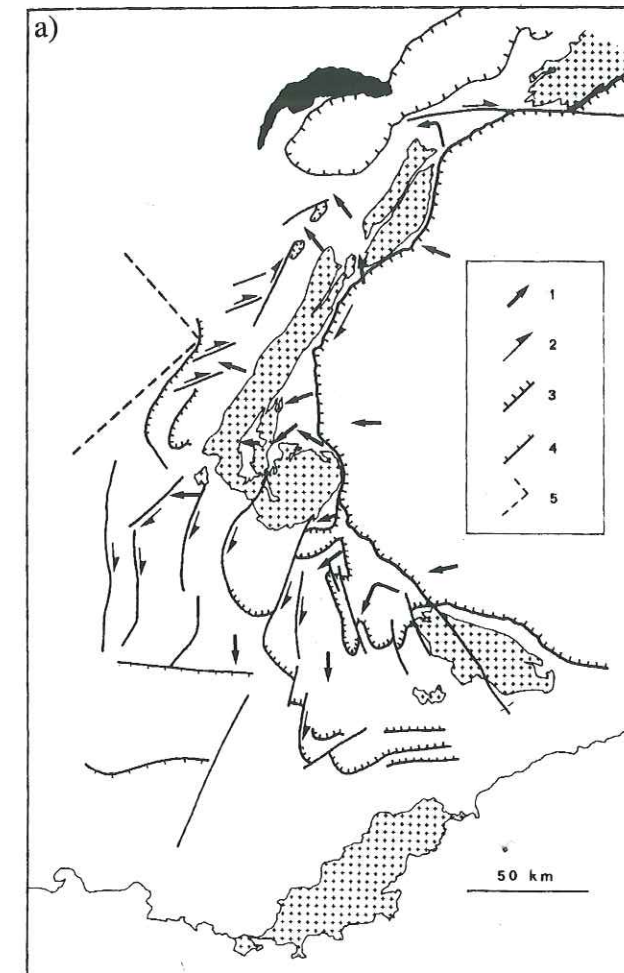
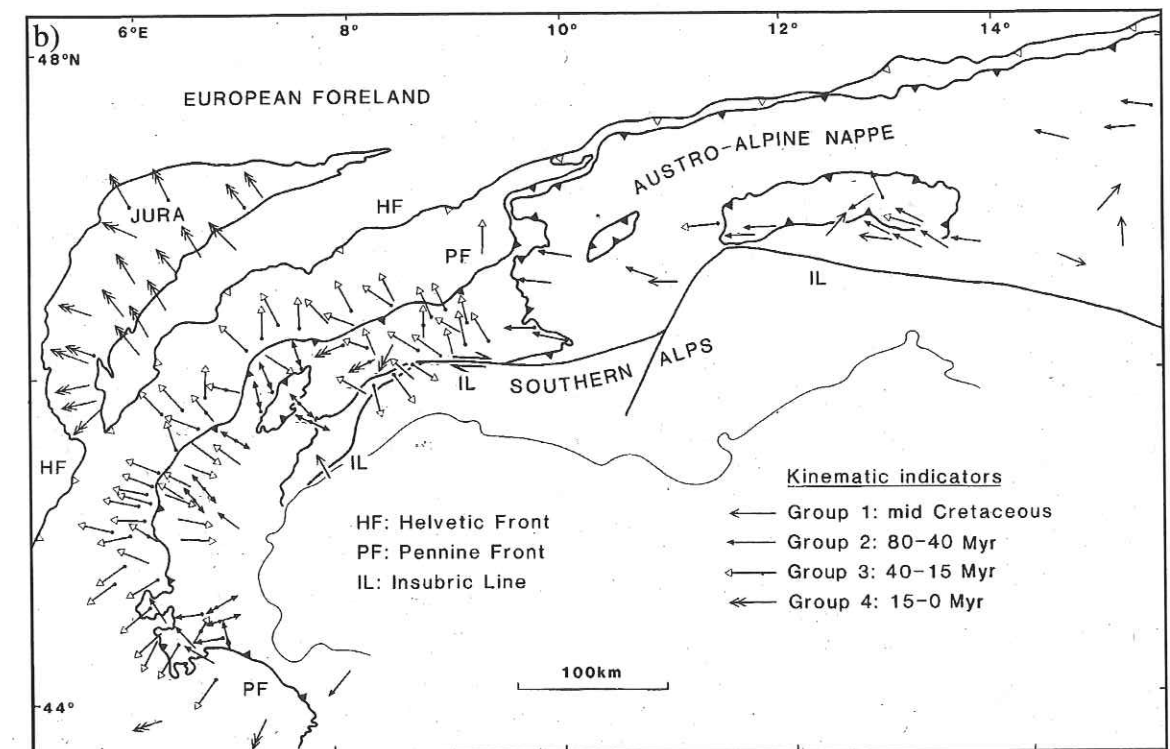


Fig. 1.3:
Main tectonic displacement directions as a basis for two different radial models (shown in Fig. 1.4) for the evolution of the western Alpine arc. Note that the divergence over the same area in a) is much larger than in b), depending on the choice of representative source data.

a) From Vialon *et al.* (1989): helitic pattern since the Miocene (25 Ma).
1) transport of nappes and stretching lineations,
2) dextral strike-slip faults,
3) main thrust limits,
4) thrusts between Provencal and Subalpine domains,
5) margin of the fixed platform in the foreland.

b) From Platt *et al.* (1989): kinematic data from the Alps plotted by age. Data show a regular divergent displacement pattern.



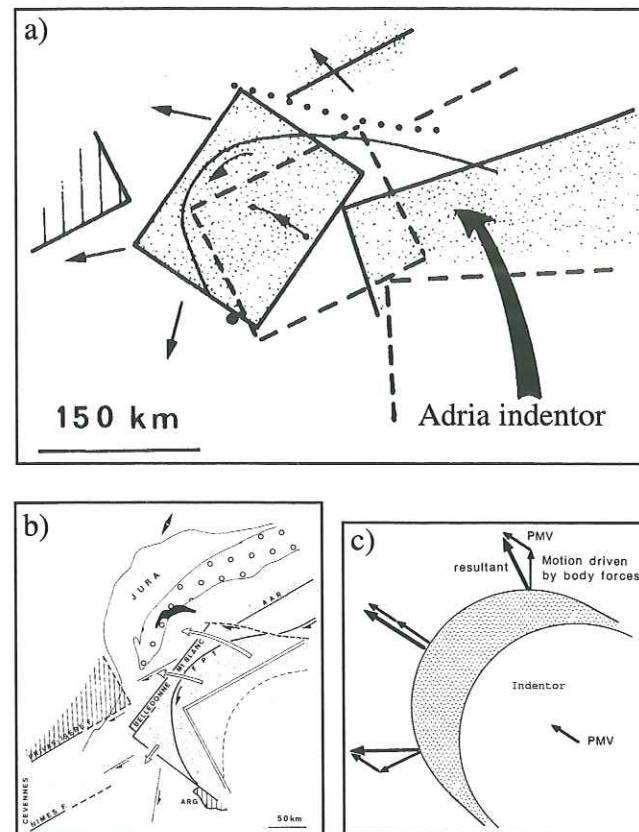


Fig. 1.4: Development of the western Alpine arc: radial models based on the kinematic maps shown in Fig. 1.3.

a) and b): Ring shear model applied to the Alps, slightly modified from Vialon et al. (1989). Interactions of translation of the Adria indenter and rotation of the Mont Blanc - Belledonne - Pelvoux block. Present position of the units shaded, assumed initial positions white and dashed. Angular buttress in the foreland is vertically hatched. a) Sketch map showing the possible lateral expulsion-translation and rotation of the western block along the sidewall of the Adria indenter, the motion of which is shown by the large black arrow. b) Present position of displaced block carrying the previously-thrusted internal units limited by the Frontal Pennine Thrust (FPT).

c) The radial thrusting model from Platt et al. (1989). Transport directions produced by the interaction between the plate-motion vector (PMV) and the body forces acting normal to the trend of a mountain belt.

The 'corner hypotheses'

Ricou (1984) and Ricou and Siddans (1986) interpreted the Alps as a strike-slip collision belt. In their model general NW-ward collision constrained laterally by N-S strike-slip faults from Late Cretaceous (80 Ma) to Eocene (40 Ma) is related to northward motions of the Adriatic promontory (Fig. 1.5a). It is followed by Oligocene (or post-Oligocene) to Pliocene westward displacement between a northern dextral (e.g. Insubric Line) and a southern sinistral, strike-slip zone. This westward movement of the Adriatic promontory independent of Africa caused the westward thrusting of the external crystalline massifs and the thin-skinned fold and thrust tectonics in the Subalpine chains and the Jura. They identified 5 major sinistral N-S strike-slip zones in the internal Alpine zone and along the boundary to the external zone.

Butler *et al.* (1986) argued against strike-slip motions along the FPT. They analysed the rocks of the external zone and concluded that thrusting from the Mont Blanc to the Pelvoux massif was constantly towards the WNW (restored width is at least 140 km, between the externalmost front and the Frontal Pennine Thrust). They proposed that all the displacements represented by the NW external Alpine Thrust Belt are transferred onto the base of the Embrunais-Ubaye nappes, with the formation of a lateral hangingwall ramp on a flat-lying WNW sinistral displacement zone (Fig. 1.5b). With

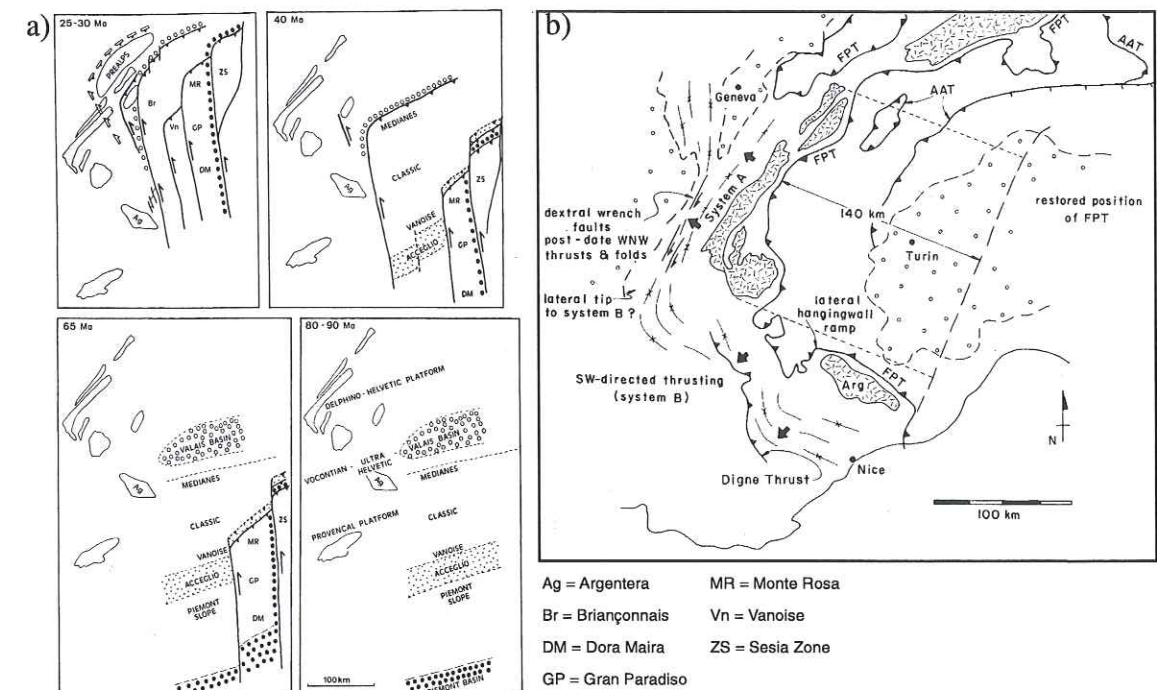


Fig. 1.5: Development of the western Alpine arc: corner models.

a) From Ricou and Siddans (1986). Diagrammatic representation of the strike-slip collision model since Cretaceous times. The Argentera massif is taken as a fixed datum in stable Europe. Médiannes, Classic, Vanoise, Acceglio refer to parts of the Briançonnais Zone (s.l.). Single lines of circular symbols represent closed basins (ophiolitic sutures). Open strike-slip and thrust symbols represent the extent of superficial gravity gliding of the Prealps.

b) From Butler *et al.* (1986). Map of the restored position of the NW external Alpine thrust system and its relationship to the, in this model later, SW-directed thrust system in the southern Subalpine chains.

such a model the resultant lateral hangingwall culmination may have been sufficiently high to allow gravity driven SW-directed thrusting. Furthermore, they argued that basement thrusting in the Argentera massif and thrust sheet activity post-dating thrusting in the northern Subalpine chains indicate that the southern Subalpine chains, south of the Pelvoux massif, constitute a second, entirely independent thrust system, probably in the footwall to the floor thrust carrying the NW-directed thrust system (Fig. 1.5b).

A similar conclusion comes from Fry (1989) who proposed that the dominant features of the western Alps are the WNW-directed ($290\frac{1}{2}$) and the SW-directed ($230\frac{1}{2}$) thrust systems. He concludes that both systems have been active simultaneously, each accommodating hundreds of kilometres shortening during tens of millions of years.

Approach: gap in data

The main controversy between the models described above arises from the interpretation of the tectonic transport pattern. Collations of transport directions around

the external western Alps (Goguel, 1963; Malavieille *et al.*, 1984; Choukroune *et al.*, 1986; Platt, 1986; Gillcrist *et al.*, 1987; Gratier *et al.*, 1989; Platt *et al.*, 1989; Vialon *et al.*, 1989: see Figs. 1.2 1.3 & 1.5b) clearly document the WNW–NW-directed shortening of the northern Subalpine chains and the WSW–SW-directed shortening of the southern Subalpine chains. But there is uncertainty about the transition between these two arms around the Pelvoux-Belledonne massif (Fig. 1.6). Thus, any study investigating the relationship between the northern and southern Subalpine chains must focus into this region.

Working around the arc, Arpin *et al.* (1988), Mugnier *et al.* (1990), Butler (1992b) and many others documented dominant late Alpine WNW-directed thrusting in the northern Subalpine chains which extends southward to La Mure (Fig. 1.6). About 30 km further south the Neogene sediments of the Dévoluy area record WSW-directed deformation (Meckel *et al.*, 1996; Meckel, 1997). To the east, the kinematic data from the Pelvoux massif (Gillcrist *et al.*, 1987; Coward *et al.*, 1991) are rather complex (Fig. 1.6). These authors propose that the structures are related to the inversion of passive margin structures which makes these data very difficult to interpret in terms of regional transport direction. Additionally, no Tertiary sediments are preserved (Debrand-Passard *et al.*, 1984b) and the age of the observed structures is uncertain. To the northeast and east of the Pelvoux massif NW to W-directed thrusting and folding involving Tertiary sediments at Aiguilles d'Arves (Bravard, 1982; Bravard, 1983; Serre *et al.*, 1985) and at Rocher de l'Yret (Butler, 1992a) have been reported (Fig. 1.6). Beach (1980; 1981b; 1982) argues that the deformation in the Mesozoic cover is WNW-directed. All these structures to the north of the Pelvoux massif have been related to the WNW–NW-directed deformation in the northern Subalpine chains. However, to the southeast of the Pelvoux massif the deformation pattern becomes complex. According to published data the late Alpine transport direction changes from SW–WSW in the Champsaur-Prapic area (Gidon, 1965; Plotto, 1977; Bravard and Gidon, 1979) to WNW and N-directed in the Soleil Boeuf area (Gidon and Pairis, 1980–1981). The relative timing and relationship of the structures of these two areas has remained unclear. To the south predominantly SW-directed deformation has been reported (e.g. Elliot *et al.*, 1985; Lawson, 1987; Fry, 1989) although there are exceptions: WNW-directed displacements in the Faucon-Turriers area in the footwall of the Digne thrust (Arnaud *et al.*, 1977) and NW-directed deformation within the upper Embrunais-Ubaye nappes (Parpaillon nappe; Merle and Brun, 1984); their significance is controversial (Fig. 1.6). With these data alone it is not possible to decide between the 'radial' and the 'corner' hypotheses.

Therefore this project concentrates on this central part of the western Alps with the aim to clarify the kinematic transition between the northern and the southern Subalpine chains and is directed towards a better understanding of the evolution of the external

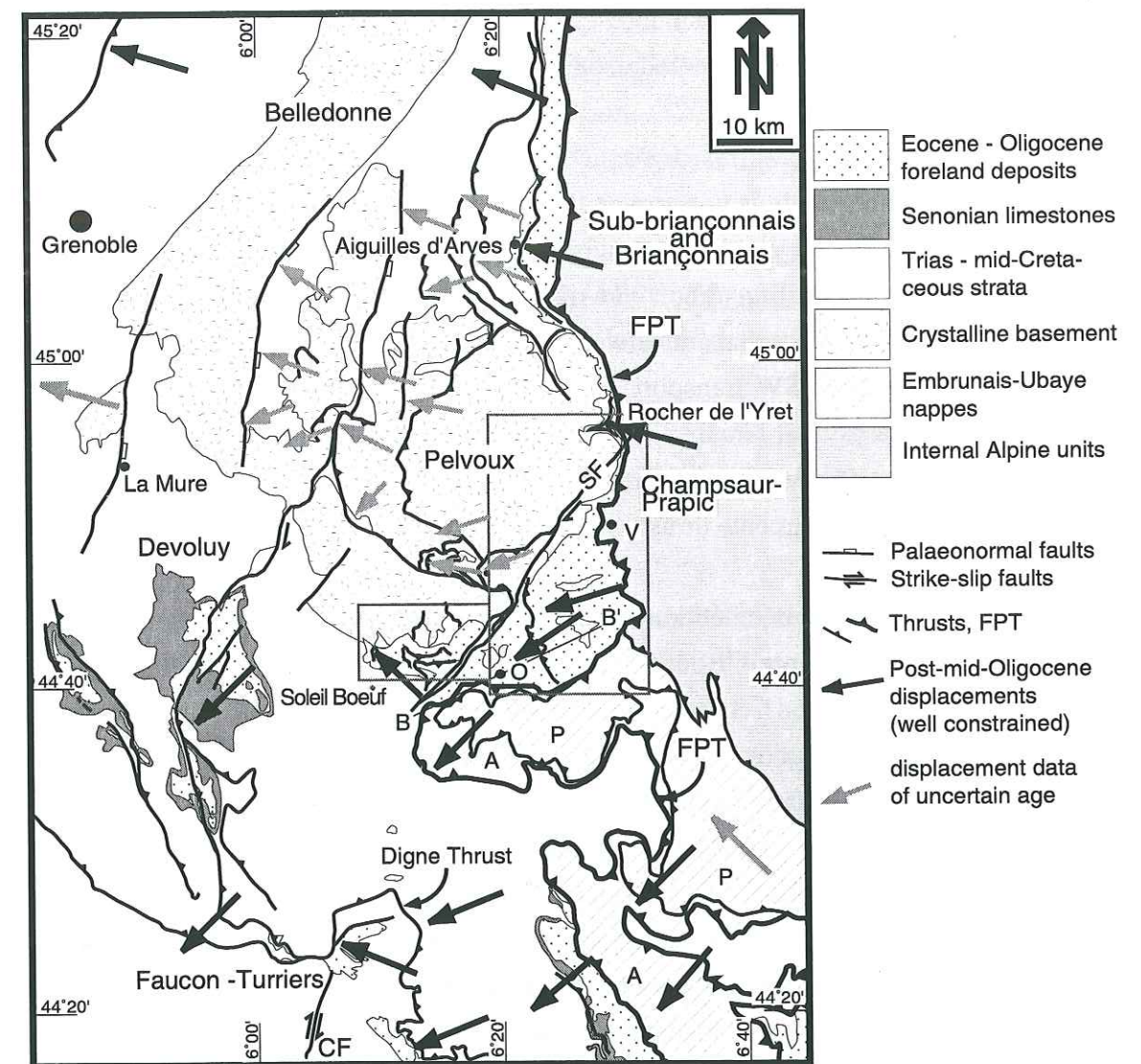


Fig. 1.6: Directions of late Alpine tectonic transport in the external zone around the Pelvoux massif. Data compiled from Gidon (1965), Plotto (1977), Bravard and Gidon (1979), Beach (1981), Bravard (1982), Bravard (1983), Serre *et al.* (1985), Butler (1987), Gillcrist *et al.* (1987), Fry (1989), Coward *et al.* (1991) and Butler (1992), Meckel (1997) and this study. Boxes outline Fig. 2.1 (Champsaur-Prapic) and Fig. 3.1 (Soleil Boeuf). A = Autapie nappe, B–B' = profile trace of Fig. 2.7, CF = Clamensane Fault, O = Orcières, P = Parpaillon nappe, V = Vallouise.

western Alpine arc. The main problems in the Pelvoux region are a lack of kinematic data of well constrained age, poor understanding of the relative timing of NW and SW-directed deformation and poor understanding of their mutual relationship. Therefore it was decided to focus on the Tertiary foreland basin remnants because only there can the late Alpine structures be clearly distinguished from older structures. In the larger framework of this project the thesis by L. D. Meckel (1997) has clarified the sedimentological and structural history of the Dévoluy area whereas this study focuses on the tectonic evolution of the Soleil Boeuf and the Champsaur-Prapic areas further

east. These areas are of particular interest because they record different displacement directions which are pivotal for the understanding of the evolution of the Alpine arc.

1.1.3 Objectives and aims of this study

The purpose of this study is to examine the geodynamic development of the external western Alpine arc. The approach to this subject involves a combination of detailed field work and analogue modelling. The field research aimed to fill a critical gap in the kinematic data set of the external arc between the NW transport direction in the northern Subalpine chains and the SW transport direction in the southern Subalpine chains and thus focuses on the pivotal Champsaur-Prapic and Soleil Boeuf areas. The obtained information will be integrated and compared to sand-silicone analogue models which focus on the formation of arcuate thrust systems.

In order to identify the detailed kinematic and mechanical relationships between the Champsaur-Prapic and Soleil Boeuf areas the detailed aims of this thesis are the following:

- 1) to examine the direction, distribution, relative timing, amount of shortening and nature of the deformation in the Champsaur-Prapic and Soleil Boeuf areas;
- 2) to define the kinematic history and the role of the Selle-Fault which separates the Soleil Boeuf area from the Champsaur-Prapic area;
- 3) to develop a regional kinematic model and to use these data to evaluate earlier models of the formation of the western Alpine arc.

The results will be compared to analogue sand-box modelling which focuses on

- 4) the role of pre-existing features such as paleogeographic highs in the development of the arc and the related kinematic pattern;
- 5) the production of variable transport directions ahead of an indenter with oblique and curved motion paths.

1.1.4 Methods

The investigated area lies at the southern rim of the Pelvoux basement massif, a very mountainous region with peaks reaching up to 4102 m (Barre des Ecrins). In the sedimentary cover along the rim of the massif the topography is less extreme but still many mountain peaks reach over 3000 m. The area is accessible from valleys to the east (Durance valley) and to the southwest (Drac valley). Navigable roads lead up to 1500 m the rest has to be reached on foot. Most field work was carried out between 1500 and 2800 m.

The field data presented in this study were collected by detailed structural mapping in key areas at the scales of 1:10'000 to 1:2'500. The structural mapping used as a base the

geologic maps of the BRGM which are very accurate. The data were taken from the following maps 1:50'000 sheets *Guillestre* (847) (Debelmas *et al.*, 1966), *Orcières* (846) (Debelmas *et al.*, 1980), *St.-Christophe-en-Oisans* (822) (Barféty *et al.*, 1984), *Briançon* (823) (Barféty *et al.*, 1995) and the 1:80'000 map sheet *Briançon* (189) (Lemoine *et al.*, 1969).

Orientation data were analysed using the software packages Stereoplot v.3 (Mancktelow, 1989-1995), FaultKin v.3.8a (Allmendinger *et al.*, 1989-94) and Faille v.3.5 (Etchecopar, 1990-1994). All stereonet plots are on lower hemisphere, equal area projections.

The field data were combined with the analysis of aerial photographs and other field photographs, with tectonic fabric analysis in thin sections, and with profile construction and restoration.

1.2 Geological overview of the western Alps and the Pelvoux area

The Soleil Boeuf area and the Champsaur-Prapic fold zone are part of the external western Alps, just south of the Pelvoux basement massif. The basement massifs of the external western Alps are composed of Variscan crystalline basement. During Mesozoic rifting the basement massifs were part of the northern continental margin of Tethys. Major tilted crustal blocks, a few tens of kilometres wide, can be either reconstructed or directly observed in the Pelvoux and Belledonne basement massifs east of Grenoble (Lemoine *et al.*, 1981: Fig. 1.6). The passive margin extension reactivated the NNE-SSW trending Cevennes fault system (Debelmas and Lemoine, 1970; Rousset, 1986). During the Alpine compression, graben structures were partially inverted or their footwall blocks buttressed the deformation. These structures have been extensively analysed (e.g. Davies, 1982; Gillcrust *et al.*, 1987; Butler, 1989; Coward *et al.*, 1991; Huyghe and Mugnier, 1995; Sue *et al.*, 1997).

Rifting started in the Early Jurassic, after deposition of Triassic evaporites and shallow water carbonates. The Triassic sequence is rather thin above the basement massifs (0 - 100 m) compared to the Subalpine chains (100 - 400 m) (Debrand-Passard *et al.*, 1984b; Lemoine *et al.*, 1986). Rifting continued until late Middle Jurassic and was followed by oceanic spreading until the early Cretaceous (Lemoine *et al.*, 1986). In the Pelvoux region the Jurassic sediments (mainly shales and limestones) fill asymmetric half-grabens with an irregular relief. Over 4 km of Liassic sediments in deeper parts of the grabens may be condensed to only a few metres on top of the horsts, where locally even the basement was eroded (Debelmas and Kerckhove, 1980; Lemoine *et al.*, 1986).

Contemporaneous with the earliest phase of continent collision in the eastern Alps the pre-Senonian folding phase (during the Late Cretaceous but prior to 88 Ma) affected the

southern Subalpine chains (Siddans, 1979). It is characterised by generally E-W oriented upright to N-facing folds which have been linked to N-S compression (Flandrin, 1966; Siddans, 1979).

From Late Cretaceous (locally Paleocene) to Early Eocene a period of uplift occurred with widespread subaerial erosion throughout the external Alps (Trümpy, 1980). It seems to correspond to a general slowing down of crustal shortening (Dewey *et al.*, 1989) but it also has been interpreted as related to uplift of a flexural forebulge in advance of the Alpine thrust-wedge (Allen *et al.*, 1991). In the south-western Alps, during the Paleocene to Middle Eocene, in the Provence and to a lesser extent in the southern Subalpine chains the Pyrenean-Provençal phase was active. It is recorded by E-W trending folds and thrusts (Lemoine, 1972; Siddans, 1979) and by uplift of the Pelvoux massif (Ford, 1996). The Pelvoux basement massif was uplifted 1 - 3 km while the basement cover interface and the overlying thin Mesozoic cover were folded. The recumbent basement involved folds face outward and rapidly die out away from the massif. As a result the Pelvoux massif formed a paleogeographic high (Ford, 1996).

Orogenic up-building in the internal Alps led to increased loading of the crust, which caused flexural subsidence and the formation of the Alpine foreland basin in the external domain (Fig. 1.1) since Late Eocene (Homewood *et al.*, 1986). The foreland basin succession is separated from the underlying Mesozoic passive-margin succession by a marked unconformity. To the south of the Pelvoux massif the foreland basin sediments transgressed over a continuously older substratum towards the north (Fig. 1.7) (Haug, 1894; Ravenne *et al.*, 1987). Slight detachment above the Triassic evaporites allowed gentle buckling of the foredeep (Lickorish and Ford, 1998). The typical stratigraphic trilogy of the underfilled foreland basin comprises from bottom to top (1) carbonate deposition on the cratonic margin of the basin (Nummulitic Limestone), (2) hemipelagic sedimentation offshore from the cratonic margin of the basin (Globigerina Marl), and (3) deep water turbiditic siliciclastic sedimentation toward the orogenic margin of the basin (Sinclair, 1997). Fig. 1.8 shows the westward prograding transgression onto the foreland. In the investigated area the Upper Eocene to Lower Oligocene stratigraphy comprises four formations (Fig. 1.9). The Basal Conglomerate Formation which consists of local fluvial incision channels up to 100 m deep (Gupta, 1997), the Nummulitic Limestone Formation which is characterised by a variable thickness of 5 - 50 m. There is evidence that extensional faulting was active during its deposition (Fabre *et al.*, 1985). It grades upwards into the Globigerina Marl Formation which consists of silty to very fine-grained hemipelagic shales and marls. Its thickness varies between 0 - 50 m. Above lies the Champsaur Sandstone Formation which constitutes a well stratified, regular alternation of turbiditic sandstones and shale. The sand layers are commonly coarse-grained, often

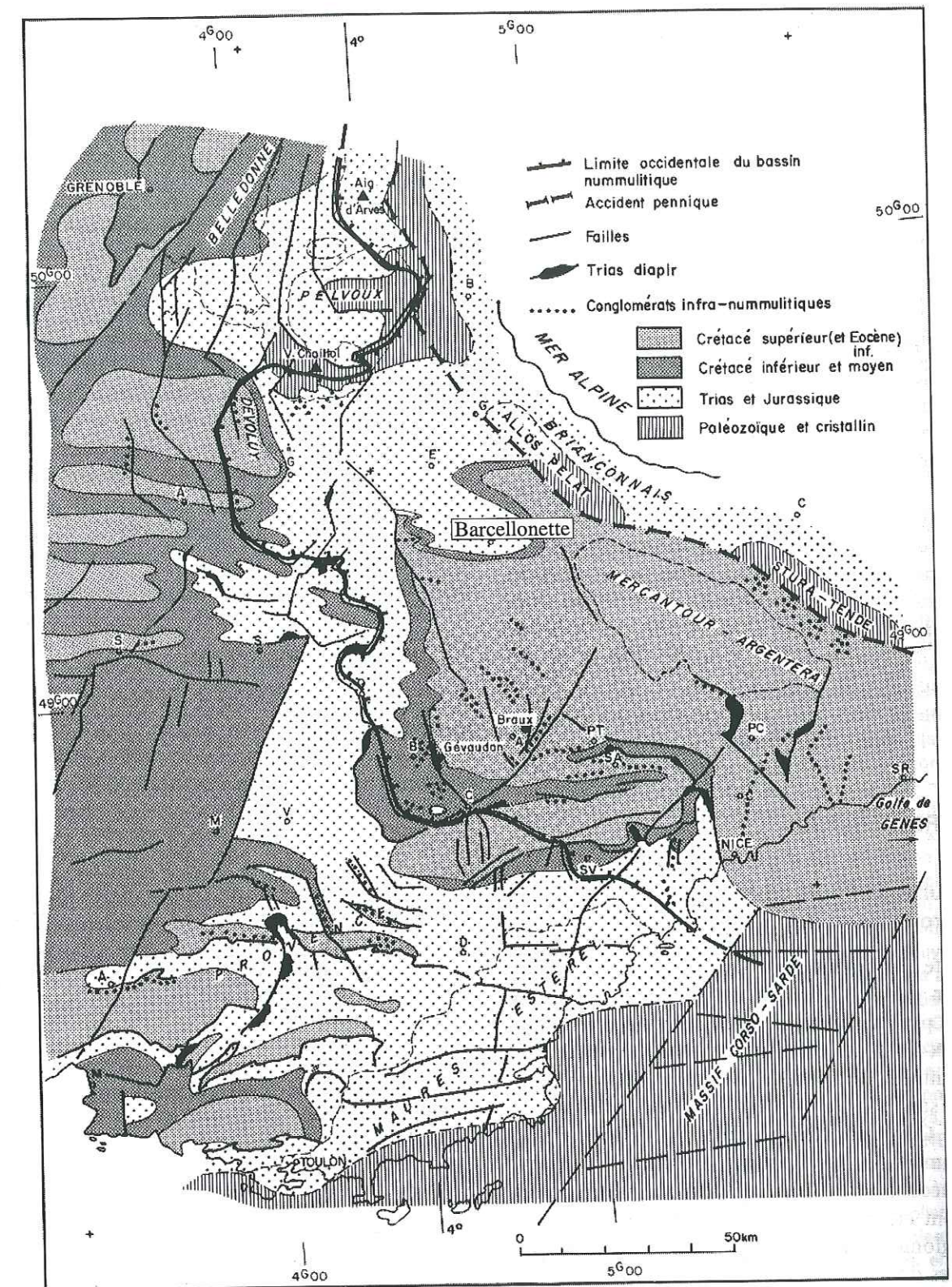


Fig. 1.7: Reconstruction of the substrate to the Tertiary foreland basin deposition. It reveals the structuration resulting from the Pyrenean-Provençal phase. The basement-cover interface rises northwards (north of Barcelonnette) and is exposed in the Pelvoux area. From Ravenne *et al.* (1987).

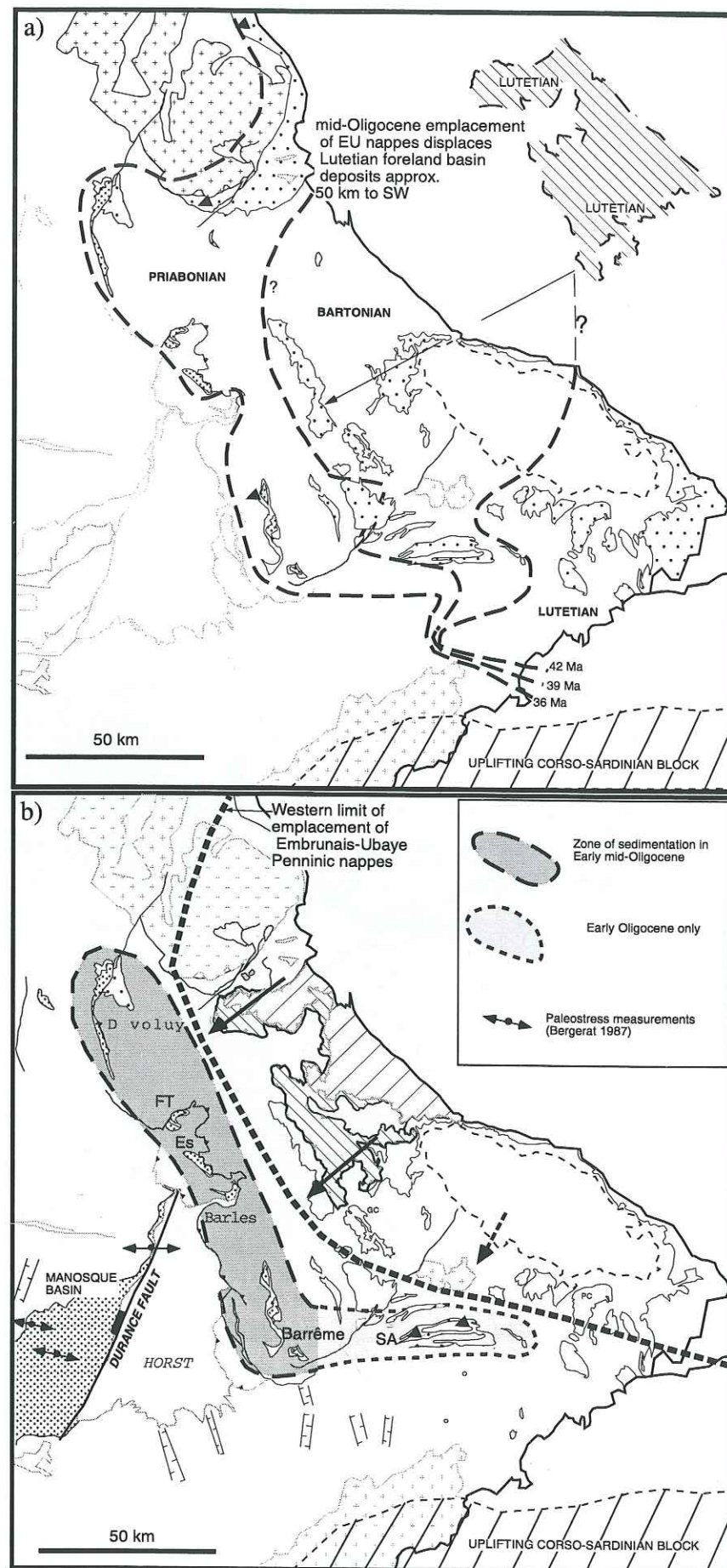


Fig. 1.8: Simplified map of southeastern France showing the distribution of sedimentation. From Ford et al. (subm.)

a) Late Eocene: transgression. Heavy lines representing the western limit of the transgression at 42, 39 and 36 Ma. Black triangles mark the presence of volcanic material.

b) Early-mid-Oligocene: emplacement of Embrunais-Ubaye nappes.

conglomeratic and thick-bedded (Perriaux and Uselle, 1968; Waibel, 1990). The thickness ranges from approximately 650 m in the Soleil Boeuf area to 1200 m in the eastern part of the Champsaur-Prapic area. In some parts of the foreland basin the siliciclastic sediments contain volcanic debris (Debrand-Passard *et al.*, 1984b). In my area both volcanic and non-volcanic facies occur, and the deposits in the Soleil Boeuf area contain up to 50% of volcanic detritus (Waibel, 1990). K/Ar whole-rock dating on andesitic pebbles from the Soleil Boeuf area (Fontignie *et al.*, 1987) yielded maximum ages (due to the effects of argon over-pressure) for the volcanic activity of 37.6 ± 1.3 Ma and 40.2 ± 1.3 Ma. Recent $^{39}\text{Ar} - ^{40}\text{Ar}$ dating of amphibole from andesite pebbles in the same sandstones by G. Feraus (pers. comm.) yielded an age of 34.3 ± 1.0 Ma. These ages must be older or at least equal to the stratigraphic age and therefore indicates that sedimentation in the Soleil Boeuf area continued until at least Early Oligocene (mid-Rupelian).

During Late Eocene and Oligocene times, western Europe underwent E-W extension, which initiated the N-NE oriented Rhine-Bresse-Rhône graben system (Fig. 1.1) which extends from central Germany south-southwestward through southeastern France to join the Mediterranean Sea near the Rhône delta (Bergerat, 1987).

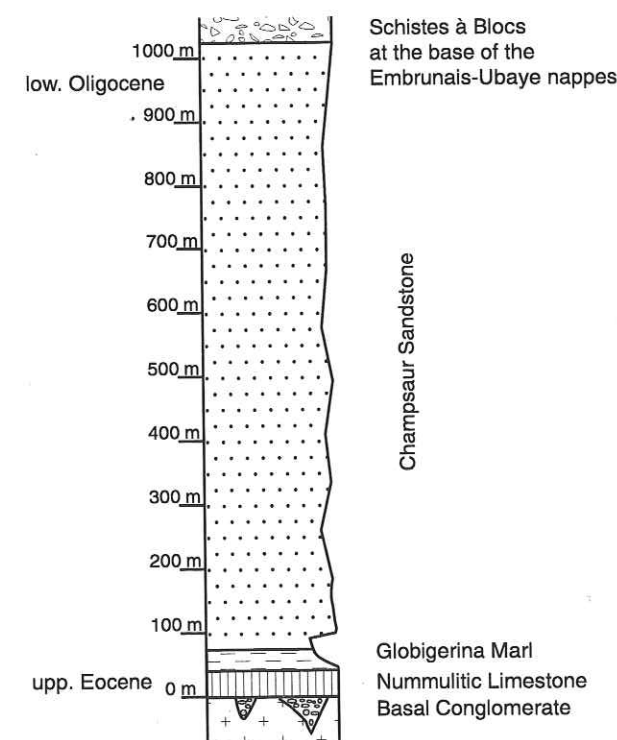


Fig. 1.9: Simplified stratigraphic column.

During the mid-Oligocene, Alpine deformation reached the external western Alps. The foreland basin was filled and overridden by internally derived nappes (Fig. 1.1). In the southern Subalpine chains, the deposition of the siliciclastic sandstones abruptly ceased due to the deposition of the Schistes à Blocs, a tectono-sedimentary marine mélange (Kerckhove, 1969). This unit underlies the Embrunais-Ubaye nappes everywhere and has been interpreted by Kerckhove (1969) to include debris which were shed into the basin from the front of the advancing nappes. The Embrunais-Ubaye nappes were emplaced during the Rupelian (Early Oligocene) (Fry, 1989; Lickorish and Ford, 1998). Kinematic data from the 'Schistes à Blocs' and other structural data (Lawson, 1987; Fry, 1989; Ritz, 1991; Lickorish and Ford, 1998) show that this nappe stack was emplaced toward the SW-WSW ($220\frac{1}{2}$ - $240\frac{1}{2}$) onto the Alpine foreland. The internal tectonic history of the Embrunais-Ubaye nappe stack and its relation to the FPT is complex and controversial (Kerckhove, 1969; Tricart, 1980; Merle and Brun, 1984; Fry, 1989).

During the Late Oligocene, foreland deposition shifted to the Barrême and Dévoluy areas, and sedimentation was limited and became continental (Elliot *et al.*, 1985; Evans and Mange-Rajetzky, 1991; Meckel *et al.*, 1996; Meckel, 1997; Lickorish and Ford, 1998). From late Early Miocene (Burdigalian) to Pliocene up to 2000 m thick continental and shallow marine clastics were deposited in the Valensole basin (Debrand-Passard *et al.*, 1984a).

In the north Alpine foreland basin in the mid-Oligocene a change occurred from a deep marine, underfilled foreland basin to a filled or overfilled basin with shallow-marine or continental molasse sediments (Trümpy, 1980; Sinclair, 1996). In contrast to the southern Subalpine chains, the foredeep migrated regularly to the north to northwest and continuous sedimentation filled the Oligocene to Miocene molasse basin. Its greatest thickness (5000 - 6000 m) is found along the southern side below the front of the Alpine nappes (Trümpy, 1980).

2. The Champsaur-Prapic fold zone: overthrust shear deformation of a foreland basin

2.1 Introduction

2.1.1 Geological setting and previous work

The Champsaur-Prapic fold zone is situated at the southeastern rim of the Pelvoux basement massif (Fig. 1.6). It is covered by the 1:50'000 geologic maps of Orcières (Debelmas *et al.*, 1980), St.-Christophe-en-Oisans (Barfétty *et al.*, 1984), Briançon (Barfétty *et al.*, 1995) and Guillestre (Debelmas *et al.*, 1966). A regional angular unconformity separates the strata of the southwestern Alpine foreland basin, from the Variscan crystalline basement and its Mesozoic cover. Within the Champsaur-Prapic fold zone the Mesozoic cover was completely eroded except in the Dormillouse inlier, where few meters of Triassic rocks are preserved. Along the margin of the Pelvoux massif, basement and Mesozoic cover rocks were folded together by the Pyrenean-Provençal deformation (Late Cretaceous to Eocene), uplifted and deeply eroded (Ford, 1996 and references therein), providing a rapidly varying substrate for the Tertiary sediments (Fig. 2.1). The Upper Eocene to Lower Oligocene stratigraphy comprises local fluvial incision channels filled by a basal conglomerate (0 - 10 m), shallow-water Nummulitic Limestone (5 - 50 m), hemipelagic Globigerina Marl (0 - 50 m) and turbiditic sandstones (700 - 1200 m), the Champsaur Sandstone. The latter onlap their substrate from east to west and are of the non-volcanic facies.

The Champsaur-Prapic fold zone extends westward for some 14 km from the Frontal Pennine Thrust (FPT) (Fig. 2.1). The study area is divided in two by the Champsaur Thrust which separates the main Champsaur fold zone from the narrower Prapic fold zone to the west. No major folds occur in the Tertiary succession west of Orcières (south of the Selle-Fault; Fig. 1.6). For purposes of description, the Champsaur fold zone is divided into 3 domains (Fig. 2.1): the central domain, including the Fournel basement inlier, the northern domain north of Vallouise and along the border to the Pelvoux massif and the southern domain, around the Dormillouse basement inlier and further south. Folds in the Champsaur Sandstone record shear strain variations across the region while intense shear fabrics characterise the Globigerina Marl and the Nummulitic Limestone in the basal shear zone below.

The N-S trending FPT separates the Tertiary sediments from the internal Sub-briançonnais units. Further east the Frontal Briançonnais Thrust carries the Briançonnais zone on top of the Sub-briançonnais zone (Fig. 2.1). Late normal displacements on both faults (Tricart *et al.*, 1996) probably thinned the Sub-briançonnais to few metres thickness in the Fournel valley. To the south, the Tertiary sediments are tectonically

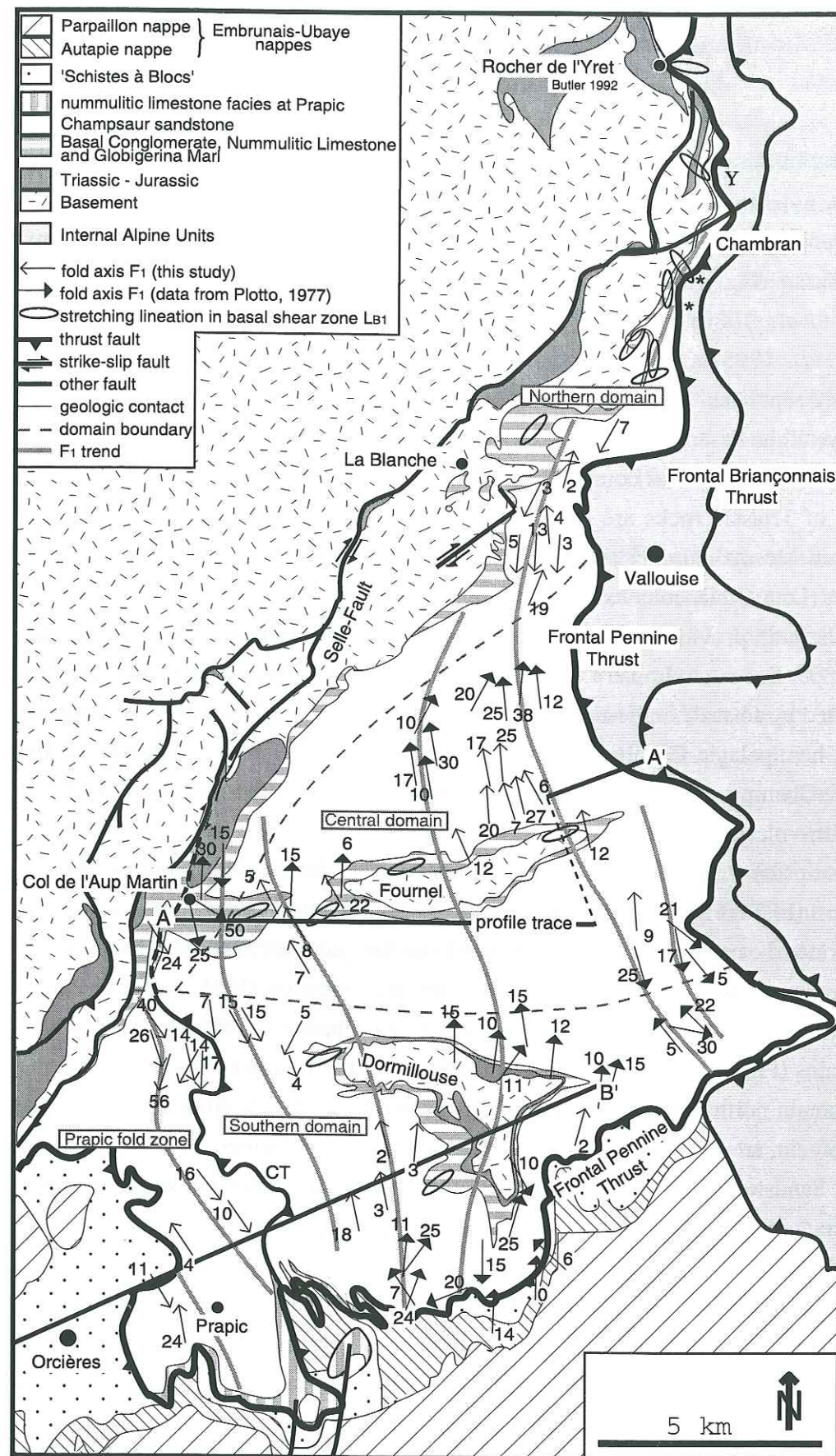


Fig. 2.1: Simplified geological map of the Champsaur-Prapic fold zone adapted from BRGM maps 1:50000 and own work. Arrows give fold axis orientation of chevron folds in the Champsaur Sandstone. The fold axial trends are marked by thick grey lines. A-A' (note that the line is in two parts) and -B' (see Fig. 1.6 for full section line) are the traces of the reconstructed profiles in Figs. 2.4 & 2.7, respectively. CT = Champsaur Thrust; * = location of NNE-SSW trending open folds in basal shear zone; Y indicates the northern limit of observed FB2 folds.

overlain by the Embrunais-Ubaye nappes, a more complex assemblage of Cretaceous Helminthoid flysch, Sub-briançonnais and Briançonnais units (Fig. 1.6). Structural and metamorphic evidence (Aprahamian, 1974; Debelmas and Kerckhove, 1980) indicates that internal thrust sheets overrode the whole Champsaur-Prapic fold zone. The Embrunais-Ubaye nappes are separated from their foreland substrate by the 'Schistes à Blocs' (Fig. 2.1), described by Kerckhove (1969) as a marine sedimentary mélange implying that submarine emplacement of the lowest of these nappes (Autapie) terminated foreland basin sedimentation. Kinematic data from the 'Schistes à Blocs' (see Fig. 2.7b) and other structural data (Lawson, 1987; Fry, 1989; Lickorish and Ford, 1998) show that the nappes were emplaced toward the SW-WSW ($220\frac{1}{2}$ - $240\frac{1}{2}$).

Most previous work was carried out to investigate the relationship of the Pelvoux massif and its Mesozoic and Tertiary cover at the rim of the Pelvoux massif (e.g. P. Gidon, 1953; M. Gidon 1965). Structural studies of the Champsaur-Prapic area itself have been carried out by Plotto (1977) and Tricart (1980) in the Central and Southern domain of the Champsaur-Prapic fold zone. Plotto (1977) described and quantified the extent and continuity of the deformational styles whereas Tricart (1980) concentrated on the relationship between the cover and the basement and between the cover and the Frontal Pennine Thrust. However, these studies did not investigate the Northern domain or the Prapic fold zone. The most recent study of the Prapic fold zone is by Kerckhove *et al.* (1978) which served as a basis for the BRGM map sheet Orcières (Debelmas *et al.*, 1980).

2.1.2 Overthrust shear and development of folds in simple shear

In thrust belts, stratified sequences can become folded by simple shear within a broad shear zone, usually below an overthrusting mass. The resulting asymmetrical fold trains show a transition from upright to overturned folds and may describe larger asymmetric nappes. Such structures have been analysed in several external orogenic belts: e.g. in the Variscan belt of southwest England (Sanderson, 1979), from back-arc basin deposits in the southern Andes (Bruhn, 1979; Tanner and Macdonald, 1982), in the Helvetic Alps (Ramsay *et al.*, 1983; Dietrich and Casey, 1989; Rowan & Kligfield, 1992; Casey and Dietrich, 1997) and previously in the present study area by Plotto (1977) and Tricart (1980, 1984, 1986). This phenomenon has become known as overthrust shear. All these areas show some or all of the following characteristics: (1) folds show consistent facing and asymmetry across a large area, (2) there is a clear correlation between fold tightness and axial plane attitude which (3) both record a systematic increase in strain in one direction, (4) folds are non-cylindrical and (5) fold axis orientation is variable with respect to the stretching lineation (Gibson and Gray, 1985).

The issue of how folds are initiated in simple shear is problematical. The first mathematical and geometrical models for fold development in simple shear argue that to initiate folding in a shear zone, the shear plane has to be initially at a low angle to the layering (Ghosh, 1966; Sanderson, 1979, 1982). However other authors have argued that to initiate folding in a shear zone at a low angle to layering, small perturbations within an anisotropic multilayer sequence on which folds can nucleate and amplify are necessary (Casey and Huggenberger, 1985). Alternatively, the bulk strain must deviate from ideal simple shear for example, if there is a component of shortening parallel to the shear direction (Ridley and Casey, 1989). For fold development in simple shear (Sanderson, 1979) bedding lies at a low angle to the shear zone with a constant strain profile (Fig. 2.2a). Symmetrical buckle folds initiate by layer-parallel shortening with axial planes at a high angle to the shear zone and subsequently rotate, tighten and become more asymmetrical as the strain increases. This model has been applied to asymmetrical fold trains where the folds are all of the same order (Bosworth and Vollmer, 1981; Tanner and Macdonald, 1982), being slightly modified to estimate shear strain by Gibson and Gray (1985) and Rowan and Kligfield (1992). In the case of the Millook nappe in SW England (Sanderson, 1979) and the Helvetic nappes of Switzerland, folds record a marked increase in shear strain downwards across a large-scale recumbent nappe fold (Fig. 2.2b). For the Helvetic nappes, Ramsay *et al.*, (1983) proposed that the nappes were first emplaced over their footwall ramps to give a hangingwall anticline before the onset of progressive simple shear. Dietrich and Casey (1989) and Casey and Dietrich (1997) instead propose that these nappes evolved by contemporaneous superposition of pure shear and heterogeneous overthrust shear.

In this Chapter asymmetrical folding is described and analysed from the Champsaur-Prapic fold zone which lies in the footwall of the Frontal Pennine Thrust (FPT), the tectonic boundary between the external and internal units of the western Alps. The general geometries of asymmetrical chevron folds agree very well with the simple shear model of Sanderson (1979; Fig. 2.2a) and the characteristics of overthrust shear described above. However this area also has distinctive geometrical characteristics which suggest a more complex distribution of shear strain than shown in previous studies. Shear strain increases toward the hinterland indicating that it was generated by emplacement of the over-riding internal thrust sheets with highest strains recorded at the rear (Plotto, 1977; Tricart, 1980). No major nappe folds have developed. Instead the deformation is concentrated in high strain zones which cut at a variable angle through sub-horizontal bedding, forming diffuse ramps linking floor and roof shear zones. The folds of Champsaur-Prapic have previously been described and analysed in the theses of Plotto (1977) and Tricart (1980). Their work is incorporated and discussed in this study.

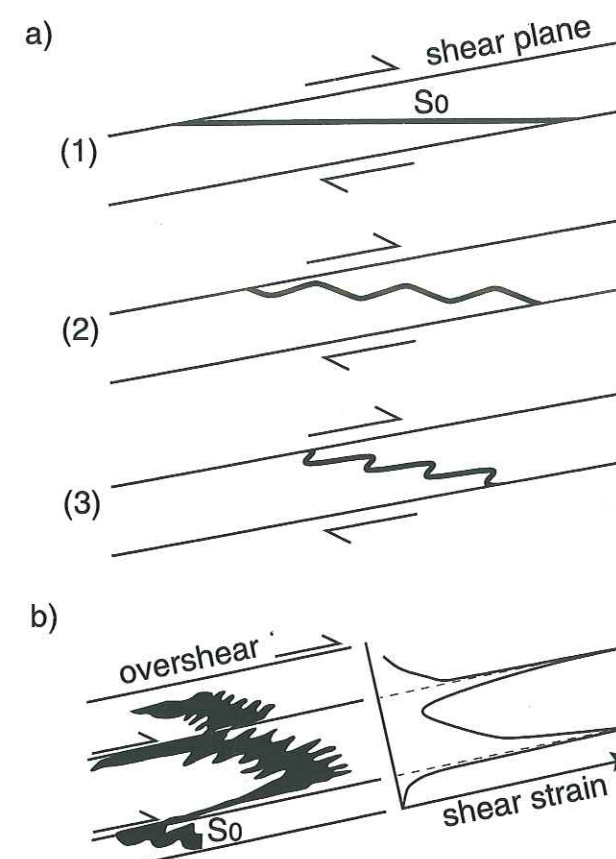


Fig. 2.2: Simplified cross sections of overthrust shear models:

a) Conceptual model of the progressive development of folds by simple shear (modified after Sanderson, 1979). (1) Undeformed geometry: a shear zone with a constant strain profile is at a low angle to layering; (2) initial generation of symmetric buckle folds; (3) development of asymmetry by passive rotation of axial planes.

b) Nappe geometry resulting from distributed simple shear originally oblique to the stratigraphic sequence (as in a) which concentrates at the lower nappe boundary (from card deck experiments). The graph to the right shows how the shear strain varies, the two peaks refer to the base of the nappes (modified after Casey and Dietrich, 1997).

2.2 The Champsaur fold zone

The turbidite sequence forms regular trains of gently plunging chevron folds. Individual folds die out laterally and cannot be traced for more than 4.5 km. Fold axes and axial trends, compiled from Plotto (1977) and this study, are shown on Fig. 2.1. A single axial planar cleavage is associated with the folds (Fig. 2.3). In the narrow northern domain, fold axes plunge toward N–NNE and S–SSW (Figs. 2.1 & 2.3a). Poles to bedding and cleavage define similar cluster distributions, giving an average planar dip of 40–50° E, approximately parallel to the FPT (Figs. 2.3a & b). In the central domain fold axes plunge gently NNW and coincide well with the Π -pole (346–12) to the best fit great circle for bedding (Figs. 2.1 & 2.3c). The elongate cluster of poles to axial planar cleavage (Figs. 2.3d & f) is generated by the east-west transition from moderately to steeply dipping axial planes. In the southern domain measured fold axes plunge dominantly to S–SSE but display a considerable scatter which is also reflected in the broad girdle distribution of poles to bedding (Figs. 2.1 & 2.3e). Fold orientation can vary within a single fold pair suggesting that the folds may be weakly curvilinear in this region. In summary, fold axial trends curve from NNE in the northern domain to NNW in the central and southern domains. This curvature becomes more pronounced toward the east (Fig. 2.1).

The majority of folds show angles of axial transection Δ (Borradaile, 1978; Johnson, 1991) between $+27^\circ$ and -16° . The degree of axial transection may be related to fold trend: N-S to NW-SE folds tend to have smaller (or even negative) Δ -values than NE-SW trending folds.

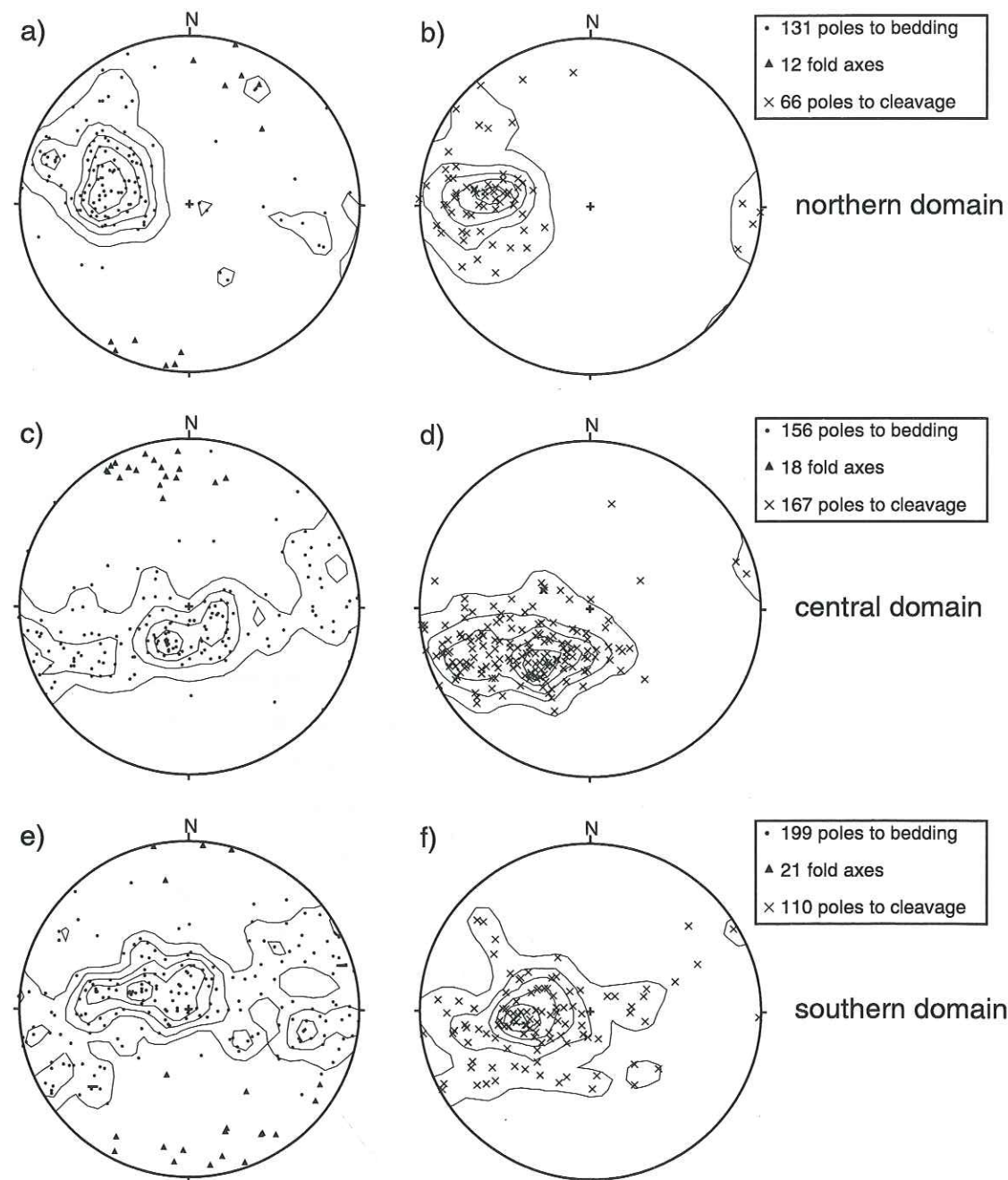


Fig. 2.3: Equal area lower hemisphere projections of structural elements (bedding, cleavage, fold axes) in the Champsaur Sandstone turbidite sequence of a) & b) the northern domain, c) & d) the central domain and e) & f) the southern domain. Bedding poles and poles to cleavage are contoured at 1 2 3... times uniform. For further description see text.

2.2.1 The northern domain

The northern domain is only 1 - 4 km wide and thus lateral variations in geometrical parameters of folds cannot be observed. In addition, this zone has been tilted 20 - 30½ to the SE by late uplift of the Pelvoux basement massif so that, for example, the dip of axial planes cannot be used to calculate shear strain. Interlimb angles however are not affected by later tilting and give a range similar to those of zones D to E in the central domain (see next paragraph).

2.2.2 The central domain: the Fournel profile

The southern side of the E-W Fournel valley (Fig. 2.1) provides an excellent 14 km long profile (1.5 to 0.8 km high) through the central domain from the FPT in the E to the Selle-Fault in the W. The valley cuts down into basement, thus exposing the basal shear zone in the lower Tertiary units (Fig. 2.1). This continuous profile, first documented by Plotto (1977), is re-drawn in more detail from rectified photographs for analysis of fold geometry (Fig. 2.4; see figure caption for details of correction procedure). Five zones of folding, labelled A to F, with widths varying from 0.4 to 2 km are separated by 0.3 to 1.6 km wide zones of moderately east-dipping strata. The dip of the fold zones decreases from west to east (Fig. 2.4; Table 2.I). The size of folds is controlled largely by the percentage of sand and shale within the turbiditic succession and the thickness of sandstone- and shale dominated packages. Wavelengths range between 50 and 450 m, amplitudes from 30 - 200 m. The typical chevron forms have long straight limbs, narrow hinge zones, rounded hinges in sandstone-dominated facies and angular hinges in mudstone-dominated facies (Fig. 2.5a). Limb-thrusts and hinge-collapse are relatively common in upright chevron folds (Fig. 2.5b). In sections with strongly marked layer thickness variations, the fold limbs become curved. The fold enveloping surface dips gently west. In the east it dips eastward below the Sub-briançonnais units.

Table 2.I summarises the main geometrical features of the five fold zones and Fig. 2.6 (a, b) presents plots of fold interlimb angle vs. distance from the FPT and interlimb angle vs. axial plane dip. Two main trends characterise the deformation: mean interlimb angle and mean fold axial surface dip both decrease from west to east, together with an increase in relative shortening across the fold zones (calculated using bed length). The observed axial plane rotation and fold tightening are consistent with progressive non-coaxial deformation. Using the axial planes as passive markers that rotated from an original dip of 90½ toward the shear direction with increasing shear (Sanderson, 1979), variation in shear strain within each fold zone (Table 2.I; Fig. 2.6c) was calculated. Although individual fold zones show a wide range of shear strains (Fig. 2.6c) the mean value clearly increases toward the east. However zone F does not fit with this trend. In this zone axial planes have become parallel to the FPT. As they can no longer rotate they

cannot be used to calculate shear strain. One best fit line is constructed through these data and extrapolated to find the shear strain at the FPT. The line gives a shear strain of 2.2 at the FPT. This is a minimum estimate. Bulk fold shortening in this profile is ~22%. Plotto (1977) estimated 30% because he assumed that folding was homogeneously developed across the region.

fold zone	ILA range [°]	average ILA	shortening (l_0-l)/ l_0 [%]	average AP-dip [°]	shear strain γ	average zone dip [°]
A	75 - 134	102	19	78	—	—
B	49 - 106	70	~36	50	0.9	~30 - 53
C	57 - 77	66	~46	40	1.1	48
D	26 - 90	54	~42	36	1.4	~32
E	22 - 55	34	65	32	1.7	28
F	26 - 101	63	—	41	—	20

Table 2.I: Geometric fold data from the Fournel profile (Fig. 2.4). ILA = fold interlimb angle. AP = fold axial plane. Shear strain $\gamma = \tan(90-\alpha)$, where α is the dip of the axial plane.

In the westernmost zone A fold axial planes dip steeply east or west. Folds are tighter in the west than in the east (Fig. 2.6a) indicating that they were either tightened against the Pelvoux massif or by a later activity on the Selle-Fault. Within the fold zones themselves shear strain tends to increase downward (Zones B and D), however deformation is strongly affected by mechanical stratigraphy and thus no consistent vertical variation in strain can be detected. For example, shear strain clearly increases at the thick shale-dominated horizon in zones B, C and D, as shown by the narrowing and flattening of the fold zones as they cross this level. There are also individual fold packages bounded by unfolded but sheared shale-rich horizons (Fig. 2.5a). The fold package in Fig. 2.5(a) displays all the features of a duplex, but without discrete thrust surfaces. Axial surfaces are sigmoidal and, towards the shale-rich beds above and below, fold amplitude and interlimb angle decrease.

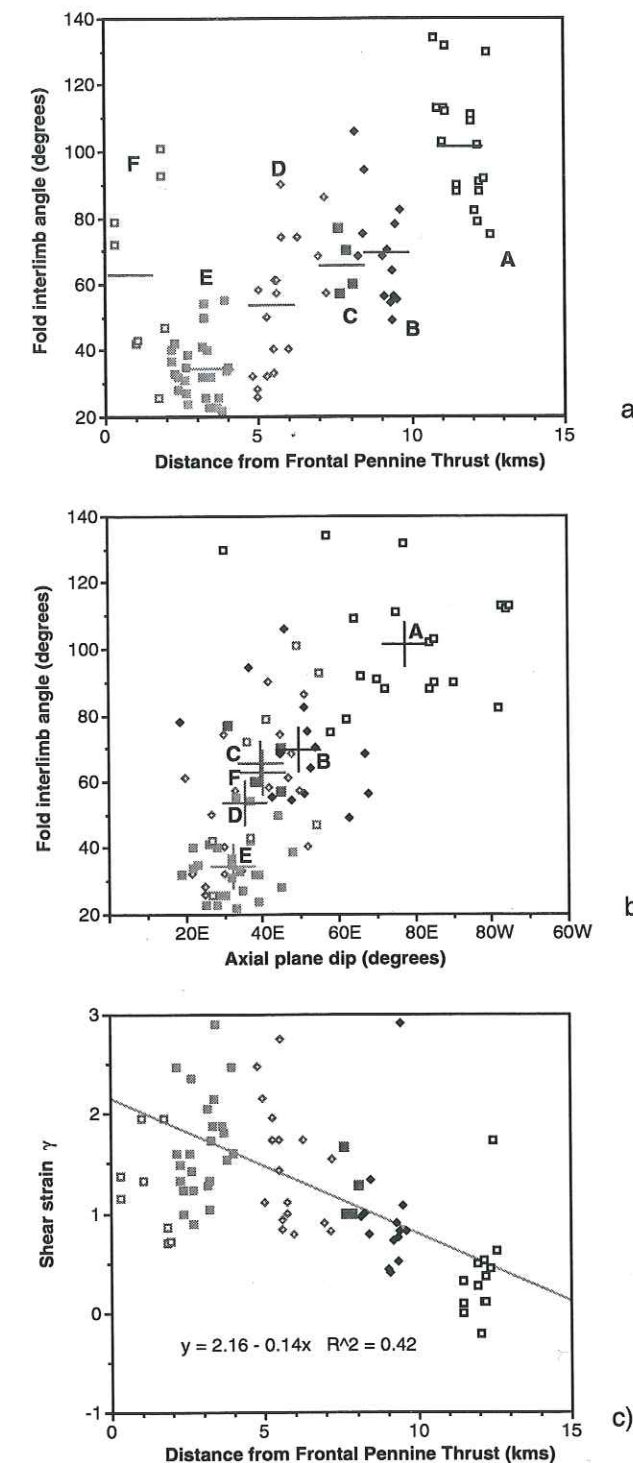


Fig. 2.6: Plots of geometric parameters of the Fournel chevron folds (Fig. 2.4). a) Fold interlimb angle vs. distance from a fixed point on the Frontal Pennine Thrust in the east. Horizontal bars represent the mean values of fold interlimb angles calculated for each inclined fold zone A - F. They decrease gradually towards the Frontal Pennine Thrust, with the exception of zone F in the immediate footwall of the thrust. b) Fold interlimb angle vs. axial surface dip of the same folds. Crosses represent the mean values for each zone. They show a linear relationship except for zones E and F which are bent down below the Frontal Pennine Thrust. c) Shear strain ($\gamma = \tan(90-\alpha)$, where α is the dip of the axial plane; Sanderson, 1979), vs. distance from a fixed point on the Frontal Pennine Thrust. The curve was calculated without the data from zone F and extrapolated to the Frontal Pennine Thrust. For further explanations see text.

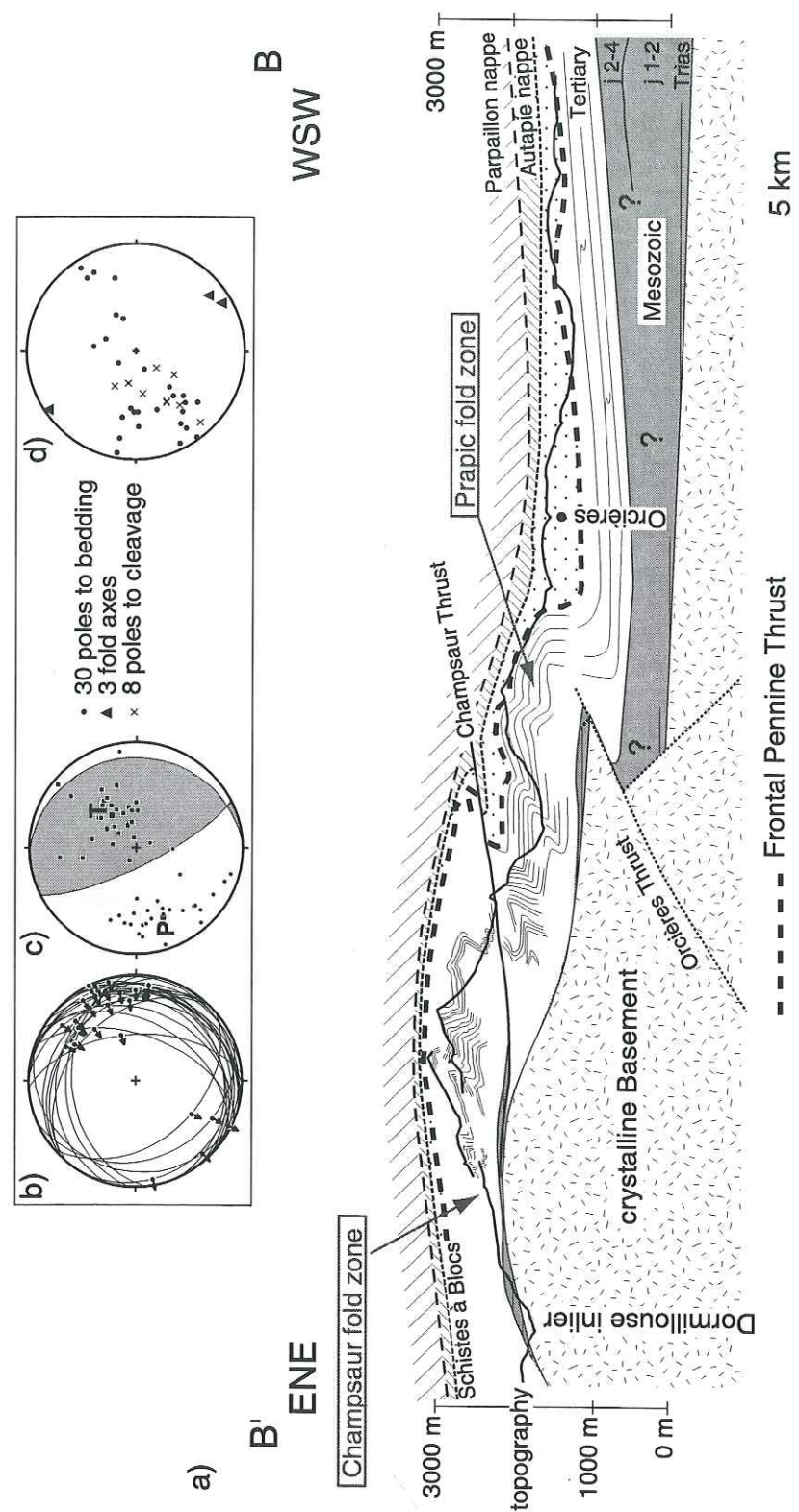


Fig. 2.7: a) ENE-WSW profile (localised in Fig. 2.1) across the Dormillouse basement inlier and the Champsaur Thrust. The strong deformation in the footwall of the Champsaur Thrust rapidly dies out towards the WSW. The change from basement-dominated substrate to thick Mesozoic substrate is related to a Mesozoic half graben structure. j 1-2 = marly limestones (Bajocian - Low. Bathonian), j 2-4 = Terres Noires (Up. Bathonian - Oxfordian). The stratigraphy of the Embrunais-Ubaye nappes (Parpaillon and Autapie) is Up. Cretaceous - Paleocene. For further discussion see text. b) Equal area lower hemisphere projection plots of fault kinematic data from the Schistes à Blocs around Orcières. c) Fault plane solutions derived with the FaultKin programme of Allmendinger (1989-94), showing the P and T axes for individual slip surfaces ($n = 29$) and the mean T (055-59) and P (248-30) axes for the data set. d) Structural elements (bedding, cleavage, fold axis) in the Champsaur Sandstone turbidite sequence from the footwall of the Champsaur Thrust.

2.2.3 The southern domain

In the southern domain, folds in the Champsaur Sandstone, observed around the Dormillouse basement inlier, record a similar strain gradient to that in the central domain. Fig. 2.7(a) depicts the western part in the hangingwall of the Champsaur Thrust with the transition from asymmetric to upright chevron folds. Interlimb angle and axial plane dip both decrease from west to east (Figs. 2.8a & b). The calculated shear strain

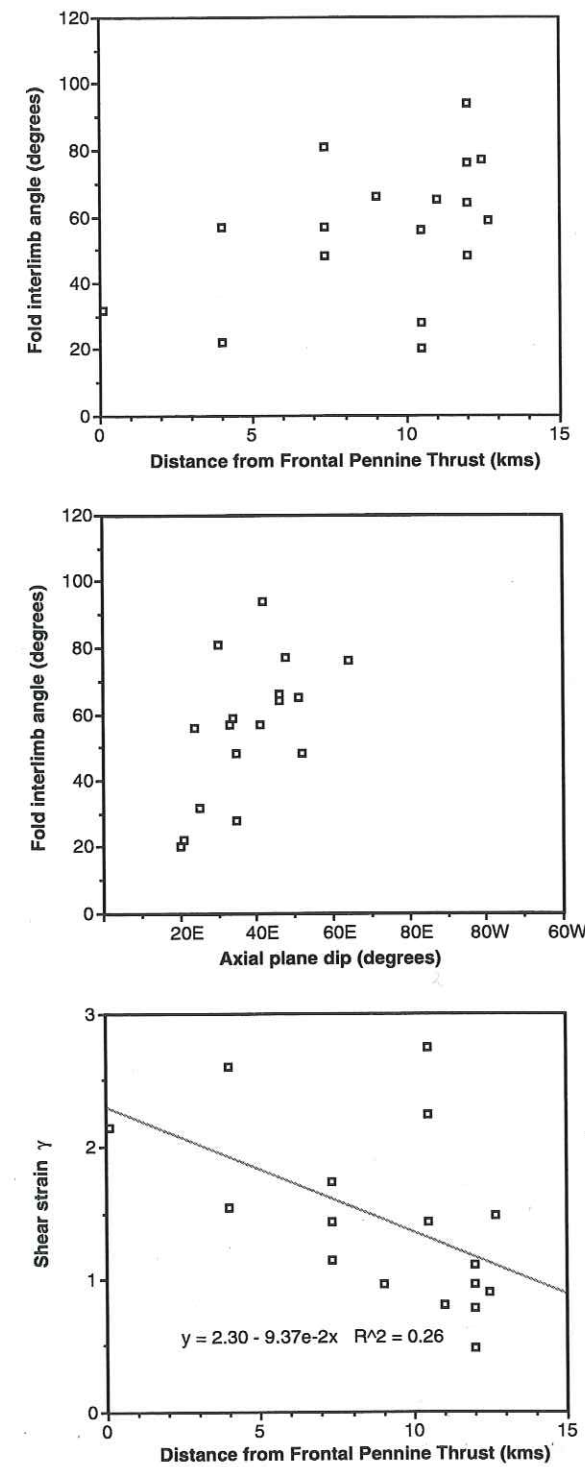


Fig. 2.8: a) - c) Plots of geometric parameters of the chevron folds in the southern domain. These data show the same relationships as in the Fournel profile (Fig. 2.6). a) Fold interlimb angle vs. distance from a fixed point on the Frontal Pennine Thrust. The values gradually decrease towards the Frontal Pennine Thrust. b) Fold interlimb angle vs. axial surface dip of the same folds. c) Shear strain ($\gamma = \tan (90-\alpha)$) vs. distance from a fixed point on the Frontal Pennine Thrust.

thus increases toward the FPT giving a minimum value of $\gamma = 2.3$ at the fault itself (Fig. 2.8c).

2.3 The Prapic fold zone

The Prapic fold zone lies in the footwall of the Champsaur Thrust (Figs. 2.1 & 2.7). The Champsaur Thrust dips 10 - 30½ east and can be traced northward where it links to the basal shear zone (Figs. 2.1 & 2.4). Displacement on the Champsaur Thrust decreases northward.

In the Dormillouse area the Champsaur Thrust almost doubles the Tertiary stratigraphy and the thrust is marked by a sudden change in chevron fold morphology (Fig. 2.7a). In the hangingwall, close to the thrust plane, chevron folds become overturned and minor asymmetric folding affect the limbs. In the footwall the turbidite sequence is folded in large tight recumbent asymmetrical SW-vergent folds. All folds have subhorizontal fold axes trending NW-SE (145½; Fig. 2.7b). Most of the deformation is accommodated in a narrow (~3 km) zone in the footwall of the thrust. Restoration of bed lengths give at least 1 km shortening in this zone. The orientation and vergence of these folds suggest that they were generated during SW movement on the Champsaur Thrust.

To explain the presence of nummulitic limestone facies at the base of the 'Schistes à Blocs' south of Prapic (Fig. 2.1) Kerckhove *et al.*, (1978) proposed an early large-scale recumbent nappe-like syncline, overturned towards the NW (well illustrated on the 1:50'000 geologic map of Orcières; Debelmas *et al.*, 1980). They described overturned bedding in the underlying turbidites to represent a major upper overturned fold limb. In the present study no evidence for such an overturned fold was found (Fig. 2.7a). I therefore suggest that this nummulitic limestone sequence is either part of the 'Schistes à Blocs' or the overlying Sub-briançonnais sequence. A nummulitic limestone unit in a similar tectonic position was described above the turbidites of the Aiguilles d'Arves north of the Pelvoux massif (Fig. 1.6) by Bravard (1982) who proposed that these are in stratigraphic position.

East of Orcières, large-scale folding ends in a regional open anticline (Orcières Anticline) which drops the top of the turbidite sequence ~1 km down to the west (Fig. 2.7a). I propose that this large NW-SE-trending anticline is related to a blind basement thrust (Orcières Thrust) which carries the hangingwall ~1 km towards the SW. Further SW only rare minor (<10 m) SW-vergent folds occur within the Tertiary sequence. This change in deformational style may be related to a change in the substrate. West of Orcières the Tertiary sequence is underlain by a thick sequence of Mesozoic rocks, especially the Middle to Upper Jurassic shales (Terres Noires), whereas east of Orcières the substrate is crystalline basement with a local thin Triassic cover (Fig. 1.6). I therefore

speculate that the blind Orcières Thrust is located on a Mesozoic normal fault (Fig. 2.7a). This large anticline and the Champsaur Thrust cut and involve the lower parts of the Embrunais-Ubaye nappes ('Schistes à Blocs' and Autapie nappe) (Figs. 2.1 & 2.7; Kerckhove *et al.*, 1978) implying that these lower units were emplaced over the Prapic fold zone during ongoing SW-directed deformation.

2.4 The basal shear zone: progressive shearing of the Nummulitic Limestone and Globigerina Marl

Between the Champsaur Sandstone and the crystalline basement lies a 5 - 60 m thick basal Tertiary sequence comprising local pockets of basal conglomerate, the Nummulitic Limestone and the Globigerina Marl. In general the basal conglomerates remain undeformed. The gradation between the two upper formations produces a smooth upward decrease in mechanical strength. The basal shear zone overprints this mechanical stratigraphy and can be divided into lower (Nummulitic Limestone), intermediate (transitional marly limestones) and upper (marls) levels with an upward increasing strain gradient. The basal Tertiary stratigraphy (and therefore the basal shear zone) is thicker (up to ~60 m) in the central domain (Fournel) than in the southern domain (22 m; Dormillouse). It thins dramatically to the north of Fournel to less than 5 m in places. Structural data and characteristic synthetic profiles through the basal shear zone are shown on Fig. 2.9 (see also Plotto, 1977; Tricart, 1980). Small-scale structures in the basal shear zone record a history of progressive shear with a vertically increasing strain gradient. In order to describe this progressive deformation I have distinguished four generations of structures, numbered B1 to B4. This numbering system is only applicable within the basal shear zone.

2.4.1 The main foliation (B1)

The main foliation (S_{B1}) is subparallel to bedding and carries a well developed stretching lineation. It is not associated with any folding. Morphologically S_{B1} changes from a weak anastomosing cleavage in the lower level to a continuous cleavage in the intermediate, and slaty cleavage in the upper levels indicating a strong vertical deformational gradient (Figs. 2.9b & c). In areas of thinner basal Tertiary strata and thus higher shear strains, the spacing of S_{B1} decreases upwards within 5 metres from ~6 cm to ~4 mm. In the central and southern domains S_{B1} dips around 30° towards the NE-ENE (Figs. 2.9b & c) and the stretching lineation clusters around NE or is folded and distributed along a WSW-ENE trending great circle as in the case of the central domain (Fig. 2.10a). In the northern domain, S_{B1} dips moderately E (Fig. 2.9a) and the stretching lineation plunges NNE-NE, with the exception of the northernmost Chambran area where the stretching lineation changes to NW-SE and N-S trending (see Figs. 2.1 &

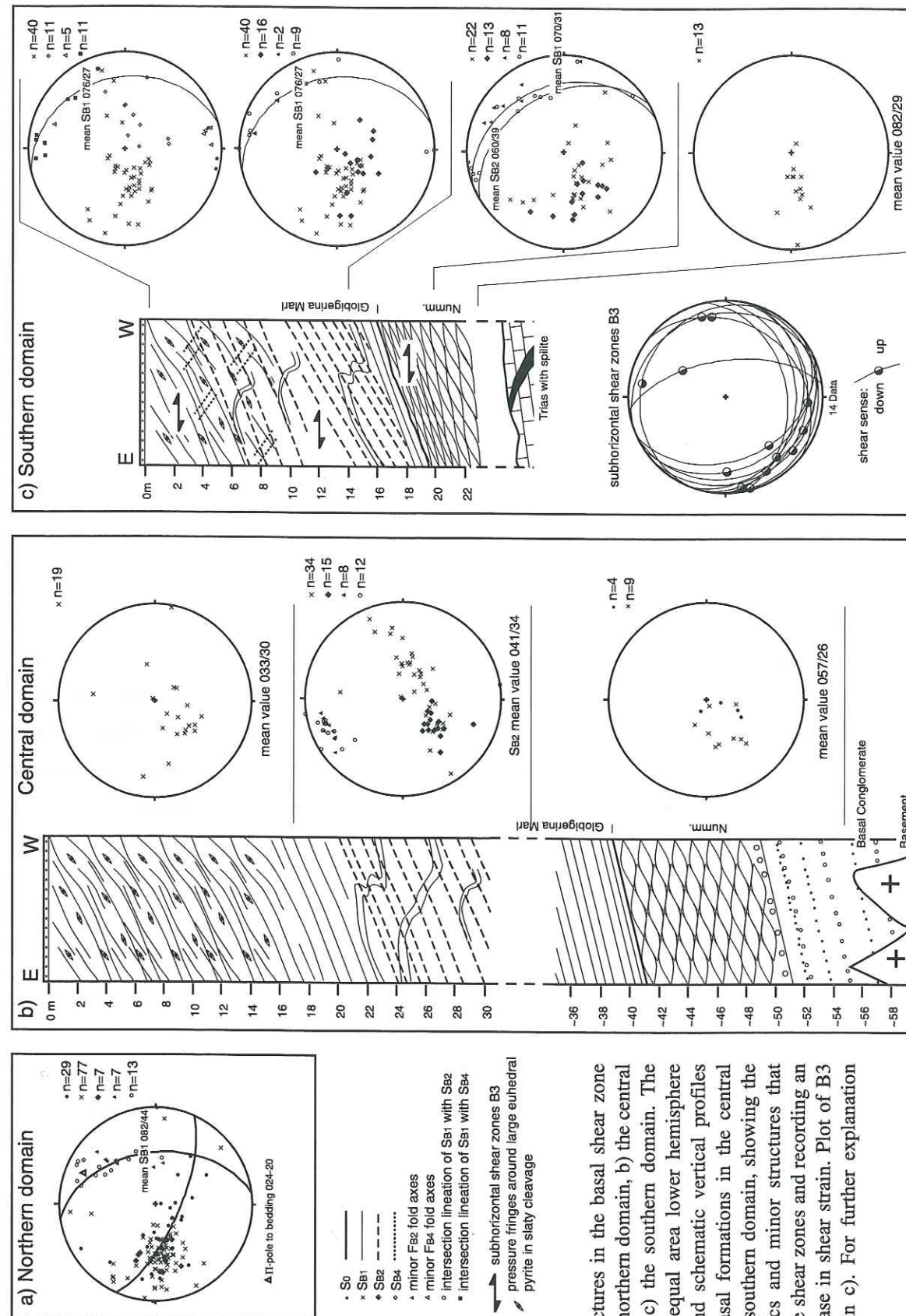


Fig. 2.9:

B1 - B4 structures in the basal shear zone across a) the northern domain, b) the central domain, and c) the southern domain. The data include equal area lower hemisphere stereoplots and schematic vertical profiles across the basal formations in the central domain, and southern domain, showing the various fabrics and minor structures that develop in the shear zones and recording an upward increase in shear strain. Plot of B3 shear zones in c). For further explanation see text.

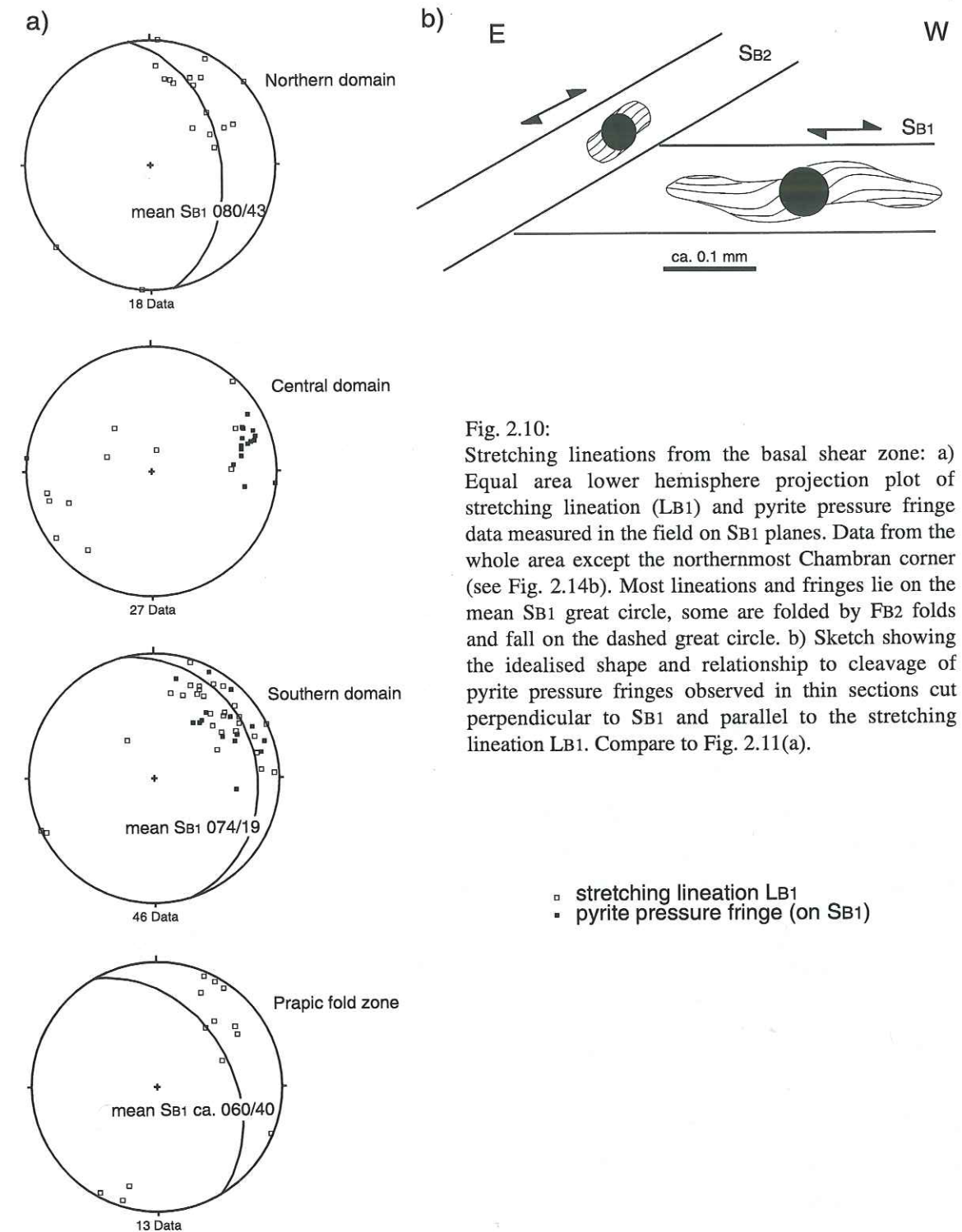


Fig. 2.10:

Stretching lineations from the basal shear zone: a) Equal area lower hemisphere projection plot of stretching lineation (LB1) and pyrite pressure fringe data measured in the field on SB1 planes. Data from the whole area except the northernmost Chambran corner (see Fig. 2.14b). Most lineations and fringes lie on the mean SB1 great circle, some are folded by FB2 folds and fall on the dashed great circle. b) Sketch showing the idealised shape and relationship to cleavage of pyrite pressure fringes observed in thin sections cut perpendicular to SB1 and parallel to the stretching lineation LB1. Compare to Fig. 2.11(a).

- stretching lineation LB1
- pyrite pressure fringe (on SB1)

2.14). In the lower levels the microlithons between the cleavage selvages are lozenge-shaped with the long axis subparallel to the stretching lineation on SB1.

Euhedral pyrites in the upper level and small framboidal pyrites in the intermediate level often have antitaxial strain fringes. Most pressure fringes lie within SB1 but some

short pressure fringes also occur within S_{B2} (see below) (Fig. 2.10b). Stretching lineation and quartz fibre orientations from larger pressure fringes (Fig. 2.10a) clearly record a constant WSW–SW-directed stretching. The quartz fibres in the pressure fringes are slightly curved in the XZ-plane of finite strain recording a non-coaxial strain path (Figs. 2.10b & 2.11a).

In thin sections of the Globigerina Marl an sedimentary lamination has been accentuated by S_{B1} and consists now of ~1 mm thick fully recrystallized calcite-rich laminae (lozenge shaped grains ~30 μm long) separated by thinner pressure solution seams, variably enriched in phyllosilicates with a high degree of preferred orientation (< 0.2 mm wide) (Fig. 2.11b). Asymmetric tails around detrital grains (quartz, white mica, fossils) indicate W-directed shearing and stretching within S_{B1} (Fig. 2.11c). In some places cleavage-parallel boudinage of phyllosilicate-rich pressure solution seams records ongoing stretching parallel to the principal cleavage (Fig. 2.11d). S_{B1} slaty cleavage in the upper level of the basal shear zone is defined by the preferred orientation of aligned phyllosilicate grains, elongate quartz grains showing undulose extinction and interstitial calcite grains. In less strained areas, around heterogeneities, the slaty cleavage becomes anastomosing and domainal. Here the microlithon domains show some relicts of bedding (Fig. 2.11e).

2.4.2 Folding of the main foliation (B_2)

In the intermediate level the bedding and S_{B1} cleavage are locally folded in asymmetrical WSW-vergent, mesoscale, gentle to open folds (F_{B2} ; Fig. 2.12), causing the girdle distributions on pole plots of S_{B1} (Fig. 2.9). Amplitudes range from centimetres to decametres and wavelengths range from centimetres to few metres. In the central domain where strain is lowest, all F_{B2} fold axes plunge shallowly towards the NNW, perpendicular to the shear direction (Fig. 2.9b). In the northern domain and especially in the southern domain measured fold axes and intersection lineations (Figs. 2.9a & c) show a wide distribution of orientations which all fall on the great circle of the mean S_{B1} cleavage. In the field these F_{B2} fold axes are clearly curvilinear (Fig. 2.12e). The F_{B2} folds are associated with an axial planar cleavage (S_{B2}), expressed as cm-spaced, pressure solution seams. S_{B2} dips in the same direction as the mean S_{B1} (E–NE) but tends to be slightly steeper (Fig. 2.9). S_{B2} is best developed in the short limbs and hinge areas of F_{B2} folds, where the compositional layering S_{0-B1} is thicker than in the surrounding rock mass (Fig. 2.12). Large amounts of material have been removed by pressure solution on S_{B2} , making compositional layering highly discontinuous (Fig. 2.12b). Slight buckling in the short limb of some F_{B2} folds results in second order forelimb-folds (Ray, 1991). The limbs of these second order folds are thinned (Fig.

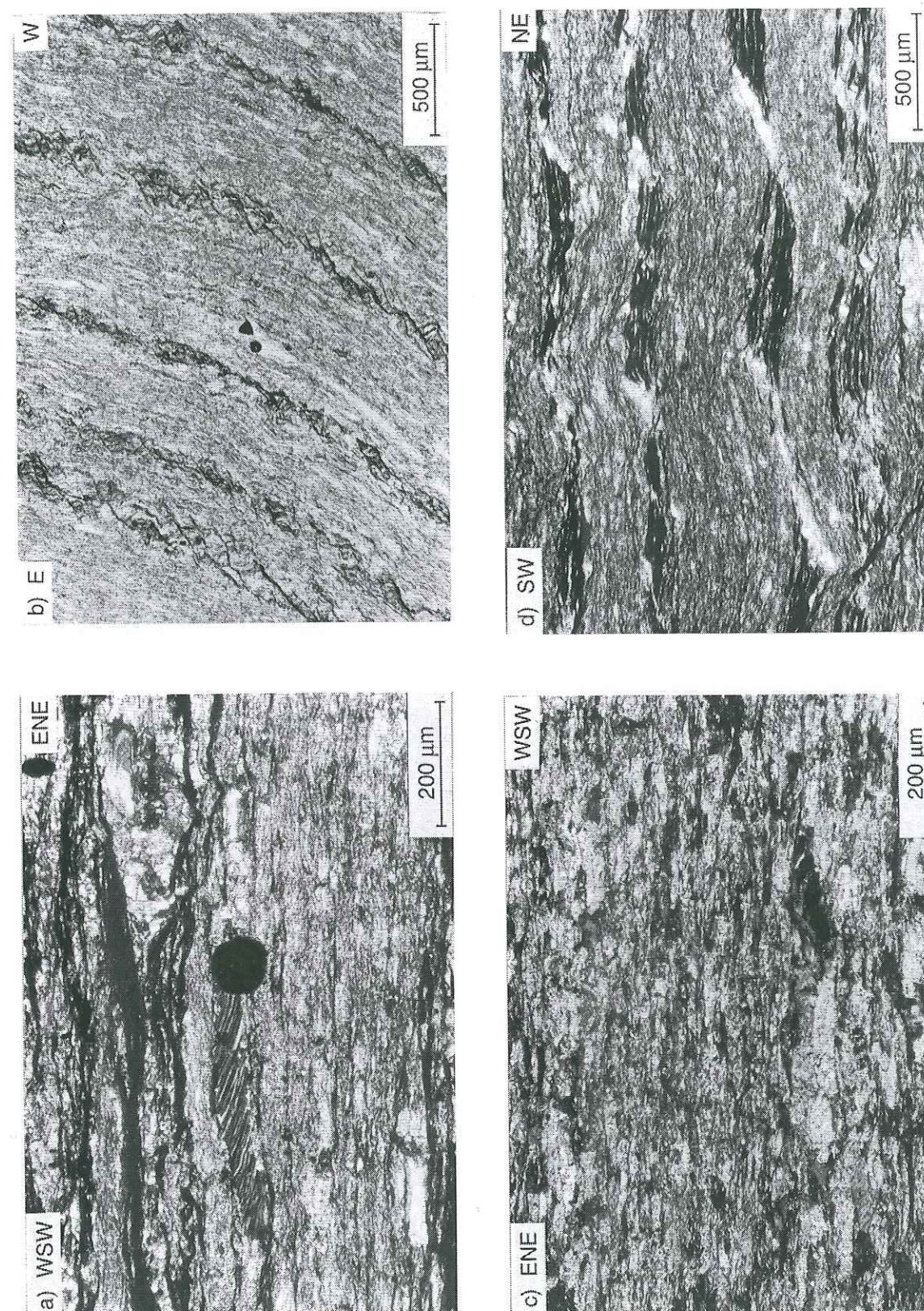


Fig. 2.11:

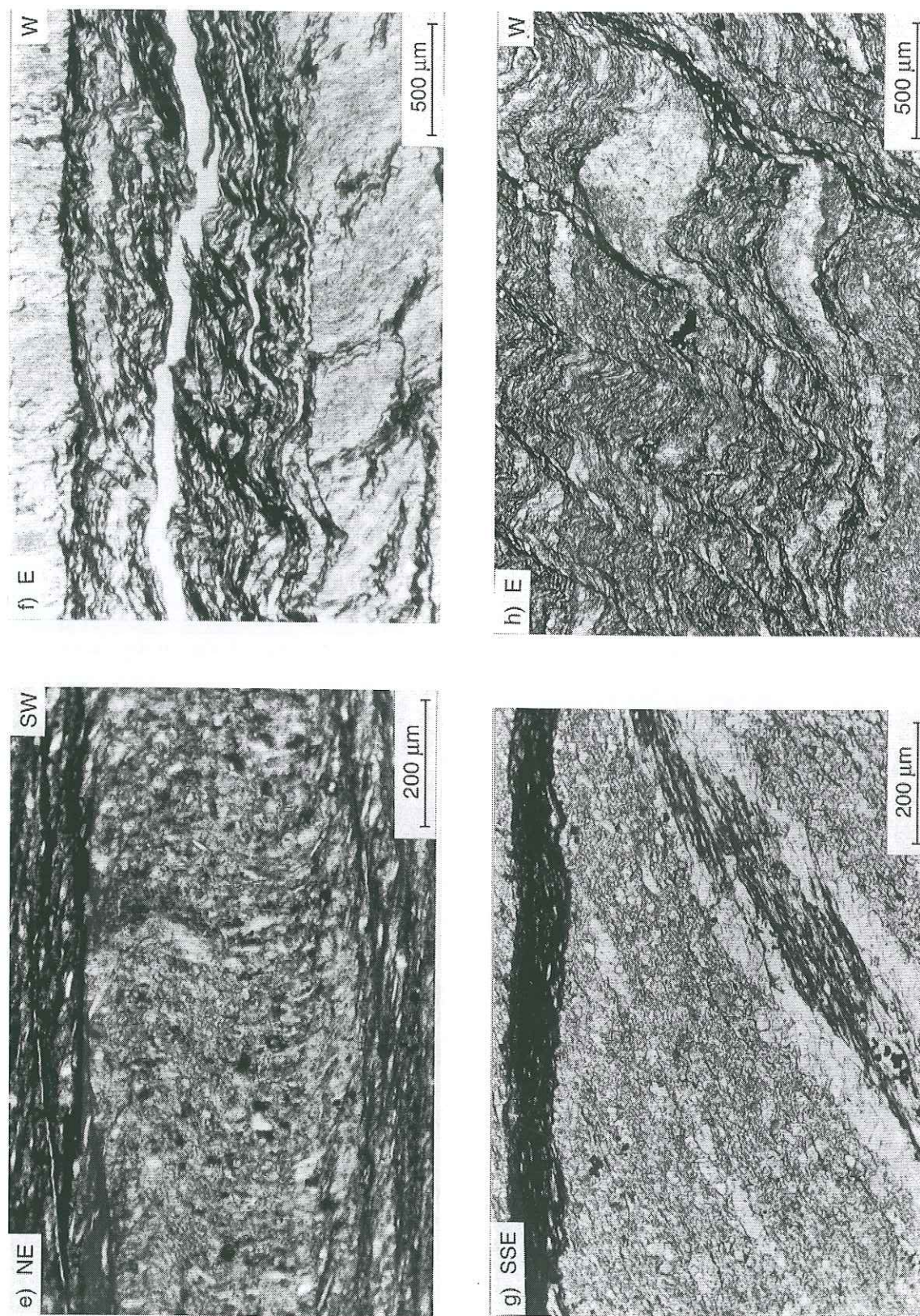


Fig. 2.11:
continued

Fig. 2.11: Photomicrographs of thin sections cut perpendicular to SB_1 and, unless stated otherwise, parallel to the stretching lineation LB_1 . a) Southern domain: spherical framboidal pyrite with quartz pressure fringe to the left and calcite fringe to the right in finer grained calcite matrix. SB_1 (horizontal on this photo) is marked by phyllosilicate seams. The quartz fibres in the pressure fringes were rotated anticlockwise in sinistral non-coaxial flow while being pulled away from the pyrite. Calcite pressure fringes are also seen around fossil debris (in the lower left corner). Crossed polarizers. b) Southern domain: hinge area of an FB_2 fold (cut perpendicular to fold axis): S_0 - B_1 lamination is defined by calcite separated by accumulations of phyllosilicates and insoluble residues. Elongate large calcite grains and pyrite pressure fringes lie subparallel to SB_1 . The phyllosilicate rich seams are crenulated by SB_2 (subhorizontal in this view). c) Central domain: asymmetric tails around a quartz grain within a highly sheared SB_1 fabric (give top to the W sense of shear). Crossed polarizers. d) Central domain: asymmetric boudinage of SB_1 phyllosilicate seams (black) with interstitial growth of large calcite crystals (white). e) Central domain: SB_1 slaty cleavage (subhorizontal in photo) with folded primary lamination preserved in a microlithon. f) Southern domain: thick SB_2 seam of phyllosilicates and insoluble residues crosscutting S_0 - B_1 (subvertical in photo) in the hinge area of a FB_2 fold. Differential crenulation cleavage dips steeply left (Selle-Fault cleavage) in the thick SB_2 seam. Thin section cut perpendicular to the FB_2 fold axis. g) Southern domain: S_0 - B_1 fabric is oriented from top right to lower left corner. A thick SB_2 seam is seen along the upper rim of the photo. SB_2 pressure solution cleavage is also intensely developed within the dark seam in the centre of the photo (dipping left). Large rectangular calcite crystals are aligned subparallel to SB_2 on either side of this seam. Thin section cut perpendicular to the FB_2 fold axis. h) Selle-Fault cleavage crenulating subhorizontal S_0 - B_1 fabric. Thin section cut perpendicular to the Selle-Fault folds.

2.12c). Some FB_2 mesofolds are localised on heterogeneities such as quartz-calcite veins (Fig. 2.12d). In these cases the fold amplitude dies out rapidly along the axial plane. The axial planar SB_2 cleavage curves into sub-parallelism with the SB_1 planes and spacing between seams decreases, until they are indistinguishable. At higher shear strains (i.e. in the southern domain), SB_2 is omnipresent in the intermediate and upper levels and cleavage domains strongly dismember the FB_2 folds (Fig. 2.12e). In the hinges of FB_2 folds SB_1 is well preserved in the microlithons and forelimb-folds are curvilinear. At Col de l'Aup Martin (Fig. 2.1), near the Selle-Fault, FB_2 folds occur in a diminishing number indicating that the shear strain was lower.

In thin section SB_2 generally forms dark through-going surfaces up to 2 mm wide, with aligned phyllosilicates and accumulations of insoluble residues (Fig. 2.11f). In some samples where SB_2 is at a high angle to S_0 - B_1 , small microfolds of SB_1 are observed in the microlithons. In other cases SB_2 develops as a crenulation cleavage associated with pressure solution (Fig. 2.11b). In the southern domain where SB_2 is well developed, it can be observed in certain laminae that large calcite crystals (~ 0.1 mm long), aligned parallel to SB_2 , grew over the SB_1 pressure solution seams (Fig. 2.11g). Clear truncations at SB_2 cleavage surfaces suggest that strong pressure solution took place along SB_2 . Sigmoidally shaped S_0 - B_1 offsets at SB_2 surfaces also indicate shearing on SB_2 which may have caused the curvilinear shape of FB_2 folds.

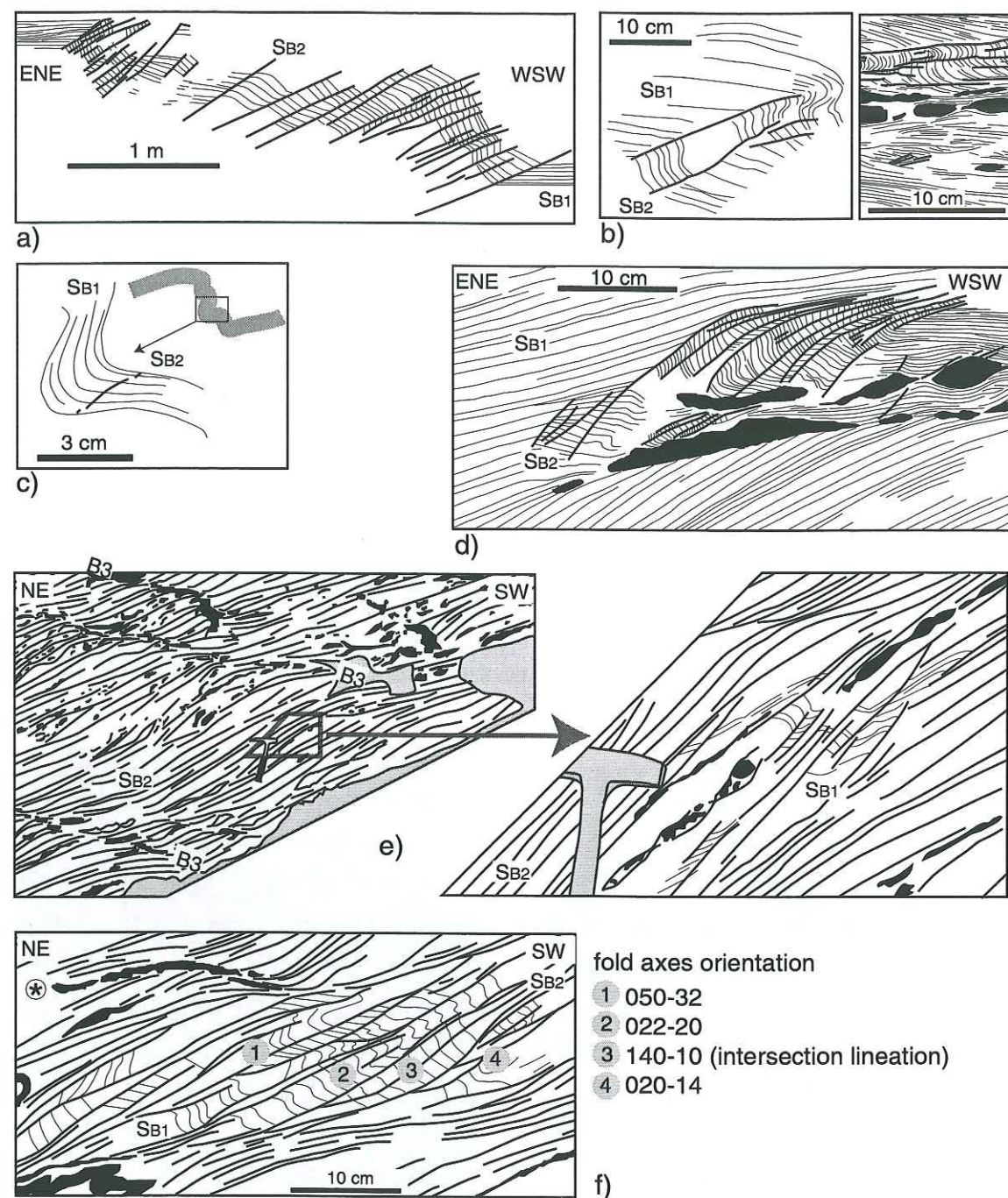


Fig. 2.12: Field sketches showing profile shapes of B2 folds in the basal shear zone. a) - d) Examples from the central domain. a) Large B2 folds with concentration of SB2 on the steep limbs. b) Two examples where strong pressure solution on SB2 dissolved much of the fold hinge, which results in a highly discontinuous SB1. c) Detail from a second order forelimb fold showing thinning of the limbs. d) B2 fold zone with strong SB2 localised on a quartz-calcite vein (black). Prior to FB2 the vein was boudinaged by the B1 deformation. The fold amplitude dies out rapidly along the axial plane until SB2 merges with SB1. e) & f) B2 fold zone from the southern domain where SB2 dominates. e) Sub-horizontal B3 shear zones, marked by aligned quartz-calcite veins (black). In detail a slightly dismembered B2 fold is preserved in the microlithons. (Hammer for scale). f) Strongly dismembered B2 fold. Minor fold hinges in such microlithons are highly curvilinear see orientations of fold axes at localities 1 to 4. The orientation of fold axes varies from one microlithon to another. * indicates a sub-horizontal B3 shear zone.

2.4.3 Sub-horizontal shear zones (B3)

In the northern and southern domains, higher shear strain led to the development of discontinuous subhorizontal metre-scale shear zones in all levels (Fig. 2.9c). They cut across B1 and B2 structures (Fig. 2.12e). Slicken-fibre lineations on these shear surfaces and the curvature of older foliations indicate a top to the WSW-sense of shear (Fig. 2.9c). They are interpreted as shear bands (White *et al.*, 1980) which develop only in higher strain zones probably late during shear zone activity.

2.4.4 West-dipping cleavage (B4)

In the southern domain, the principal foliation SB1 is locally cut by a west-dipping crenulation cleavage SB4 (Figs. 2.9c & 2.13). Discontinuous bedding indicates a large amount of pressure solution. This cleavage is related to minor buckle folds with a thinned western limb (Fig. 2.13). The thinned limb sometimes merges into a distinct cleavage surface. No cross-cutting relations to B2 and B3 structures was found. The geometry makes it difficult to relate this structure to shear zone development. It is a very local feature and may be related to differential movement in the basement. Tricart (1980) suggested that this cleavage relates to late Alpine backthrusting, however, the very local distribution is not compatible with a regional event.

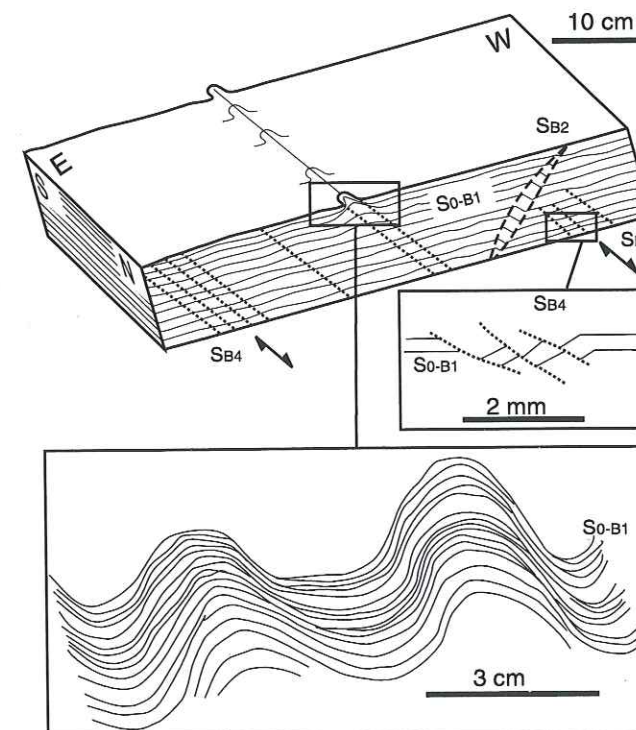


Fig. 2.13: Schematic block model showing the geometry and relationship of B4 structural elements to S0-B1 and SB2. Insets show thinning on FB4 limbs and apparent extensional geometries across some SB4. For further explanation see text.

2.4.5 Chambran: transition to WNW-directed deformation

In Chambran, the narrow northernmost part of the Champsaur fold zone, the orientation of the stretching lineation in the basal shear zone changes northwards within 2 km, from NE-SW to NW-SE (Fig. 2.1) with a small number of N-S lineations measured within the transition zone. To the north at Rocher de l'Yret (Fig. 2.1) a series of WNW-directed ($290\frac{1}{2}$) thrusts in the footwall of the FPT carry basement onto Mesozoic and Tertiary cover (Butler, 1992a). B1 and B2 structural elements (Figs. 2.9a & 2.14a) persist northward to location Y (Fig. 2.1). The F_{B2} folds are highly curvilinear. Within the transition zone (starred localities in Fig. 2.1) additional metre-scale NNE-SSW trending open folds occur in the upper level of the basal shear zone. They fold the S_{0-B1} layering and are associated with an east dipping axial planar cleavage (Fig. 2.14a). Unfortunately no cross cutting relationship between the F_{B2} folds and these open folds could be observed but assuming that the F_{B2} structures are related to the WSW-SW-directed deformation I propose that the WNW-directed deformation was at least in part later because the open folds would have been obscured by the more intense B2 structures.

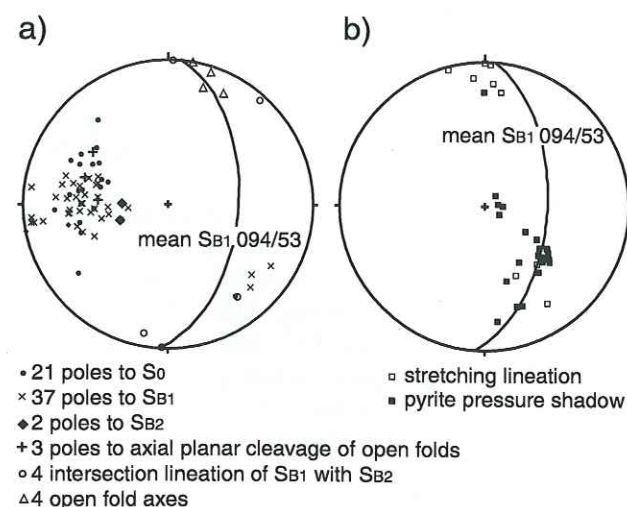
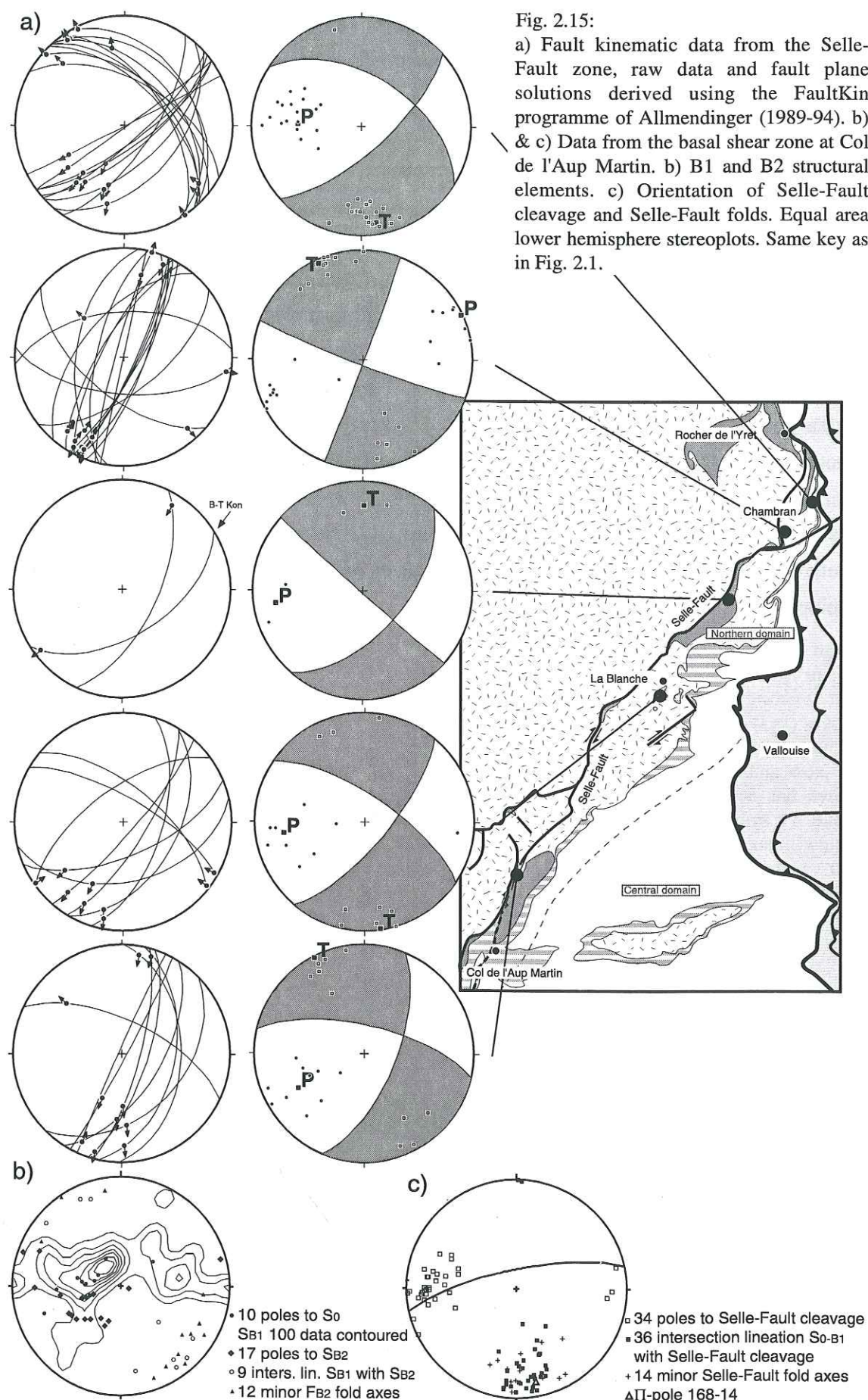


Fig. 2.14:
Structural data from the basal shear zone at Chambran in the northern domain where the stretching lineation (LB_1) is N-S to NW-SE-directed (Fig. 2.1): a) Cleavage and bedding data. b) Stretching lineation and pyrite pressure shadow data. Stretching directions which plunge north belong to the transition zone. Equal area lower hemisphere stereoplots.

2.4.6 A model of progressive shear

The structures described ($B_1 - B_3$) can be linked within a single progressive shear history. The principal S_{B1} cleavage and associated stretching lineation are the main fabrics produced within the shear zone. As shearing progressed, heterogeneities within the marls (such as veins) caused small asymmetrical folds to fold bedding, the principal cleavage and the stretching lineation. Small flow perturbations were sufficient to rotate S_{B1} into the field of incremental shortening initiating S_{B2} and F_{B2} to accommodate the continuing shear strain (Gray, 1995). S_{B2} , a strong axial planar cleavage to these local (F_{B2}) folds merged with the continuously developing principal fabric S_{0-B1} away from the folds. Where shearing became strong enough (e.g. in the northern and southern domains) the F_{B2} folds became curvilinear. F_{B2} folds, initially oriented almost perpendicular to the stretching direction, passively rotated towards the stretching direction (Donath and Parker, 1964). During later stage shear zone activity the large shear bands (B_3) cut through B_1 and B_2 structures. They indicate a slightly east-dipping shear zone boundary subparallel to bedding. B_1 , B_2 and B_3 structures are thus genetically linked. Talbot (1964) and Laubach *et al.*, (1989) report similar cleavage development in shear zones.



2.5 Selle-Fault

The NE-SW trending Selle-Fault cuts mainly through basement and Mesozoic rocks, however, in a few places smaller satellite faults also affect Tertiary strata (Fig. 2.1). Slicken-fibres on brittle faults and shear zones, displaced veins, shear bands etc., all indicate dextral shear with a slight downthrow component dropping the southeastern block down (Fig. 2.15a). To the north the conjugate sinistral fault set becomes of equal importance (Fig. 2.15a) and increases to the north of the Pelvoux massif (Bravard and Gidon, 1979; Gidon, 1979). The corresponding compression-axis (P) is towards WSW-W (Fig. 2.15a). To the north, next to the Frontal Pennine Thrust, the Selle-Fault bifurcates and individual branches die out within the internal units (Fig. 2.1: Barf  ty *et al.*, 1995). The two dextral main branches offset the Nummulitic Limestone approximately 380 m (heave 350 m, throw 160 m), and the Frontal Pennine Thrust by about 80 m (heave 70 m, throw 40 m). Therefore total dextral displacement is estimated to be in the range of 500 m. 30 km further southwest, west of Orci  res (Fig. 1.6), the Selle-Fault accommodates ~870 m downthrow to the south (see Chapter 3). The increasing downthrow component is probably related to differential uplift of the Pelvoux massif. This indicates that the Selle-Fault was of local significance during the late Alpine deformation although it may have had an earlier history.

Observations from the basal shear zone at Col de l'Aup Martin (Fig. 2.1) show that near the Selle-Fault the F_{B2} folds (Fig. 2.15b) are overprinted by the Selle-Fault cleavage. The Selle-Fault cleavage is axial planar to metre-scale, upright, asymmetric, W-vergent folds with subhorizontal fold axes trending N-S (Figs. 2.11h & 2.15c). These folds are clearly restricted to a narrow zone (< 1 km) close to the Selle-Fault. But the Selle-Fault cleavage occurs even several km further east, as a very fine differentiated crenulation cleavage in thick pelitic seams (Fig. 2.11f). These structures are clearly related to a late dextral transtension on the Selle-Fault post-dating activity along the basal shear zone.

2.6 Burial and exhumation history of the Champsaur-Prapic fold zone

The metamorphic grade of the Champsaur-Prapic fold zone has previously been estimated by illite crystallinity measurements (Aprahamian, 1974). According to these data the illite crystallinity in the Champsaur-Prapic area increases northwards and eastwards. North of the Dormillouse inlier the metamorphic facies changes from zeolite facies to greenschist facies (Debelmas and Kerckhove, 1980). Fabre (1988) concluded from K/Ar ages of the fine fraction of the Nummulitic Limestone that peak metamorphism occurred at 30 Ma or later.

As part of a larger project ten samples from the Champsaur-Prapic fold zone (Fig. 2.16) have been dated by the fission track method (Seward *et al.*, submitted).

Five zircon ages come from the Champsaur Sandstone; the zircon fission track age of sample JB77 (4.0 ± 0.6 Ma, 2σ) is younger than the depositional age (fully reset), the others are much older (single crystal ages ranging from 30 to 310 Ma) and are inherited ages. The fission-track age of zircon is expected to be fully reset when the crystals are heated to $250 \pm 50^\circ\text{C}$. The old ages, i.e. ages greater than depositional age, have not been annealed and were therefore not heated to more than $200 \pm 50^\circ\text{C}$. The fully reset zircon age of sample JB77 in the immediate footwall of the Frontal Pennine Thrust however reached temperatures in the order of $250 \pm 50^\circ\text{C}$. Assuming a geothermal gradient of $25 \pm 5^\circ\text{C}/\text{km}$ this sample was at 4 Ma buried 8 - 12 km.

The apatite ages range from 4 to 13 Ma (Fig. 2.16). All samples have been exposed to temperatures in excess of $120 \pm 50^\circ\text{C}$ (generic algorithm modelling confirms burial to $> 120 \pm 50^\circ\text{C}$; D. Seward pers. comm.). On an age-altitude plot (Fig. 2.16) the samples do not lie on a single straight line. However, without the two samples to the west of Prapic (94/21 and 94/P12) and without the one to the north of the Selle-Fault (JB80), a positive age-altitude correlation results, with a low exhumation rate of about 0.1 mm/y (Fig. 2.16). This implies that the Champsaur-Prapic fold zone did not behave as a single block and that there must have been differential uplift after the rock passed through the closure temperature. The younger age to the north of the Selle-Fault indicates that the Selle-Fault was active after 4 Ma. The two older apatite samples to the west of Prapic probably are less exhumed, i.e. exhumation stopped earlier than in the rest of the area.

Assuming a geothermal gradient of $25 \pm 5^\circ\text{C}/\text{km}$ the Champsaur-Prapic fold zone was buried at least 5 km. The maximum burial is 8 km (resetting the time for the zircon fission track clock) although the zircon age of sample JB77 demands burial ranging from 8 to 12 km. As the samples have been exposed to temperatures above $120 \pm 50^\circ\text{C}$ the fission tracks contain no information about the burial history. But modelling gives evidence that the samples passed below depths equivalent to $120 \pm 50^\circ\text{C}$ around 10 Ma, except for the sample JB77, which passed below $250 \pm 50^\circ\text{C}$ around 4 Ma.

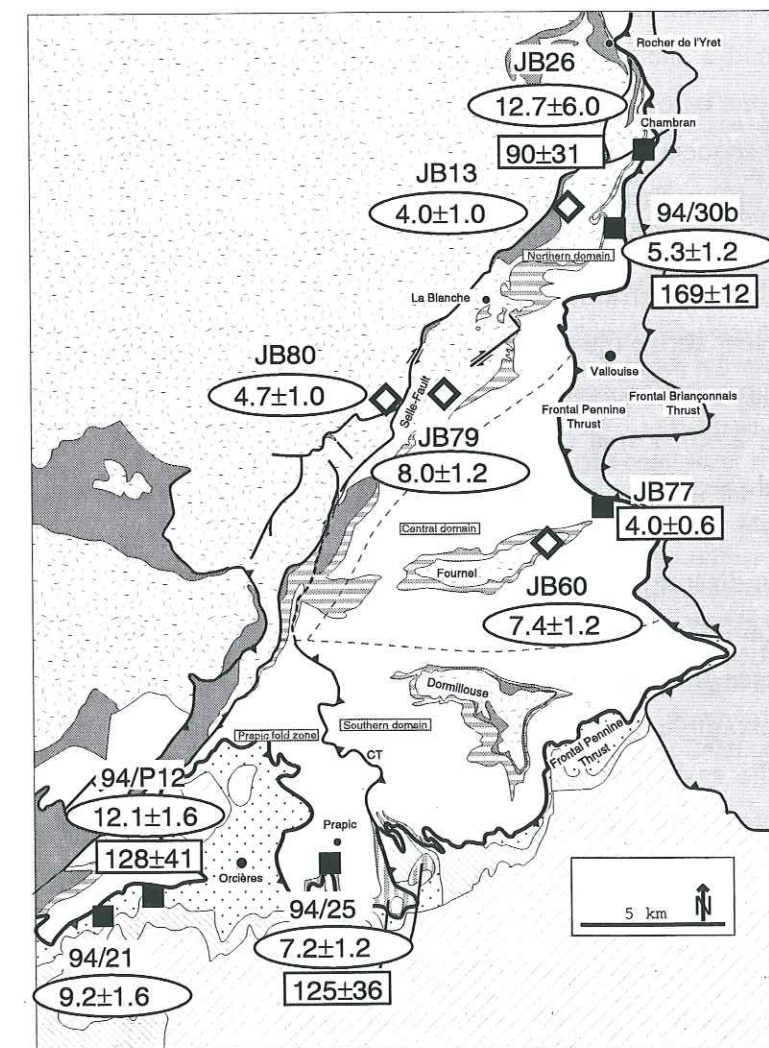
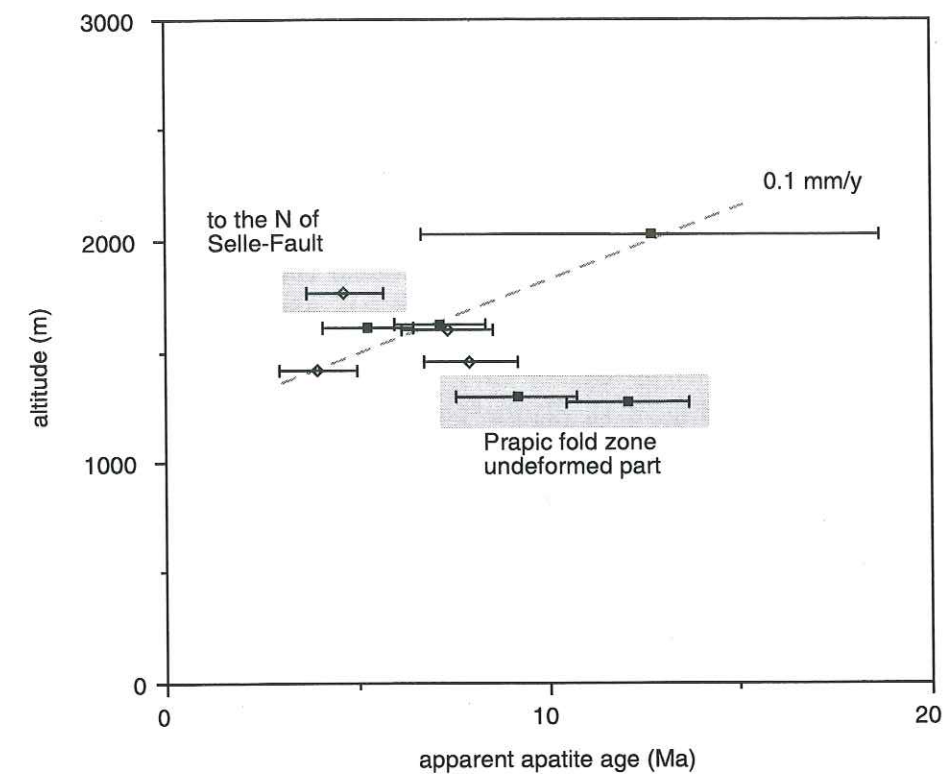


Fig. 2.16: Age-altitude plot and simplified map of Champsaur-Prapic area (same key as Fig. 2.1) for apatite fission-track ages from crystalline basement (open diamonds) and Tertiary Champsaur Sandstone (black squares). Apatite ages shown within ellipses and zircon ages within rectangles.

2.7 Interpretation and discussion

2.7.1 Overthrust shear model

From the description above, I can deduce that the deformation documented in the Fournel profile (Fig. 2.4) is due to one continuous deformation that was dominated by top to WSW overshear. A tectonic model for the Fournel profile must account for the geometrical information of large and small-scale structures. The main structural features which must be explained by any model are: (1) the progressive eastward change from large, open chevron folds with vertical axial planes to close, chevron-like folds with gently inclined axial planes (Fig. 2.4), (2) the positive correlation between interlimb angle and axial plane dip (Fig. 6b), (3) the concentration of folds in E-dipping zones which become shallower towards the E (Table 2.I), and (4) mesofolds and cleavage development in the basal shear zone. All these features reflect an increase in shear strain towards the hinterland (i.e. FPT) indicating that the shear strain was generated by emplacement of the over-riding internal thrust sheets as previously suggested by Plotto (1977) and Tricart (1980).

This leads to an overthrust shear model (Fig. 2.17). I propose that the Tertiary foreland basin succession formed a shear zone bounded above by the Frontal Pennine Thrust and by the basal shear zone below. Along the Fournel profile, the thickness of the Champsaur Sandstone turbidite sequence increases from ~700 m in the W near the Selle-Fault to ~1200 m approximately 8 km further east (Figs. 2.4 & 2.7) giving the shear zone a wedge shape. Movement of the Frontal Pennine Thrust hangingwall towards the WSW over the foreland caused high shear strains in the lower incompetent units of the underlying Tertiary succession just above the crystalline basement. The Champsaur fold zone offers a particularly well preserved record of overthrust shear deformation because of low shear strains (γ -3; Fig. 2.6c). Zonal deformation (diffuse ramps), a horizontal shear strain gradient and a basal shear zone are integral parts of the deformation pattern.

The development of folds in discrete zones whose dip decreases from vertical in the west to 20°E below the FPT (Table 2.I) requires further discussion. Restoration of folds across the Fournel profile causes the zone dips to increase but to preserve the same eastward decrease in value, for example, the dip of zone E increases from 28° to 45° after restoration. This implies that the eastward decrease in zone-dip is an original feature. Casey and Dietrich (1997) proposed that vertical zones of pure shear (diffuse ramps) can develop between non-overlapping upper and lower flats within a layered sequence deforming under pure shear (Fig. 2.17a). I propose an adaptation of this model in which: (1) the basal shear zone (below the Tertiary foreland succession) propagates forward in a position below and behind the overthrusting mass of internal nappes (Fig. 2.17b); (2)

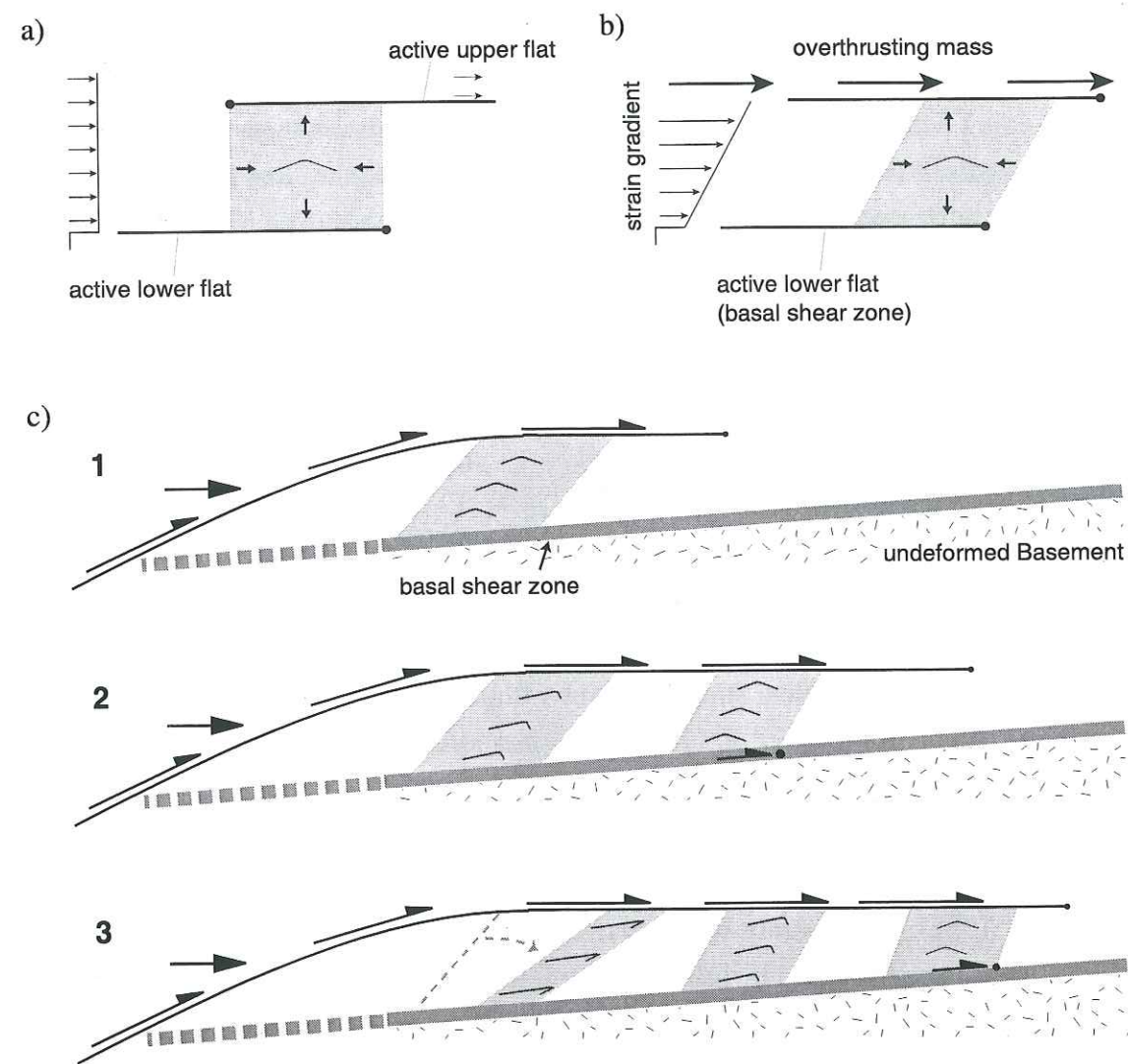


Fig. 2.17: Overthrust shear model. a) Within a layered sequence deforming under pure shear a vertical diffuse ramp (shaded) develops by simultaneous movement on overlapping upper and lower flats. The diffuse ramp deforms in pure shear and leads to the initiation of buckle folds (modified after Casey and Dietrich, 1997). b) Modification of a). An increasing vertical strain gradient links the active lower flat (i.e. the basal shear zone) with the overthrusting mass. The lower flat lags behind the overthrusting mass. If the lower flat gets stuck a diffuse ramp propagates upward through the layered sequence in which upright buckle folds initiate. The vertical strain gradient controls the dip of the diffuse ramps so that the higher the strain gradient between the floor and roof shear zones, the shallower the dip of a ramp that connects them. c) Overthrust shear model for the Fournel profile depicted on Fig. 2.4. A wedge shaped turbidite sequence overlies the basal shear zone. The first diffuse ramp formed next to the overthrusting mass and sequentially newer ramps developed toward the foreland with progressively steeper dips. The initially symmetric buckle folds rapidly amplified asymmetrically (Casey & Huggenberger, 1985). Continued shear further tightened and rotated the chevron folds and fold zones.

there is a decreasing vertical strain gradient downward between the FPT and the basal shear zone; (3) the basal shear zone from time to time gets stuck and a diffuse ramp propagates upward through the Tertiary sequence in which upright buckle folds initiate; (4) the vertical strain gradient controls the dip of the diffuse ramps so that the higher the

strain gradient between the two sub-horizontal shear zones, the shallower the dip of a ramp that connects them (Fig. 2.17b); (5) once a diffuse ramp is initiated (at whatever angle) folding within it proceeds following the classic overthrust shear model (Fig. 2.2) and the zone itself is rotated to a shallower dip. This model implies that the vertical strain gradient diminishes westward until the most westerly diffuse ramp on the Fournel profile is vertical (Fig. 2.17c). Thus not only fold geometries but also the dip of the fold zones themselves record a rapid decrease in overthrust shear deformation toward the west. Thus the strain gradient (from zone A to zone F; Fig. 2.4) represents the progressive development of structures through time and space (Fig. 2.17c). Similar observations of fold behaviour in the Southern domain (Fig. 2.8) allow us to propose that this model applies for the whole Champsaur fold zone.

Previously documented overthrust shear examples may show zonal shear strain gradients similar to the Fournel profile (Bosworth and Vollmer, 1981; Rattey and Sanderson, 1982) or a vertical strain gradient within a nappe or thrust sheet (Fig. 2.2b) (Sanderson, 1979; Ramsay *et al.*, 1983; Gibson and Gray, 1985; Dietrich and Casey, 1989; Rowan and Kligfield, 1992; Casey & Dietrich, 1997).

In the first group of examples deformation in the footwall of an overthrusting mass is accommodated in listric zones of high shear strain shallowing downward (Rattey and Sanderson, 1982). Shear strain decreases forward and downward. Detailed structural observations are complicated by high shear strains and overprinting deformation phases. However, unlike in the Fournel profile the high strain zones do not ramp from a distinct floor shear zone but are unconstrained scattered shear zones which probably follow less competent rock assemblages. They are not controlled by a restricted shear zone thickness. Therefore the boundary constraints and the distribution of easy glide horizons critically influence the shear strain distribution. In the second case overthrust shear causes rapidly increasing strains towards the base of a thrust sheet. The shear strain concentration at the base can be so high that a nappe structure with an overturned lower limb forms (Fig. 2.2b). In the Fournel profile shear strains are too low and the stratigraphic pile is probably too thin to form a nappe. Therefore the shape, thickness, and boundary constraints of the overthrust zone and the distribution of easy glide horizons critically influence the shear strain distribution.

The deformation in the Prapic fold zone was similarly caused by overthrust shear on the Champsaur Thrust and overriding internal nappes. Style of folding and transport direction fit the deformation in the Champsaur fold zone (Fig. 2.7). I therefore propose that one regionally continuous WSW-SW-migrating overthrusting mass caused the deformation in the Champsaur-Prapic fold zone. The WSW-SW-directed shortening of the Champsaur-Prapic fold zone is relatively small: ~3 km for the Champsaur fold zone

(Fig. 2.4; Table 2.1) and ~2 km for the Prapic fold zone (Fig. 2.7).

2.7.2 Curvature of axial trends and late Alpine transport directions

On a regional scale, the investigated area lies within the core of the external Alpine arc. Recent work has documented the magnitude of late Alpine shortening in the NW-directed (>100 km) and SW-directed (~21.5 km) sectors of the external Alps (Fry, 1989; Butler, 1992b and references therein; Lickorish and Ford, in press).

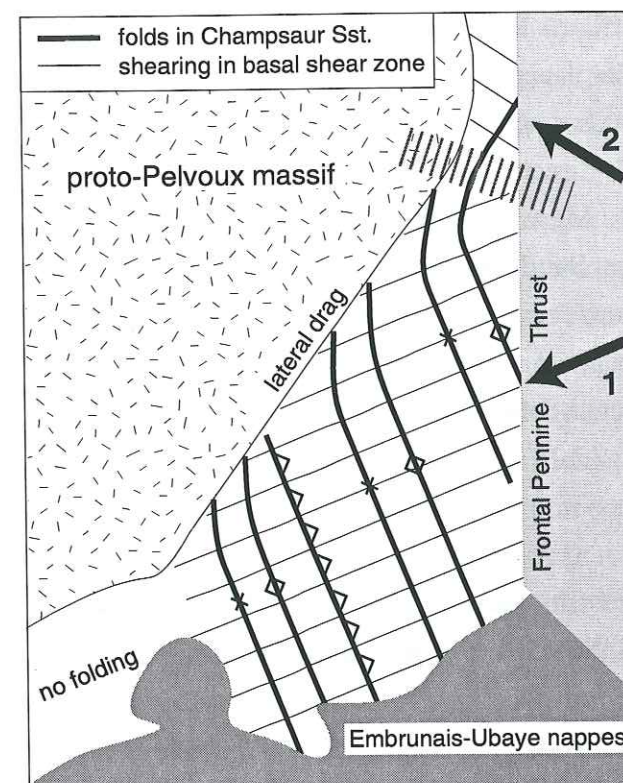


Fig. 2.18: Schematic map showing the large-scale relationship of structural elements at the SE corner of the Pelvoux massif. Overthrust shear causes folding of the turbidite sequence and reorientation of fold axes by lateral drag against the proto-Pelvoux massif. Below the basal shear zone shows constant shearing towards the WSW-SW. To the north this shear direction changes to NW which is sub-perpendicular to the reoriented chevron folds. The NW tectonic transport is partially later than the SW transport. For further explanation see text.

The clockwise curve in map view by ~40% of fold axial trends in the Champsaur Sandstone (Fig. 2.1) suggests variable transport directions which could be related to a regional radial transition of the SW to the NW thrusting direction. But in the basal shear zone the stretching lineation remains WSW-directed (except for the Chambran area) (Fig. 2.18). This suggests that the chevron folding of the Champsaur Sandstone is affected by local perturbations whereas the basal shear zone structures document the regional undisturbed transport direction. The curvature of fold axial trends in the Champsaur Sandstone may have been caused by lateral drag against the proto-Pelvoux massif (Tricart, 1980; 1981) and is thus unrelated to the Western Alpine arc. Similar processes may also be responsible for cleavage transection. But as I have argued above, the Selle-Fault fabrics post-date all other structures in the basal shear zone and therefore

could not cause bending of fold axes as suggested by Plotto (1977). Additionally the displacement on the Selle-Fault dies out towards the NE where the curvature of axial trends becomes most marked.

The regional transport direction in the basal shear zone changes from WSW–SW-directed to NW-directed around Chambran in the northern domain. As shown on Fig. 2.1 this change occurs 4–6 km south of Rocher de l'Yret. The change in orientation of the stretching lineation in the basal shear zone is not abrupt and is not segmented with any significant fault zone (Fig. 2.1). The northern terminations of the Selle fault, which accommodate in total ~500 m of dextral displacement, lies to the north of the transition zone and cannot be used to partition the two transport directions. NW-thrusting continues at Rocher de l'Yret where a series of WNW-directed ($290\frac{1}{2}$) thrusts in the footwall of the Frontal Pennine Thrust carry basement onto Mesozoic and Tertiary cover (Butler, 1992a) and further north in the Aiguilles d'Arves Sandstones (Fig. 1.6) (Serre *et al.*, 1985). Therefore the basal shear zone at Chambran records the change from the NW-directed sector to the SW-directed sector of the external Alps in the immediate footwall of the FPT. And as argued above the WNW-directed deformation in part post-dates the WSW–SW-directed deformation at Chambran (Fig. 2.18).

2.7.3 The problem of the hangingwall

Which WSW–SW migrating overthrusting mass caused the deformation in the Champsaur-Prapic fold zone? At least the 'Schistes à Blocs' and the Autapie nappe are affected by the overthrust shear deformation (Fig. 2.7) which implies that the deformation occurred simultaneously with or after their deposition. This brings up the question about the relationship of the Embrunais-Ubaye nappes with the more internal units. Today, further north, the Champsaur-Prapic fold zone is not overlain by the Embrunais-Ubaye nappes. Instead the Frontal Pennine Thrust brings Sub-briançonnais units on top of Tertiary sediments. Further east the Frontal Briançonnais Thrust carries the Briançonnais zone on top of the Sub-briançonnais zone (Fig. 2.1). Late normal displacements on both faults (Tricart *et al.*, 1996; Sue *et al.*, 1997) probably thinned the Sub-briançonnais to few metres thickness in the Fournel valley (Fig. 2.4).

Tricart (1980 & 1986) argued that the external zone rocks (including the Champsaur Sandstone) and the overlying Autapie and Parpaillon nappes (Figs. 2.1 & 2.7) share a common Oligocene cleavage-forming deformation, associated with westward shear of the Briançonnais zone. He therefore proposed that the Frontal Briançonnais Thrust is the major structural boundary between the external and internal zones. However, some authors (Kerckhove, 1969; Kerckhove *et al.*, 1978; Fry, 1989) emphasised that the base of the Parpaillon nappe cuts external zones and Autapie nappe structures. The Parpaillon

nappe was thought to have been emplaced onto a Miocene erosion surface together with the Briançonnais zone in a single Early Miocene overthrust event. According to Kerckhove (1969) and Kerckhove *et al.* (1978) the deformation in the Champsaur-Prapic fold zone must have occurred before that, probably during the emplacement of the Autapie nappe, although Fry (1989) argued that the Champsaur-Prapic fold zone was deformed during both SW-directed thrusting events, resulting in indistinguishable structures.

Therefore, using the present Bureau de Recherche Géologiques et Minières (BRGM) geological maps, it is difficult to define which overthrusting nappe stack caused the WSW–SW migrating overthrust shear recorded in the Champsaur-Prapic fold zone. New data are awaited from the internal zones to clarify the identity of this overthrusting mass.

Although, the Embrunais-Ubaye nappes have traditionally been interpreted as the result of gravitational emplacement (Debelmas and Kerckhove, 1973; Merle and Brun, 1984; Merle, 1990), Fry (1989) stressed that all the features of the Embrunais-Ubaye nappes can be better interpreted with thrusting from depth in the hinterland.

The data from the Champsaur-Prapic fold zone and from further south (e.g. Lickorish and Ford, 1998) suggest that the foreland basin was overridden and filled by the Embrunais-Ubaye nappes almost simultaneously with detachment and thrusting from depth (Triassic evaporites). This implies that both processes were ongoing at the same time suggesting that the emplacement of the Embrunais-Ubaye nappes caused shortening in their footwall. In the Champsaur-Prapic fold zone the deformation increases towards the rear, whereas in gravitational spreading nappes the deformation increases towards the front and the base of the nappe (Merle, 1990). Therefore also the development of the Champsaur-Prapic fold zone requires additional dynamic overthrust shear components.

2.7.4 Summary

The Champsaur-Prapic fold zone is a particular example of overthrust shear deformation in the footwall of internal alpine nappes. The main characteristics of the deformation in the Champsaur-Prapic fold zone are: (1) WSW-directed shear deformation which decouples from the basement below the overthrusting internal nappes. Above, the Champsaur Sandstone is folded in chevron-like folds. Variations in chevron fold shape, axial plane dips and zonal distribution of folding indicate progressively higher shear strains towards the Frontal Pennine Thrust in the east. (2) To the north (at Chambran) late Alpine deformation changes to WNW–NW-directed partly post-dating the WSW–SW-directed deformation further south.

3. The Soleil Boeuf area northwest of the Selle-Fault zone: NW-directed folding and thrusting

3.1 Introduction

The Soleil Boeuf area is covered by the 1:50'000 geologic map sheet of Orcières (Debelmas *et al.*, 1980). In this area Tertiary foreland basin sediments (Upper Eocene to Lower Oligocene) unconformably overlie folded basement and Mesozoic rocks (Ford, 1996 and references therein). On top of this autochthonous sequence lie several klippen of Mesozoic and Tertiary sediments which were emplaced after the mid-Oligocene. The purpose of this Chapter is to investigate the kinematics of the klippen emplacement.

3.1.1 Geological setting

Physiography

The Soleil Boeuf area includes Tertiary outcrops on the southern side of the Pelvoux crystalline massif, north of the Selle-Fault zone (Fig. 1.6). It is subdivided physiographically by the Drac Champoléon river which cuts a N-S valley through the Tertiary sequence (Fig. 3.1). On the eastern side of this valley rises the Méollion zone which culminates at Aiguille de Cédéra (2883 m). On the western side lies the Soleil Boeuf klippen zone which is a distinct mountainous region where the klippen form the peaks of the area which are from east to west (Fig. 3.1): Croix de l'Estang (2209 m), La Pousterle (2401 m), La Prouveyrat (2467 m), Le Palastre (2279 m), Pic du Clot Lamiande (2461 m), Soleil Boeuf (2595 m), Pointe Sud de la Venasque (2620 m), and Pointe Nord de la Venasque (2637 m). Two important tributaries join the Drac Champoléon (Fig. 3.1). The Torrent du Tourond deeply erodes into the Mesozoic substrate adjacent to the Pelvoux crystalline massif creating a steep cliff on the southern side which shows a complete Tertiary section from the substrate up to the klippen; in a similar way the valley cut by the Torrent de Méollion to the east has created steep cliffs which reveal the relationships of the Soleil Boeuf area with the Champsaur-Prapic area to the southeast of the Selle-Fault zone. The westernmost part of the Soleil Boeuf area with no klippen is called the Queyrel zone.

Stratigraphy

In the Soleil Boeuf region the stratigraphy below the Tertiary unconformity consists of Triassic dolomites and basaltic spilitic dikes overlying and crosscutting the Pelvoux basement (Fig. 3.1), overlain by Lower Jurassic marls and limestones (Tourond and Méollion valleys), Mid-Jurassic (Aalenian - Lower Bathonian) marls and marly limestones together with Middle - Upper Jurassic (Upper Bathonian - Oxfordian) black

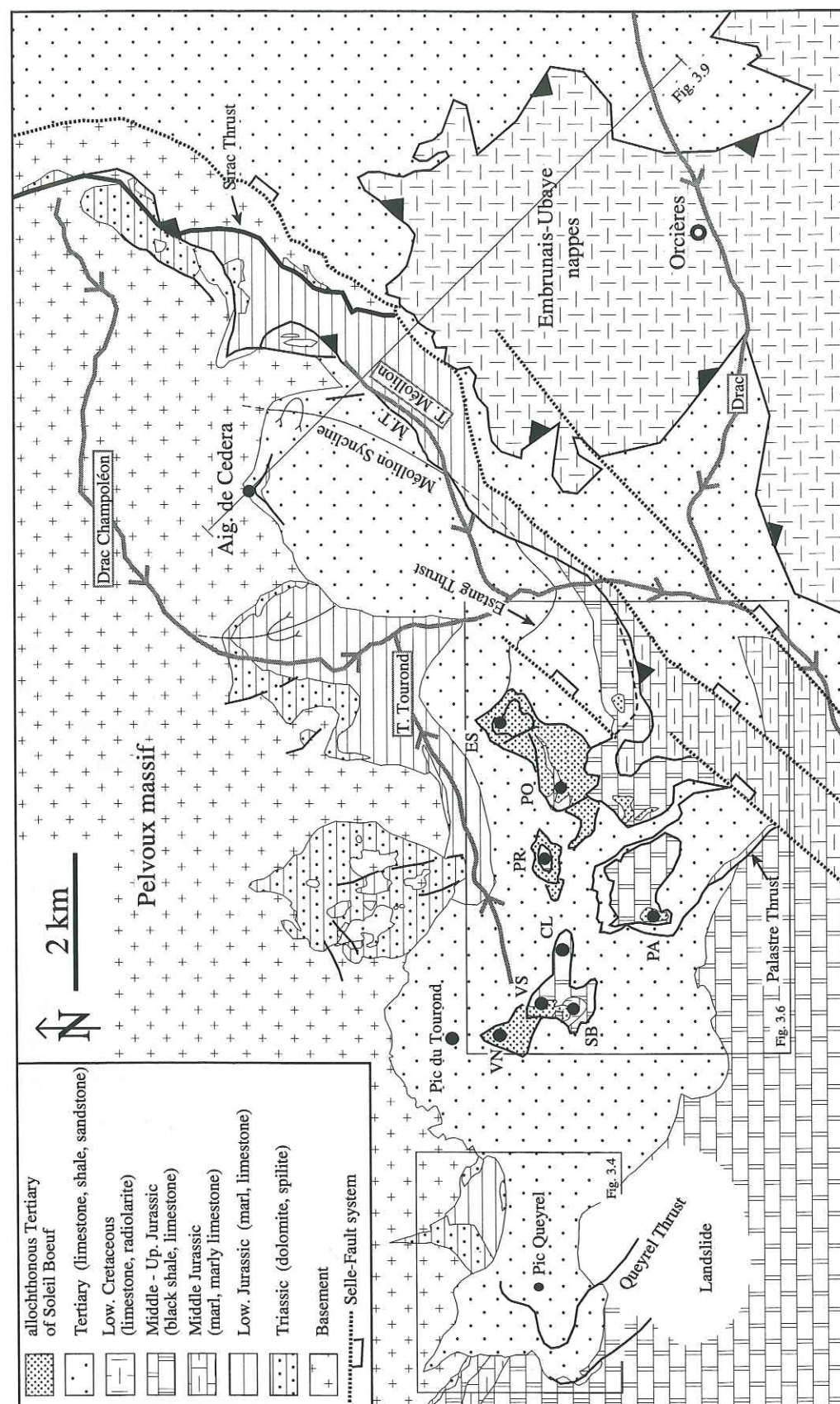


Fig. 3.1: Simplified geologic map of the Soleil Boeuf area. Adapted from BRGM map 1:50 000, sheet Orcières (Debelmas *et al.*, 1980) and own work. Letter shortcuts label the peaks within the Mesozoic klippen: CL = Pic du Clot Lamiande, ES = Croix de l'Estang, PA = Le Palastre, PO = La Pouterle, PR = La Prouveyrat, SB = Soleil Boeuf, VN = Pointe Nord de la Venasque, VS = Pointe Sud de la Venasque. M.T. = Méollion Thrust. Insets of Figs. 3.4 and 3.6 and the profile trace of Fig. 3.9 are shown.

shales and marls ('Terres Noires'; Drac valley). All these rocks were deformed together during the Pyrenean-Provençal deformation phase (Late Cretaceous to Early Eocene) by an early phase of basement uplift which folded the southern rim of the Pelvoux basement massif in south-facing recumbent folds (Ford, 1996 and references therein) (see Drac Champoléon transect on Fig. 3.1).

The basement uplift is documented by pre-Upper Eocene Basal Conglomerate which infills incised valleys cut into basement and Mesozoic strata, and comprise breccias, conglomeratic red beds, and paleosols. The fluvial valley fills are 100 - 500 m wide and 50 - 100 m deep. The clasts within the breccias and conglomerates are predominantly of local basement compositions (Gupta, 1994; Gupta, 1997). The subsequent marine transgression is documented by, shallow marine Nummulitic Limestone (5 - 50 m) and Globigerina Marl (0 - 50 m) indicating increasing water depth. They are overlain by up to 650 m of Champsaur Sandstone (Waibel, 1990). In the Soleil Boeuf region the Champsaur Sandstone is a volcanoclastic, turbiditic graywacke containing andesitic rock fragments. The amount of andesitic rock fragments averages 20 - 30% near the base of the Champsaur Sandstone and rises progressively to 40 - 50% near the top (Waibel, 1990). In contrast, in the Champsaur Sandstone to the southeast of the Selle-Fault zone (i.e. in the Champsaur-Prapic area; Chapter 2) andesitic debris appear only in trace amounts < 0.3%. The correlation between these two successions is still a problem.

The Mesozoic stratigraphy in the klippen ranges from Mid-Jurassic marly limestones (Bajocian - Lower Bathonian), black shales and marls (Upper Bathonian - Oxfordian), and Upper Jurassic limestones (Kimmeridgian - Portlandian) to small fragments of Lower Cretaceous bedded limestones (Neocomian) and radiolarites (Barremian - Aptian). The Lower Cretaceous sediments are only preserved in the peak of Soleil Boeuf and this is the only outcrop of Cretaceous strata in the whole Pelvoux region (Debelmas *et al.*, 1980; Debrand-Passard *et al.*, 1984b). The Tertiary sediments in the klippen are characterised by a highly variable amount of volcanoclastic debris in the coarse sand fraction of the Champsaur Sandstone, ranging from 0.1 - 50% (Waibel, 1990). The percentage becomes progressively less from NW to SE, i.e. from the lower to the higher units.

3.1.2 Previous work

The Soleil Boeuf area has attracted geologists from the beginning of Alpine geology. At the beginning of the 19th century the basic stratigraphy, the Tertiary angular unconformity and klippen characteristics were defined and reviewed in Haug (1894). At that time the tectonic interpretation was bound to the folding theory, Lory writes (1894: p. CLXIV): "...une poussée du sud-est a déterminé la production d'un grand anticlinal déversé, dont l'axe jurassique occupe les pentes sud-est de la vallée de Méollion... De la

sorte les pentes au N de Pont-du-Fossé sont revêtues, sauf là où l'érosion a mis à nu le substratum de Flysch, d'Oxfordien et de Kimmérien, surmontés par du Nummulitique. Ce recouvrement s'étend jusqu'aux Pics du Palastre et de Soleil-Boeuf,..." More detailed observations (e.g. see Fig. 3.2a) were collected during mapping campaigns from 1899 - 1903 (Haug, 1899-1900; Lory, 1899-1900; Lory, 1900-1901; Lory, 1901-1902; Lory, 1903-1904) for the geologic map sheet 1:80'000 of Gap (Haug *et al.*, 1905). Later, three main units bounded by major dislocations were distinguished (Fig. 3.2b): (1) the autochthonous Tertiary (progressively less deformed away from the Pelvoux massif), (2) the extremely complicated imbricates within the klippen and (3) the upper Tertiary unit in the footwall of the overthrusting Embrunais-Ubaye nappes (Gignoux *et al.*, 1932). More detailed mapping (Beuf, 1959; Debelmas *et al.*, 1980: Fig. 3.2c) led Gidon & Pairis (1980-1981) to suggest that the klippen were emplaced during sedimentation (gravitational gliding) at the last stage of the Champsaur Sandstone deposition and were due to WNW-directed overthrusting and that they were afterwards affected by northward motions.

However, opinions diverge regarding what caused the NW-directed deformation in the Soleil Boeuf area. Some geologists relate the deformation in the Soleil Boeuf area to the emplacement of the Embrunais-Ubaye nappes (Haug, 1894; Gignoux *et al.*, 1932; Gignoux and Moret, 1937; Beuf, 1959; Ford, 1996), for others the klippen in Soleil Boeuf result from movements along the Selle Fault (Gidon, 1975; Arnaud *et al.*, 1978; Gidon and Pairis, 1980-1981). These authors argued that deformation in Soleil Boeuf is similar to the NW-directed deformation in the Faucon-Turriers area (Arnaud *et al.*, 1977: Fig. 1.6). In contrast to this Arlhac and Rousset (1979) and Rousset (1986) relate the klippen of Soleil Boeuf to W-directed deformation at the base of the Digne nappe.

In order to study this area transect mapping, additional collation of kinematic data in key areas, cross-section construction and restoration has been carried out. These structures will be described in 2 groups, first the deformation in the autochthon of the whole Soleil Boeuf area, later kinematics of the allochthons within the Soleil Boeuf klippen zone.

Fig. 3.2: b) Schematically compiled cross-section through the western part of the Soleil Boeuf area continued from Gignoux and Moret (1937: their Fig. 3). Three tectonic units were distinguished: (1) The lower Eocene cushion (coussinet éocène inférieur) which is progressively more strongly deformed away from the Pelvoux massif, e.g. simple folding at Queyron (I), stretched folds in the Palastre cliff (II), and tectonic slabs at Clot-Lamiande (II). (2) A stack of mainly Jurassic imbricates (imbricate III in Fig. 3.2b), highly deformed and of extremely complicated structure in detail. and (3) the upper Eocene cushion (imbricate IV in Fig. 3.2b) which is overthrust by the lowest of the Embrunais-Ubaye nappes along thrust ϕ . c) Three detailed NW - SE cross sections from the BRGM map 1 : 50'000 (Debelmas *et al.*, 1980). This interpretation is based on nappe-like folding of tectonic contacts which previously strongly imbricated the Tertiary and Jurassic sediments. Thus large-scale folding does in part also affect the autochthonous Tertiary. The steep normal faults of the Selle-Fault system are taken into account (same labels as in Fig. 3.6).

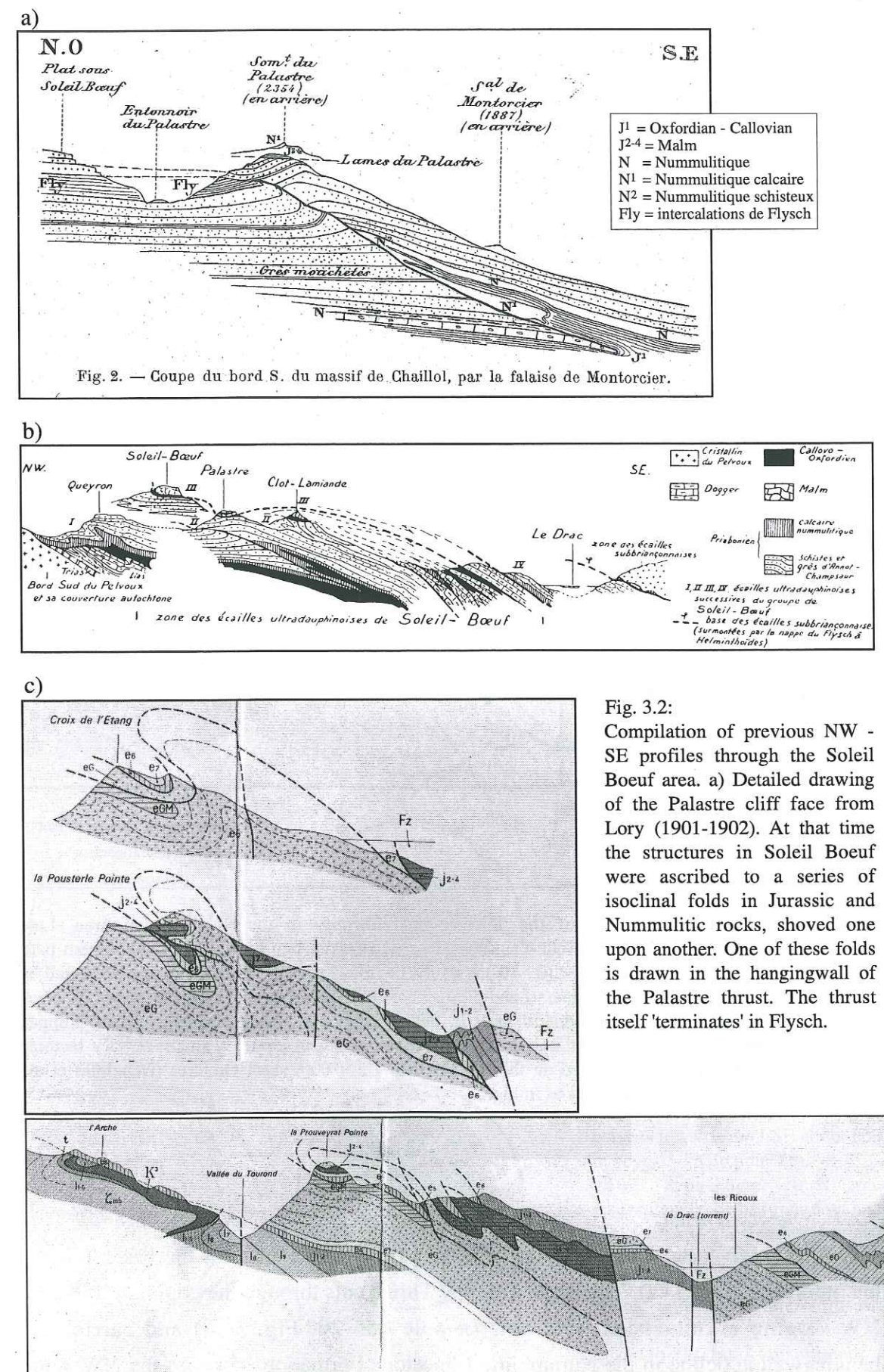


Fig. 3.2: Compilation of previous NW - SE profiles through the Soleil Boeuf area. a) Detailed drawing of the Palastre cliff face from Lory (1901-1902). At that time the structures in Soleil Boeuf were ascribed to a series of isoclinal folds in Jurassic and Nummulitic rocks, shoved one upon another. One of these folds is drawn in the hangingwall of the Palastre thrust. The thrust itself 'terminates' in Flysch.

3.2 Folding and thrusting in the autochthon

The autochthonous Tertiary unconformity is cut by several thrust faults with associated folding. The larger of these structures are, from west to east, the Queyrel Thrust, the Palastre Thrust, the Estang Thrust and the Méollion Syncline and Méollion Thrust (Fig. 3.1). They will be described below, working from west to east. After the main post-mid-Oligocene deformation regional basement uplift caused southward tilting of the autochthon and overlying nappes. Mapping the base of the Tertiary sequence (Fig. 3.3) reveals that tilting up to $30\frac{1}{2}^\circ$ occurred along an E-W trending band to the north of the preserved klippen. Elsewhere the base of the Tertiary sequence dips $0\frac{1}{2}^\circ$ - $10\frac{1}{2}^\circ$ southeast.

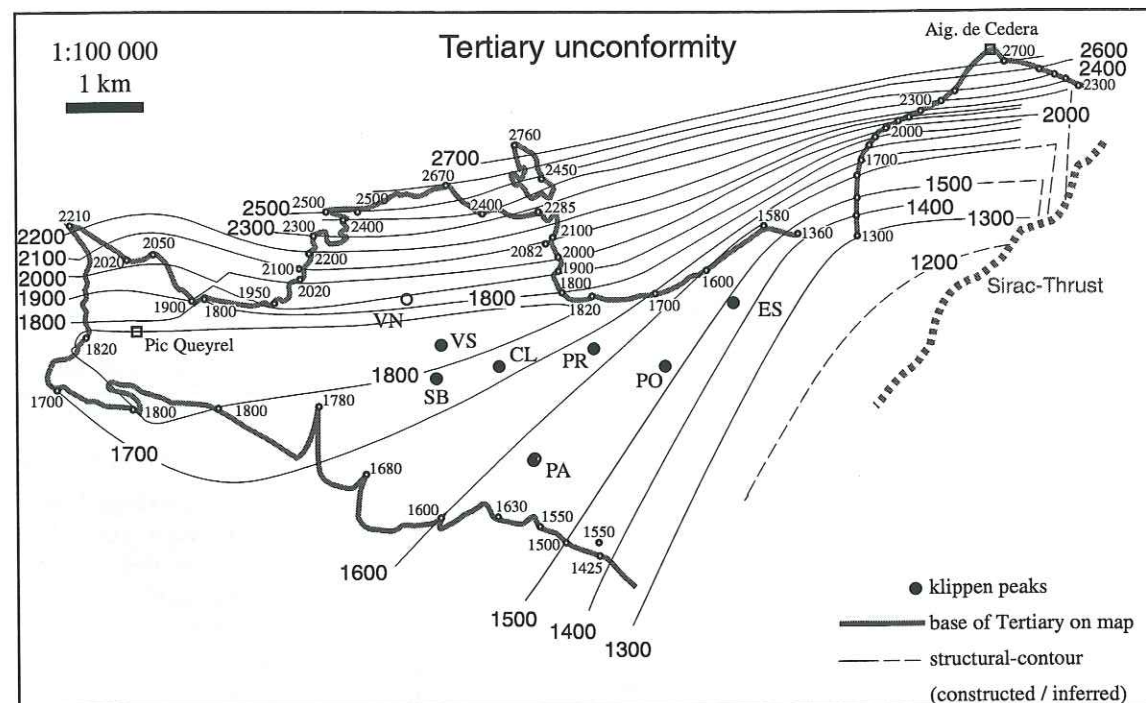


Fig. 3.3: Structure-contour map of the Tertiary unconformity in the Soleil Boeuf area. Late displacements along the Selle-Fault system are not taken into account. In the southern part, the Tertiary is slightly tilted ($0 - 10^\circ$) towards the SE. The northern part is strongly affected by the uplift of the Pelvoux massif and dips $\sim 30^\circ$ S. All Mesozoic klippen (represented by black dots) lie in the flatter southern part. In the northern part tilting clearly postdates klippen emplacement and only at Pointe N de la Venasque (open circle) a small Tertiary tectonic outlier is preserved. Based on the BRGM map 1:50'000, sheet Orcières (Debelmas et al., 1980). Same abbreviations as in Fig. 3.1.

3.2.1 Queyrel Thrust

In the south face of Pic Queyrel (Fig. 3.1) two thrust faults cut the basal Tertiary unconformity (Fig. 3.4a). The larger Queyrel Thrust cuts through the common limb of a NW-verging asymmetrical fold pair (π -pole 054-20; Fig. 3.4c) and carries the hangingwall anticline in the Nummulitic Limestone Formation ~ 1 km to the NW. Fault

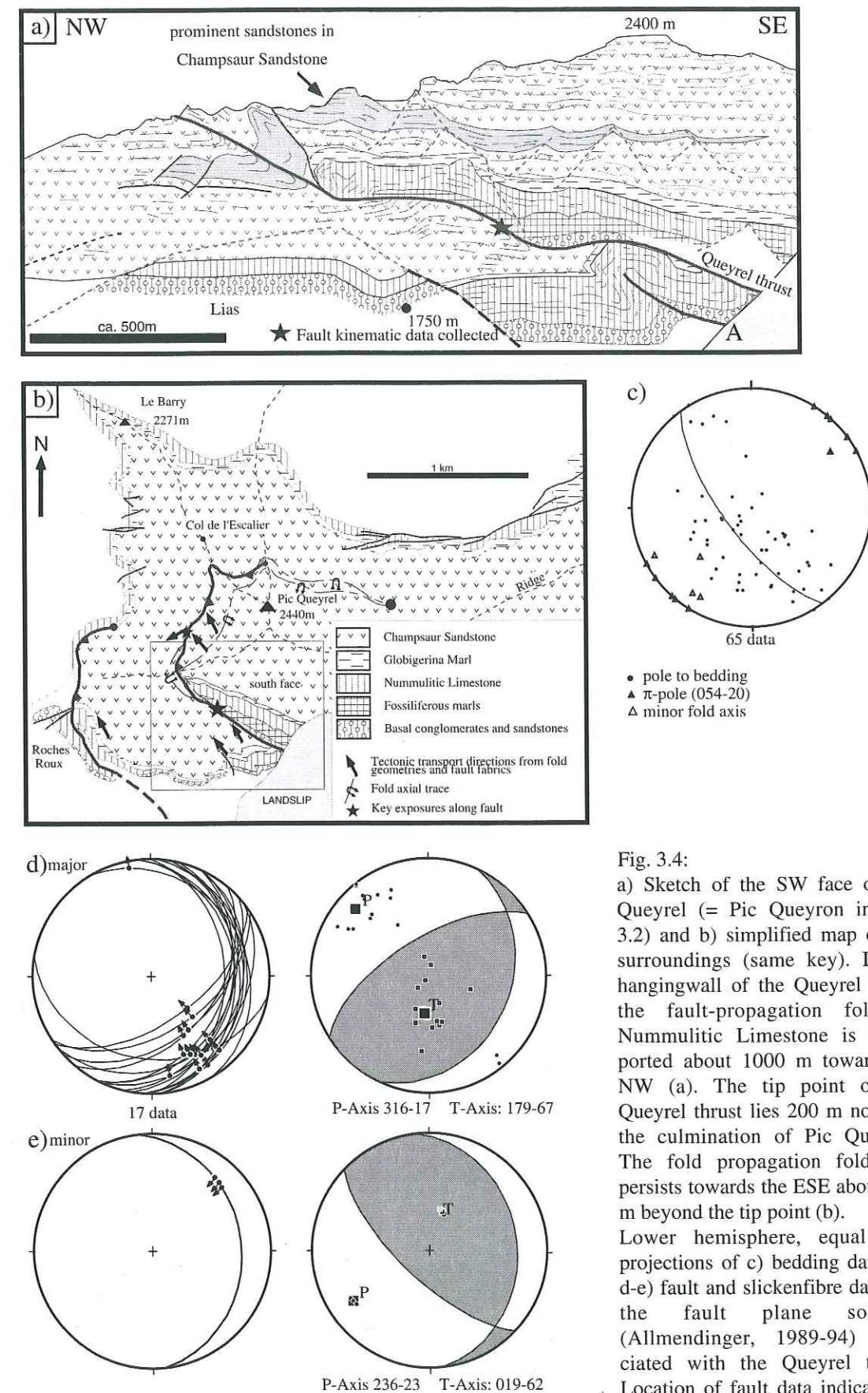


Fig. 3.4:

a) Sketch of the SW face of Pic Queyrel (= Pic Queyron in Fig. 3.2) and b) simplified map of the surroundings (same key). In the hangingwall of the Queyrel thrust the fault-propagation fold in Nummulitic Limestone is transported about 1000 m toward the NW (a). The tip point of the Queyrel thrust lies 200 m north of the culmination of Pic Queyrel. The fold propagation fold pair persists towards the ESE about 800 m beyond the tip point (b). Lower hemisphere, equal area projections of c) bedding data and d-e) fault and slicken fibre data and the fault plane solution (Allmendinger, 1989-94) associated with the Queyrel thrust. Location of fault data indicated in a) and b). (M. Ford, unpublished).

striations and fibre lineations measured at two key exposures along the Queyrel Thrust (Fig. 3.4b) give dominant NW-directed displacements (Fig. 3.4d) which kinematically agree with the orientation of the fold pair (Fig. 3.4c). Very few striations indicating SW-directed thrusting (Fig. 3.4e) occur also in the same fault zone. The field data give no evidence whether these are relicts of an earlier SW-movement or if they indicate SW-directed reworking. To the north the Queyrel Thrust dies out while the asymmetrical fold pair extends a distance beyond of the fault tip indicating that the displacement on the fault is consumed by folding (Fig. 3.4b) (Gidon and Pairis, 1980-1981). The asymmetric fold-pair is medium sized with an amplitude of less than 250 m. In the immediate footwall of the Queyrel Thrust a smaller thrust fault rapidly dies out within the Nummulitic Limestone and the shortening is consumed by a fold pair (Fig. 3.4a). Similar thrusting occurs further west at Roches Roux (Fig. 3.4b).

This kind of deformation, with decreasing bed displacement upwards on a thrust fault terminating in a fold pair is commonly referred to as fault-propagation folding (Williams and Chapman, 1983; Suppe and Medwedeff, 1984; Suppe and Medwedeff, 1990) which is characterised by simultaneous faulting and folding. Folds form at the tip of propagating thrust faults and as deformation progresses faulting breaks through the common limbs (Fig. 3.4a).

3.2.2 Palastre Thrust

In a similar way the Palastre Thrust further east (Fig. 3.1) accommodates ~600 m displacement towards the NW (Fig. 3.5). In this case fault-related folding is restricted to a minor footwall syncline (with no well developed hangingwall anticline) well marked

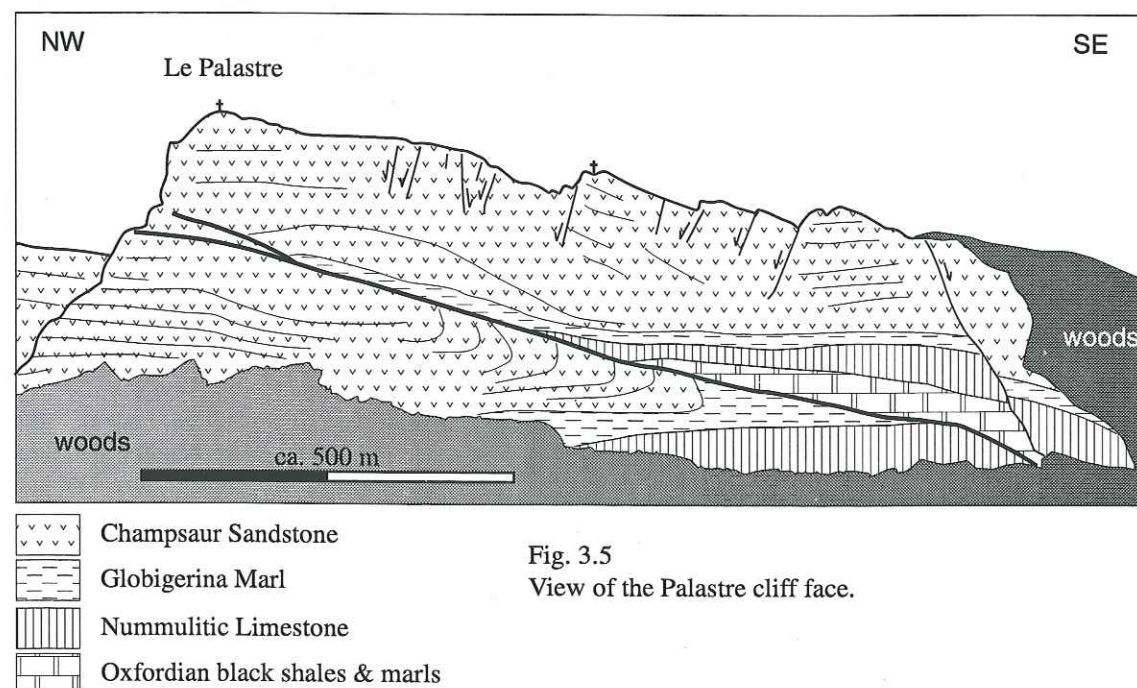


Fig. 3.5
View of the Palastre cliff face.

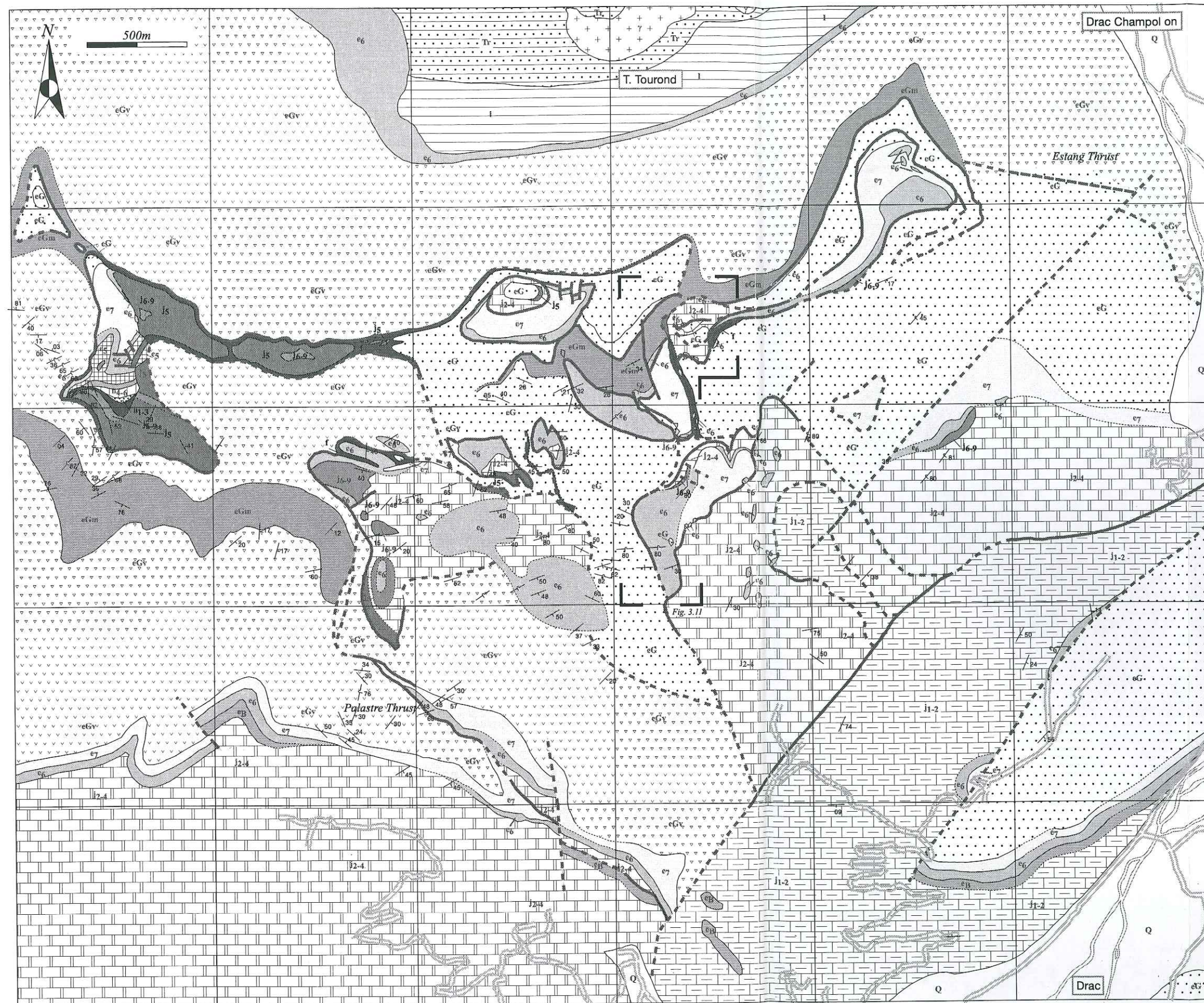


Fig. 3.6:
Detailed geologic map of the Soleil Boeuf
klippen zone (located in Fig. 3.1). Inset of
Fig. 3.13 is shown. Based on mapping by H.
Lickorish, M. Ford and J. Býrgisser.

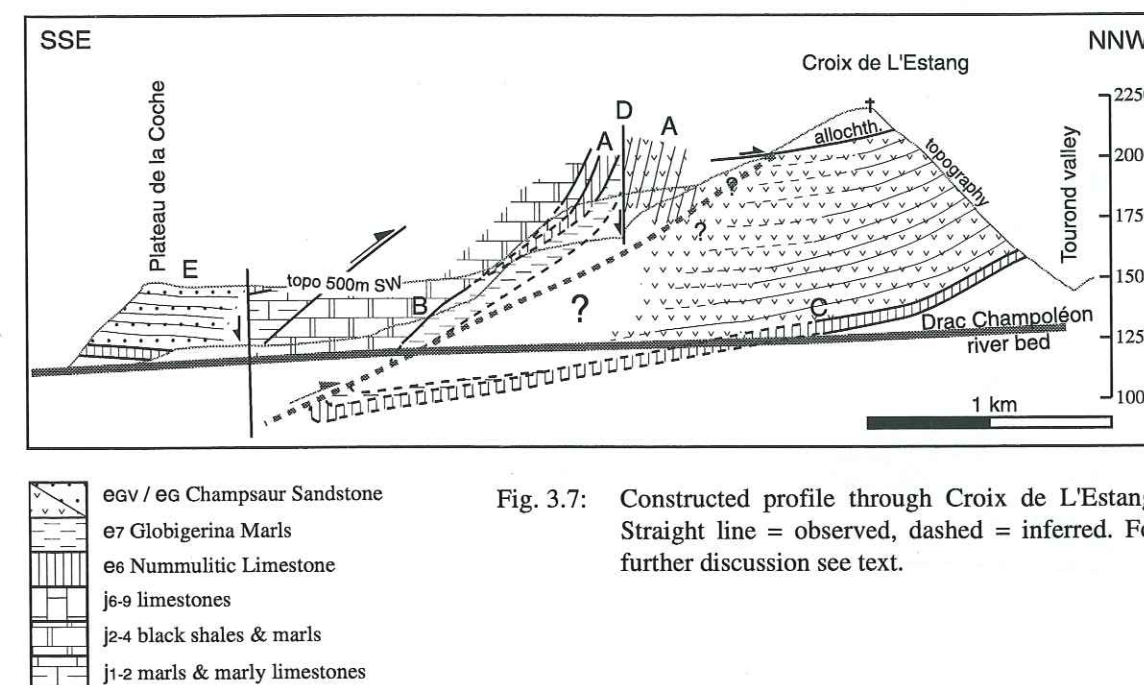
Legend

Q	Quaternary
eG	Champsaur Sandstone - Eocene volcanic facies
eGm	siltstone
e7	Globigerina Marl - Eocene
e6	Numulitic Limestone - Eocene Cerithium beds
e3	Basal conglomerate
r	fault shear zone
j4-6	radiolarite - Barremian
j1-3	limestones - Neocomian
j6-9	limestones - Tithonian
j5	limestones - Upper Jurassic
j2-4	Up. Bathonian - Oxfordian black shales
j1-2	Bajocian - Lo. Bathonian marls
l	Liassic
Tr	Triassic
+	basement
---	fault
---	stratigraphic contact
---	road
---	river

by the Champsaur Sandstone and Globigerina Marl Formations (Fig. 3.5; compare to Lory (1901-1902) and Gignoux & Moret (1937) interpretation: Fig. 3.2a & b). The size of the footwall syncline ranges within less than 100 m. No detailed data could be collected, but Gidon & Pairis (1980-1981) give a fault plane orientation (180/40) which seems too steep.

3.2.3 Estang Syncline and Thrust

In the western cliff of the Drac Champoléon valley the trace of the Estang Thrust can be recognised (Figs. 3.1, 3.6 & 3.8) which is thought to cut through the Estang Syncline.



The Estang Syncline is inferred from the stratigraphic sequence (Middle Jurassic black shales and marls, Upper Jurassic limestones, Nummulitic Limestone, Globigerina Marl and Champsaur Sandstone) which lies up-side down on the autochthonous Champsaur Sandstone just west of the Drac Champoléon (Figs. 3.6). A profile construction (Fig. 3.7) combines the poor outcrop data. At (A) the overturned sequence dips with $80\frac{1}{2}^\circ$ to the southeast and seems to flatten out downwards (contact Jurassic to Globigerina Marl at B). The contacts between the different formations at A are stratigraphic (H. Lickorish pers. comm.) except at the normal fault (D) which belongs to the Selle-Fault zone. In the autochthon the southward continuation of the Nummulitic Limestone (at C) was inferred from the structural contour map (Fig. 3.3), it is not well constrained. Two kilometres to the southeast (at E) the Tertiary sequence is again upright.

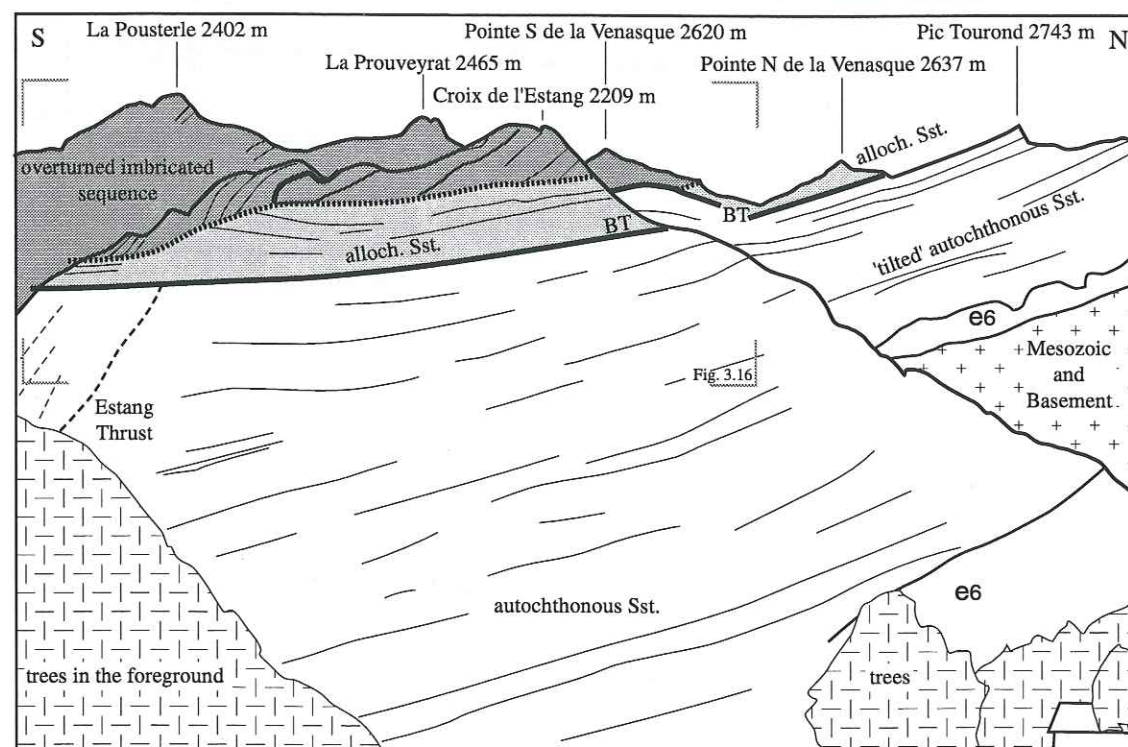


Fig. 3.8: Photograph and interpreted drawing looking towards W into the Soleil Boeuf area with Mesozoic and Tertiary klippen (shaded) sitting on top of the autochthonous Tertiary sequence (white). In the northern 'tilted' part the autochthonous sediments and the Basal Thrust (BT) dip south below Pic Tourond and Pointe N de la Venasque, southwards they become subhorizontal (e.g. at Pointe S de la Venasque). In the middle left margin steeply dipping overturned sediments overlie the autochthonous sandstone along the Estang Thrust. In this view, two units can be distinguished in the allochthons: the allochthonous sandstone sheets (light shaded), an imbricated overturned and upright sequence (dark shaded). In the foreground is the Estang-profile which is described in more detail in Fig. 3.16 (inset is shown).

The overturned sequence is interpreted to form the steep limb of a large syncline (Estang Syncline). The amplitude must be > 1 km. In the field the synclinal hinge was not found. This is inferred to be due to the Estang Thrust which subsequently cut through the syncline and carried the hangingwall northwestwards.

The structure probably continues east of the Drac Champoléon (Fig. 3.1).

3.2.4 Méollion Syncline

In the upper Méollion valley a large-scale syncline affects the autochthon (Figs. 3.1 & 3.9). The normal limb dips moderately south and covers the southern slopes of Aiguille de Cedera. Close to the valley bottom bedding in the Champsaur Sandstone becomes steep to overturned. The synclinal closure can be picked up just west of the abandoned village Méollion. The stereoplot of poles to bedding gives a NE-SW trending fold axis (π -pole 217-15; Fig. 3.9b). Further south Globigerina Marl and Nummulitic Limestone complete the Tertiary sequence in the steep to overturned limb. The stratigraphic contacts between the formations are tectonized. These autochthonous rocks are tectonically overlain by a thick, southeast dipping Lower Jurassic normal sequence of

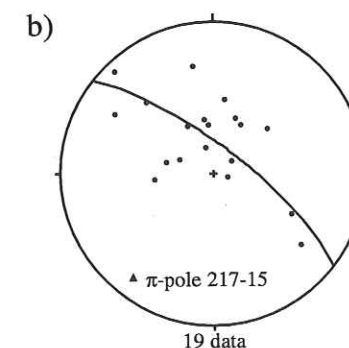
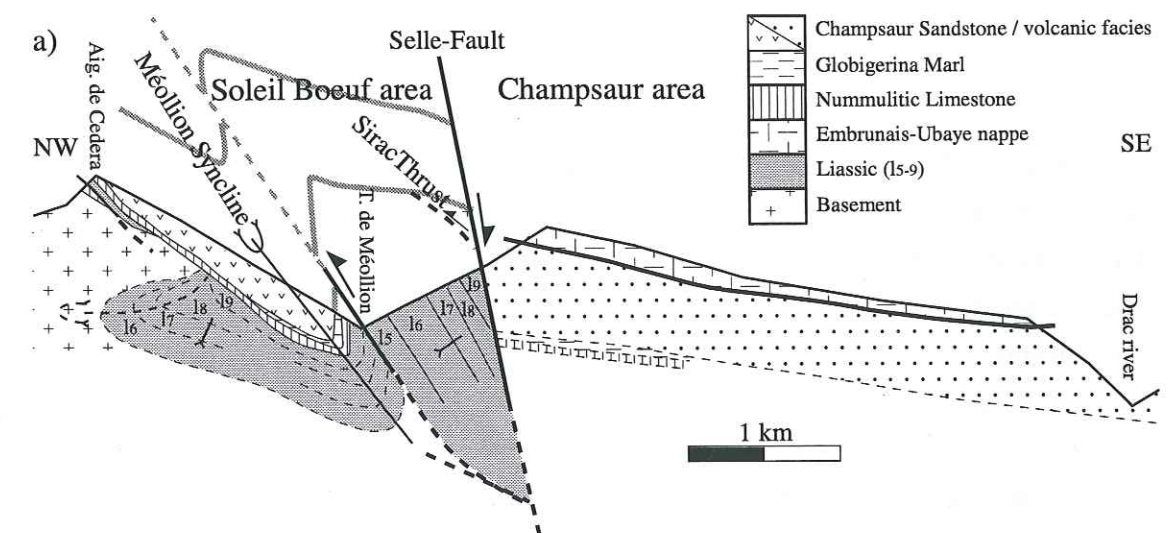


Fig. 3.9: NW-SE profile across the Méollion valley. The southern slopes of Aig. de Cedera are covered with Tertiary sediments which unconformably overlie folded basement and Mesozoic rocks. The Méollion syncline is overthrust by thick upright Liassic sediments. Just north of the profile trace they are thrust by the Sirac basement thrust sheet. Further southeast normal displacement on the Selle-Fault juxtaposes the Champsaur area against the Soleil Boeuf area (minimum displacement is about 750 m). The continuation of the Méollion fold pair is schematically drawn with grey lines. b) Lower hemisphere, equal area projection of poles to bedding associated with the Méollion syncline. Data from turbiditic sandstone layers and Nummulitic Limestone beds.

marls and limestones in the footwall of the Sirac basement thrust sheet. This thrust cuts through the steep limb and further northeast also through the normal limb, where only patches of Basal Conglomerate give evidence for the former Tertiary cover (Fig. 3.1). Restoration of the late Selle-Fault displacement (Fig. 3.9a) clearly shows the size of the Méollion Syncline which has an amplitude of about 1.5 km.

3.2.5 Discussion

All the thrusts and folds described above occur in the so-called autochthon. They all involve Tertiary sediments and therefore can be clearly distinguished from older deformation features in the autochthon (Ford, 1996 and references therein) and can be dated as post-mid-Oligocene.

Around the Drac Champoléon valley the evenly dipping basal Tertiary unconformity is affected by a major fold and associated thrust, the Estang Syncline to the west and the Méollion Syncline to the east. These structures roughly correlate along strike (NE-SW) and are therefore interpreted as parts of the same structure. A fault-propagation fold model is proposed for this major structure in analogy to the much smaller fault-propagation fold at Pic Queyrel (Fig. 3.4).

The large asymmetric synclines verge towards the NW in the general thrust transport direction which indicates that they are related to the same dynamic process. Therefore it is probable that thrusting and folding were ongoing simultaneously as it has been documented for the smaller structures in the Queyrel zone (Fig. 3.4). The Estang and Méollion Thrusts sole in detachment horizons within the Mesozoic sequence; close to the Pelvoux basement massif the faults are forced to ramp upwards and asymmetric folds formed in the Tertiary cover at the tips of the propagating thrusts. Ongoing thrusting broke through the Estang and Méollion Synclines and obscured their original fault-propagation origin.

3.3 Geometry of the allochthonous units

Figure 3.8 shows the klippen which were emplaced over the autochthonous Champsaur Sandstone (e.g. at Pointe N de la Venasque) along the Basal Thrust. The Basal Thrust is the lower boundary of all allochthonous units. Numerous small preserved fragments of tectonic slices can be divided into three major groups of thrust sheets which from bottom to top are, the allochthonous sandstone sheets, an imbricated overturned sequence (the Pousterle Imbricates) and an imbricated upright sequence (Bonne Herbe Thrust Imbricates and the Palastre-Venasque Thrust Sheet) (Fig. 3.10). The field data will now be presented for each major group of thrust units from bottom to top.

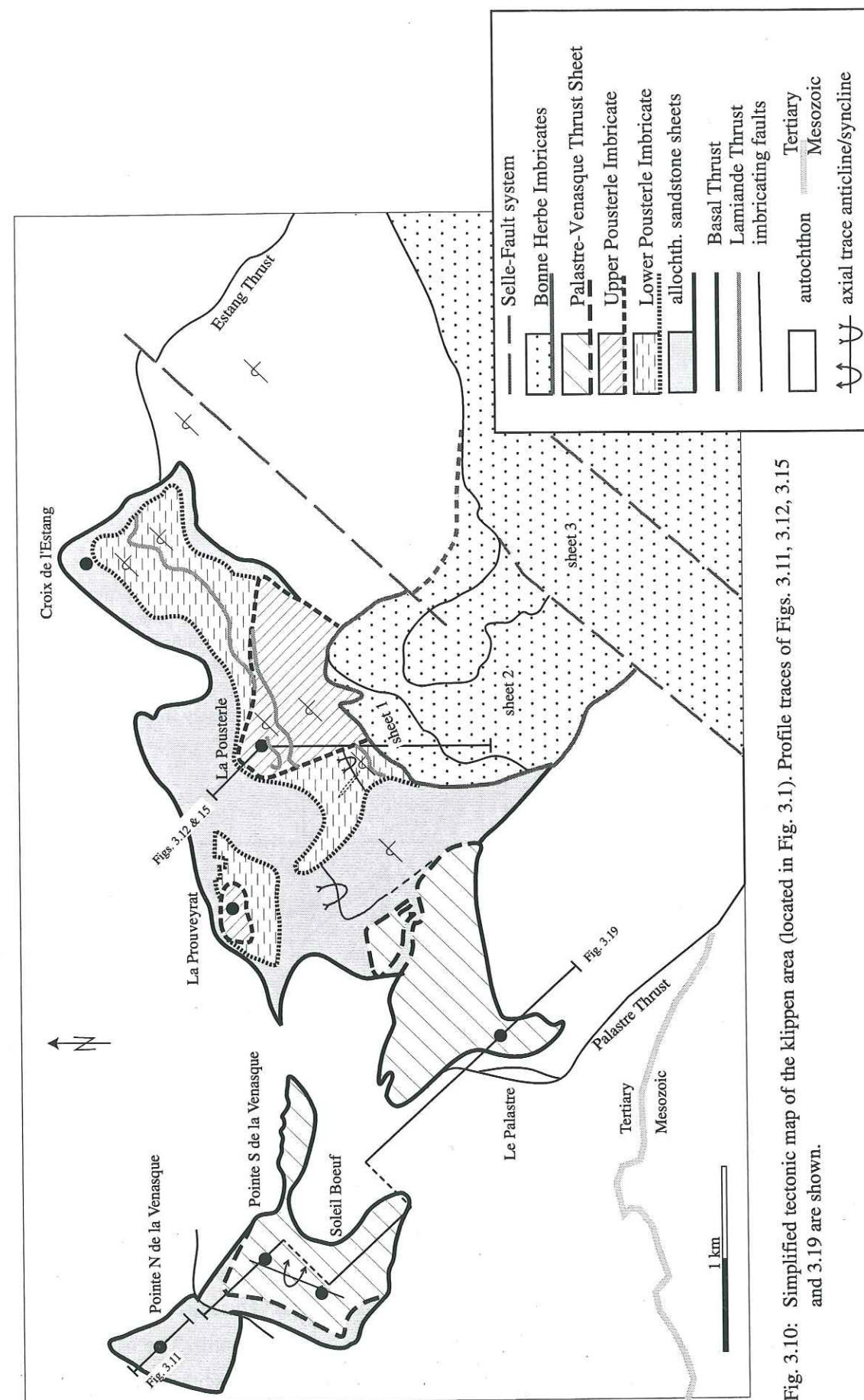


Fig. 3.10: Simplified tectonic map of the klippen area (located in Fig. 3.1). Profile traces of Figs. 3.11, 3.12, 3.15 and 3.19 are shown.

3.3.1 The allochthonous sandstone sheets

The autochthonous sandstone is first overlain by allochthonous Champsaur Sandstones (Fig. 3.10). They are preserved as a large continuous sheet underneath the imbricates of Croix de l'Etang, La Pousterle and La Prouveyrat, and as a smaller isolated patch further west around Pointe Nord de la Venasque (Figs. 3.8 & 3.10). Unlike in the autochthonous substrate mesoscale folds and faults are common in these sheets.

An allochthonous sandstone sheet is nicely exposed at Pointe Nord de la Venasque (Fig. 3.11b). The peak itself contains a tight upright minor antiform emplaced onto a sheet with open upright folds, blind thrusts and associated minor folding cut by normal faults. The Basal Thrust is bedding-parallel and follows a silt-rich sequence (eGM) within the autochthonous Champsaur Sandstone (Fig. 3.6). Bedding data indicate NW-SE-directed shortening (π -pole 235-03; Fig. 3.11a). To the south the allochthonous sandstone unit is cut out by the Palastre-Venasque Thrust Sheet (Fig. 3.10).

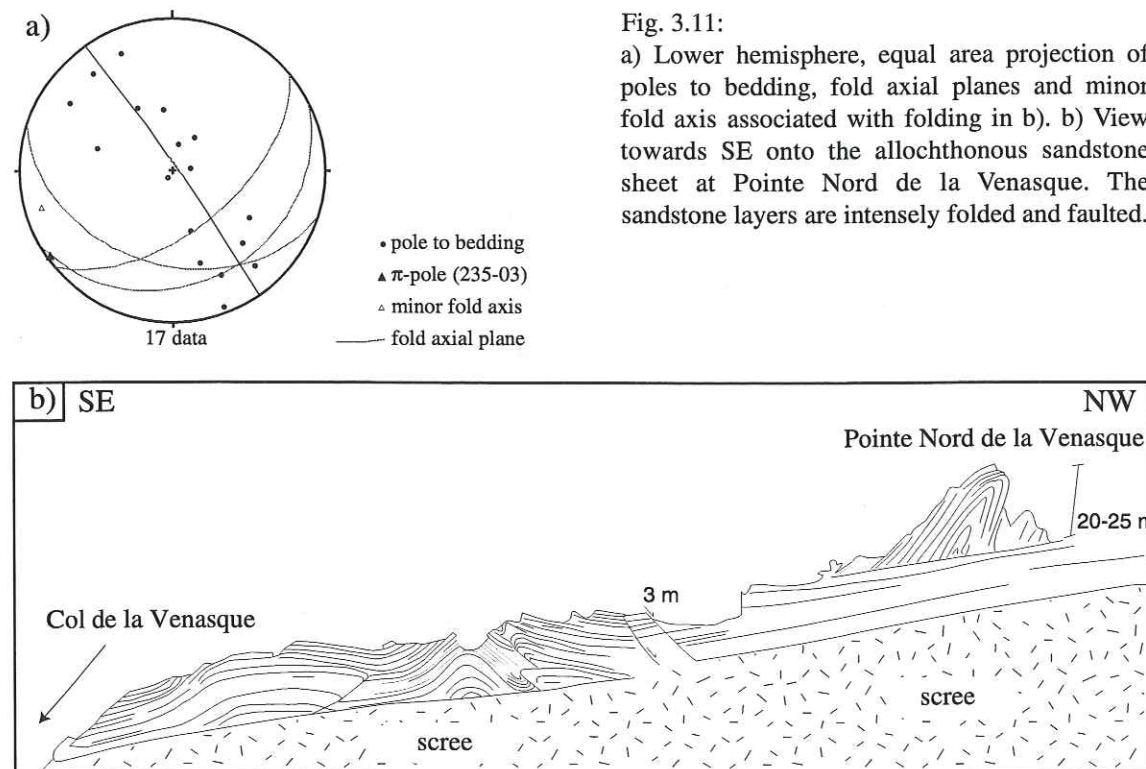


Fig. 3.11:

a) Lower hemisphere, equal area projection of poles to bedding, fold axial planes and minor fold axis associated with folding in b). b) View towards SE onto the allochthonous sandstone sheet at Pointe Nord de la Venasque. The sandstone layers are intensely folded and faulted.

In the southern part of the large eastern allochthonous sandstone sheet bedding is constantly overturned and steeply dipping southeast for at least 400 m (Figs. 3.6 & 3.12). This must be the steep limb of a large syncline (see discussion). The northern part of the allochthonous sandstone sheet is right way up and dips shallowly south. The trace of the large syncline is shown in Fig. 3.10. At several other locations mesoscale folding can be

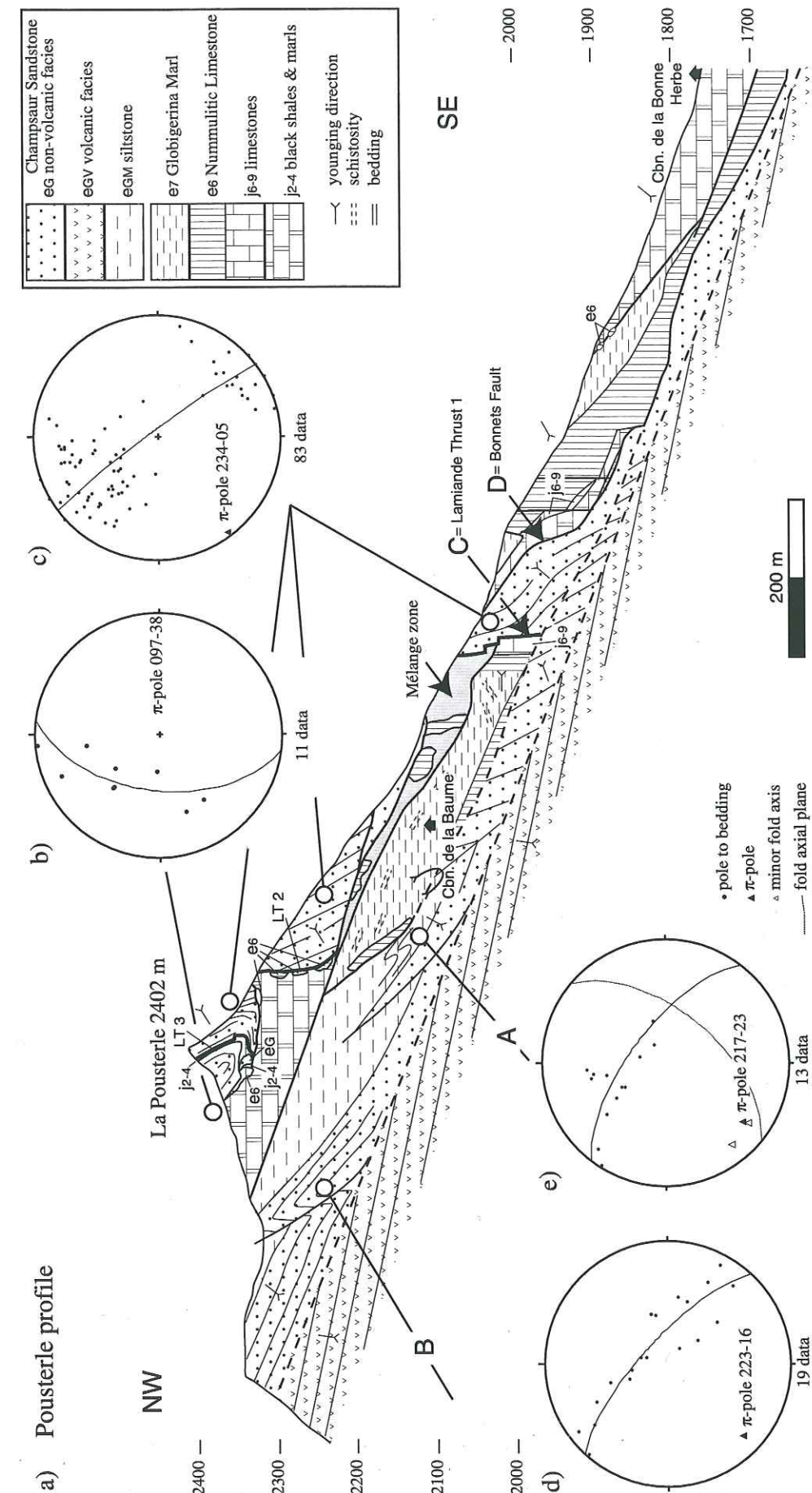


Fig. 3.12: a) Detailed geologic profile across the Pousterle ridge (for the tectonic interpretation see Fig. 3.15). Lower hemisphere, equal area projections of bedding data associated with b) meter-scale folding of Champsaur Sandstone in the Pousterle Imbricate, d) and e) folding of sandstone layers (d) and siltbeds (e) in the allochthonous sandstone sheet. Profile trace is located in Fig. 3.10. LT=Lamiande Thrust

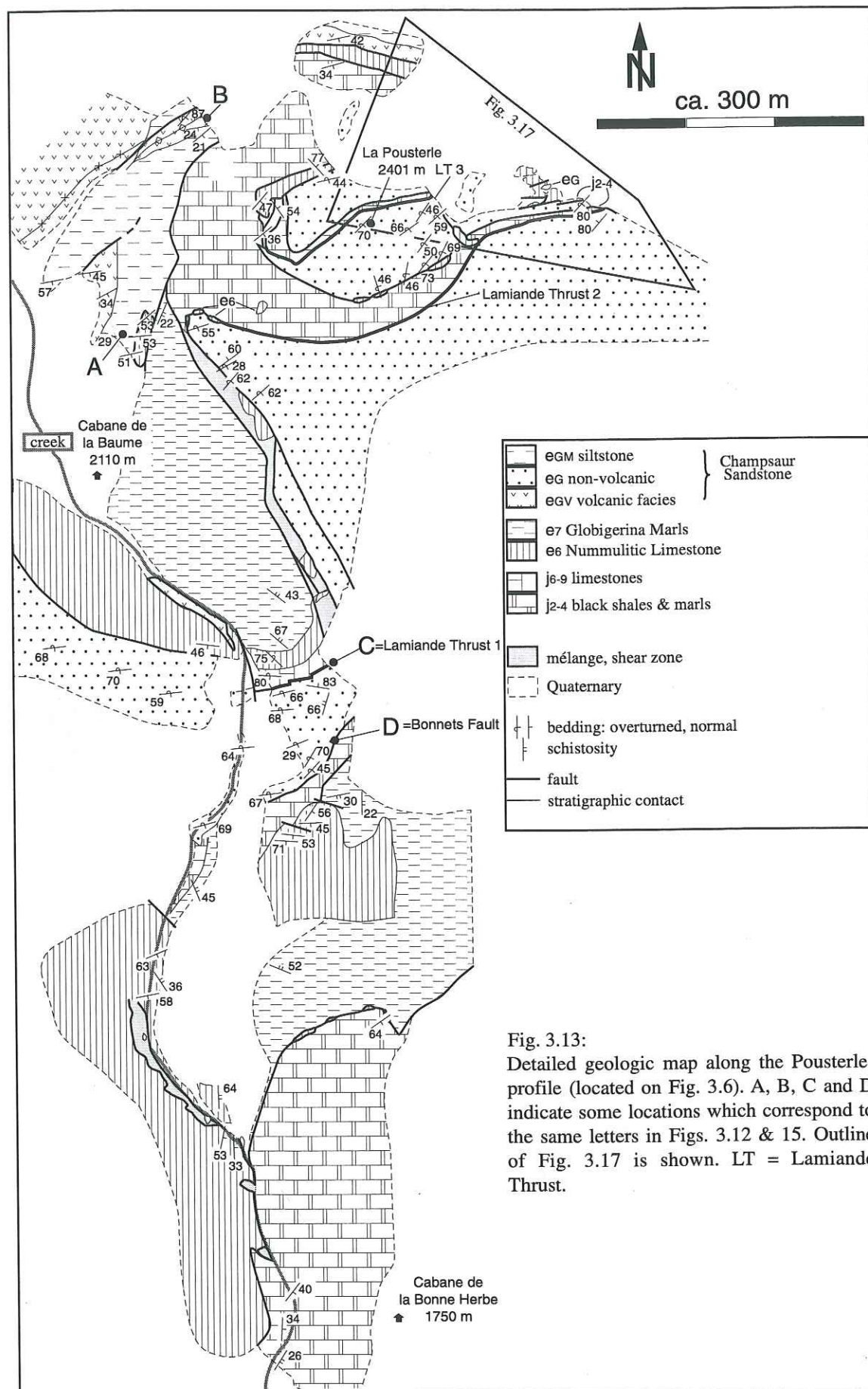


Fig. 3.13:
Detailed geologic map along the Pousterle-profile (located on Fig. 3.6). A, B, C and D indicate some locations which correspond to the same letters in Figs. 3.12 & 15. Outline of Fig. 3.17 is shown. LT = Lamiande Thrust.

observed, e.g. below the Pousterle peak. Here, thin silt beds (EGM) form tight, asymmetric, NW-vergent folds (Figs. 3.12 & 13: location A). They have 1 - 3 m wavelengths and up to 1 m amplitudes. The π -pole (217-23: Fig. 3.12e) coincides with minor fold axes. About 200 m further north, near the topographic crest, a sandstone layer marks the hinge of a NE-SW-trending anticline surrounded by a siltstone rich sequence (Figs. 3.12 & 13: location B). The hinge zone (π -pole 223-16: Fig. 3.12d) becomes less tight towards the SW across 20 m so that the sandstone layers are buried by shale. Immediately to the northwest lie steeply SE-dipping, overturned turbidites which become subhorizontal further northwest. This resolves into a fold pair with a thrust fault cutting through the common limb (Fig. 3.12).

Discussion

Fig. 3.14 compiles the above observations into a simple model for the eastern allochthonous sandstone sheet. The autochthonous turbidite sequence was overthrust layer-parallel towards the NW by a relatively thin sheet (~50 m) of turbiditic sandstones and siltstones. This caused minor internal folding and thrusting. In the southern part, the broad panel of steeply dipping Champsaur Sandstone younging northwards requires a large-scale syncline. The Basal Thrust cut through the steep limb and carried it several hundred meters towards the NW over the undeformed autochthon.

The smaller western allochthonous sandstone sheet is a local feature in the footwall of the frontal part of the Palastre-Venasque Thrust Sheet. To the south it is cut out by the Palastre-Venasque Thrust Sheet. It is best explained as a footwall shortcut with low amounts of displacements.

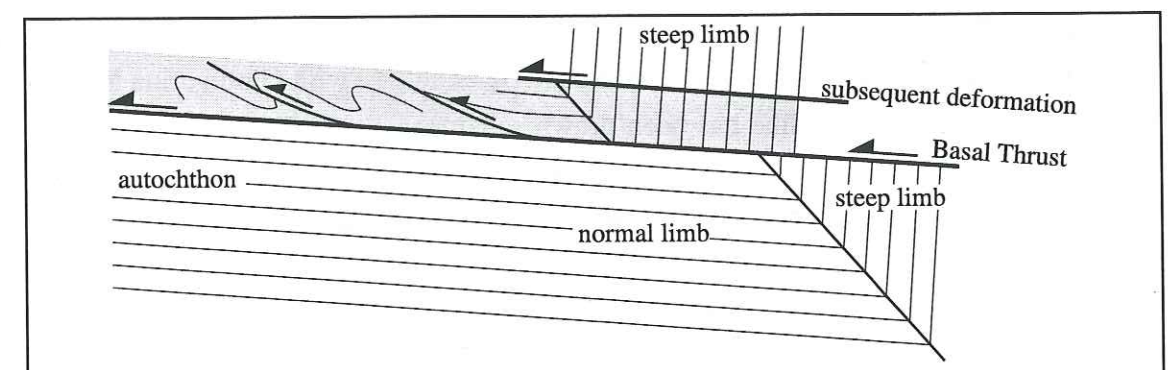


Fig. 3.14: Interpretational sketch (not to scale) to explain the structures observed in the large eastern allochthonous sandstone sheet (shaded). The autochthonous substrate is folded in a large scale syncline. The Basal Thrust cuts through the syncline scraping off and deforming the uppermost layers of the autochthonous Champsaur Sandstone in the normal limb and carrying the steep limb over undeformed autochthon towards the NW. Subsequent deformations behind the steep limb and may have further accentuated the internal deformation of the allochthonous sandstone sheet.

3.3.2 Imbricated overturned sequences

The next unit is the most complex and involves an imbricated sequence of Mesozoic and Tertiary rocks which is characterised by a largely overturned stratigraphy and a synclinal structure. This unit comprises two imbricates separated by a low angle thrust (Fig. 3.10: Lower and Upper Pousterle Imbricates). Two generations of thrusts are involved. The older thrusts have been folded and partly reactivated by later thrusts during NW compression. Thus the Lower and Upper Pousterle Imbricates are defined by late thrusts and therefore incorporate the older thrust structures. Abundant minor slip surfaces have strongly dismembered the stratigraphic formations and detailed mapping was required to resolve the structure. This mapping concentrated around La Pousterle, along a N-S transect following a creek system which has eroded deeply into the klippen and their footwall rocks (Fig. 3.13).

The Lower Pousterle Imbricate

The Lower Pousterle Imbricate is preserved in the middle part of the Pousterle profile (Figs. 3.12 & 3.15). It is composed of several tectono-stratigraphic units which are from southeast to northwest (Fig. 3.12): ~150 m steeply dipping non-volcanic turbidites (eG) younging north, ~10 m steeply dipping Upper Jurassic limestones (j6-9: Kimmeridgian - Portlandian), 2 - 3 m steeply dipping Nummulitic Limestone overlain by Globigerina Marl of indeterminable dip which extends ~350 m northwestward until it again meets a south dipping Nummulitic Limestone sequence thrust towards the NW over siltstones of the underlying allochthonous sandstone sheet. Across the creek, to the west, a thick unit of Nummulitic Limestone immediately sits on the allochthonous sandstone unit (Fig. 3.13) and underlies the Globigerina Marl. It extends north to La Prouveyrat where it is stratigraphically overlain by Globigerina Marl (Fig. 3.6). Therefore the Nummulitic Limestone can be traced around a syncline (Pousterle Syncline) with Globigerina Marl in the core (the Pousterle Syncline has been drawn schematically in Fig. 3.15). The steep panel to the south lies on the southern limb of the syncline. Primary thickness variations and subsequent tectonization can explain the rapid thickness changes of the Nummulitic Limestone.

On the southern steep limb north-younging overturned Champsaur Sandstone (eG) is in tectonic contact to Upper Jurassic limestones (j6-9) to the north; this contact is called the Lamiande Thrust₁ (Fig. 3.12). Minor faults within this cataclastic contact zone resolve into a conjugate fault set which comprises (Fig. 3.15b): subvertical sinistral strike-slip faults parallel to the contact zone and southwest-dipping dextral strike-slip faults. The fault plane solution indicates N-directed compression. Because the dextral strike-slip faults clearly offset the Lamiande Thrust₁ and adjacent beds towards the

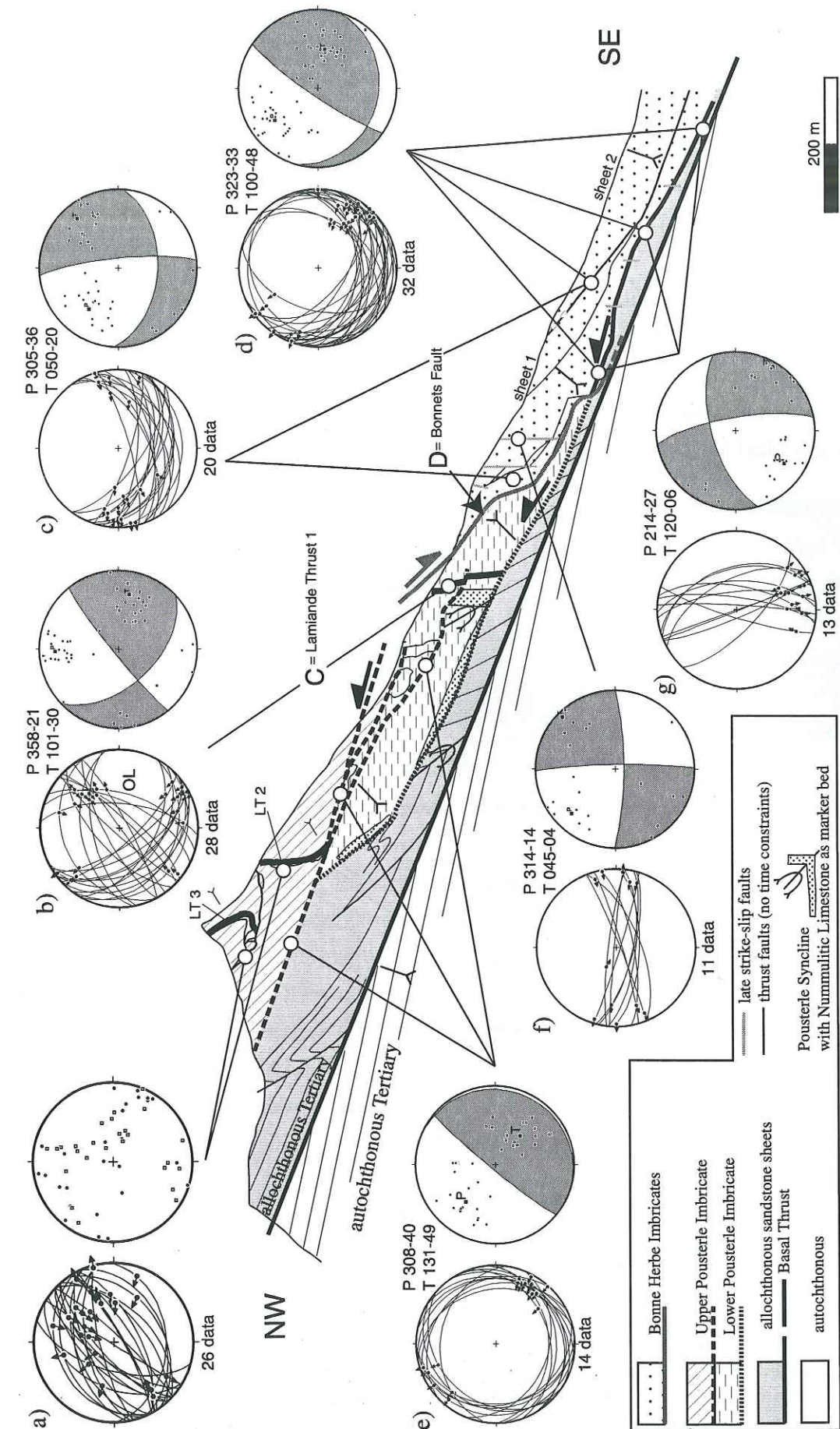


Fig. 3.15: Simplified tectonic profile across the Pousterle ridge (for geologic profile see Fig. 3.12). The different tectonic units and imbricates are shown. Lower hemisphere, equal area projections of fault planes and striae and to the right the fault plane solutions derived with the FaultKin programme (Allmendinger, 1989-94) (P: compression, T: extension). Profile trace is located in Fig. 3.10.

northwest this conjugate fault set is interpreted as reworking of the Lamiande Thrust₁ during the emplacement of the Pousterle Imbricates. In other words, the Lamiande Thrust₁ is an older fault within the Lower Pousterle Imbricate. It has been folded around the Pousterle Syncline, thus the Lower Pousterle Thrust at the base of the Nummulitic Limestone along the flat limb of the Pousterle Syncline reactivates the Lamiande Thrust₁.

A similar tectonic situation occurs in the Lower Pousterle Imbricate at Croix de l'Etang further east (Fig. 3.16). The allochthonous sandstone sheet is overthrust by a sequence which comprises from S to N: ~250 m overturned non-volcanic turbidites (eG), a 2 m wide strongly weathered cataclastic zone, ~20 m Nummulitic Limestone, ~40 m Globigerina Marl and again non-volcanic turbidites. This sequence is similar to the one

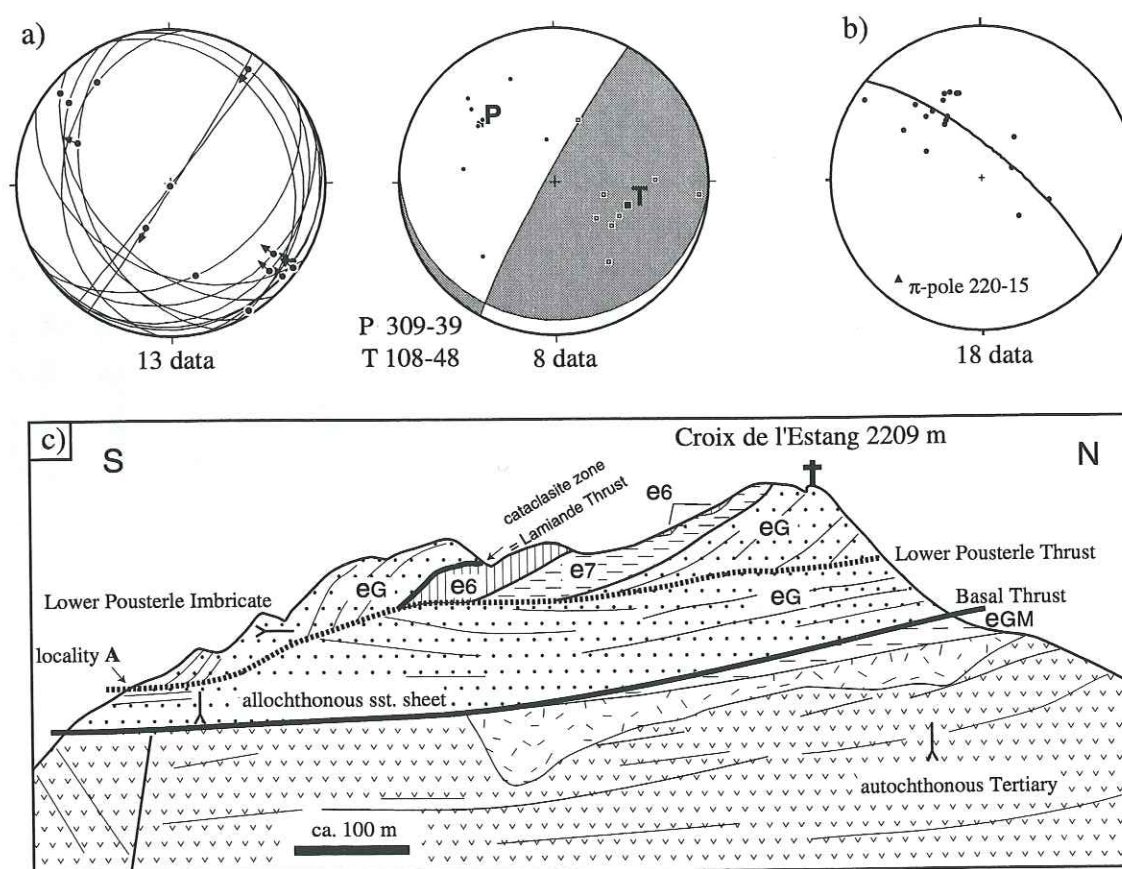


Fig. 3.16: The Estang klippe: Lower hemisphere, equal area projections of a) minor faults from locality A (fault planes & striae, fault plane solution (Allmendinger 1989-94)) and b) bedding data from Lower Pousterle Imbricate. c) Interpretational geologic sketch of profile view across the Drac Blanc valley (detail from Fig. 3.8). The Basal Thrust cuts layer-parallel (except at the left margin) through the autochthonous sediments using siltbeds (eGM) as an easy-glide horizon. The allochthonous sandstone sheet in the hangingwall is not folded. Clearly, at locality A, a thrust fault emplaces overturned Tertiary beds of the Lower Pousterle Imbricate towards the NW over the allochth. sst. sheet. A thin cataclastic zone marks the Lamiande Thrust between overturned Champsaur Sandstone in the hangingwall and overturned Nummulitic Limestone in the footwall. Same patterns as on Fig. 3.13.

described in the Pousterle profile in that it shows again doubling of Tertiary stratigraphy within an overturned southeast dipping sequence. The Upper Jurassic limestone is missing but the cataclasite zone indicates where a major tectonic contact was. Thus the Lamiande Thrust₁ from the Pousterle profile (Fig. 3.15) links eastward below higher imbricates with the cataclasite zone on the Estang profile (Fig. 3.10).

The Lower Pousterle Imbricate was emplaced over the allochthonous sandstone sheet towards the NW on a low angle Lower Pousterle Thrust whose striations are plotted with their fault plane solution in Fig. 3.16a. Bedding data give a π -pole perpendicular to this NW-directed shortening (Fig. 3.16b). The lower, upright limb of the Pousterle Syncline is not present in the Estang profile (Fig. 3.16), it must have been cut off during the emplacement by the Lower Pousterle Thrust.

The Upper Pousterle Imbricate

The Upper Pousterle Imbricate in the peak of La Pousterle is separated from the Lower Pousterle Imbricate by the late low angle Upper Pousterle Thrust (Figs 3.10 & 3.15). The Upper Pousterle Thrust bifurcates southeastwards into several thrust faults and a ~30 m thick *mélange* zone (Fig. 3.12). Fault kinematic data give NW-directed thrusting (Fig. 3.15e). On the western slope of La Pousterle the southern part of the Upper Pousterle Imbricate consists of overturned non-volcanic turbidites steeply southeast-dipping which to the north are in tectonic contact (the Lamiande Thrust₂) with Middle Jurassic black shales and marls (j2-4) of indeterminable dip (Fig. 3.12). The Lamiande Thrust₂, marked by Nummulitic Limestone blocks is cut by the late low-angle Upper Pousterle Thrust below. Therefore the Lamiande Thrust₂ is an old fault pre-dating the emplacement of the Upper Pousterle Imbricate.

Within the peak, Lamiande Thrust₃ along a thin strip of Middle Jurassic black shales (j2-4) separates two blocks of overturned southeast-dipping Champsaur Sandstone. These units describe a minor northwest-facing syncline (Figs. 3.12 & 3.15) and tectonically overlie Middle Jurassic sediments.

In the eastern slope of La Pousterle (Fig. 3.17) the Middle Jurassic sediments north of the Lamiande Thrust₂ narrow to a thin strip. Adjacent to the north underneath the peak lies a wedge-shaped highly tectonized zone with large blocks of Nummulitic Limestone and several lenses of Champsaur Sandstone and Jurassic shales (Figs. 3.13 & 3.17). There is no evidence for folding in the eastern side of the peak.

The relation between the structures seen on the western and eastern slopes is unclear. All major faults are marked by aligned blocks of Nummulitic Limestone (Fig. 3.12). In general fault kinematic data from within The Upper Pousterle Imbricate do not give any resolvable pattern (Fig. 3.15a). But the projection of poles to bedding gives a broad girdle distribution with a corresponding NE-SW trending π -axis (234-05; Fig. 3.12c)

which again indicates a SE–NW directed shortening. However, minor folds may deviate from this general direction (Fig. 3.12b).

In the peak of La Prouveyrat Champsaur Sandstone tectonically overlies Mesozoic rocks (Fig. 3.6). They are interpreted to be a small tectonic outlier of the Upper Pousterle Imbricate (Fig. 3.10). Underneath, right way-up Nummulitic Limestone and Globigerina Marl of the Lower Pousterle Imbricate tectonically overlie the allochthonous sandstone sheet. They are the northern continuation of the lower normal limb of the Pousterle Syncline. The overturned limb is cut off by the Upper Pousterle Thrust.

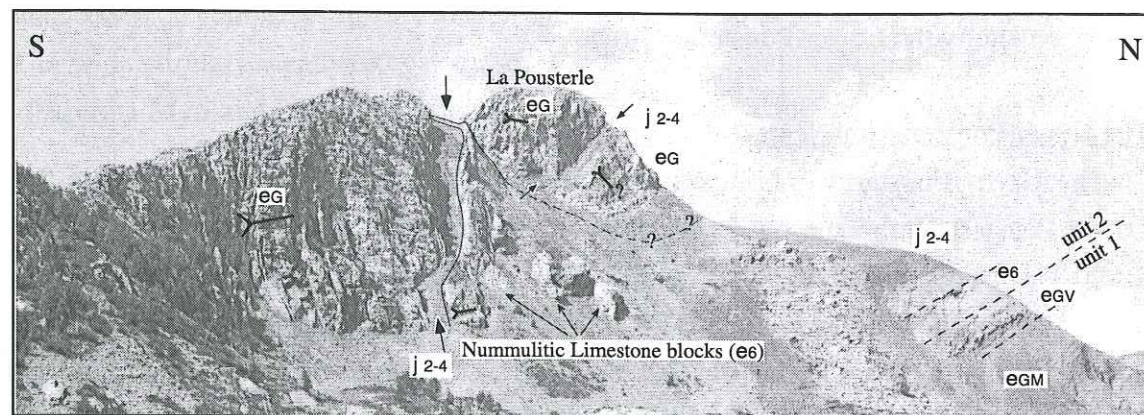


Fig. 3.17: View towards W at la Prouveyrat (Upper Pousterle Imbricate). Subvertical Champsaur Sandstone (eG), younging north, is in tectonic contact with thin Jurassic black shales and marls (j2-4). The Jurassic ribbon (marked by arrows) is slightly offset in the lower third. Adjacent to the north lies a wedge-shaped assemblage of Champsaur Sandstone, Nummulitic Limestone (e6) and Jurassic sediments. These rocks are tectonically broken up and imbricated in a very complex way. In the hangingwall of this zone, in the Pousterle peak, two large blocks of overturned Champsaur Sandstone are separated by a thin strip of Jurassic black shales (marked by arrows). Further north the contact between unit 1 and unit 2 crops out. This view is localized on the detailed geologic map Fig. 3.13.

Discussion

To summarise, the Pousterle Imbricates document at least three different stages of deformation (Fig. 3.18):

- 1) The normal stratigraphic sequence was doubled by the Lamiande Thrusts₁₋₃ (Fig. 3.15): when the Pousterle Syncline is unfolded it becomes clear that early thrusting on the Lamiande Thrust₁ brought Upper Jurassic limestones and their Tertiary cover over the Champsaur Sandstone (Figs. 3.12 & 3.18a). In the Upper Pousterle Imbricate the hangingwall stratigraphy varies from tens of meters of Mesozoic sediments (Lamiande Thrust₂) to very thin Mesozoic sediments directly overlain by Champsaur Sandstone (Lamiande Thrust₃) (Figs. 3.12 & 3.16). The Lamiande Thrusts₁₋₃ are interpreted as different segments of a single early thrust

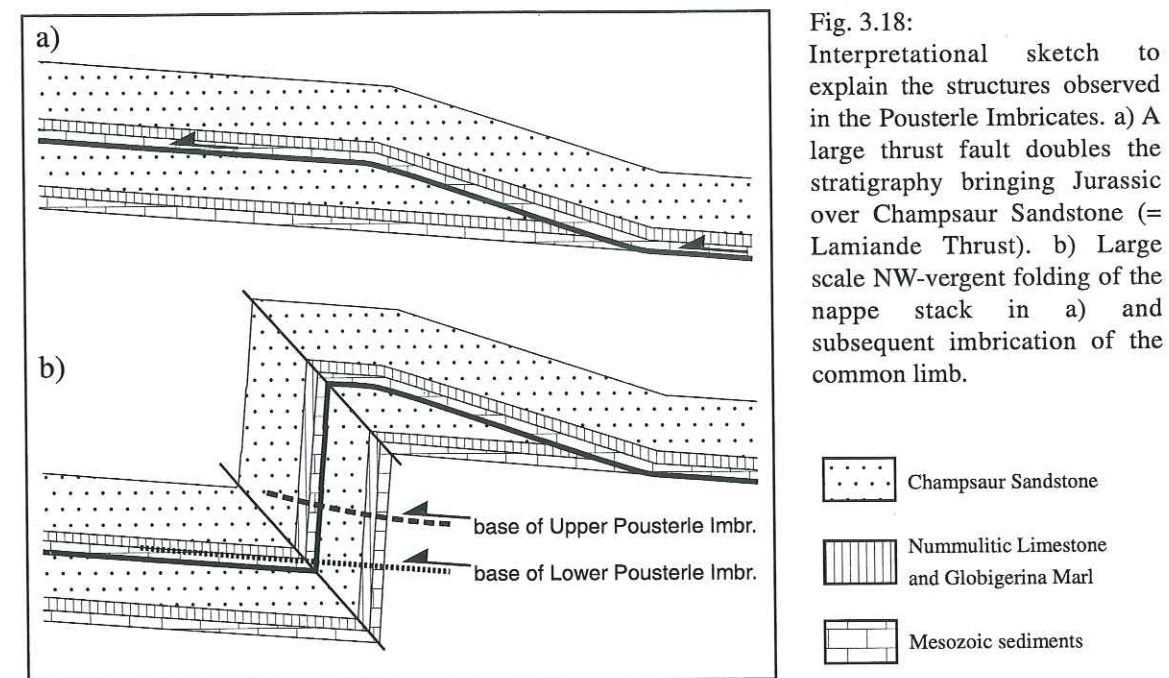


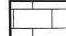


Fig. 3.18:

Interpretational sketch to explain the structures observed in the Pousterle Imbricates. a) A large thrust fault doubles the stratigraphy bringing Jurassic over Champsaur Sandstone (= Lamiande Thrust). b) Large scale NW-vergent folding of the nappe stack in a) and subsequent imbrication of the common limb.

-  Champsaur Sandstone
-  Nummulitic Limestone and Globigerina Marl
-  Mesozoic sediments

which carried the Mesozoic to Tertiary sequence over Champsaur Sandstone (Fig. 3.18a). The Lamiande Thrust accommodated significant displacement.

- 2) A large-scale NW-vergent asymmetric fold-pair developed as demonstrated by the synclines described above (Fig. 3.18b). The stratigraphy in the short limb (including the Lamiande Thrust) rotated to steep dips.
- 3) Subsequently low angle thrusts (Lower and Upper Pousterle Thrust) cut through the common limb of this large fold pair and sliced it up to imbricates (Fig. 3.18b).

3.3.3 Imbricated upright sequences

The remaining imbricates are largely in upright position. They are divided into the Palastre-Venasque Thrust Sheet in the western part of the Soleil Boeuf klippen zone and the Bonne Herbe Imbricates to the south of the Pousterle Imbricates (Fig. 3.10).

Palastre-Venasque Thrust Sheet

The geometry of the Palastre-Venasque Thrust Sheet is relatively simple (Fig. 3.19): the autochthon containing the Palastre Thrust is directly overlain by upright Mesozoic sediments and Nummulitic Limestone dipping shallowly to the north (Fig. 3.6). This normal stratigraphic sequence continues in the Soleil Boeuf peak and terminates around Pointe Sud de la Venasque in a major frontal anticlinal closure (π -pole 053-04; Fig. 3.19). It is in this part of the profile where we meet again all three Tertiary formations in a vertical to overturned position in the core of a major recumbent anticline. The anticline

was thrust over the allochthonous sandstone unit of Pointe Nord de la Venasque.

Southeast of the Soleil Boeuf peak the tectonic contact between autochthonous Champsaur Sandstone and allochthonous Upper Jurassic limestones is a ~1.5 m thick cataclastic shear zone (Fig. 3.20). Shear veins with NW–SE-trending fibre lineations are predominant. Slicken-fibres indicate a top to the NW movement. The sigmoidal shape of cm-large limestone and sandstone clasts confirm the top to the NW movement. Other fault striae on slickensides trend NNE–SSW (Fig. 3.20b), they indicate a minor SW displacement and are very rare.

The Palastre-Venasque Thrust Sheet laterally truncates the Palastre Thrust. Deformation in the autochthon therefore predates the emplacement of the allochthons. To the east the Palastre-Venasque Thrust Sheet overlies the eastern allochthonous sandstone sheet (Fig. 3.10) and lies therefore at the same tectonic level as the Pousterle Imbricates further east. The lateral relationship to the Pousterle Imbricates is problematic (see below).

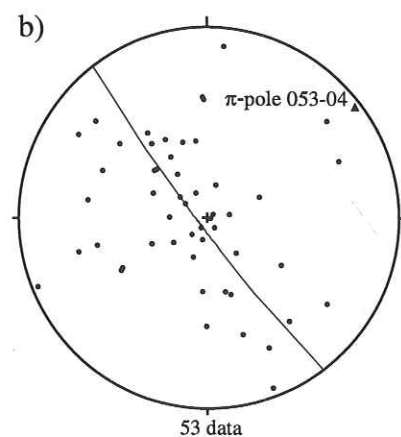
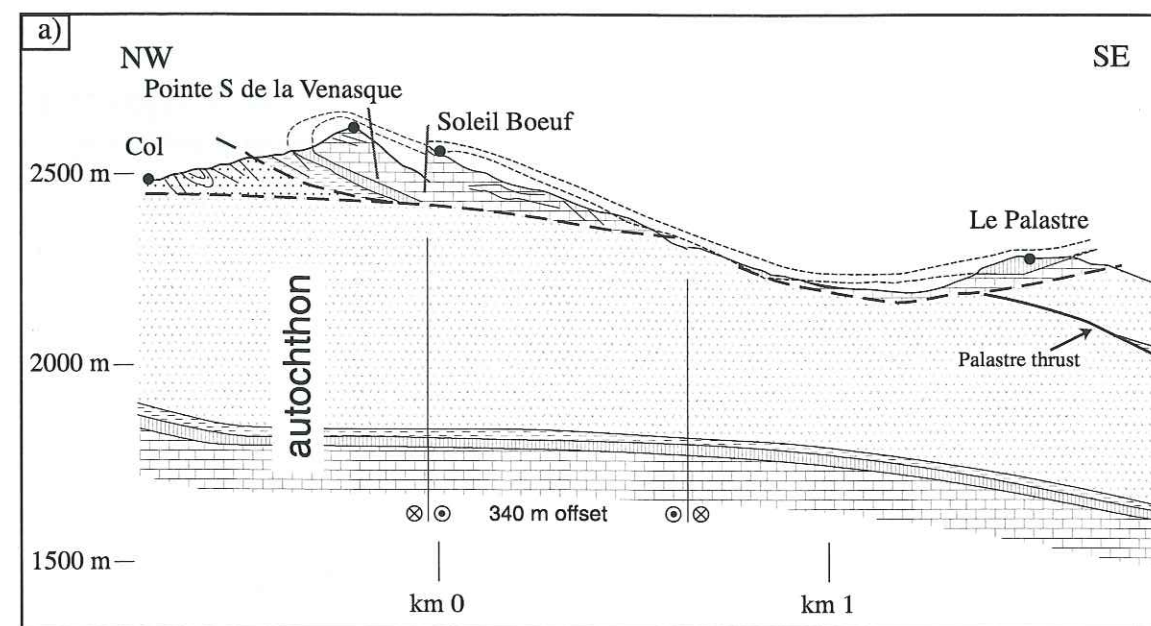


Fig. 3.19: a) Schematic profile through the Palastre-Venasque Thrust Sheet. The profile trace is located in Fig. 3.10, note the offset in the middle part. The hangingwall of the Palastre thrust is cut-off by this thrust sheet. The anticlinal closure to the NW is offset by steep normal faults. A footwall shortcut thrust caused the development of the small allochthonous sandstone sheet (same key as Fig. 3.13). b) Lower hemisphere, equal area projection of poles to bedding associated with the anticlines at Pointe S de la Venasque and Soleil Boeuf.

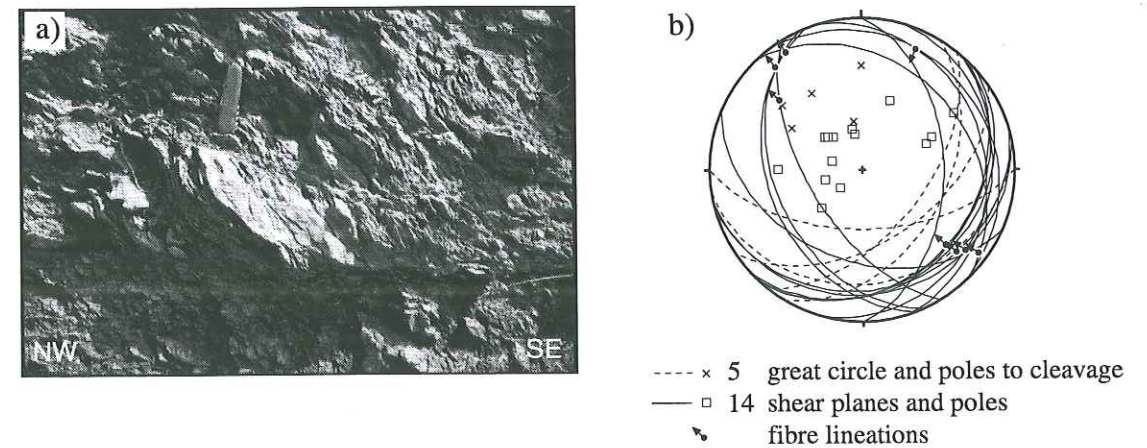


Fig. 3.20: a) Detail from cataclastic shear zone (pocket knife for scale). Sigmoidal clasts give top to the NW sense of shear. b) Equal area lower hemisphere stereoplot summarizing measured shear planes and cleavages from the base of the Palastre-Venasque Thrust Sheet.

Bonne Herbe Imbricates

The Bonne Herbe imbricates consist of three thrust sheets (Figs. 3.6 & 3.10). The normal stratigraphic sequence of the lowest thrust sheet 1, comprises Mesozoic sediments, Nummulitic Limestone and Globigerina Marl (Fig. 3.12). The Bonnets Fault is the tectonic contact to the overturned Champsaur Sandstone in the Lower Pousterle Imbricate to the north (Figs. 3.12 & 15). Fault kinematic data from within the fault zone indicate that it acted predominantly as a normal fault, (M. Ford pers. comm.). Therefore the Bonnets Fault is very important, because it displaced the upright Bonne Herbe Imbricates at least 400 m down against the largely overturned Lower Pousterle Imbricate (Fig. 3.15). Along the tectonic contact to the allochthonous sandstone sheet below, the displacement data on minor faults give predominant NW-directed low-angle thrusting (Fig. 3.15d). Minor N–S-trending dextral strike-slip faulting affects this contact (Fig. 3.15g) whereas, further north E–W-trending dextral strike-slip faults offset bedding (Fig. 3.15f). But these strike-slip structures are minor and clearly post-date the thrust sheet emplacement.

To the south, the Globigerina Marl is overthrust by Middle Jurassic black shales and marls (j2-4) of thrust sheet 2 (Fig. 3.12). The fault zone contains numerous fragments of Nummulitic Limestone. Two sets of minor faults occur within the contact zone: NW-directed low-angle thrusts and dextral strike-slip faults, both record NW-directed compression (Fig. 3.15c & d).

The Middle Jurassic black shales and marls are tectonically overlain by older marly limestones (j1-2). Nummulitic Limestone boulders aligned within the contact zone demonstrate again the tectonic origin and Tertiary age of this thrust sheet 3 (Figs. 3.6 & 3.10) which includes Nummulitic Limestone, Globigerina Marl and Champsaur

Sandstone of non-volcanic facies (Debelmas *et al.*, 1980).

Discussion

Fig. 3.21 depicts schematically the structures in the imbricated upright sequences. The Palastre-Venasque Thrust Sheet is a large thrust sheet with a leading anticline. It immediately overlies the autochthon which gives a minimum displacement of 5 km. In the frontal part the Palastre-Venasque Thrust branches off the Basal Thrust and overthrusts the allochthonous sandstone unit of Pointe Nord de la Venasque (Fig. 3.21a). The continuation of the Basal Thrust underneath the allochthonous sandstone unit of Pointe Nord de la Venasque is interpreted as a footwall shortcut. The correlation of the Palastre-Venasque Thrust Sheet with the more complex imbricate stack to the east will be discussed later. However, the eastern allochthonous sandstone sheet is too large to be interpreted as a footwall shortcut to the Palastre-Venasque Thrust (Fig. 3.10).

The Bonne Herbe Imbricates consist of three individual thrust sheets which must be treated as a separate unit. The main feature is the normal displacement on the Bonnets Fault which juxtaposes largely overturned sequences to the north (Lower and Upper Pousterle Imbricates) against the upright Bonne Herbe Imbricates. The Bonnets Fault is inferred to post-date the thrust sheet stacking and it probably roots along the Basal Thrust where it flattens out which means that the movement on the Basal Thrust was inverted.

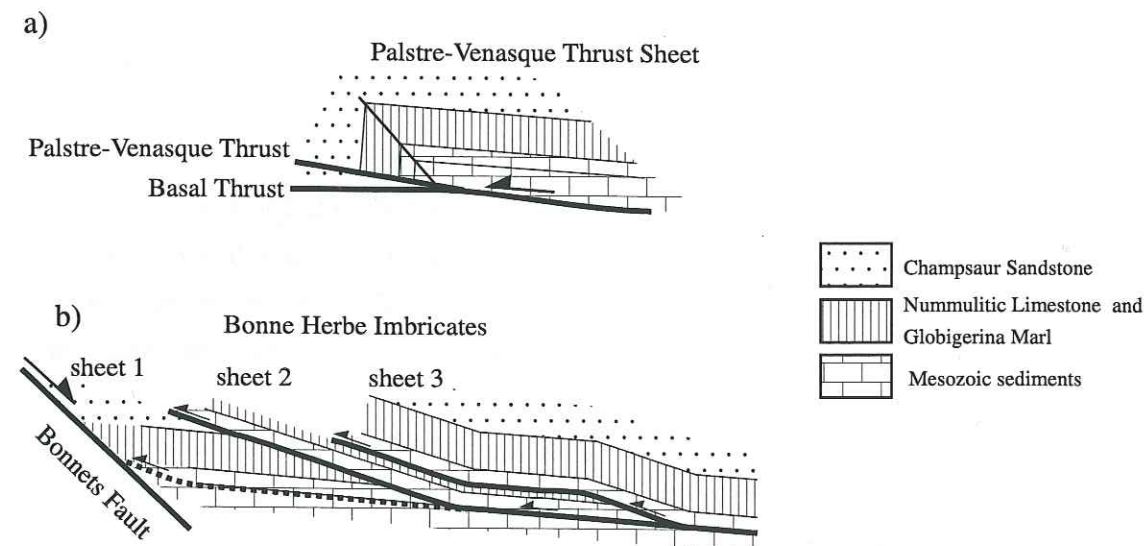


Fig. 3.21: Interpretational sketch to summarize the structures observed in the imbricated upright sequences. a) The anticlinal closure of the Palastre-Venasque Thrust Sheet with a footwall shortcut. b) A normal fault bounds to the left the Bonnes Herbes Imbricates. The relation between a) and b) is unclear. For further discussion see text.

3.4 Burial and exhumation history of the Soleil Boeuf area

The only data constraining the thermal history of the region until now is the occurrence of prehnite-pumpellyite grade metamorphism in the Champsaur Sandstone which indicates a burial to at least $170 \pm 10^\circ\text{C}$ (Martini and Vuagnat, 1965; Waibel, 1990). As part of a larger project three samples from the Soleil Boeuf area have been dated by the fission-track technique (Seward *et al.*, submitted). All samples come from the Champsaur Sandstone (Fig. 3.22a).

The one zircon age (159 ± 40 Ma, error is 2σ) is much older than the depositional age of the host formation, indicating that there has been no significant annealing. The burial temperature of the Champsaur Sandstone was therefore not over $200 \pm 10^\circ\text{C}$.

The three apatite ages range between 6 and 15 Ma with very large error margins. All samples have been exposed to temperatures in excess of $120 \pm 10^\circ\text{C}$ (generic algorithm modelling confirm burial $> 120 \pm 10^\circ\text{C}$; D. Seward pers. comm.). The data show a rough age-altitude correlation (Fig. 3.22b). Samples 94/9f and 94/33b are similar in altitudes but with variable ages (which do overlap statistically). They give exhumation rates of about 0.1 mm/y to 0.05 mm/y.

These data bracket the metamorphism between $> 120 \pm 10^\circ\text{C}$ and $< 200 \pm 10^\circ\text{C}$ which is in agreement with Waibel (1990). Assuming a geothermal gradient of $25 \pm 5^\circ\text{C}/\text{km}$ the Soleil Boeuf area was buried to least 5 km but no more than 8 km. As the samples have been exposed to temperatures above $120 \pm 10^\circ\text{C}$ the fission tracks contain no information about the burial history. But modelling gives evidence that the samples passed below depths equivalent to $120 \pm 10^\circ\text{C}$ around at 10 Ma, hence exhumation started prior to that.

3.5 Interpretation and discussion

When comparing structures from the autochthon with structures from the different allochthonous units described above it becomes clear that they all show a similar style of NW-vergent asymmetric folding and thrusting. Using the best documented and most complex profile through the Pousterle peak as a model, a 5 stage evolution of the nappe stack in the eastern part of the Soleil Boeuf area is proposed. The applicability of this model for the whole Soleil Boeuf area will be discussed.

3.5.1 Interpretation of the Pousterle profile

Fig. 3.23 presents in sequential steps the evolution of the Pousterle profile. This model involves 1) thrusting of Mesozoic and Tertiary rocks over the autochthonous Tertiary succession 2) the formation of a large asymmetric, NW-verging fault-propagation fold ahead of a thrust, 3) breakthrough faults dissecting the common steep limb, 4) N-S extension along normal Bonnets Fault and 5) late normal displacements on NE-SW trending Selle-Fault zone.

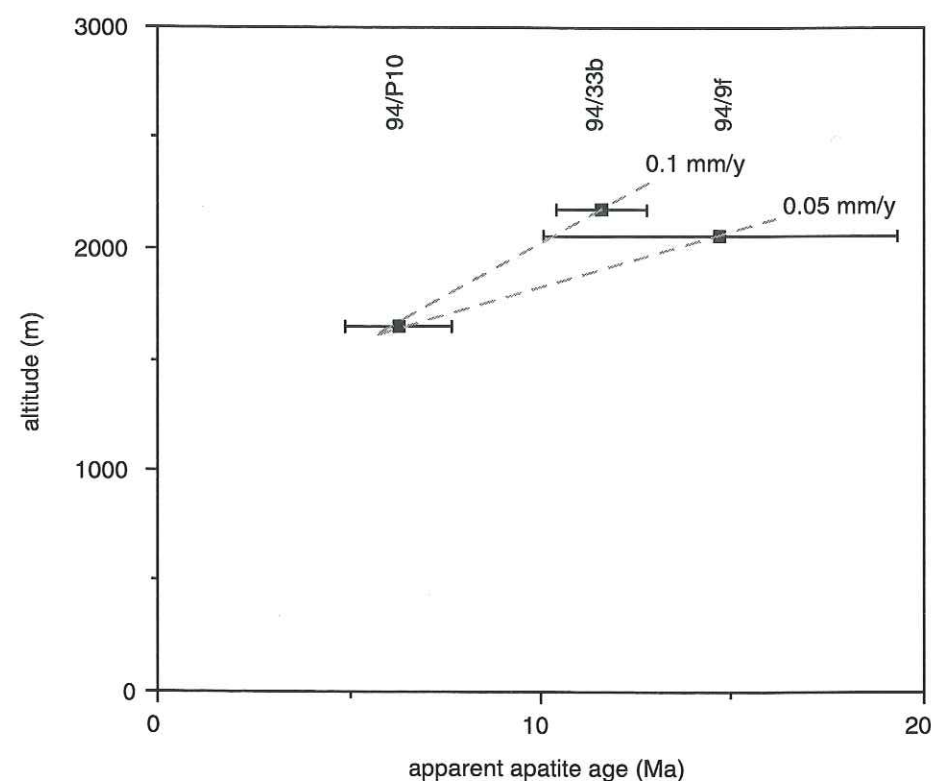
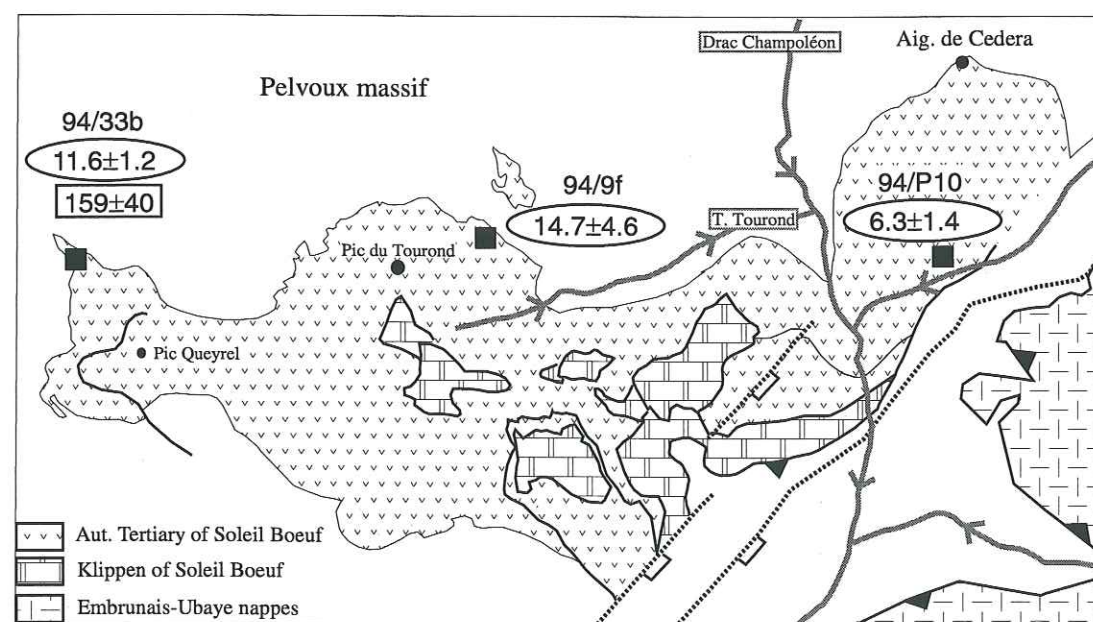


Fig. 3.22: Age-altitude plot and simplified map of Soleil Boeuf area for apatite fission-track ages from Tertiary Champsaur Sandstone. Apatite ages shown within ellipses and zircon ages within rectangles.



Step 1 (Fig. 3.23a): Sometime after the mid-Oligocene an imbricate thrust system formed an array of overlapping thrusts branching from within the Mesozoic sediments. The early doubling of Tertiary and Mesozoic sediments in the Pousterle Imbricates by the Lamiande Thrust and the thrust sheets of the Bonne Herbe imbricates (Fig. 3.15) are preserved remnants of this early imbrication. Shortening estimates are difficult: a minimum of 2 km is reasonable for the Lamiande Thrust whereas shortening on the Bonne Herbe Imbricates can be several hundred meters or much more. The direction of thrusting is probably towards the NW, but no kinematic data are available because all outcrop of such early contacts were overprinted by later motions.

Step 2 (Fig. 3.23b): A deeper ramp in the footwall of this imbricated thrust system propagated towards the NW, and the overlying imbricate stack was folded as part of the hangingwall tectonic stratigraphy in a major NW facing asymmetric fault-propagation fold pair with an amplitude of 1 - 2 km. This fold pair is necessary to obtain the overturned sequences in the Pousterle peak (the Lower and Upper Pousterle Imbricates and in the eastern allochthonous sandstone sheet) (Figs. 3.12 & 15) where part of the synclinal closure (Pousterle Syncline) can be observed. A minimum solution requires at least 700 m of shortening during folding.

Step 3 (Fig. 3.23c-e): low-angle breakthrough thrusts cut the common limb of the fault-propagation fold and dismembered earlier structures. They pushed the allochthonous sandstone sheet, the Lower Pousterle Imbricate and the Upper Pousterle Imbricate towards the NW onto the undisturbed foreland (autochthon of Soleil Boeuf). Nearly all collected fault kinematic data record this stage of deformation (Fig. 3.15), they show ubiquitous NW-directed thrusting. Minimum thrust displacements are ~1.8 km, ~0.5 km and ~1.8 km for the three individual imbricates, which gives a total of 4.1 km shortening.

Step 4 (Fig. 3.23f): the Bonnets Fault cut through the imbricate stack and dropped the upper normal limb of the anticline containing the Bonne Herbe Imbricates about 800 m down to the south so that it was juxtaposed against the overturned limb in the footwall. In Fig. 3.23(f) the corresponding displacement is ~1 km (heave ~600 m, throw ~800 m). This fault is shown to merge with the Basal Thrust at depth.

Step 5 (Fig. 3.23g) Late displacements on the Selle-Fault zone are distributed over three major normal faults. The total downthrow to the south is ~870 m. This movement is probably related to late differential uplift of the Pelvoux massif.

With this model a total shortening of 6.8 km is required for the Pousterle profile, not taking account of the early thrust sheets in the Bonne Herbe Imbricates. This is a minimum solution for the main features observed in the field. Complex structures may

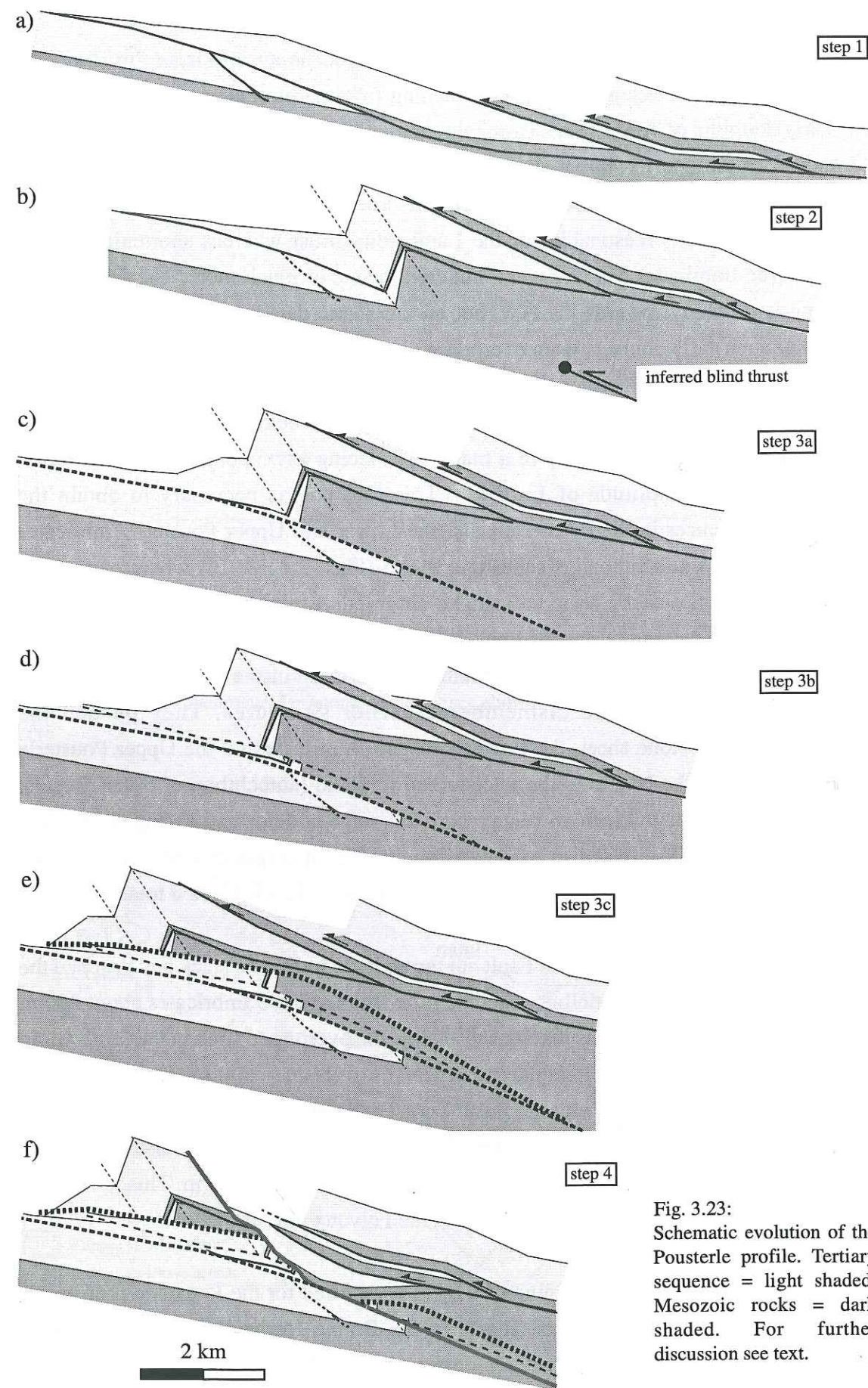


Fig. 3.23: Schematic evolution of the Pousterle profile. Tertiary sequence = light shaded, Mesozoic rocks = dark shaded. For further discussion see text.

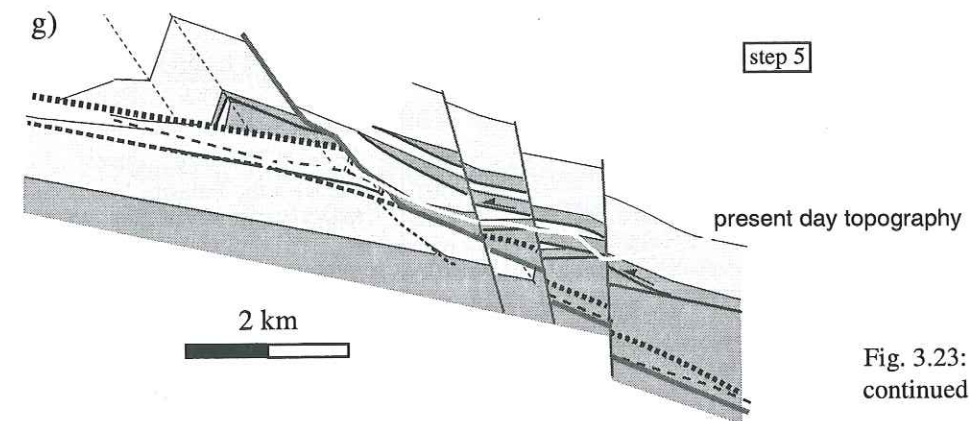


Fig. 3.23: continued

require more than one larger-scale fold. For example the fact that the syncline in the allochthonous sandstone sheet has been displaced further NW than the Pousterle syncline in the overlying Lower Pousterle Imbricate: this implies that either the Lower Pousterle Imbricate has been somehow displaced at least 300 m southeastwards opposite to the main structural trend or the two synclines can not be part of the same large syncline. Another point is the rapidly varying hangingwall stratigraphy of the early Lamiande Thrusts₁₋₃ in the dismembered common fault-propagation fold limb. It could be better explained to be different portions of more than one larger-scale fold. This would increase the total amount of shortening

3.5.2 Applicability of model to the whole Soleil Boeuf area

The footwall syncline of the fault-propagation fold pair (step 2) can be correlated with the Méollion and Estang Synclines in the autochthon (Figs. 3.7 & 3.9). These large synclines affected the entire Tertiary sequence and were subsequently cut by thrusts. Such a correlation constrains the original position of the fault-propagation fold pair to lie immediately SE of the Soleil Boeuf klippen zone. Therefore the minimum shortening estimates from the Pousterle profile (Fig. 3.23) probably do not significantly underestimate the real amounts of shortening.

The Palastre-Venasque Thrust Sheet in the western part of the Soleil Boeuf klippen zone may represent the highest and furthest travelled of the imbricates (step 3) in the Pousterle profile (Fig. 3.23e). In this model this imbricate, which has been eroded in the Pousterle profile, is therefore inferred to cut-down westwards so that it directly overlies the autochthon in the western part of the Soleil Boeuf klippen zone (Fig. 3.24). This requires a major lateral ramp to accommodate the different amounts of displacement. Unfortunately, the allochthonous units are eroded from the proposed lateral ramp zone and the model cannot be tested.

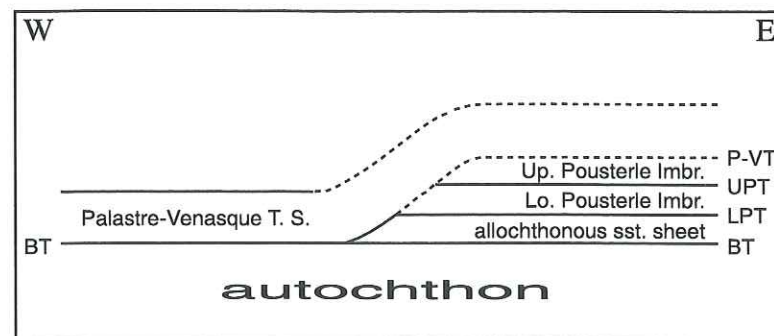


Fig. 3.24: Schematic longitudinal W-E section. The Pousterle Imbricates branch onto the Palastre-Venasque Thrust. To the west the Palastre-Venasque Thrust cuts down section and becomes the Basal Thrust where it directly overlies the autochthon. Dashed line = inferred, BT = Basal Thrust, LPT & UPT = Lower and Upper Pousterle Thrust, P-VT = Palastre-Venasque Thrust.

Another solution is to propose lateral variations along the structural trends of the Soleil Boeuf area. In the autochthon, the shortening in the Méollion zone is accommodated by km-scale folding and thrusting whereas in the Queyrel zone, to the west, structures are smaller with a lesser amount of shortening. A similar westward decrease of the amount of shortening may also occur in the allochthonous units. The complex structures in the eastern part of the Soleil Boeuf klippen zone and the more simple structures in the western part can be related to along-strike variations in fold and thrust geometry (Fischer and Woodward, 1990). However, such lateral variations in deformational style also require transfer zones.

In general the proposed model for the Pousterle profile does apply to the deformation in the whole Soleil Boeuf area, which therefore can be described as a simple deformation history of NW-directed thrusting and fault-propagation folding. The few SW-directed kinematic indicators recorded in the Queyrel Thrust and Palastre-Venasque Thrust zones (Figs. 3.4e & 3.20b) are of very minor importance and cannot be related to large-scale structures in the Soleil Boeuf area. The relative timing between these minor SW-directed structures and the NW-directed deformation remains unclear from the field data. Hence the NW-directed deformation is the only major deformation event in Soleil Boeuf and it must be largely responsible for the 5 - 8 km overburden recorded by the fission track data. I therefore have assumed that the NW-directed thrusts carried in their hangingwall a nappe pile several km thick. The NW-directed deformation roots down to a deeper detachment in the Mesozoic cover underneath the Tertiary foreland basin sequence to the southeast which is overlain by the Embrunais-Ubaye nappes (Fig. 3.1). It is therefore reasonable to assume that the NW-directed deformation carried not only the Tertiary sequence but also the overlying Embrunais-Ubaye nappes onto the Soleil Boeuf area. As a consequence the NW-directed deformation post-dates the SW-directed emplacement of the Embrunais-Ubaye nappes (for further discussion see Chapter 4).

3.5.3 Discussion of previous work

Gidon and Pairis (1980-1981) is the only modern published paper on the structures and kinematics within the Soleil Boeuf area. Their few data and their interpretations differ in several points from the results of this study. Gidon and Pairis suggested that the deformation of Soleil Boeuf results from a polyphase deformation comprising WNW-directed overthrusting of the allochthonous units, overprinted by northward motions which also affected the autochthonous substrate.

Gidon and Pairis (1980-1981) proposed WNW-directed overthrusting of all the allochthonous units based on minor structures at the base of the Palastre-Venasque Thrust Sheet and the orientation of its leading anticline. But as shown in Figs. 3.20 & 3.19 and discussed in the text, the Palastre-Venasque Thrust Sheet was emplaced towards the NW. Additionally this study presents more detailed data from the other klippen (Figs. 3.11, 3.12, 3.15, 3.16) which confirm the NW-directed emplacement.

Gidon and Pairis (1980-1981) proposed a second phase of N-directed compression assuming a) that the Palastre Thrust links to the Upper Pousterle Thrust which cuts through previously stacked allochthonous units and assuming b) N-directed compression from the orientation of the Queyrel Thrust and the Palastre Thrust fault planes and from the trend in strike of the overturned limb of the Pousterle Syncline without presenting any additional data. But my data clearly show that a) the Palastre Thrust is truncated by the allochthonous units (Fig. 3.19) and b) all these structures are related to NW-directed compression (Figs. 3.4, 3.9, 3.12 & 3.15).

In summary this study does not corroborate a two-phase deformation. The deformation is better explained as a continuous evolution of simultaneous thrusting and folding towards the NW.

3.5.4 Summary

Although the Soleil Boeuf area and especially the Soleil Boeuf klippen zone show a wide variety of complex structures the data can be explained by a simple deformation history which comprises early thrusting (probably NW-directed) followed by NW-directed fault-propagation folding and thrusting.

4. Significance of new data for the evolution of the western Alpine arc

4.1 The relationship between the Soleil Boeuf area and the Champsaur-Prapic fold zone

4.1.1 *Spatial relationship*

How are the late Alpine deformation histories of the Champsaur-Prapic fold zone and the Soleil Boeuf area related? Fission track data indicate that both areas were buried to between 5 and 8 km and underwent a similar exhumation history. As demonstrated in Chapter 3 the autochthonous Soleil Boeuf Tertiary sequence with the volcanoclastic Champsaur Sandstone is thrust over by Champsaur Sandstone of non-volcanic facies similar to that of the Champsaur-Prapic fold zone. The highest klippe is therefore correlated southeastward across the Selle-Fault zone to the south-westernmost part of the Prapic fold zone (Figs. 3.1 & 3.23). Fig. 4.1 shows schematically the spatial relationship of the different units.

Southeast of the Selle-Fault lies the Champsaur-Prapic fold zone with WSW-directed chevron-like folds. As documented in Chapter 2 this deformation is characterised by decreasing deformation towards the southwest and has been related to overthrust shear induced by the overriding internal nappes. The Orcières anticline then lowers the Tertiary sequence to the west by roughly 1 km and further southwest no major deformation occurs within the Tertiary sequence (Fig. 2.7). To the northwest of the Selle-Fault in the Soleil Boeuf area the klippen record early thrusting of non-volcanic Champsaur Sandstone and Jurassic strata over the autochthonous Tertiary sequence containing volcanic detritus, followed by NW-directed folding and thrusting. This second stage is characterised by large-scale fault-propagation folding preceding thrusting (Fig. 3.23). Hence the northwestern continuation of the sediments in the Prapic fold zone was in the hangingwall of the klippen in the Soleil Boeuf area and the main faults in Soleil Boeuf root below the Prapic fold zone where they probably ramp from a single detachment surface in Jurassic marls. This means that the Champsaur-Prapic fold zone was thrust toward NW over the Soleil Boeuf area. Later activity on the Selle-Fault zone, probably related to the uplift of the Pelvoux massif, dropped the Champsaur-Prapic fold zone down to the south and thus juxtaposed the upper limb of the Soleil Boeuf fault-propagation fold pair against the autochthon in the Soleil Boeuf area to the north (Fig. 4.1).

The Selle-Fault zone today appears to separate two areas of different foreland basin facies (Fig. 4.1). The variable amounts of volcanic detritus in the Champsaur Sandstone must be related to different source areas which supplied the Alpine foreland basin. A palaeogeographic reconstruction is difficult (Waibel, 1990) and the original distance

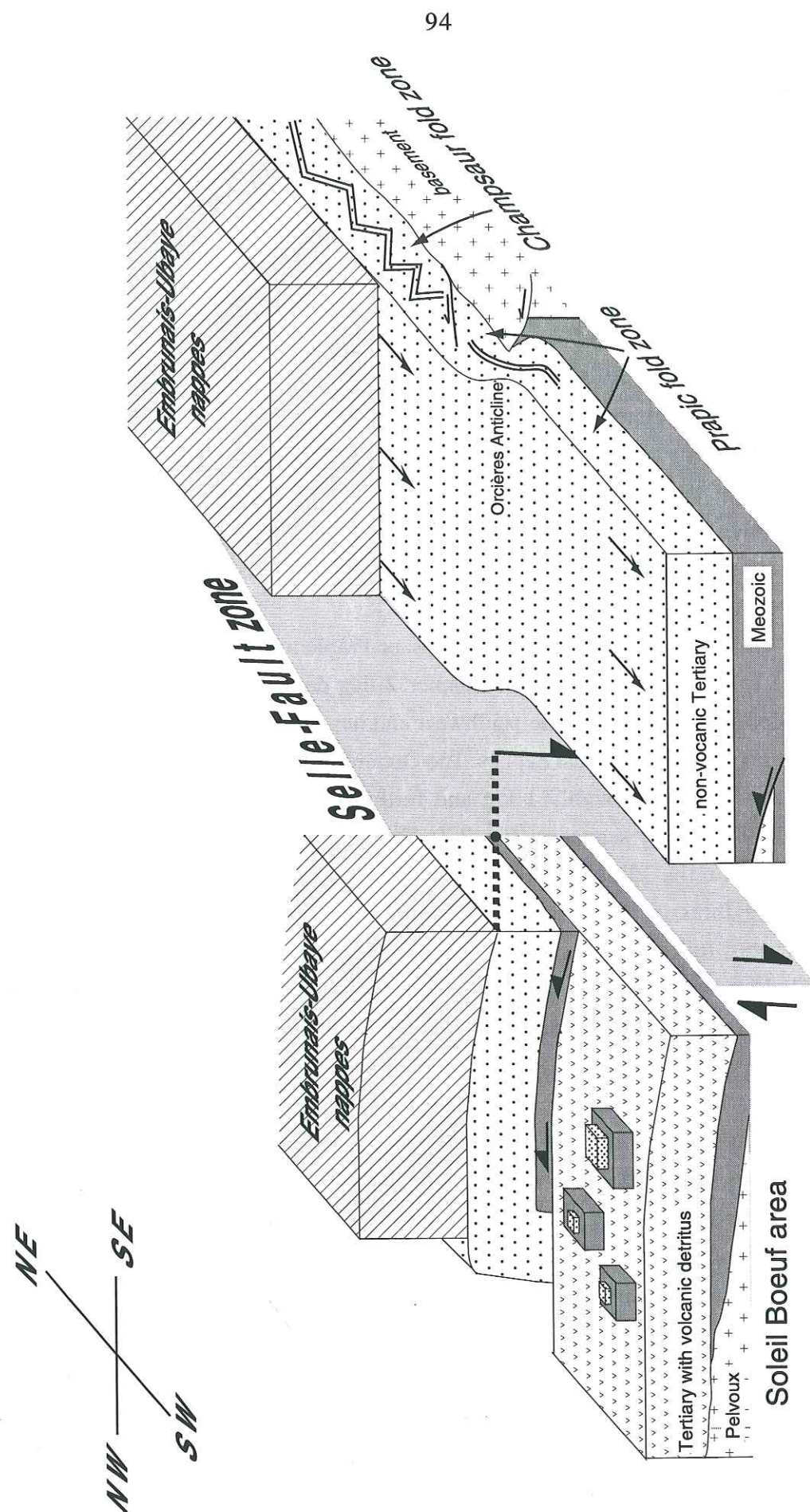


Fig. 4.1: Schematic block model showing the geometric relationship between the Champsaur-Prapic fold zone and the Soleil Boeuf area.

between these two different depositional realms is unknown. However, a minimum estimate can be derived from the shortening within the Soleil Boeuf area. With their variable amounts of volcanoclastic debris (Waibel, 1990), the Champsaur Sandstone fragments in the allochthons of Soleil Boeuf probably derive from the transitional facies zone. The lower imbricates are similar to the autochthonous Champsaur Sandstone rich in volcanic debris whereas the highest imbricates are closely related to the Champsaur Sandstone from the Prapic fold zone without volcanic debris (Waibel, 1990). The 6.8 km minimum shortening estimate from restoration of the Pousterle profile is thus a minimum estimate of the original distance between the two depocentres.

4.1.2 Influence of variable substrate to deformational style

The detailed structural analysis of the two areas document two completely different deformation styles: meso-scale chevron-like folding in the Champsaur-Prapic fold zone (Chapter 2) and large-scale fault-propagation folding and thrusting in Soleil Boeuf (Chapter 3). This must be at least partly related to the variable substrate because the thickness and mechanical stratigraphy of the overlying Tertiary foreland basin succession are approximately the same in both areas. In the Champsaur fold zone and the northern part of the Prapic fold zone the Tertiary sediments transgressed directly onto basement rocks whereas in the southern part of the Prapic fold zone and in most of the Soleil Boeuf area the Tertiary sediments are underlain by several hundred meters thick Mesozoic sediments (Ménard, 1979; Debelmas *et al.*, 1980; Debrand-Passard *et al.*, 1984a; Ravenne *et al.*, 1987) (Fig. 4.1). In Soleil Boeuf the northern rim overlies basement rocks (Figs. 3.1 & 3.2c).

It has been argued, that the overall style of deformation in the northern Subalpine chains is thin-skinned with a detachment between basement and cover, and thrust ramps branching at irregularities in the detachment surface (Butler, 1989). A similar behaviour can be observed in the southern Subalpine chains where the main detachment is again within the Triassic evaporite horizon (basement-cover interface). Displacement ramps up to minor detachments in Mesozoic shale levels (Lickorish and Ford, 1998). Towards the north-east, the basement-cover interface and overlying Mesozoic cover were locally folded during early uplift of the Pelvoux massif (Ford, 1996) Thus the basement-cover interface rises abruptly north of Barcelonnette (Fig. 1.7). Furthermore the Triassic evaporite horizon, the main detachment horizon, was not deposited or was eroded in the Pelvoux massif area (Debrand-Passard *et al.*, 1984a: p. 84; Lemoine *et al.*, 1986). This must have forced the main detachment to cut up-section at some distance south of the Pelvoux massif. In the Champsaur-Prapic fold zone the cover is detached within the Globigerina Marl a few meters above basement. The deformed stratigraphic pile is much thinner and is therefore characterised by thin-skinned 'duplex-like' deformation.

4.1.3 Relative timing of NW motion in Soleil Boeuf and SW transport in Champsaur-Prapic

In the Champsaur-Prapic fold zone, SW-WSW-directed shortening of 5 km was mainly accommodated by mesoscale chevron folding in the footwall of the Autapie nappe and Sub-briançonnais unit. In the Soleil Boeuf klippen area at least 6.8 km NW-directed shortening by fault-propagation folding and thrusting occurred in the footwall of the Prapic fold zone. Although no structural interference patterns were observed in the investigated area, the relative timing can be inferred: for several reasons the WSW-SW-directed deformation pre-dates the NW-directed thrusting in Soleil Boeuf.

- 1) The deposition of the Champsaur Sandstone ceased abruptly with the emplacement of the Schistes à Blocs, a tectono-sedimentary mélange in front of the advancing nappes (Kerckhove, 1969). Kinematic data from within the Schistes à Blocs indicate WSW-directed thrusting (Fig. 2.7).
- 2) The subsequent thrusting of the lower Embrunais-Ubaye nappes (Autapie nappe and Sub-briançonnais units) immediately followed the deposition of the Schistes à Blocs; and these units were deformed during their emplacement (and later) together with the external cover (Kerckhove, 1969; Debelmas and Kerckhove, 1973) (Fig. 4.2). Kinematic data indicate that these nappes were also emplaced towards the SW onto the external domain (Tricart, 1980; Fry, 1989). The close association of the Champsaur-Prapic deformation with the emplacement of these internally derived nappes is the strongest evidence that the SW-directed motion was first and was the principle regional deformation south of the Pelvoux massif.

If the NW-directed thrusting and fault-propagation folding were first, it had either to occur extremely rapidly during the very last stages of Champsaur Sandstone deposition, or at a reasonable deformation rate combined with growth structures during most of the deposition of the Champsaur Sandstone. Field observations do not support both of these hypotheses. So, there was no time for a first NW-directed deformation phase between the final deposits of the Champsaur Sandstone and the SW-directed emplacement of the internally derived nappes.

- 3) Additionally, as presented in Chapter 2, the WNW-directed deformation in Chambran (the northern end of the Champsaur fold zone) post-dates the WSW-SW-directed deformation.

Merle and Brun (1984) proposed that the upper part of the Embrunais-Ubaye nappes (Parpaillon nappe) had a continuous curved translation path: large-scale folding towards the NW was immediately followed by folding and thrusting towards the SW. This sequence is based on incremental strain analysis of quartz and calcite fibre growth in

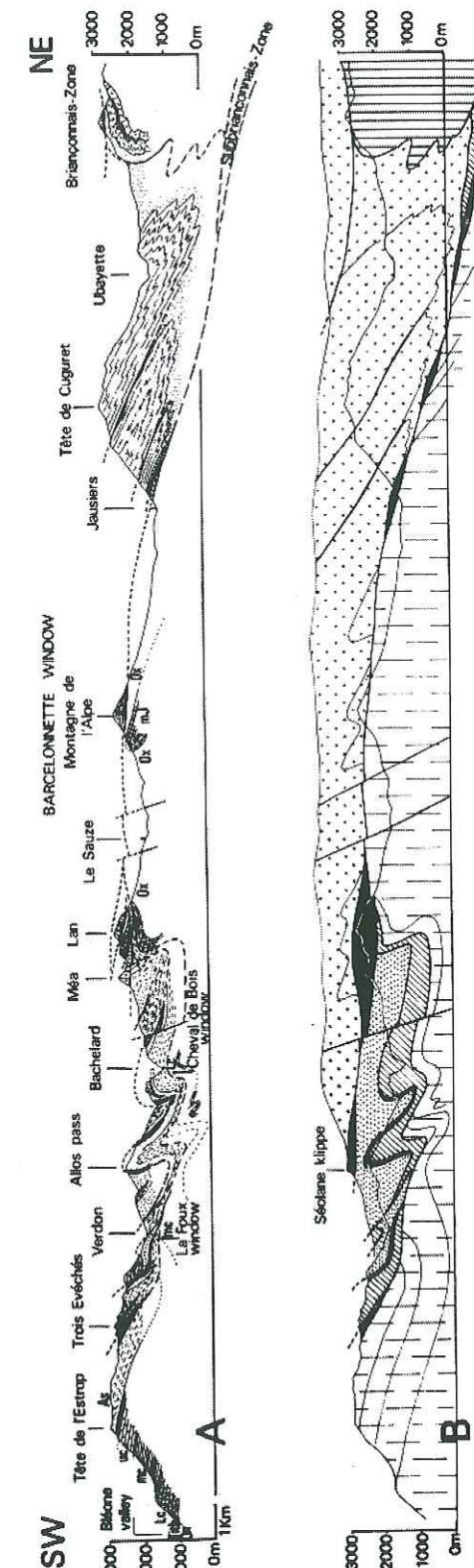
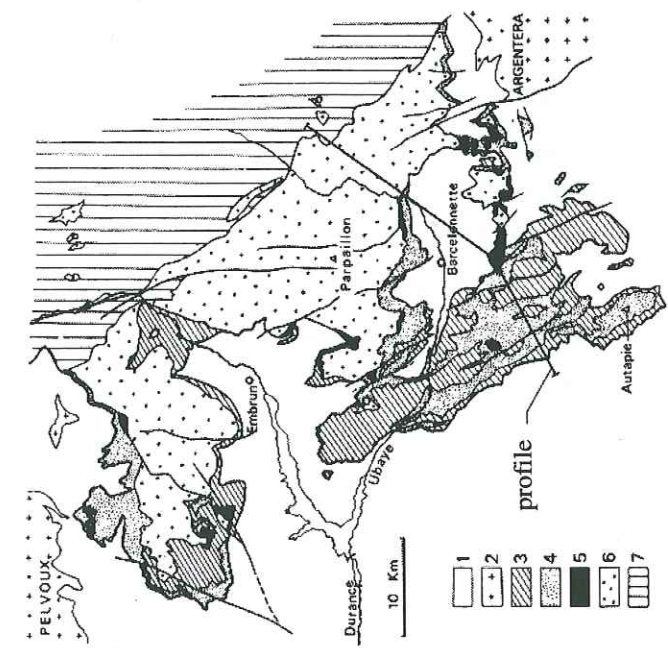


Fig. 4.2:
Structural map of the Embrunais-Ubaye nappes and (A) geological cross section and (B) structural units of the same section before Quaternary erosion (the present relief is shown by a line as in (A)). Modified from Debelmas and Kerckhove (1973).



veins and pressure shadows. However, their incremental strain analysis contains errors (D. Durney pers. comm.). In the text they claim that the calcite fibres in the pyrite pressure shadows have an antitaxial growth sense (new vein material grows at the pyrite or quartz grain surface), but on the figure they interpret the data according to syntaxial fibre growth (new vein material grows between the pressure shadow and the surrounding matrix; compare Fig. 5 of Merle and Brun, 1984 to Fig. 12 of Durney and Ramsay, 1973). The interpretation of pressure shadows as syntaxial or antitaxial is critical for the reconstruction of the strain history. Therefore the relationship of NW and SW-directed transport in the Parpaillon nappe is unclear and cannot be directly related to the presence of the two transport paths in the foreland. An early NW-directed translation of the Parpaillon nappe far away from the external Alps is probable (Merle and Brun, 1984).

Kerckhove *et al.* (1978) proposed from stratigraphic observation in the Prapic fold zone that the NW-directed deformation was refolded by SW-directed deformation. But as shown in section 2.4 the NW-directed large-scale fold does not exist in this area and therefore their argument for relative timing is untenable.

Local model

As argued above, the NW-directed deformation in Soleil Boeuf post-dates the SW-directed deformation in Champsaur-Prapic. Field evidence suggests that the SW-directed deformation did not significantly affect the Soleil Boeuf area (Chapter 3). This requires that the Embrunais-Ubaye nappes overrode a limited area to the south. This observation can be used to develop a new model for the tectonic evolution along the southern rim of the Pelvoux massif. The model is illustrated in Fig. 4.3 and comprises 3 stages.

- 1) Originally within the Alpine foreland basin, the Champsaur-Prapic area was separated by a facies transition zone (at least 6.8 km wide) from the Soleil Boeuf area. The Embrunais-Ubaye nappes had a limited extent and possibly advanced into a depression between the later Pelvoux massif and Argentera massif (Debelmas and Lemoine, 1970; Tricart, 1981; Merle and Brun, 1984) without affecting the southern margin of the Pelvoux massif. Additionally the Soleil Boeuf area lay in the 'shadow' of the massif which may also explain why it escaped any SW-directed thrusting (Fig. 4.3a).
- 2) The NW-directed deformation carried the Champsaur-Prapic area with the overlying Embrunais-Ubaye nappes over the Soleil Boeuf area. (Fig. 4.3b & c). The northern and southeastern continuation of the NW-directed thrusting is unknown. To the north the fault trace disappears below the WSW-directed Sirac thrust sheet (see below) (Fig. 3.1).

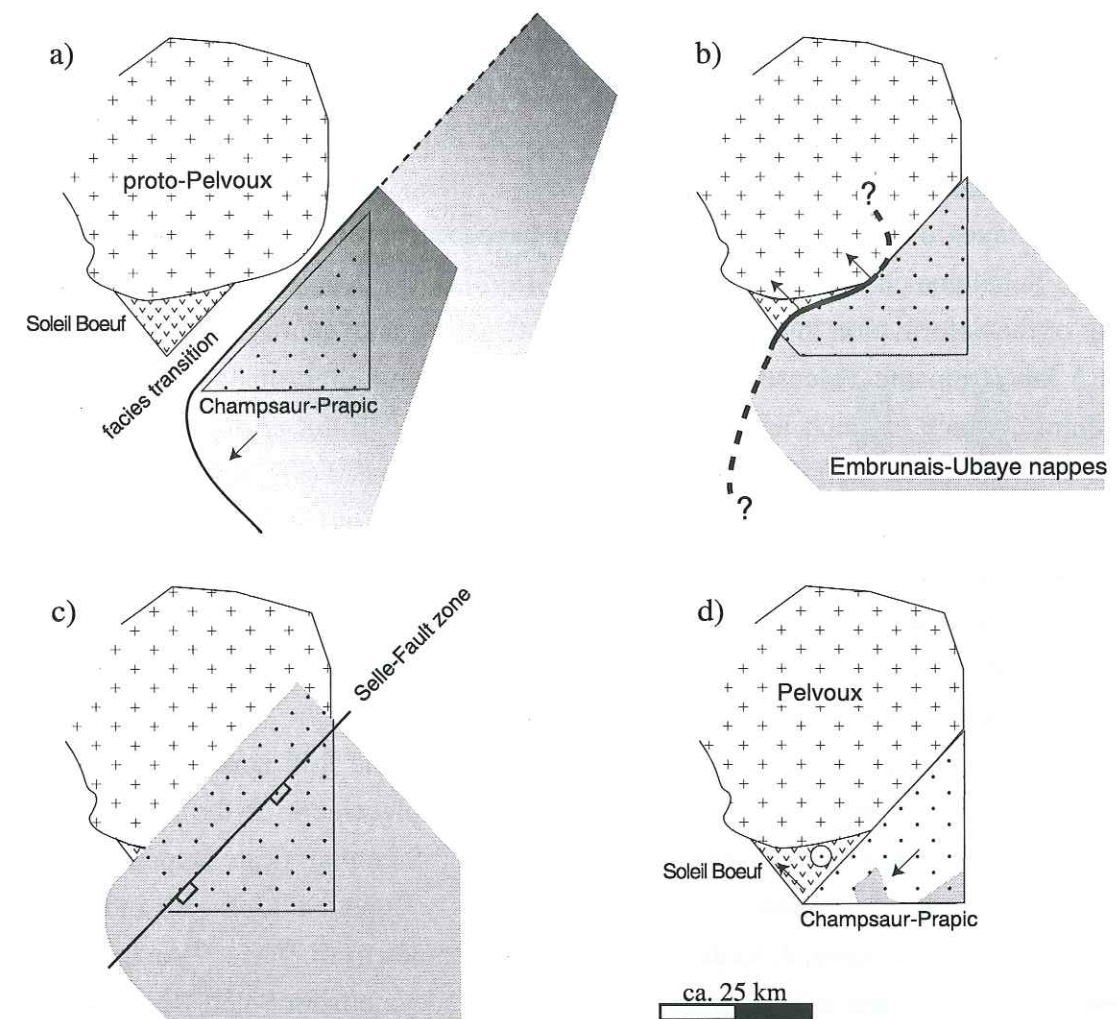


Fig.4.3: Local model in sequential time steps from a) to d). a) The depocentre of Champsaur-Prapic is separated from the Soleil Boeuf area which contains volcanic detritus. The overriding internal nappes do not affect the Soleil Boeuf area which is sheltered behind the proto-Pelvoux massif. b) NW-directed thrusting from depth carries part of Champsaur-Prapic and the overlying Embrunais-Ubaye nappes over the Soleil Boeuf area. c) The NE-SW trending Selle-Fault zone cuts through the nappe stack and drops the southern part down. d) Subsequent exhumation removes most of the hangingwall from the Soleil Boeuf and Champsaur-Prapic areas.

- 3) The Selle-Fault zone cut through the nappe stack. Displacements progressively increase from several tens of metres downthrow next to the FPT to about 900 m downthrow south of the Soleil Boeuf area. This normal component is probably related to the uplift of the Pelvoux massif. Finally the erosion removed most of the overthrust cover from the Soleil Boeuf area, leaving the few klippen remnants (Fig. 4.3d).

4.2 Correlation with the kinematics of the surrounding region

4.2.1 Timing and relation of NW and SW-directed deformation on a regional scale

Late Tertiary tectonic transport directions in the external western Alps vary from NW- to SW-directed (Figs. 1.3 & 1.6).

Three stages of SW-directed deformation have been recently established in the southern Subalpine chains (Lickorish and Ford, 1998). They document the location and timing of the deformation in the Digne thrust system. The total shortening was restored to 21.5 km (from the Valensole basin to the FPT, without Embrunais-Ubaye nappe shortening), which is much less than previously estimated (Elliot *et al.*, 1985). Three stages of SW-directed (220 - 240°) shortening were distinguished (Fig. 4.4): 1) about 1.5 km shortening by detachment and gentle buckling of the floor of the foredeep during the Late Eocene. 2) about 9.5 km shortening during Early to mid-Oligocene overthrust shear related to the emplacement of the Embrunais-Ubaye nappes. And 3) 10.5 km shortening from Miocene to Pliocene expressed in the uplift of the Argentera massif and thrusting of the Digne sheet over the Valensole basin.

The WSW-directed deformation in the Champsaur-Prapic fold zone is due to the emplacement of the internal nappes. The timing of emplacement of the Embrunais-Ubaye nappes has been bracketed between Lutetian and Stampian (Late Rupelian: Fry, 1989) and was further constrained to be Sannoisian (Early Rupelian: Lickorish and Ford, 1998) in the Barrême basin. A further time constraint comes from $^{39}\text{Ar} - ^{40}\text{Ar}$ dating in amphibole from andesite pebbles in the Champsaur Sandstone from Soleil Boeuf which yielded an age of 34.3 ± 1.0 Ma (G. Feraus pers. comm.). The emplacement of the Embrunais-Ubaye nappes which terminated Champsaur Sandstone deposition must be post 34 Ma. This is in agreement with the stratigraphic data from further south (Fry, 1989; Lickorish and Ford, 1998). Therefore the onset of the WSW-directed deformation in Champsaur-Prapic is well constrained to mid-Rupelian (Fig. 4.4).

About 40 km further west to the foreland of the Champsaur-Prapic area lies the Dévoluy area, another remnant of the Tertiary foreland basin. The stratigraphic relationships allow to distinguish late post-Oligocene to Pliocene folding and faulting from pre-Senonian and Paleocene to Priabonian deformation. The Late post-Oligocene (27 Ma) to Pliocene deformation documents foreland migrating SW-directed compression and 2 - 3 km shortening. Emplacement of thrust sheets was followed by folding, and later the SW compression partitioned into westward thrusting on the Median Dévoluy thrust and N-S dextral shear (Meckel *et al.*, 1996). A time-temperature model of the burial and exhumation history of a partially reset apatite fission track sample in the footwall of the Median Dévoluy thrust indicates that the area reached maximum burial of about 4 km (assuming a geothermal gradient of 25°C/km) around 21 - 16 Ma (Meckel, 1997; D. Seward pers. comm.). There is no evidence for a later burial event during the

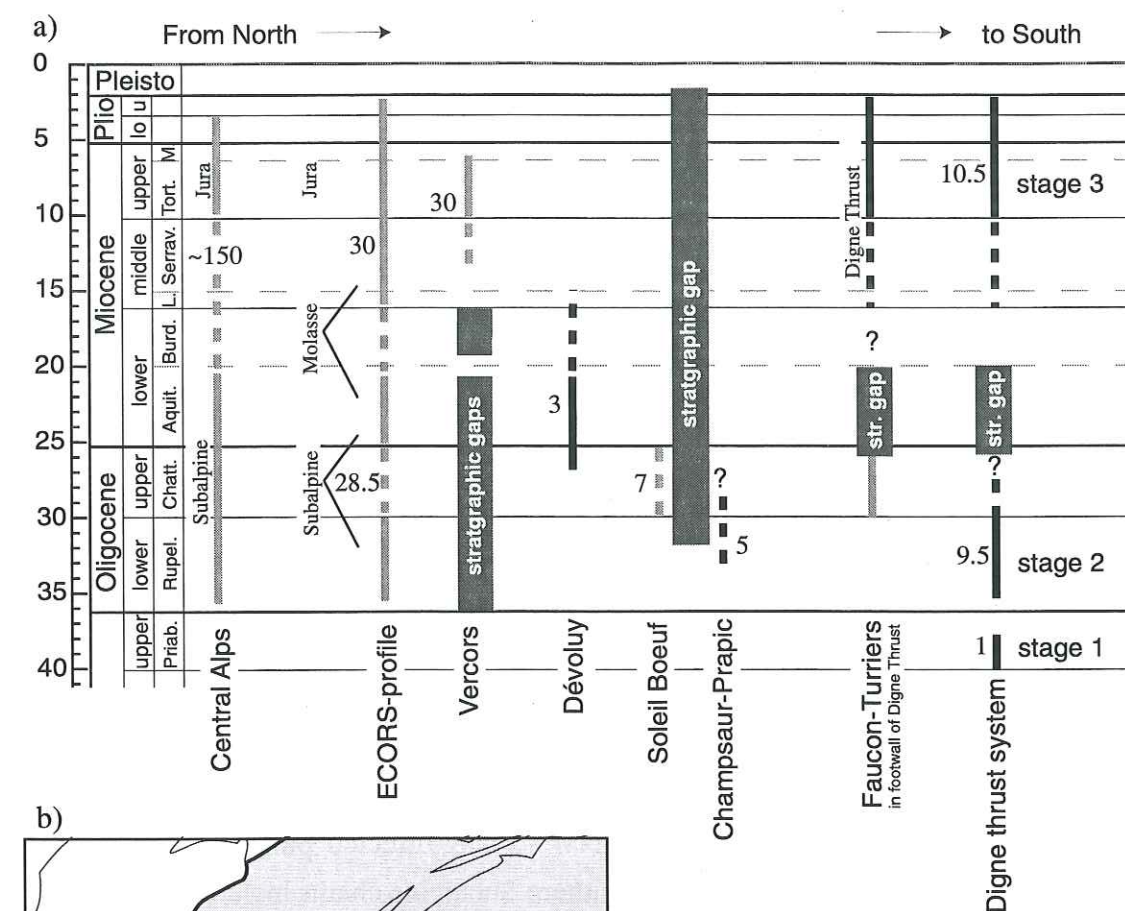


Fig. 4.4:
a) Timing of late Alpine deformation events in the external domain around the western Alps. Small numbers give shortening estimates in km. SW-directed shortening in black lines, NW-directed shortening in grey. Boxes indicated important stratigraphic gaps.
b) Simplified outline map of the western Alps, the external basement massif are dashed. Extension of the WNW to NW-directed deformation (light shaded) and the WSW to SW-directed deformation (dark shaded) in the external Alps are shown. B = Barrême, C-P = Champsaur-Prapic, D = Dévoluy, DTS = Digne Thrust system, EU = Embrunais Ubaye nappes, FPT = Frontal Pennine Thrust, F-T = Faucon-Turriers, V = Vercors
Data from Lickorish and Ford (1998), Arnaud *et al.* (1977), Meckel *et al.* (1996), Meckel (1997), Arpin *et al.* (1988), Gratier *et al.* (1989), Butler (1987), Guellec *et al.* (1990), Homewood *et al.* (1986) and this study.

Late Miocene - Pliocene Digne thrusting which constrains the main burial in Dévoluy from latest Oligocene through Early Miocene (Fig. 4.4). These constraints suggest that the SW-directed deformation front continuously migrated to more external domains and arrived at Dévoluy roughly 6 Ma later than in the Champsaur-Prapic area.

Simultaneously with this migrating SW-directed deformation, the Faucon-Turriers area (Fig. 1.6), a half-window in the footwall of the Digne thrust, underwent WNW-directed deformation (Arnaud *et al.*, 1977). Growth structures indicate that the thrust imbricates developed before and during the deposition of the red continental molasse, i.e. during the Late Oligocene (Fig. 4.4). A correlation of the NW-directed deformation in Soleil Boeuf with the WNW-directed deformation in Faucon-Turriers has already been suggested (Gidon, 1975; Arnaud *et al.*, 1978; Gidon and Pairis, 1980-1981) and if accepted, constrains the NW-directed deformation in Soleil Boeuf to immediately follow the WSW-directed deformation in the Champsaur-Prapic fold zone. The SW-directed deformation front concurrently migrated further west, so that the onset of the main deformation in Dévoluy largely post-dates the NW compression phase (Fig. 4.4).

4.2.2 Models to explain simultaneous thrusting

Models that may explain a distinct WNW to NW-directed pulse of deformation during ongoing WSW-SW motion in the southern Subalpine chains include regional and local solutions.

Case 1: Lateral effects of SW-directed gravitational spreading or thrusting

It has been proposed that the Embrunais-Ubaye nappes were emplaced by gravitational spreading (Fig. 4.5a) (Kerckhove, 1969; Merle and Brun, 1984). The kinematics of gravitational spreading involve (Merle, 1990) an increase of the amount of deformation towards the front and the base of the spreading nappe, and a radial displacement pattern dominated by pure shear in the upper part of the nappe (stretching concentric and perpendicular to the displacement) and by simple shear in the lower part of the nappe (stretching divergent and parallel to the displacement) (Fig. 4.5a). It could be suggested that the Soleil Boeuf area represents the lateral portion of such a spreading nappe. But then the displacement direction should change gradually from SW to NW which is not observed in the field. However, the major problem with gravitational spreading is that the deformation does not deeply penetrate into the substrate and thus cannot cause the thrusting from deeper detachments in the Soleil Boeuf area.

Synchronous with the superficial emplacement of the Embrunais-Ubaye nappes more deeply detached deformation in the SW-directed southern Subalpine chains decreases northwards from 21.5 km shortening in the Digne system (Lickorish and Ford, 1998) to 2 - 3 km in Dévoluy (Meckel *et al.*, 1996) and 5 km in Champsaur-Prapic, suggesting that

the SW-directed thrust system dies out towards the Pelvoux massif. This brings up the idea that the structural patterns in the Soleil Boeuf area could be explained in terms of lateral tip structures (Coward and Potts, 1983) to the SW-directed thrusting. Coward and Potts (1983) suggest that differential movement at the lateral tips of a propagating thrust system may lead to lateral thrust ramps characterised by folding oblique to the thrust transport direction and shear strains parallel to the thrust transport direction (Fig. 4.5b). However, in Soleil Boeuf, this is not the case: folding is NW-directed, i.e. perpendicular to the SW-directed thrust system, not oblique, and no NE-SW-trending dextral shear strain has been documented. Additionally, it is only the thrust sheet above the thrust plane that will be affected by thrust tip structures, whereas in Soleil Boeuf the NW-directed deformation roots below the SW-directed deformation. Another weakness of the model is that the Faucon-Turriers area does not lie at a lateral tip of the SW-directed thrust system and therefore requires another explanation.

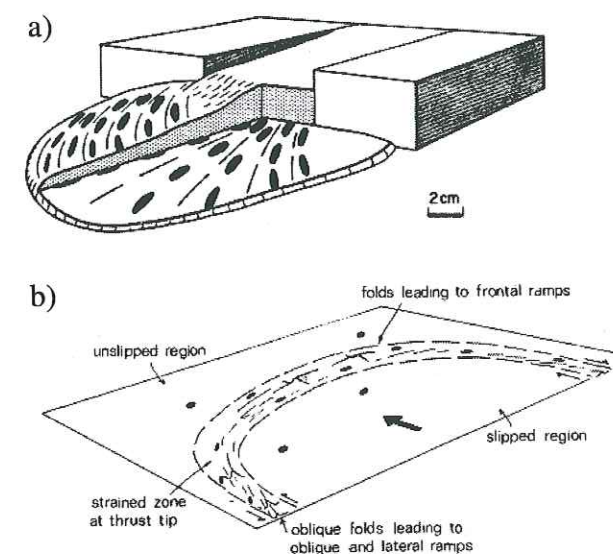


Fig. 4.5:

a) Schematic representation of a gravitational spreading nappe, movement path of particles is divergent. Variation of the stretching is shown; concentric stretching towards the top (pure shear deformation) and radial stretching towards the bottom (simple shear deformation). From Merle (1990).

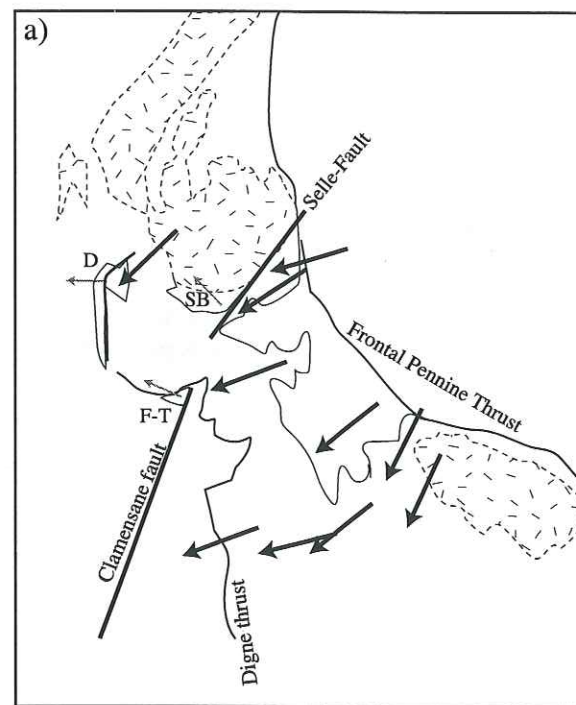
b) A thrust plane showing the strained tip region between the slipped and unslipped regions. From Coward and Potts (1983).

Case 2: Local strain partitioning along strike-slip faults

The Soleil Boeuf and the Faucon-Turriers areas are both situated to the west of NE-SW trending faults, the Selle-Fault and the Clamensane fault (Figs. 1.6 and 4.6a). They are segments of the Aix-en-Provence fault (Rousset, 1978), an old lineament (Arnaud *et al.*, 1978; Rousset, 1986). It is believed that this lineament acted in various ways during successive stages of Alpine deformation and was also active as early as Permian and Jurassic times, when it influenced sedimentation. The relatively narrow localisation of WNW-NW thrusting has been linked to a local complex strain field related to the Clamensane fault in Faucon-Turriers (Arnaud *et al.*, 1977) and to the Selle-Fault in Soleil Boeuf (Gidon, 1975; Arnaud *et al.*, 1978; Gidon and Pairis, 1980-1981).

When the localisation of WNW-NW thrusting in Soleil Boeuf and Faucon-Turriers is

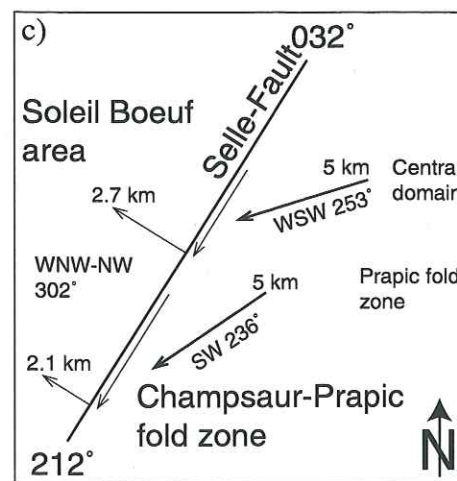
related to the faults, it has to do with stress partitioning. In simplified partitioning models, compressional stress oblique to a fault zone is partitioned into components of movement perpendicular and parallel to the zone (Fig. 4.6b). It has been shown that across thin-skinned, limited-length transcurrent faults, such models are valid (Odonne and Costa, 1991). A problem which arises with a partitioning model is that the imposed compression in the southern Subalpine chains is only at a small angle of $41\frac{1}{2}^\circ$ - $24\frac{1}{2}^\circ$ to the Selle-Fault (Fig. 4.6c) which is not much different for the Clamensane fault which has a similar strike ($019\frac{1}{2}^\circ$) (Fig. 4.6a). Therefore the partitioned component perpendicular to the fault zone should always be smaller than the component parallel to the fault zone. Partitioning of 5 km WSW-directed shortening in Champsaur-Prapic at the Selle-Fault would give 2.7 - 2.1 km shortening perpendicular to the Selle-Fault in Soleil Boeuf only (Fig. 4.6c). This is much less than the 7 km minimum shortening estimate (Chapter 3). Another weakness of the simple partitioning model is that it assumes that the NE-SW



b)

Fig. 4.6:

a) Simplified map of southeastern France to illustrate the situation of NW-directed deformation in Soleil Boeuf (SB) and Faucon-Turriers (F-T) to the west of NE-SW trending faults. Reported partitioning in Dévoluy (D) at the Median Dévoluy thrust (Meckel et al., 1996) is also shown. b) General partitioning model showing discrete divergence in slip vectors across a thin skinned fault of limited length (after Odonne and Costa (1991)). c) Partitioning solution for the Selle-Fault. 5 km WSW to SW-directed shortening in the Champsaur-Prapic fold zone would partition into 2.7 to 2.1 km shortening perpendicular to the Selle-Fault in the Soleil Boeuf area.



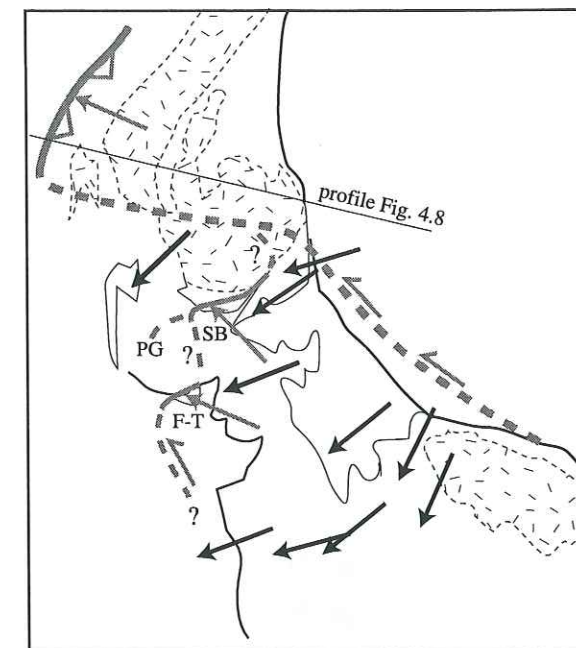
oriented faults acted as thin-skinned, limited faults. However, as the faults probably belong to the Aix-en-Provence lineament which already acted as a passive margin fault during Mesozoic extension this assumption is not necessarily valid.

Case 3: Satellite system of northern Subalpine chains

This model invokes a short-lived satellite fault system related to the Oligocene NW-directed thrust system (Fig. 4.7). The following constraints result from such a model:

Fig. 4.7:

Simplified map of southeastern France to illustrate the satellite fault solution for the NW-directed deformation in Soleil Boeuf (SB) and Faucon-Turriers (F-T) and Pic de Gleize (PG). Interference of SW-directed deformation in the southern Subalpine chains (black arrows) with satellite fault to the NW-directed thrust system of the northern Subalpine chains (grey). Outlines of Frontal Pennine Thrust, Embrunais-Ubaye nappes, Digne Thrust and the external basement massif (dashed) are shown.



- 1) The two compression directions must have operated at different levels at the same time. The SW-directed deformation has been documented to develop near the surface by gravitational gliding or overthrust of the Embrunais-Ubaye nappes of at least 50 km (Kerckhove, 1969; Merle and Brun, 1984), and by simultaneous detachment along several deeper levels, e.g. within the Triassic evaporites, the Middle Jurassic shales, and the mid-Cretaceous shales (Lickorish and Ford, 1998). There are no 'free' detachment levels left for the NW-directed thrusting in the cover rocks which therefore forces the NW-directed deformation to detach in the basement. Coward *et al.* (1991) adopt WNW-NW-directed thrusting from depth (Fig. 4.8) in the Pelvoux area based on deep seismic ECORS line south of the Mont Blanc massif (Roure *et al.*, 1990). Thus the NW-directed deformation in Soleil Boeuf and Faucon-Turriers may similarly ramp up from detachments in the basement while the SW-directed deformation in the cover rocks of the southern Subalpine chains was going on (Fig. 4.8).

- 2) The southern continuation of a NW-directed detachment in the basement below the southern Subalpine chains is problematic. Somehow it would have to be linked to the main NW-directed thrust system east of the Frontal Pennine Thrust. But so far no evidence has been found for further late NW-directed thrusting in the southern Subalpine chains east of the Digne thrust nor for a transcurrent NW–SE trending sinistral fault system which could accommodate differential NW-directed shortening. Such features could, however, have been overprinted by subsequent deformation.
- 3) Another weakness of the satellite model is the northern continuation of the thrusting at Soleil Boeuf. To the west it may link to NW-directed folding and thrusting recorded in Cretaceous sediments at Pic de Gleize (Fig. 4.7; H. Lickorish pers. comm.). But northwards it appears to link into the Sirac basement thrust sheet (Fig. 3.1). In the centre of the Pelvoux massif no Tertiary sediments are preserved and the accurate dating of deformation is problematical. In the Aiguilles Morges area, recent work has shown SSW-directed large-scale folding (π -axis 116-32; Lazarre *et al.*, 1996; Murer, 1998) followed by predominant W to SW-directed thrusting (mean compression directions 239-00 in the north and 249-05 in the south, Murer, 1998) and minor WNW-directed deformation (Lazarre *et al.*, 1996). The W–SW and WNW-directed kinematic data have been both related to the emplacement of the Sirac thrust sheet during the Alpine shortening. Hence, the transfer of the NW motion of Soleil Boeuf to the northern Subalpine chains remains an unsolved problem.

With such a satellite fault model, the exact cause of the two movement directions is linked to the large-scale kinematics of the northern and southern Subalpine chains and therefore to the larger-scale Alpine tectonics of the more internal domains. The problem of two major thrust systems at right angles acting at the same time has to be solved with all of the three models presented above! The satellite model therefore seems to be the simplest solution. Additionally it can account for the nature of the deformation in Soleil Boeuf with its detachment at depth.

4.3 Kinematics and geodynamics of the western Alpine arc

What are the implications of the structural and tectonic observations made in Soleil Boeuf and Champsaur-Prapic for the geodynamic evolution of the external western Alpine arc? The most prominent models have been presented in Chapter 1 where they have been grouped in two categories: those favouring a radial forming arc, and those favouring the presence of two mutually perpendicular thrust systems.

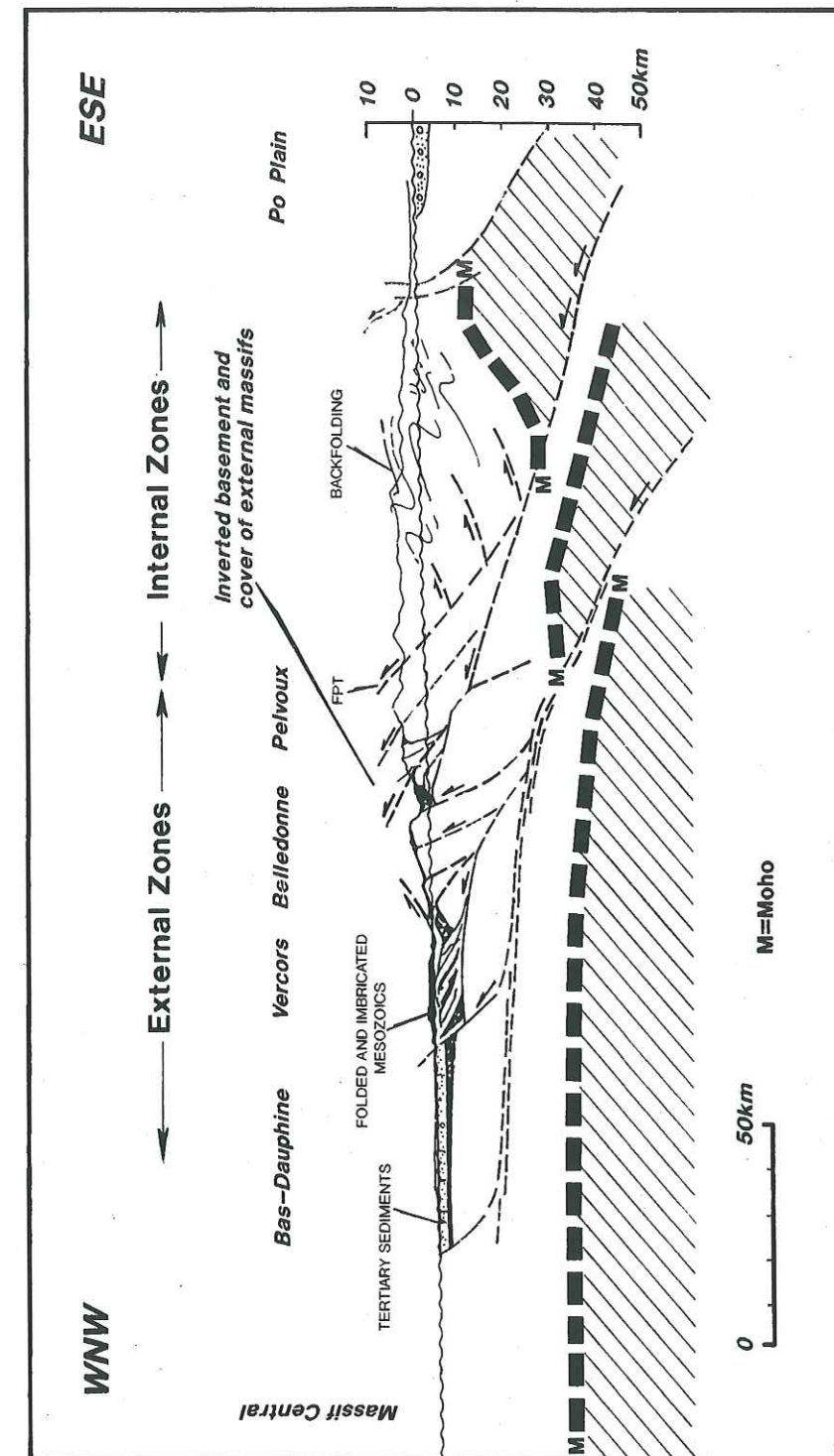


Fig. 4.8: Simplified cross-section through the Pelvoux massif. NW-directed deformation ramps up from within the basement. From Coward *et al.*, (1991). Profile trace is located in Fig. 4.7.

Observations from the area around the bend in the arc do not support a radial evolution of the arc as discussed below.

The Late Tertiary tectonic transport directions in the external western Alps to the south of the Pelvoux massif have been discussed in the previous section; they are predominantly WSW–SW with a simultaneous pulse of WNW–NW motion during the

Late Oligocene. At the same time as the Digne thrust system evolved in the southern Subalpine chains, large amounts of WNW–NW-directed deformation were accommodated in the northern Subalpine chains (e.g. Goguel, 1963; Pijolat *et al.*, 1981; Malavieille *et al.*, 1984; Butler, 1985; Choukroune *et al.*, 1986; Dietrich and Durney, 1986; Gourlay, 1986; Platt, 1986; Mugnier *et al.*, 1987; Ramsay, 1989; Butler, 1992b). Along the trace of the ECORS-profile (Fig. 4.4), for example, the Alpine compressive front progressed regularly to the west during the Tertiary (Fig. 4.4). Overall shortening between the cover of the external crystalline Belledonne massif and the front of the Jura mountain is estimated at 58.5 km (Guellec *et al.*, 1990), 30 km of them within the Molasse and Jura cover. Along the same profile, shortening of 126.5 km has been estimated between the external Belledonne massif and the Frontal Pennine Thrust (Butler, 1985). Three deformation phases migrating into the external domain could be distinguished: in the Early Oligocene, in the Early Miocene and during the Late Miocene to Pliocene. Butler (1992b) documented WNW-directed thrusting (294° to 283°), tentatively dated as post-Oligocene from the Prealps down to the Vercors area. In the Vercors area, WNW-directed main deformation occurred probably between 10 and 6 Ma during the Late Miocene (Butler, 1987). Earlier minor episodes folded and overthrust Middle Miocene molasse. The youngest preserved Tertiary sediments are local Lower Miocene units. Profile restoration gives shortening estimates of about 30 km between the Belledonne massif and the Dauphine foreland (Butler, 1987). Kinematics and displacement estimates for the northern Subalpine chains indicate that the total W to WNW shortening was between 70–80 km and 185 km (e.g. Butler, 1984; 1985; Butler *et al.*, 1986; Ménard and Thouvenot, 1987; Mugnier *et al.*, 1987; Guellec *et al.*, 1990; Mugnier *et al.*, 1990) which decreases southward towards the corner of the Pelvoux massif (Arpin *et al.*, 1988; Gratier *et al.*, 1989). Whereas in the southern Subalpine chains SW-directed shortening decreases northward from 21.5 km in the Digne thrust system (Lickorish and Ford, 1998) to ~8 km close to the Pelvoux massif (Meckel, 1997; this study).

Evidence for W-directed compression in the external Alps is recorded only within the Pelvoux massif area, where poorly dated thrust kinematics show a spread of directions from 209° to 315° (Fig. 1.6), including several W-directed data (e.g. Gidon, 1979; Gillcrust *et al.*, 1987; Coward *et al.*, 1991). Clearly these directions are related to the complex inversion of passive margin structures at some stage during Alpine collision, but the data can not be simply interpreted in terms of regional late Alpine transport directions. However, at the internal margin of the Pelvoux massif, close to the Frontal Pennine Thrust, a sudden change northwards from WSW to WNW-directed deformation has been documented within the Champsaur fold zone (Chapter 2) which continues at the easternmost corner of the Pelvoux massif (Butler, 1992a) and into the areas further north

(Bravard and Gidon, 1979; Beach, 1980; Beach, 1981b; Beach, 1981a; Beach, 1982; Serre *et al.*, 1985).

The lack of a significant component of W-directed movement at the bend in the arc suggests that the distribution of movement vectors around the Pelvoux massif is not radial, but rather, that there is a distinct break in the kinematic pattern of the arc between the NW and SW-directed transport. The models that explain the kinematic break include 1) strike-slip collision (Ricou, 1984; Ricou and Siddans, 1986), 2) lateral hangingwall collapse of the NW-directed main thrust system (Butler *et al.*, 1986), or 3) a late independent SW-directed thrust system in the footwall of the NW-directed main system (Butler *et al.*, 1986).

Models 1) and 3) assume that the SW-directed thrusting in the southern Subalpine chains post-dates the evolution of the northern Subalpine chains. But as argued above there is sufficient evidence that both deformations went on at the same time (Fig. 4.4), although in the southern Subalpine chains with lesser shortening. Model 2) considers SW motions due to lateral hangingwall collapse, but it is questionable if this process can cause thrusting from deeper levels in the hinterland as it was ongoing from the beginning of the deformation in the external Alps. Additionally, hangingwall collapse is probably restricted to the latest stage of NW-directed thrusting which again does not fit the timing observed in the field. Therefore none of these models explains all the observed features.

5. Analogue modelling of obstacles and oblique indentation

5.1 Introduction

5.1.1 Aim of this study

The previous Chapters 2, 3 and 4 have clarified the kinematics at the southern rim of the Pelvoux massif and their significance for the development of the western Alpine arc. These data strongly suggest that the external western Alpine arc was produced by two synchronous transport directions which were at approximately at right angles. The Pelvoux massif is situated in the core of the arc, where the two thrust systems intersect and its sedimentary cover records both displacement directions. This raises the question: to what extent the Pelvoux massif controlled the position of the Alpine arc or even the formation of the external arc as previously suggested by Bravard and Gidon (1979) and Tricart (1981). The Pelvoux massif is a candidate for buttressing the deformation, because: (1) the Triassic platform deposits are relatively thin and devoid of evaporites (Lemoine *et al.*, 1986), i.e. there is a pinch-out of the stratigraphic decollement horizon; and (2) between Late Cretaceous and Early Eocene the Pelvoux massif was uplifted and eroded down to basement (Ford, 1996); hence the Alpine deformation front encountered a palaeogeographic basement high covered only by Tertiary strata (Gupta, 1997).

The data presented in this study suggest that 'corner hypotheses' may be more appropriate than 'radial hypotheses' as discussed in the Chapters 1 & 4. In order to examine the validity of such models it is necessary to experimentally investigate the accommodation of the deformation around an arc formed by two perpendicular transport directions using sand box analogue modelling. The results can then be compared to the observed kinematic pattern in the external Alps which shows the strengths and weaknesses of the proposed models.

The advantage of such small-scale models is that they can be scaled to be mechanical analogues to nature, hence they should show behaviour similar to nature, and the processes involved in deformation can be studied without involving all the parameters of the more complex natural system. A number of 25 pure sand and sand-silicone experiments have been run to investigate 1) the difference in the deformation pattern with variable indentation paths and 2) the role of obstacles. The experiments have been carried out at the University of Rennes, in collaboration with P. Cobbold and H. Lickorish (H. Lickorish *et al.*, in prep.). Within this larger project, I have focused on 5 sand-silicone experiments which representatively illustrate the main results of all the experiments.

5.1.2 Previous models

Analogue models of thrust sheet interference with obstacles are rare and often investigated complex settings by mathematical and analogue modelling (e.g. England and Houseman, 1985; Haq and Davis, 1997; Tommasi and Vauchez, 1997). Some of the first work is that by Chamberlin and Shepard (1923) who placed a semicircular rigid mass into a paraffin wax experiment, opposite to the side where uniform shortening was applied. They suspected that the curvature of the obstacle might control, or at least greatly influence, the trend of the resulting fold. But the result of the experiment was that in general the trend of the fold did not conform to the shape of the rigid arcuate obstacle.

In contrast, based on experiments Beutner (1977) ascribed the small-scale thrust belt curvatures in the Rocky Mountain foreland to buttressing against basement salients and reentrants in the foreland. He showed that the curved stress trajectories, occurring where an elastic sheet (gelatine) pushed against obstacles of clay are similar to the inferred stress trajectories in nature. Similar results were obtained by Marshak (1988) and Marshak *et al.* (1992). They used a single layer damp sand model to simulate the interaction between a growing sand wedge and two stationary obstacles (glass cylinders) in the foreland. Structures that had formed prior to the interaction with the obstacles are bent, bounded by wrench shear zones along the inner sides of the obstacles, and new curved thrusts develop towards the foreland. But in both kind of experiments the materials used are rather cohesive and may not represent the behaviour of natural rocks properly.

The pinch-out of stratigraphic decollement horizons has been investigated in 2-dimensions (Souriot *et al.*, 1991) and in 3-dimensions (Letouzey *et al.*, 1995). Souriot *et al.* (1991) showed that a small gap of the ductile layer first localises a thrust fault but new thrust faults develop in front of it. Conversely, a large gap interrupts the decollement and a hinterland propagating system develops behind it. In such a way an obstacle can control the order of fault development above the decollement layer. In the 3-dimensional case study of the Jura mountains (Letouzey *et al.*, 1995) a similar effect could be observed. The curved external limit of the Jura thrust belt corresponds to a large interruption of the decollement horizon. In the analogue model the shortening concentrates at the edge of the decollement horizon in a curved thrust front and behind above the basal detachment on thrusts parallel to the backstop of the model. In the same article buttressing against a basement fault scarp with different configuration of decollement horizons has been investigated (Letouzey *et al.*, 1995) but the influence on the displacement direction was not investigated.

To summarise, the influence of obstacles on the curvature of orogenic belts has scarcely been investigated by analogue modelling. Therefore this study aims to investigate the general case of a single obstacle in the foreland of a straight thin-skinned

fold and thrust belt. The influence of the shape and thickness of the obstacle on the displacement directions are the focus of these experiments.

Previous indentation models investigated straight unidirectional motion paths. The earliest physical indentation models were made of paraffin wax (e.g. Chamberlin and Shepard, 1923; Vialon *et al.*, 1984) or plasticine (e.g. Tapponnier *et al.*, 1982; Tapponnier *et al.*, 1986). Based on their models, Chamberlin and Shepard (1923) proposed that pressure along a short straight indenter is one possibility to produce mountain arcs. Later, Vialon *et al.* (1984) did two sets of experiments with paraffin and a round-shaped rigid indenter to model the Jura mountains by indentation of the molasse basin. In a first set the rigid indenter was pushed into the foreland, in a second set the indenter was pushed down onto the foreland without lateral compression. Pushing the indenter results in a curved fold belt with shortening perpendicular to fold axes at the front and en-échelon folding due to wrench shear at the sides. In the case of loading shortening was evenly distributed around the indenter and always perpendicular to the fold axes. Thus in these models the curvature of the fold belt depends on the curvature of the indenter.

Bale (1986) produced arcuate fault patterns in sand and silicone experiments, scaled for gravity, representing the upper brittle and lower ductile part of the crust respectively. The indentation of a rectangular indenter with a protruding basal plate generated a thrust perpendicular to the displacement which amplified radially and joined faults along the lateral wrench zone. Bale concluded that the interaction between a thrust zone and a perpendicular wrench zone induces arcuate structures. The wrench zone is characterised by positive flower structures. By variation of the boundary parameters of the experiment Bale produced arcs with either external or internal vergence and compared the results to the western Alpine arc where major thrusts verge outward around the arc, and to the Ibero-Armorican Arc (Burg *et al.*, 1987) where major thrusts verge inward around the arc.

Complex 4-layer analogue models, representing the entire lithosphere were used to investigate the special case of indentation processes with different degrees of lateral confinement (Davy, 1986; Davy and Cobbold, 1988). These lateral escape models can be applied to the India-Asia collision and improve on the early simple plasticine models of Tapponnier *et al.* (1982; 1986). For our purposes the important conclusion of these experiments is that a narrow indenter leads to arcuate thrust traces with divergent thrusting of about $\pm 20^\circ$ where the lateral strain is accommodated by arc-parallel extension in the hangingwall of forethrusts and arc-parallel shortening in the hangingwall of backthrusts (Fig. 5.1). This divergent thrusting is bounded laterally by wrench faults which link back to the edges of the indenter. Divergent thrusting breaks down, either as the indenter becomes too wide, or as the lateral confinement of the

continent is relaxed.

In summary, in all these indentation models a strong curvature of thrust or fold traces was observed with a strong component of lateral wrench shear. However, the divergence of the transport directions is limited and never adequately explains the divergence of over more than 90% observed in the western Alps. As a new approach, indentation experiments with an oblique or poly-directional motion path have been performed. In such a way the divergence of the thrust motions is enhanced and the deformation characteristics within an arc can be observed.

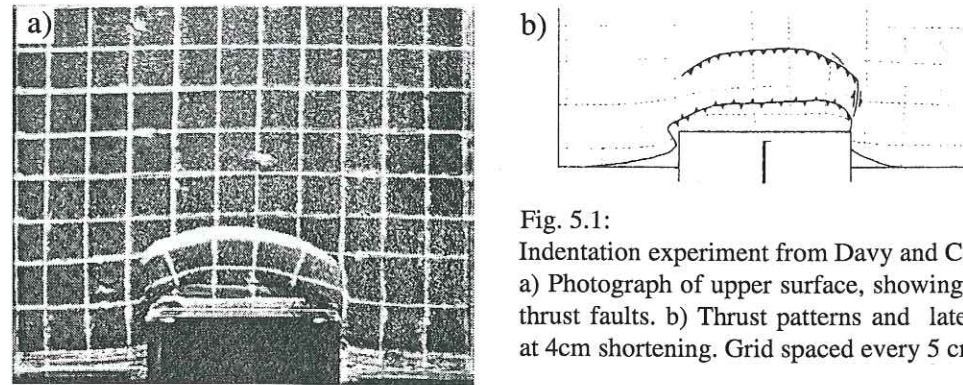


Fig. 5.1: Indentation experiment from Davy and Cobbold (1988). a) Photograph of upper surface, showing arcuate traces of thrust faults. b) Thrust patterns and lateral wrench shear at 4cm shortening. Grid spaced every 5 cm.

5.1.2 Materials and scaling

Rheology in nature

The external Alps developed due to the advance of the internal Alpine units which can be considered as an indenter with a rounded rectangular form (Fig. 1.1). The deformation of the internal units is complex whereas the evolution of the external Alps is well constrained. To simplify the analogue models, it is therefore efficient to model only the evolution of the external Alps. Such an approach also reduces the model to thin-skinned foreland tectonics which can be adequately represented by sand-silicone experiments. The sand represents the brittle behaviour of the upper crust, while the lower ductile silicone layer transfers the deformation to the foreland.

The brittle behaviour of the upper continental crust is of the Mohr-Coulomb type and can be written as:

$$\tau = \sigma_n * \tan \gamma + C \quad (5.1)$$

where τ and σ_n are the shear and normal stresses respectively, γ the angle of internal friction and C the cohesion. Characteristic numbers for natural rocks are a cohesion of 50 MPa and an angle of internal friction close to 30° (for $\sigma_n > 200$ MPa) (Byerlee, 1978). This means that the deformation is independent of the velocity and that it occurs along faults.

The ductile behaviour of the continental crust, where rocks no longer deform by fracture but by continuing flow can be described by the rheologic equation for Newtonian material:

$$\sigma_{ij} = \mu * \epsilon'_{ij} \quad (5.2)$$

where μ is the viscosity, ϵ' the velocity of the deformation and σ_{ij} the deviatoric stress. This law does not only apply to the lower crust but also for the incompetent behaviour of shales or evaporites in the upper continental crust. The viscosity of the lower crust has been estimated to be about 10^{21} Pa s (Davy, 1986, Davy and Cobbold 1991) whereas the viscosity of shale or evaporites is difficult to assess. Odé (1968) estimated evaporite viscosities to $10^{16} - 10^{19}$ Pa s.

Scaling

The application of scaling theories to earth sciences has been proposed by Hubbert (1937) and Ramberg (1967). Davy and Cobbold (1988, 1991) describe in detail the principles of the scaling analysis, while here only an outline is given.

The principles of scaling require a similarity between nature and experimental model in geometry and dynamics. An experimental model is defined by characteristic constant parameters (length (L_0), time (t_0), velocity (U_0), density (ρ_0), viscosity (μ_0), etc...). All physical parameters can be expressed by means of the three fundamental units of measurements kilogram [kg], meter [m] and second [s]. On this basis, dimensionless variables are defined which are ratios between parameters of the same units of measurement. The systems are congruent if the dimensionless variables from model and nature are identical.

To compare an experimental model with a geologic system ratios between a parameter in the model and the same parameter in the natural system are used. For example the length-ratio (L^*) is:

$$L^* = L_{\text{model}} / L_{\text{nature}} \quad (5.3)$$

The fundamental scale-ratios are the density-ratio ρ^* , length-ratio L^* and time-ratio t^* . From these 3 ratios all the others can be deduced, for example the velocity ratio $U^* = L^* / t^*$. The essential parameters are listed in table 5.I.

The models are scaled for a normal gravity field ($g^* = 1$). In the indentation models, a length ratio $L^* = 3 \cdot 10^{-6}$ was chosen, so that a sedimentary pile, 10 km thick in nature, scaled down to 3 cm thick in the model. This was enough for proper observation of structures. Note that the obstacle models are a close up with length and time scales different from those of the indentation models (Table 5.I). In a normal gravity field, the strength ratio must equal the product of the length ratio and the density ratio. A density ratio of 0.5 was chosen; the strength ratio was therefore $\sigma^* = 1.5 \cdot 10^{-6}$. In practice, for

brittle material obeying Mohr-Coulomb law, the cohesion has the dimension of stress and must therefore be scaled down in the model to become negligibly small whereas the coefficient of internal friction (dimensionless) must be the same in model and in nature. For ductile layers, strength depends upon strain-rate and so the time scale has to be considered. This is best chosen on a practical basis, so that an experiment does not last more than a few hours. A time ratio $t^* = 7.5 \cdot 10^{-11}$ (6 hours represents 10 Ma) has been used. Together with the strength ratio, this sets the viscosity ratio $\mu^* = 10^{-16}$ (the viscosity ratio must equal the product of the strength ratio and the time ratio).

	L_0 [m]	t_0 [s]	U_0 [m s ⁻¹]	ρ_0 sand [kg m ⁻³]	ρ_0 silicone [kg m ⁻³]	μ_0 [Pa s]	g_0 [m s ⁻²]	σ_0 [Pa]
NATURE	obstacle (1 km)	$9 \cdot 10^{13}$ (3 Ma)	$2.75 \cdot 10^{-10}$ (8.6 m ka ⁻¹)	2600	2600	$10^{16} - 10^{19}$	9.81	10^7 (10 MPa)
	indentation (10 km)	$3 \cdot 10^{14}$ (10 Ma)						
MODEL	obstacle (1 cm)	22'500 (6.25 h)	$1.1 \cdot 10^{-5}$ (4 cm h ⁻¹)	1400	1200	$10^4 - 10^5$	9.81	46
	indentation (3 cm)							15

SCALE RATIOS	length ratio L^*	time ratio t^*	velocity ratio U^*	density ratio ρ^*_{sand}	density ratio ρ^*_{silicone}	viscosity ratio μ^*	gravity ratio g^*	strenght ratio σ^*
obstacle	10^{-5}	$2.5 \cdot 10^{-10}$						$4.6 \cdot 10^{-6}$
indentation	$3 \cdot 10^{-6}$	$7.5 \cdot 10^{-11}$	$4 \cdot 10^4$	0.54	0.46	$10^{-15} - 10^{-11}$	1	$1.5 \cdot 10^{-6}$

Table 5.I Comparison between the natural constants and the constants used in the experimental model and the corresponding scale ratios. For proper scaling the scale ratios must fit the following relationships (Davy, 1986; Davy and Cobbold 1988; Davy and Cobbold 1991):
 $L^* = U^* \cdot t^*$
 $\mu^* = t^* \cdot \sigma^*$
 $\sigma^* = L^* \cdot \rho^* \cdot g^*$
 $\mu^* = \rho^* \cdot g^* \cdot L^{*2} / U^*$

Analogue materials

The brittle part of the continental crust is modelled by dry sand. We used dry Fontainebleau sand. This sand has an aeolian origin and consists only of quartz grains. Before use, it is sieved so that only the grain size $< 315 \mu\text{m}$ is used. The density of the sand is about 1.4 g cm^{-3} . The angle of internal friction of 30° is close to that obtained for natural rocks (Byerlee, 1978). Its weak cohesion (500 Pa) is neglectable. The sand is a Mohr-Coulomb material. The similarity of the rheological law, the angle of internal friction and the low cohesion between sand and natural competent rocks justify the use of sand as the analogue material for the brittle part of the continental crust.

The analogue material used to simulate the ductile behaviour of incompetent rocks in

the continental crust is a silicone putty (Silbione silicone, Gomme A0009, manufactured by Rhône-Poulenc, France). This is a viscose material of Newtonian type (the viscosity varies linearly with an increase of the deformation velocity). The viscosity (μ) of new silicone at room temperature, and at deformation velocities used in modelling, ranges between $10^4 - 10^5 \text{ Pa s}$ and the density is 1.2 g cm^{-3} . The use of silicone to model the ductile behaviour of the incompetent rocks of the continental crust is justified by its ability to gravitationally flow, therefore respecting the gravitational forces at deformation velocities of the laboratory experiments.

Although the scaling and the materials used allow us to scale the models appropriately according to gravitational forces and rheology, their validity in representing the complexity of nature is limited. The model represents only simplified rheologies, it does not take into account material properties varying with depth and a change of the viscous rheology in time. Therefore the results can only deliver tectonic hypotheses.

5.1.3 Experimental setup

The model (Fig. 5.2) was made 115 cm long, to allow for serial formation of structures during progressive shortening. Model width was set to 115 cm so that the influence of lateral boundary conditions, especially frictional resistance, could be minimised in the centre of the model. A rig was mounted at one end of the box which pushed either a backstop as wide as the box (115 cm) or a smaller indenter into the model (as shown in Fig. 5.2). The horizontal compression was induced by means of two or three screw-jacks coupled to computer controlled motors. Motor 1 was only used for indentation experiments, to add a lateral component to the translation path (Fig. 5.2).

Models were built from bottom to top. The box was first filled with silicon sheets of about $\sim 5 \text{ mm}$ thickness (rolled through a pastry machine at 2.5 mm thickness which then expands due to elastic viscosity) placed successively in position. The silicone was left overnight to expel any trapped air bubbles. The different obstacles or the indenter were emplaced in the box. The silicone was then covered with $\sim 2.5 \text{ cm}$ sand to give a total model thickness of 3 cm . In models which were cut at the end of the experiment sublayers, about 2 mm thick, of different coloured sand were included. Finally 5 cm spaced grid lines of coloured sand were painted on the upper surface to monitor the horizontal displacement. At the end of the experiment, the sand was stripped away to reveal the upper surface of the silicone layer to identify faults at depth and their geometry. Models with sublayers were covered with different coloured sand, damped and subsequently cut in profiles parallel to the shortening direction.

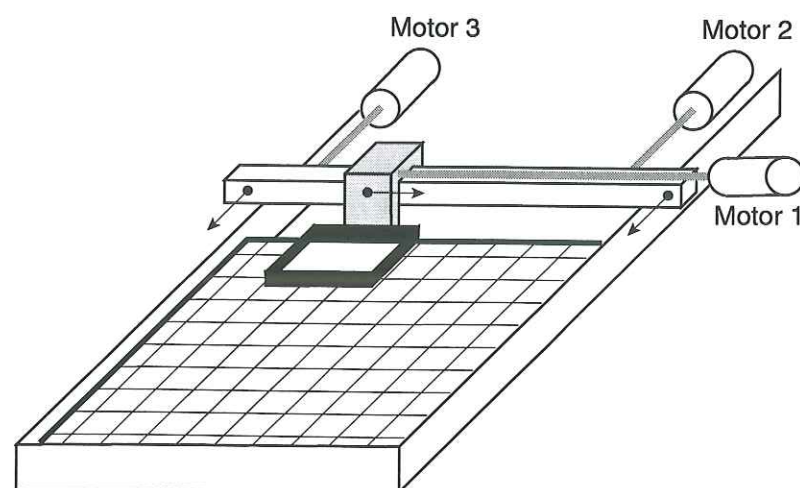


Fig. 5.2: Perspective view of experimental apparatus. The model (115 * 115 cm) is set in a rig. 3 screw-jacks coupled to computer controlled motors induce the shortening. By the means of motors 2 and 3 a wide backstop (not drawn) or an indenter (shown) can be pushed into the experiment. With the aid of motor 1 a variable lateral component can be added to the motion path of the indenter.

5.2 Obstacle experiments

Different obstacles were emplaced in the middle of the box at 25 cm from the backstop. The 115 cm wide backstop of Plexiglas was moved across the square box up to the obstacle. Horizontal compression was induced by motors 2 and 3 (Fig. 5.2), both running at 4 cm/h for 25 cm of shortening.

Two extreme types of obstacles have been used: 1) a low obstacle at the base of the experiment which is buried by sand and 2) a high obstacle, which is much higher than the upper surface of the sand. The low obstacle (1) was simulated by localised replacement of the 5 mm thick silicone layer at the base by dry sand. That way ductile shearing along the base was hindered in the silicone free zone, i.e. it faced a low obstacle at the base of a thick sedimentary pile. The high obstacle (2) was made of Plexiglas, i.e. it is a massive obstacle which can not be deformed at all. Thus these experiments are similar to the classic obstacle experiments (Beutner, 1977; Marshak *et al.*, 1992). Both types of obstacles were fixed to the bottom plate of the experimental box.

5.2.1 Experiments with a low obstacle

Two experiments with different shapes of the low obstacle were carried out.

In the first experiment (WHL-22) a rectangular silicone free zone (40 * 36 cm) was aligned with its longside parallel to the backstop. The first thrust front (T1) appeared at about 1.5 cm shortening and formed linearly along the backstop. Irregular imbricates linked longer segments of single plane thrusting (Fig. 5.3a). Almost simultaneously, a

smooth bending of the E-W grid lines on either side of the obstacle indicated that distributed flow reached far ahead of the discrete faulting and had already encountered the obstacle. The diffuse deformation propagated on either side of the obstacle whereas the obstacle itself remained undeformed (Fig. 5.3a). At about 4 cm shortening this produced a foreland-vergent thrust (obstacle thrust OT) in front of the obstacle followed immediately by a backthrust (Fig. 5.3b). At the base of the model these thrusts initiated right at the edge of the silicone, on the model surface cut-off points aligned at ~5 cm on either side of the silicone edge (Fig. 5.3b). At 5 cm shortening the second thrust front (T2) accompanied by a backthrust (B2) had nucleated in front of T1 (Fig. 5.3b). While shortening was evenly distributed on either side of the obstacle, in front of the obstacle it concentrated on T1 and on the OT (Fig. 5.3b). A similar pattern of nucleation and displacement on either side of the obstacle, combined with accumulation of shortening on the OT in front of the obstacle continued throughout the progressive development of the model (Figs. 5.3c, d & e). The movement direction of the hangingwall remained perpendicular to the backstop (no offset of N-S grid lines) except at the margins of the model box (lateral boundary effect) and very close to the undeformed obstacle (Fig. 5.3e). Similarly most of the fault trace curvature on map view could be related to side-wall friction at the walls of the box. The right half of the model was inhomogeneously heated by lighting which accentuated the curvature and caused the en-echelon array of T3 (Fig. 5.3c). However some curvature occurs at the rim of the obstacle. Connecting splay faults joined the OT with the adjacent thrust fronts T2 and T3 (Figs. 5.3c & f) and tear faults accommodated the differential displacement on both sides of the obstacle which further away in the foreland resolved into diffuse wrench zones (see E-W grid lines on Figs. 5.3d & e).

A second experiment (WHL-23) was performed with a square silicone free zone (28 cm * 28 cm) at the base of the model where the backstop faced the corner of the square, so that the sides of the obstacle made an angle of 45° with the backstop. This model was performed to investigate the influence of the shape of a low obstacle. Again T1 formed linearly along the backstop. Diffuse deformation propagated far ahead on either side of the obstacle (smooth bending of E-W grid lines: Fig. 5.4a) and became concentrated at the corner of the silicon free zone where the next foreland-vergent thrust (OT) nucleated at about 4 cm shortening, immediately followed by a backthrust (Fig. 5.4a). Thrusts took on a V-shape parallel to the sides of the obstacle and accommodated oblique displacement perpendicular to the backstop. Meantime the second thrust front (T2) accompanied by a backthrust developed in front of T1 and grew over the V-shaped backthrust (Fig. 5.4b). At 11 cm shortening deformation progressed on T3 and the related backthrust. At a first stage their lateral propagation stopped at the V-shaped backthrust

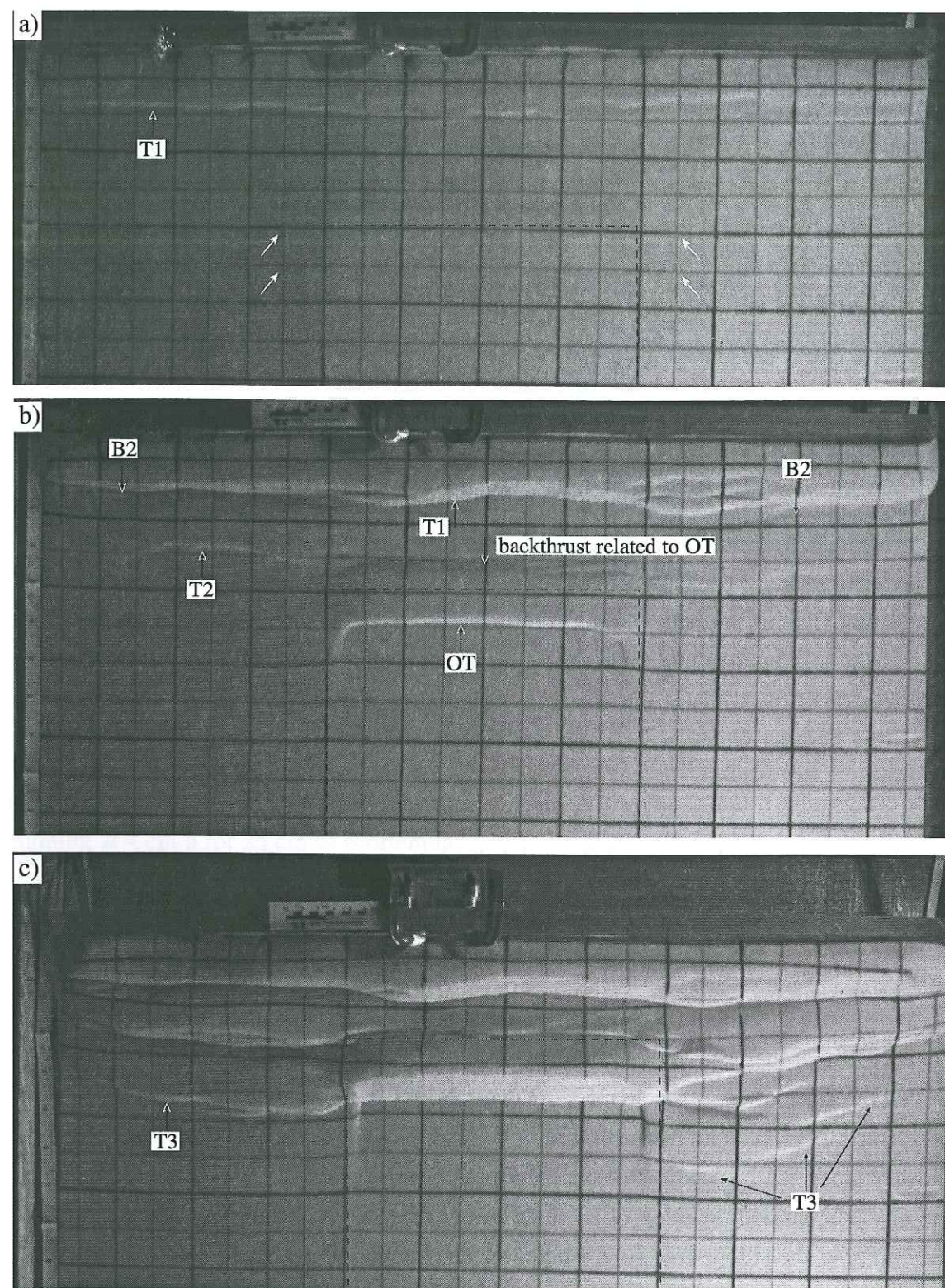
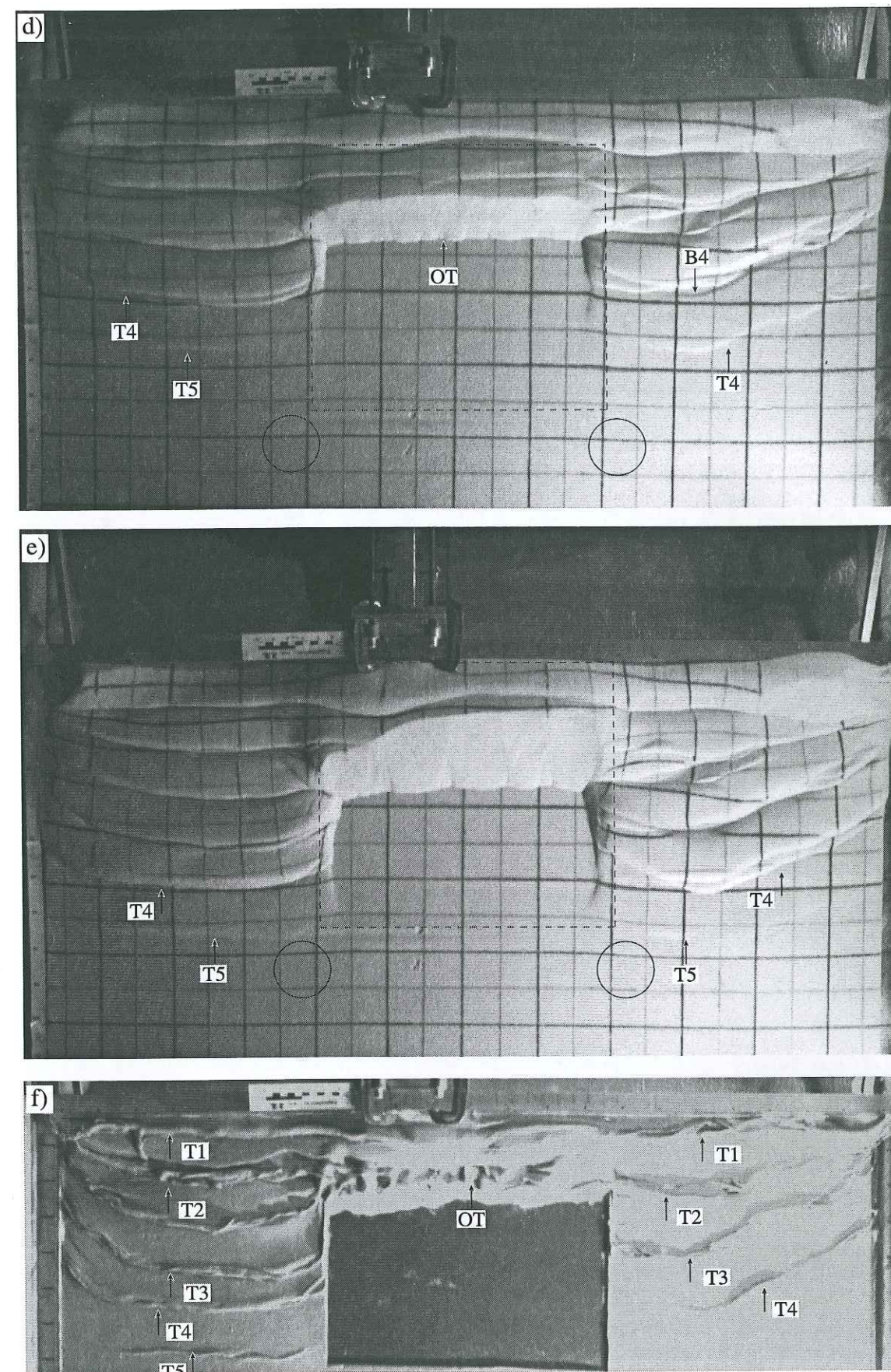


Fig. 5.3: Sequential development of experiment WHL-22, with overthrustable obstacle. Photographs of upper surface of model (lightening from right side). Sand is covered by an originally orthogonal grid of passive lines spaced every 5 cm (black and grey lines). The silicone-free zone at the base of the model, i.e. the obstacle, is marked by a thin dashed line. a) 1.7 cm shortening, white arrows mark early offset of E-W grid lines; b) 5 cm shortening; c) 11.7 cm shortening, note en-echelon array of right-hand T3; d) 18.3 cm shortening; e) 25 cm shortening; f) 25 cm shortening, upper surface of silicone. T = forethrust, B = backthrust, OT = obstacle thrust. Circles in d) & e) indicate diffuse wrench shear to the foreland of obstacle.



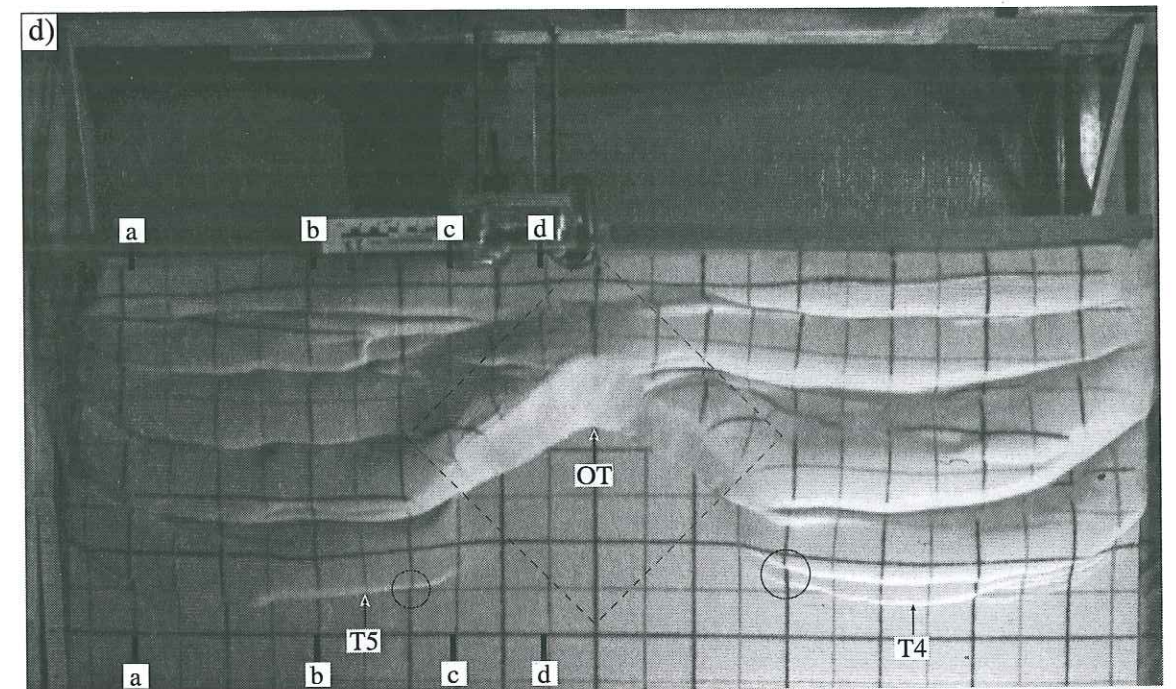
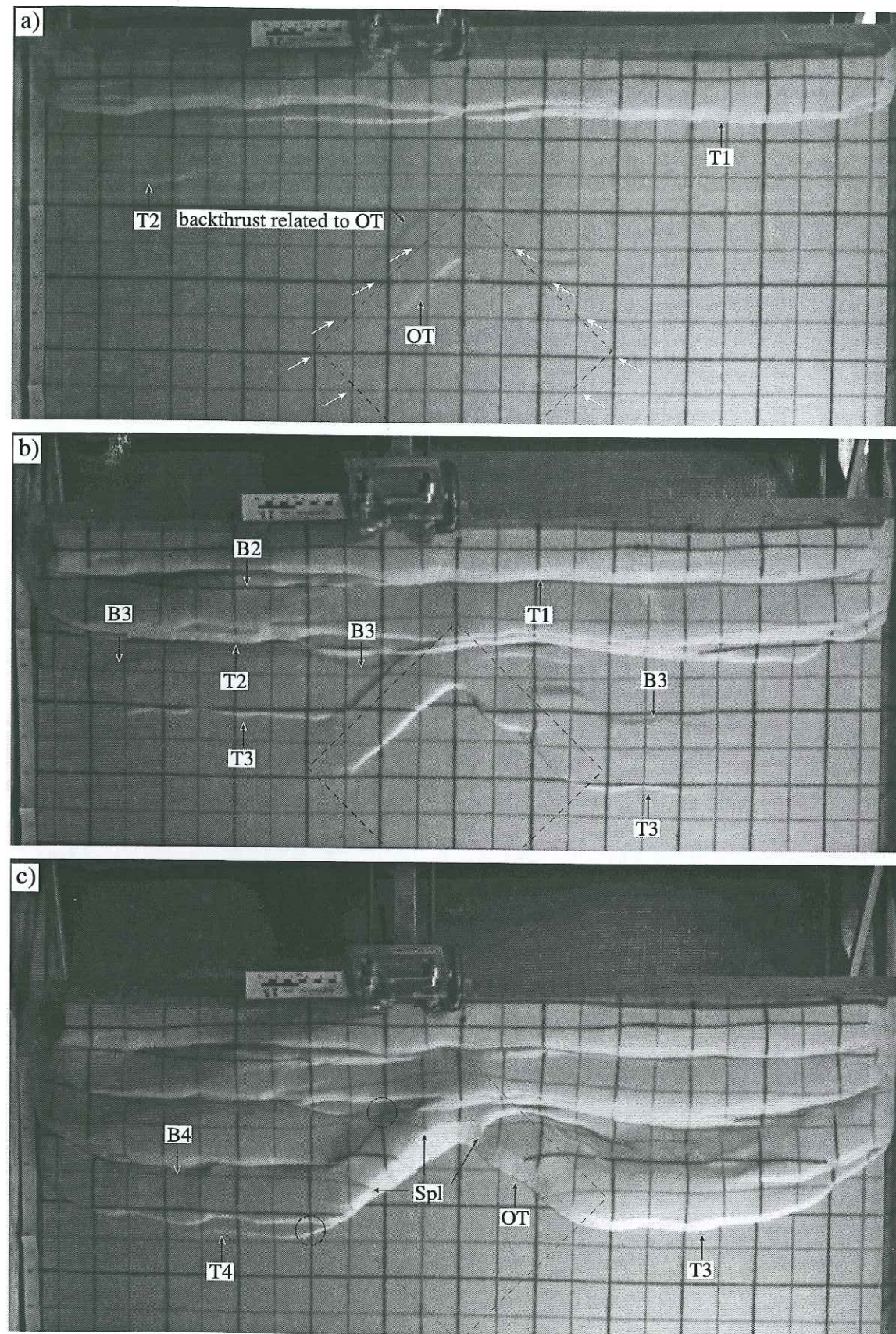


Fig. 5.4: Photographs of upper surface of model WHL-23, with a low buried diagonal square obstacle. Square grid of passive marker lines spaced every 5 cm (black and grey lines). The silicone-free zone at the base of the model, i.e. the obstacle, is marked by a thin dashed line. a) 5 cm shortening, white arrows mark beginning bending of E-W grid lines; b) 11.7 cm shortening; c) 18.3 cm shortening; d) 25 cm shortening; e) 25 cm shortening, location of profile cuts is shown. T = forethrust, B = backthrust, OT = obstacle thrust, Spl = splay fault. Circle mark offset in N-S grid lines, which indicate thrusting oblique to the backstop.

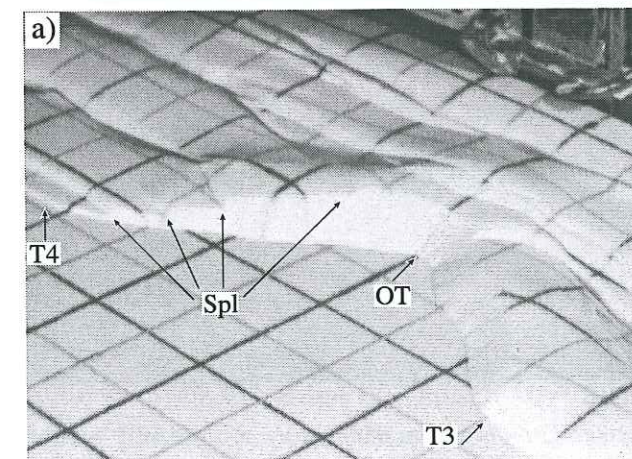


Fig. 5.5: Oblique view of upper surface of experiment WHL-23 at 18.3 cm shortening. The displacement on the OT diminishes stepwise at splay faults (=Spl) till the OT links up with T4 to the left. Compare to Fig. 5.3c.

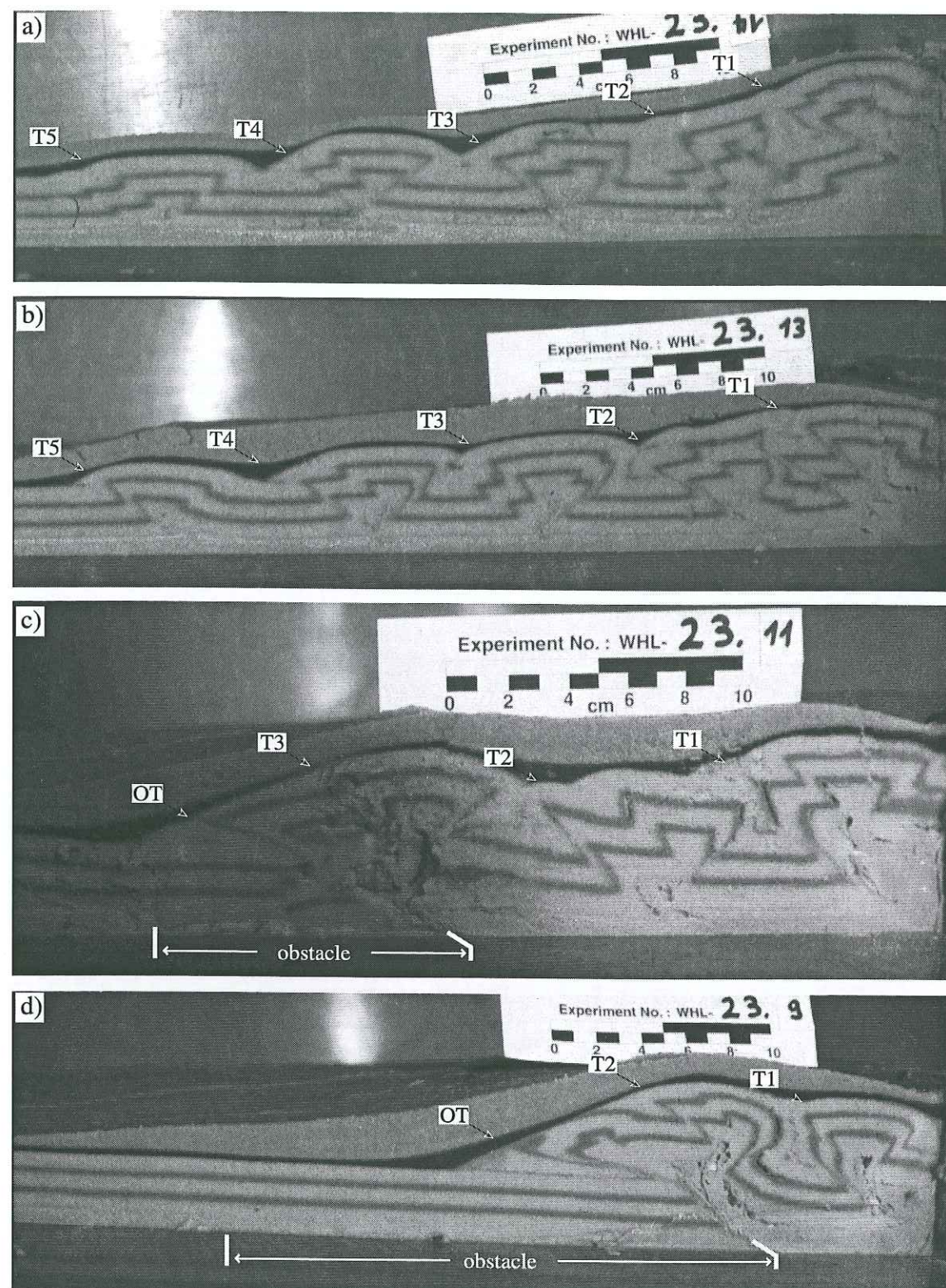


Fig. 5.6: Profile-cuts of experiment WHL-23. Internal deformation outlined by two, initially parallel darker layers. A black layer separates the model topography from the later poured protective cover of sand. a) - d) Sequential development of structures from margin to center of model, detailed location of profiles in Fig. 5.4d. Asymmetric 'pop-up' structures to the side of the obstacle. The rear of the thrust wedge is elevated adjacent to the vertical backstop. The OT overthrusts the obstacle and carries in c) T3 and B3, in d) T2 and B2 in its hangingwall. T = forethrust, B = backthrust, OT = obstacle thrust.

(Fig. 5.4b), but as deformation progressed, connecting splays transferred the shortening from T2, T3 and T4 onto the OT (Figs. 5.4c & 5.5). As a result the OT accommodated increasingly smaller displacements away from the backstop and linked from the external-most edge of the obstacle to the closest thrust front (T4 to the left, T3 to the right). Wrench systems border the further propagating thrust front at the sides (Fig. 5.4d). The obstacle itself and the area straight ahead of the obstacle remained undeformed. N-S grid lines indicated displacements perpendicular to the backstop with two exceptions: 1) friction at the lateral boundary to the box and 2) minor divergent thrusting towards the obstacle behind the OT and more clearly to the foreland of the OT (marked with circles on Figs. 5.4c & d).

Sequential profile-cuts clearly demonstrate the importance of the OT on the development of the thrust wedge. From the margin towards the centre of the model the wide, low-tapered thrust wedge (Figs. 5.6a & b) progressively narrows and steepens into a convex form suggesting a double taper geometry in the hangingwall of the OT (Figs. 5.6c & d). In order to accommodate equivalent shortening, tectonic thickening is greater adjacent to the obstacle. The deformation partitioned approximately equally between foreland-vergent thrusts and backthrusts. The foreland-vergent OT overthrusts the undeformed obstacle, it accommodated most shortening and overrode the material slumped from the thrust front (Fig. 5.6d).

5.2.2 Experiment with a high obstacle

To test the influence of a high obstacle, a rectangular Plexiglas box (35 * 26 cm, and 10 cm high) was fixed to the bottom of the model with surrounding silicone at the base (WHL-24). The box was oriented diagonally so that the sides of the box made an angle of 45° with the backstop. T1 appeared at about 2 cm shortening and T2 at about 5 cm shortening immediately followed by a backthrust. Both of these thrust fronts (T1 & T2) formed linearly along the backstop (Fig. 5.7a). The deformation front became divided at the obstacle and the two frontal positions moved progressively into the foreland with new forethrust-backthrust-pairs nucleating at an approximately uniform spacing (Figs. 5.7b, c & d). Some fault traces bifurcated near the box while others bent (marked with circles: Figs. 5.7b & c). Soon after the beginning of deformation, grid lines started to bend and evolved a characteristic pattern: E-W grid lines were smoothly curved by hindered flow along the box-edges; N-S grid lines indicated that material was being forced laterally out of the triangular zones between the backstop and the obstacle sides. There was no evidence for thrusting oblique to the backstop except for the frontal thrusts in Fig. 5.7d and perhaps close to the obstacle, but here observations were obscured by the thick pile of sand. The base of the silicone (in this model marked with circular imprints) reveals in more detail the features of deformation (Figs. 5.7e & 5.8). Shear deformation

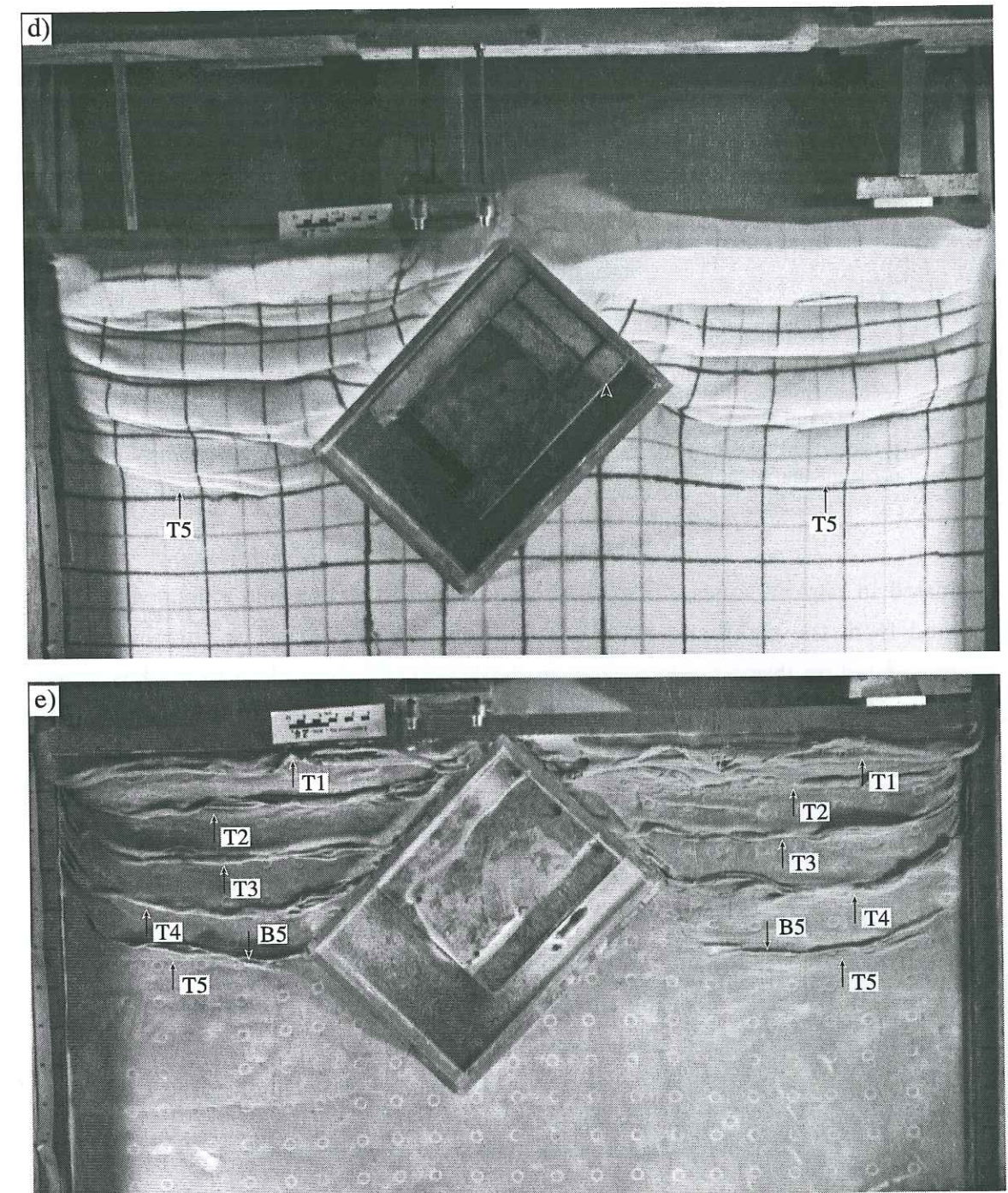
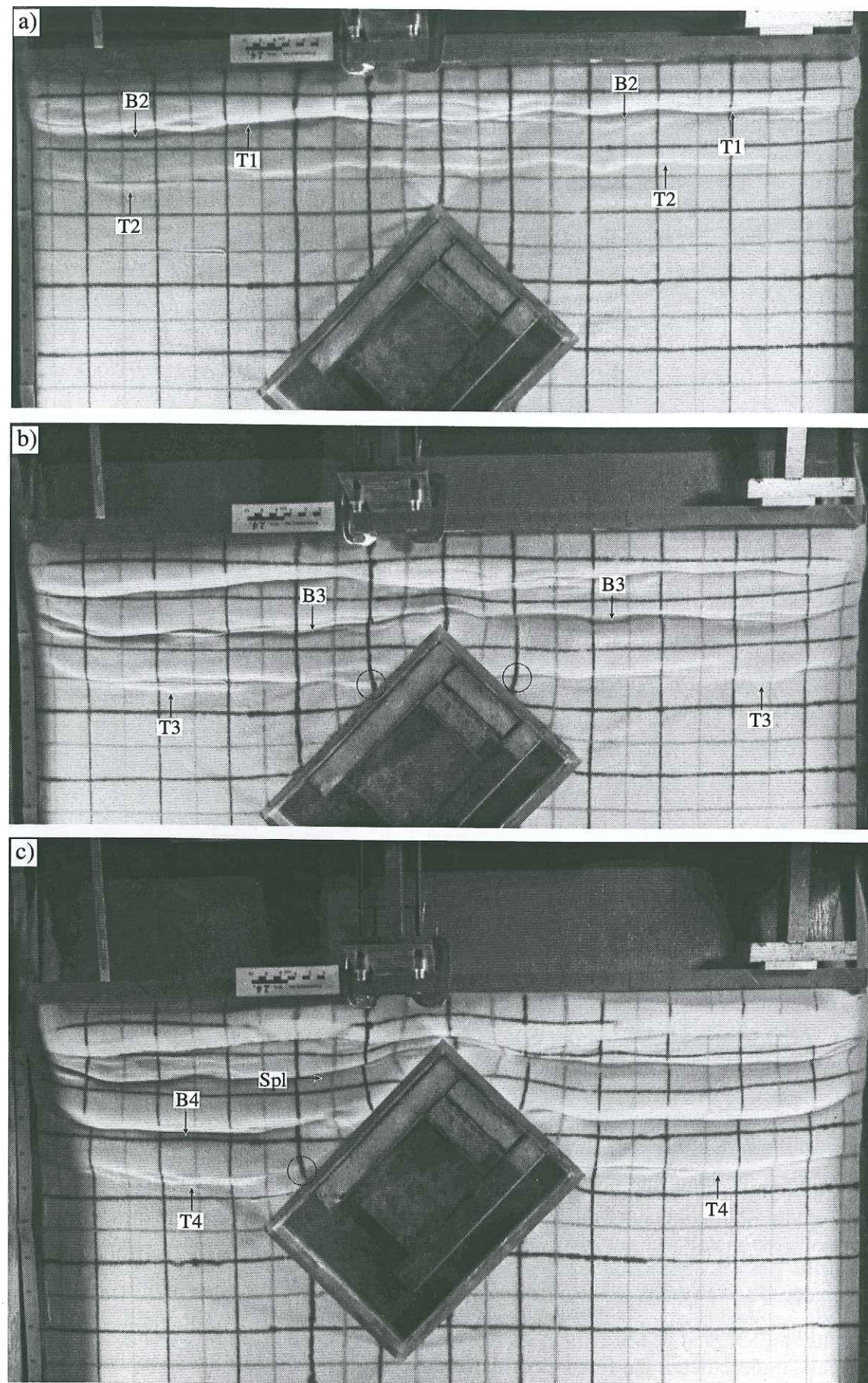


Fig. 5.7: Photograph of upper surface of model WHL-24, with a high obstacle. Square grid of passive marker lines spaced every 5 cm (black and grey lines). a) 5 cm shortening, already marked bending of N-S and E-W grid lines; b) 11.7 cm shortening; c) 18.3 cm shortening; d) 25 cm shortening; e) 25 cm shortening, upper surface of silicone. T = forethrust, B = backthrust, OT = obstacle thrust. Circle mark bending of N-S grid lines, and splay faults close to the box.

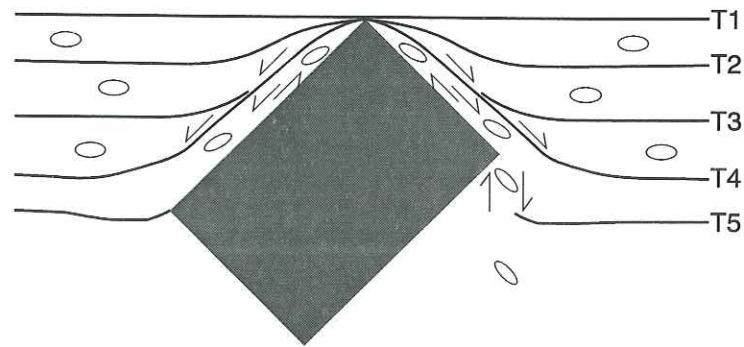


Fig. 5.8: Silicone surface in experiment WHL-24 at the end of deformation with schematic representation of the recorded strain ellipses. The fault scarps (black lines) branch onto a wrench fault parallel to the sides of the obstacle (dark grey). This fault separates a domain of predominant shear adjacent to the box from the domain of predominant thrusting perpendicular to the backstop.

dominated in narrow zones along hinterland sides of the box and extended into the foreland from the righthand box-corner (Figs. 5.7e & 5.8). The shortening was accommodated on thrust faults parallel to the backstop except close to the box where they bent and branched onto a wrench fault. This fault separated the shear domains close to the box from the thrusting domains (Fig. 5.8).

5.3 Indentation experiments

Two indentation experiments with a silicon layer at the base were carried out. A rectangular Plexiglas box (35 * 26 cm) was pushed along an oblique but straight translation path (WHL-25) and along an elliptical oblique translation path (WHL-26) to approximately the same position in the foreland (Fig. 5.9). The oblique horizontal compression was induced by three motors running at the same time: motor 2 and 3 pushing the rig with the mounted indenter to the south, motor 1 pulling the indenter to the east (Fig. 5.2). By setting the motors at different velocities any translation path can be accomplished.

5.3.1 Oblique straight translation path

In this experiment the rectangular box was pushed at an angle of 34° to the short side of the box. The velocity was held constant. Deformation initially occurred at the leading corner of the indenting box where a weak curved fault trace appeared (T1) (Fig. 5.10a). Soon after that, this fault propagated along both edges (Fig. 5.10b). The fault trace lay closer to the box along the short side than along the long side. Bending of both the E-W grid lines and to a lesser extent N-S grid lines indicated distributed flow parallel to the edges (Fig. 5.10b). The next thrusts formed as a series of en-echelon faults which started

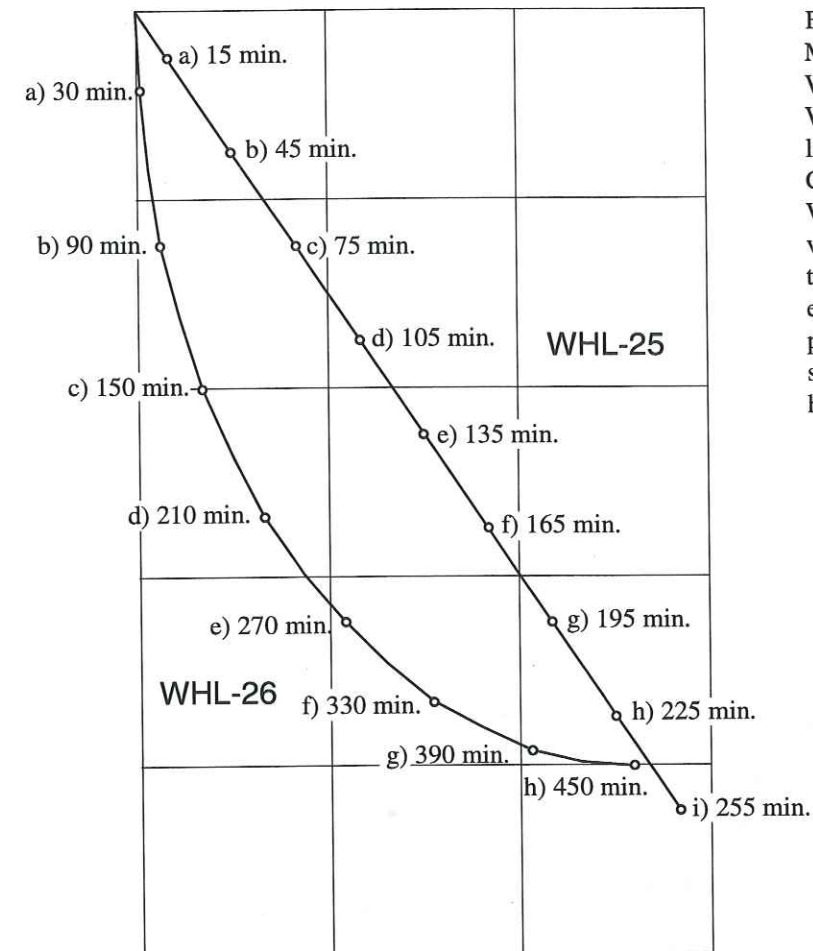


Fig. 5.9: Motion path of experiment WHL-25 (straight line) and WHL-26 (curved line). Grid lines are at 5 cm spacing. Constant velocity of 6 cm/h in WHL-25. In WHL-26 the velocity ranges from 4.2 cm/h at the beginning to 2.7 cm/h at the end. The dots represent the position and time of bird views shown in Fig. 5.9 a) - i) and a) - h) in Fig. 5.10.

to overlap and then linked to form a single fault scarp (Figs. 5.10b, c & d). A similar pattern of en-echelon nucleation and displacement continued throughout the progressive development of the model (Figs. 5.10e, f, g, h & i). The thrusts on the short side were fairly minor but usually they appeared at approximately the same time as the corresponding thrusts on the long side and could be faintly traced around the corner to link up with them. Ahead of the corner discrete faulting was very weak (Fig. 5.10j) but diffuse shortening and extension was strong (Fig. 5.10i). Thrusting was more or less perpendicular to the fault trace combined with variable amounts of diffuse wrenching causing smooth bending of grid lines. Locally a coincidence of thrusting and wrench-shear on the same fault plane led to oblique thrusting.

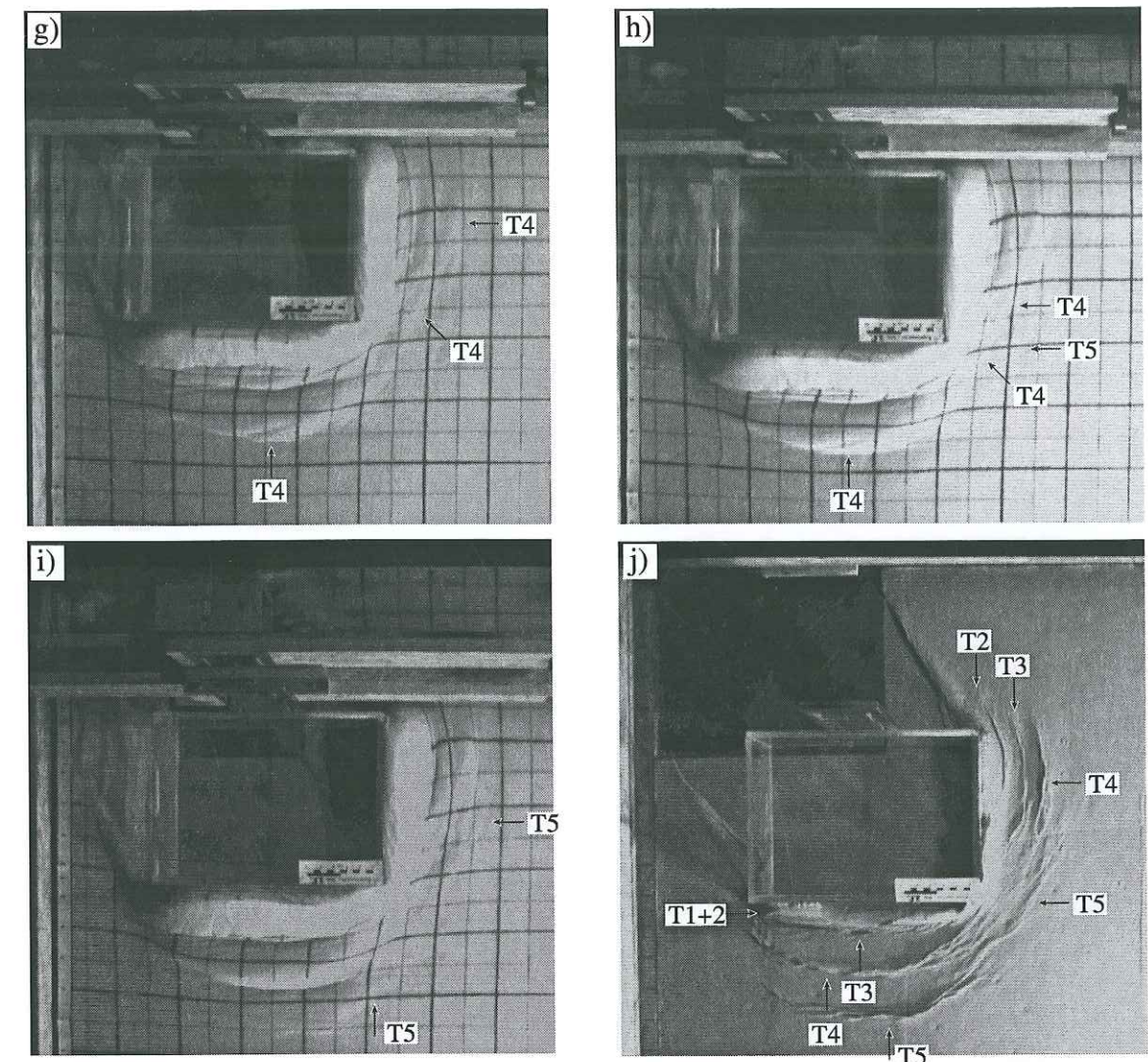
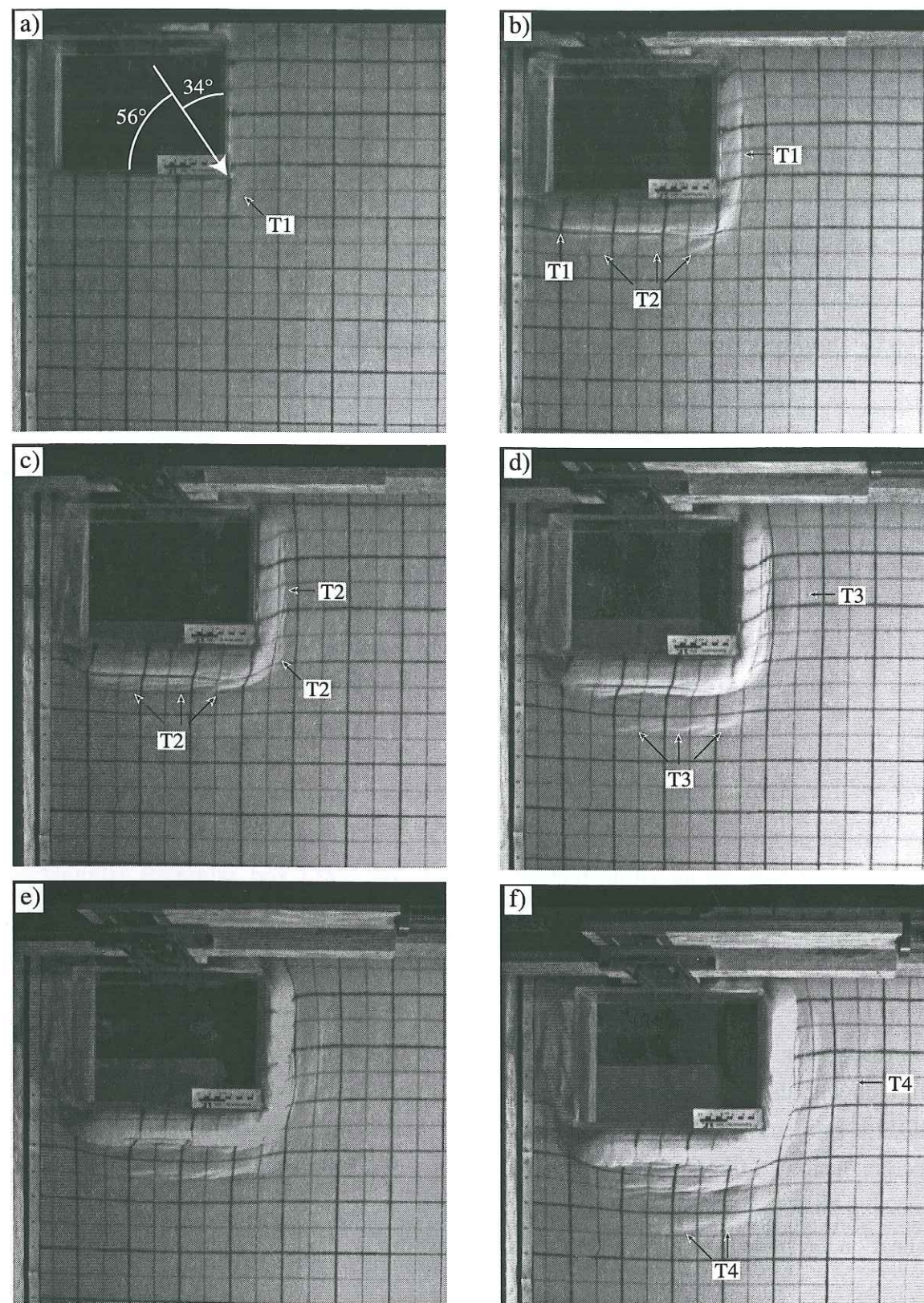


Fig. 5.10: Photograph of upper surface of model WHL-25, with rigid rectangular indenter moving oblique into foreland. Square grid of passive marker lines spaced every 5 cm (black and grey lines). a)- i): refer to Fig. 5.8 for amount of shortening. j) silicon at the base of model at the end of experiment. T = forethrust. For further description see text.

5.3.2 Elliptical translation path

The elliptical translation path was accomplished by short straight segments, each active for about 30 minutes (Fig. 5.9). The indenter first moved perpendicular to the long side of the box at 4.2 cm/h and at the end of the experiment it moved perpendicular to the short side of the box at about 2.7 cm/h. The first thrust (T1a) appeared along the long side of the box and was followed by a second thrust (T1b) in the immediate footwall (Fig. 5.11a). Only after the initiation of the second thrust front (T2) did minor thrusting along the short side occur (Ts) (Fig. 5.11b). T1 and T2 are bound by lateral wrench zones. T3 is the first thrust which links round the corner. It initiated at the long side (Fig. 5.11c) and

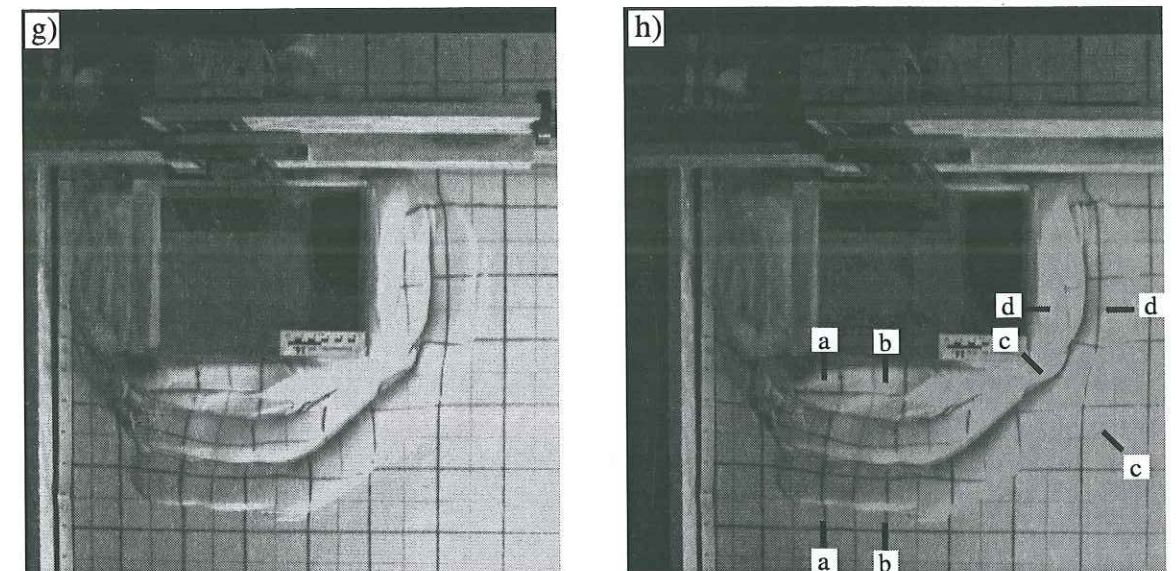
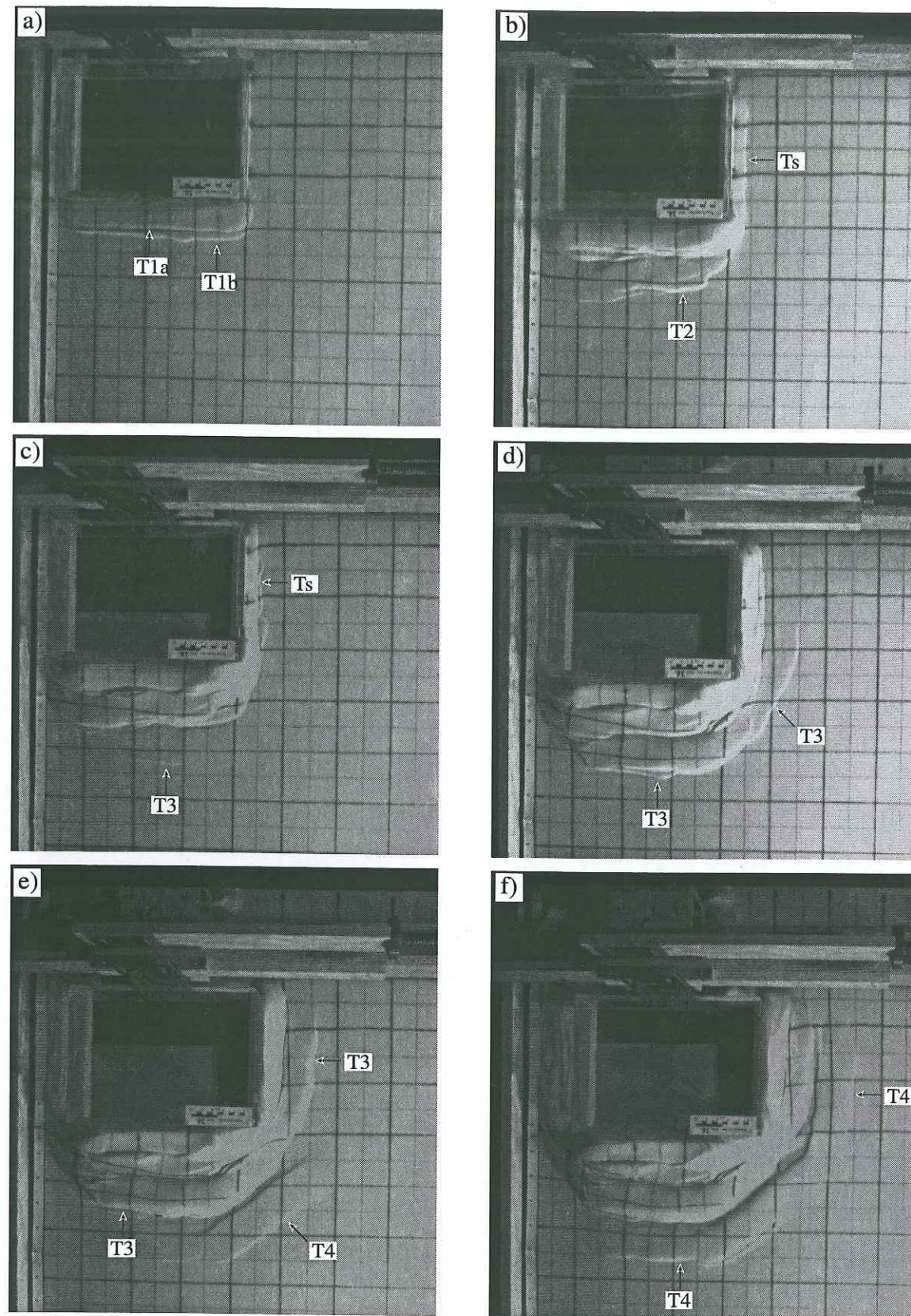


Fig. 5.11: Photograph of upper surface of model WHL-25, with rigid rectangular indenter moving along an elliptical path into foreland. Square grid of passive marker lines spaced every 5 cm (black and grey lines). a)- h): refer to Fig. 5.8 for amount of shortening. h) Location of profile cuts are shown. T = forethrust. For further description see text.

progressively propagated around the corner (Fig. 5.11d) and further along the short side (Fig. 5.11e). In contrast T4 initiated at the corner and progressively propagated along both edges (Figs. 5.11f, g & h). Thrusting was more or less perpendicular to the fault trace, i.e. radial. During the first part of the experiment diffuse shearing and small-scale wrench systems were predominant along the short side (Fig. 5.11b, c & d). At late stages of deformation the thrust wedge along the long side was increasingly sheared dextrally which was mainly accommodated on existing thrusts (Fig. 5.11d, g & h).

Profile-cuts reveal a surprisingly consistent geometry round the arc. At the long side all 4 thrust fronts (T1 - T4) are nicely preserved (Fig. 5.12a). Foreland-vergent thrust zones are always related to steeper backthrusts. Towards the corner T1 diminishes and dies out against the rigid box (Fig. 5.12b). Right at the corner only T3 and T4 occur (Fig. 5.12c). Along the short side displacement on Ts gradually increases away from the corner (Fig. 5.12d). T3 and T4 have a consistent shape around the whole arc, although the transport direction changed by over 90°.

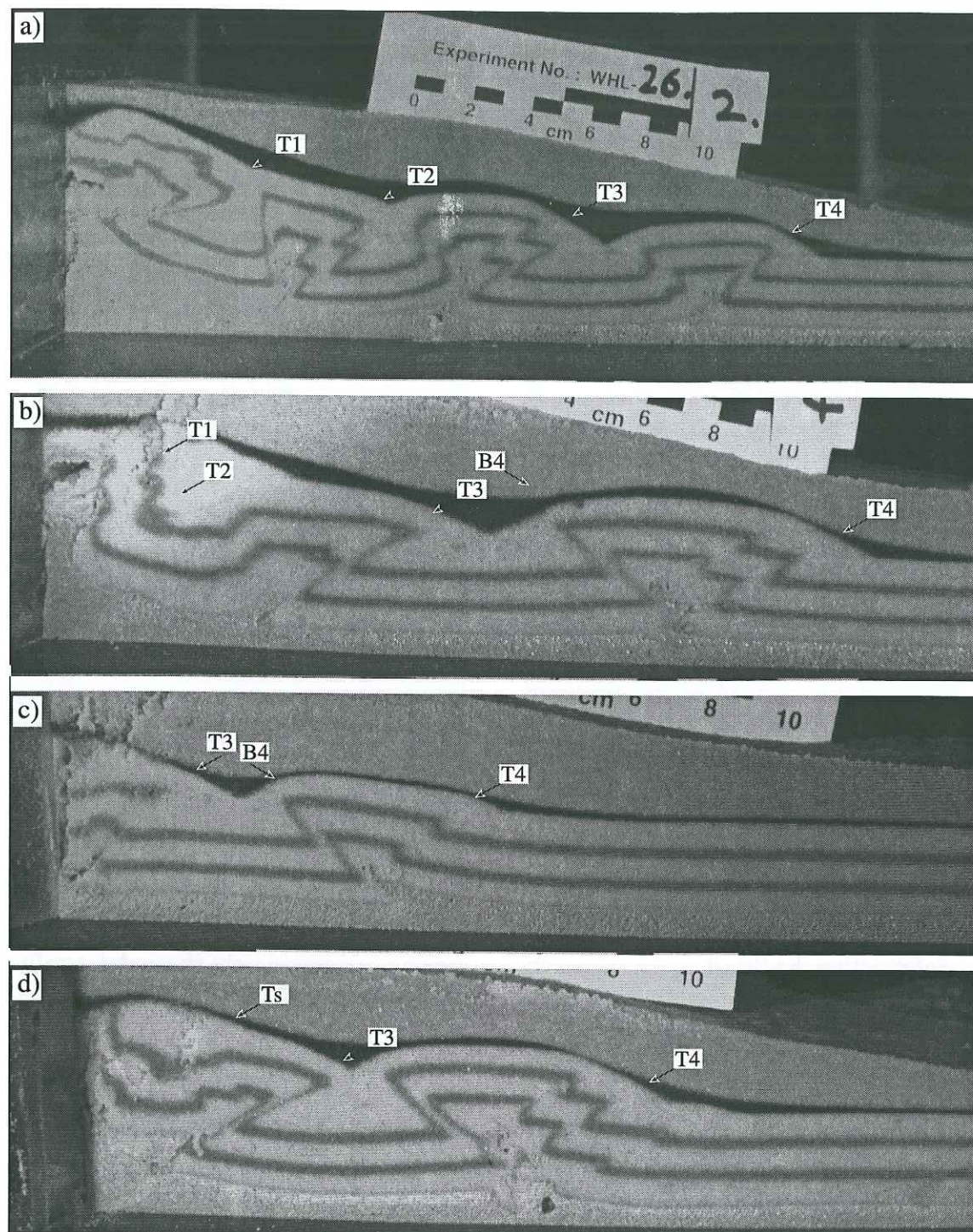


Fig. 5.12: Profile-cuts of experiment WHL-26, detailed location of profiles in Fig. 5.11h. Internal deformation outlined by two, initially parallel darker layers. A black layer separates the model topography from the later poured protective cover of sand. a) & b) Thrust-wedge development at the long flank. The rear of the thrust wedge is elevated adjacent to the vertical backstop. c) At the corner, low amount of discrete faulting. d) Perpendicular to the short flank. T = forethrust, B = backthrust.

5.4 Interpretation and significance

The analogue models presented have successfully simulated the behaviour of deformation around a foreland obstacle such as the Pelvoux massif, and on a larger scale the pattern of thrusting in an arc formed by two main transport directions generated by an oblique indenter.

In the smaller-scale obstacle experiments the undeformed rectangular obstacle should represent the Pelvoux basement massif and the propagating thrusts on either side should represent part of the northern and southern Subalpine chains. In the experiments the obstacle itself remains undeformed which is not true in nature (i.e. Pelvoux is deformed), but the experiments clearly suggest how the advancing Subalpine chains may have interacted with the rim of the Pelvoux massif. The experiments with a silicone-free zone at the base are a good equivalent for the Pelvoux basement massif buried underneath the Tertiary cover sequence. The experiment with a high obstacle represent the opposite extreme case which helps to analyse the influence of the burial depth.

The indentation experiments aimed to show the pattern of deformation related to different motion paths of an indenter. The oblique straight and oblique elliptical motion paths represent two characteristic variations of oblique Adria motion relative to stable Europe (Dewey *et al.*, 1989). The rectangular indenting box represents the inner part of the Alps, and the deforming part represents the external Alps. In the two experiments the northern and southern Subalpine chains clearly developed and the structural pattern can be compared to nature.

In all models the foreland nucleating and foreland-vergent thrust system is characterised by asymmetric 'pop-up' structures, it has been demonstrated that this is typical for fold and thrust belts with salt (low basal friction; Davis and Engelder, 1985; Davis and Lillie, 1994) which increases the number of backthrusts in the system. The curvature of fault traces (etc.) towards the margin of the experimental box is due completely to lateral friction at the walls of the experimental box and can therefore be neglected.

5.4.1 Discussion of obstacle experiments

The experiments WHL-22, 23 and 24 show that the influence of an obstacle on the development of a fold and thrust belt is restricted to the peripheral area of the obstacle.

Low obstacle

In the analogue models with a low obstacle the deformation front rapidly migrates to the edge of the obstacle and the OT is active before the thrust front on either side reaches the level of the obstacle which is similar to the strain localisation at tips of heterogeneities found in numerical modelling (e.g. England and Houseman, 1985;

Tommasi and Vauchez, 1997) and analogue modelling (Souriot *et al.*, 1991; Letouzey *et al.*, 1995). With increasing shortening, the OT ramps upwards over the obstacle and, depending on the shape of the obstacle, frontal and lateral ramps (WHL-22) or oblique ramps (WHL-23) are generated. These ramps only affect the rim of the obstacle so that the core of the obstacle remains completely undeformed. In the hangingwall of the frontal and oblique ramps the sand is locally piled up against the obstacle. This tectonic thickening is partly compensated by lateral extrusion (increased width of grid lines) behind the obstacle. This extrusion is stronger behind a straight obstacle than behind a diagonal obstacle. Thus, thrust sheets ramp over the obstacle but are also piled up against the obstacle. This is a combination of two geometric models proposed by Couples and Lewis (1988) which illustrate possible types of interaction between thrust sheets and basement blocks. Their third interaction type (the buttressed sheet comes to a halt, and a tear develops between that portion and the advancing thrust) does not occur in the analogue models because it demands a tear in the backstop.

A deflection of the transport direction away from the vertical plane perpendicular to the backstop can be observed at the lateral ramps and in the hangingwall of the oblique ramps. The deflection for the frontal ramp (in WHL-22) is zero. At the lateral ramp faults initiate at 70 - 60° to the obstacle. During the subsequent deformation they accommodate oblique thrusting towards the obstacle out of the plane perpendicular to the backstop (step-offsets of N-S grid lines). Simultaneously wrench shear enhances the curvature of the thrust traces (and bend of E-W grid lines). This deformation is similar to the divergent thrusting observed at indentation which has been explained by the stress distribution in an elastic half-space when an indenting force is applied (Laubscher, 1972; Davy and Cobbold, 1988). It is combined with the effect of passive rotation by wrench shear as can be observed at lateral boundaries of indentors (Chamberlin and Shepard, 1923; Bale, 1986). As the fold and thrust belt encounters an oblique obstacle, similar processes take place when the faults branch onto the OT. But thrusting on the OT itself has no deflection. Similar processes have been documented in the Champsaur-Prapic area (Chapter 2). The axial-trend of the chevron-like folds curves towards the oblique rim of the Pelvoux massif whereas the displacement direction in the basal shear zone remains WSW-directed (Figs. 2.1 & 2.18). The basal shear zone represents the obstacle thrust OT, where in the analogue models no deflection from the regional transport direction has been observed, and the bend in the orientation of the chevron folds corresponds to the accommodation features in the hangingwall of the OT due to buttressing.

High obstacle

In the experiment WHL-24, with an extremely high and rigid obstacle, the differences in the deformation are surprisingly small in comparison to those of the low obstacle experiments. Instead of the OT, distinct wrench shear zones develop to both sides of the obstacle. Where the propagating thrust system branches on the wrench shear zone similar deflection of the transport direction can be observed as in the hangingwall of the OT in experiment WHL-23. The main difference arises because the material can not overthrust the obstacle which 1) leads to stronger lateral extrusion than in the experiments with a low obstacle and 2) seems to slow down the propagation into the foreland (compare width of deformed zone in Fig. 5.4d to Fig. 5.7d), i.e. the same amount of shortening is taken up by stronger deformation in a narrower zone.

Generalisations

In all obstacle experiments, about 5 cm away from the obstacle, the displacement direction continues perpendicular to the backstop throughout the progressive development of the thrust wedge independent of the shape of the obstacle. In nature, 5 cm correspond to 5 km (Table 5.1) which is in perfect agreement to observations from the Champsaur-Prapic area (Fig. 2.1). Further away only the strain imposed by the motion of the backstop controls the formation of faults at the front of the thrust wedge. Therefore, in the analogue models presented, obstacles do not split the deformation on a regional scale into independent thrust systems controlled by the shape of the obstacle. Note that this is also the case for the high strong obstacle which can not be overthrust. These modelling results clearly indicate that the Pelvoux massif can not have been the cause of the two thrust systems forming the northern and southern Subalpine chains even though it lies at their juncture.

This is in contrast to the findings of Beutner (1977) and Marshak *et al.* (1992) who propose that obstacles control the formation of curved fold and thrust belts. But their analogue models are not properly scaled for the mechanical behaviour of natural rocks because they used gelatine and damp sand which have a cohesive strength far too high compared to the dry sand used in this study. This may lead to their different and misleading results.

5.4.2 Discussion of indentation experiments

The main characteristics of the indentation experiments is the development of two independent thrust systems which accommodate different amounts of shortening. The deformation is dominated by the oblique indentor margins which are clearly an important location for strain partitioning (e.g. Haq and Davis, 1997). The total indentation is resolved into a component parallel to the indentor sides, accommodated through strike-

slip faulting, and two components normal to the indenter sides taken up as contraction. This transpressive system results in the formation of new thrusts as a series of en-echelon oblique thrusts.

Differences between the oblique straight and the oblique elliptical translation path

In the case of oblique but straight indentation the deformation splits in two mirror-image transpression systems with complementary portions of strike-slip and thrusting, depending on the angle of indentation. At the beginning of the experiment, the two systems linked around the corner in curved thrusts, but with progressive deformation they became divided at the advancing corner of the indenter. In this corner zone, thrusting is radial but rather weak and strongly overprinted by lateral extension.

With an oblique elliptical translation path, indentation resulted in a complete, well developed radial thrust belt in the external part of the model while the wrench shear components concentrated in the internal parts of the thrust belts. The external radial thrusting is characterised by a progressive shift of the main deformation front from one side of the indenter, around the corner to the other side in the same sense as the curved path motion.

Generalisations and application to external Alps

These oblique indentation models can be compared to several major features of the evolution of the external western Alps (Chapter 4).

- 1) There are two sub-perpendicular thrust systems active at the same time.
- 2) The two thrust systems show different amounts of shortening which is related to the obliquity of the translation path. It can easily be adjusted to fit the large amounts of shortening in the northern Subalpine chains and the smaller amounts of shortening in the southern Subalpine chains.
- 3) Both thrust systems die out towards the centre of the semicircular arc, where shortening is lowest (Figs. 5.10j & 5.12c).

Features of the experiments which are not obvious in the external Alps are the following:

- 4) There is a diffuse wrench shear component parallel to the indenter sides. The amount of wrench shear is related to the obliquity of the translation path. The wrench shear component is highest at the edge of the indenter and decreases into the foreland.

Such shear is not yet a generally accepted feature of external Alps. Although, late NE-SW trending dextral shear has been inferred for the northern Subalpine chains (e.g. Mugnier and Gidon, 1988; Ménard, 1988). Large amounts of sinistral shear

along the Frontal Pennine Thrust in the southern Subalpine chains has already been proposed (Ricou, 1984; Ricou and Siddans, 1986). Further evidence for such a lateral ramp comes also from the foreland basin evolution around the Alps (Ford *et al.*, submitted).

- 5) Oblique thrusting occurs in the internal part, where the wrench shear coincides with a thrust plane.
- 6) In the centre of the arc, where the two thrust systems die out, the deformation is dominated by tangential extension (straight translation path) and by radial thrusting (elliptical translation path).

Large amounts of tangential extension have, however, not been reported from this area in the external Alps (e.g. Gratier, 1989).

Thus, it seems that oblique indentation is a powerful model to explain the main characteristics of the deformation in the external Alps (point 1 - 3) which previous models could not explain. The model with an oblique elliptical translation path of the indenter is favoured, because the 'problematical' wrench shear is restricted to the more internal part and because no large amounts of tangential extension occur in the central part of the model.

5.4.3 Summary

Two main conclusions can be derived from the analogue sand-silicon experiments:

An obstacle cannot split the deformation on a regional scale into independent divergent thrust systems controlled by the shape of the obstacle, neither a low overthrustable obstacle nor a high strong obstacle. Therefore the Pelvoux massif, which represents a low obstacle, did not control the formation of the external Alpine arc nor the position of the Alpine arc although it had a local influence of fold trends. It appears to be mere chance that the Pelvoux massif sits at the interference point of the two thrust systems of the northern and southern Subalpine chains.

Oblique indentation is a powerful process to produce divergent thrusting. In both types of indentation experiments two thrust systems developed at right angles, overprinted by two wrench shear systems. Therefore oblique and elliptical motions of Adria can cause the formation of the external Alpine arc. This compares well to published plate motions of Africa - Adria (e.g. Dewey, 1989).

6. General conclusions

This thesis documents the post-mid-Oligocene deformation within two foreland basin remnants at the southern rim of the Pelvoux massif which record the transition between the northern and the southern Subalpine chains. These areas bear significant information for the evolution of the external Alpine arc. The following main conclusions for the development of the Alpine arc can be drawn.

The Champsaur-Prapic area at the southeastern rim of the Pelvoux massif documents to the north, around Chambran, the change of the regional tectonic transport direction from WSW-SW-directed to NW-directed. This change records the transition from the SW-directed sector of the southern Subalpine chains to the NW-directed sector of the northern Subalpine chains which is in this locality abrupt and not segmented with any significant fault zone.

The total WSW-directed shortening in the Champsaur-Prapic fold zone is about 5 km. Thus, it marks a significant decrease of the shortening within the southern Subalpine chains northwards.

The deformation in the Soleil Boeuf area at the southern rim of the Pelvoux massif is characterised by NW-directed folding and thrusting which accommodates at least 6.8 km shortening. The deformation roots down into the basement. On a local scale the deformation in Soleil Boeuf post-dates the WSW-directed deformation in the Champsaur-Prapic fold zone, but on a regional scale it is simultaneous with the SW-directed deformation in the southern Subalpine chains.

Thus the NW-directed deformation in Soleil Boeuf is most probably accommodated on a deep satellite fault system to the main NW-directed deformation in the northern Subalpine chains simultaneously with thin-skinned SW-directed deformation in the Mesozoic and Tertiary cover sequences. Therefore, to the south of the Pelvoux massif the two branches of the northern and southern Subalpine chains evolved simultaneously but at different levels.

The results of this study do not support a radial forming arc, but rather that there is a distinct break in the kinematic pattern of the arc between the NW and SW-directed transport.

Previous models that explain the kinematic break do not consider that NW and SW-directed transport went on at the same time. According to new analogue sand-silicone experiments it could be shown that such diverging thrust systems develop ahead of oblique indentation. Experiments with an oblique elliptical translation path of the

indenter produce the main characteristics of the external arc which are: two sub-perpendicular thrust systems evolving at the same time with different amounts of shortening and both dying out towards the centre of the arc.

Additionally it was shown that obstacles do not have any regional influence on the development of arcuate fold and thrust belt systems. This signifies that the presence of the Pelvoux massif as a paleohigh in the core of the arc did not significantly influence the formation of the external arc.

Suggestions for further research

Further work should concentrate on the tectonic relationship between the external and internal units to figure out how the strain imposed by the two simultaneously divergent transport directions in the external domain is accommodated in the internal domain. In order to identify the dynamics of the southern Subalpine chains the relationship between the Embrunais-Ubaye nappes and the Sub-Briançonnais and Briançonnais units has to be clarified first. Which nappe caused the overthrust shear deformation in the Champsaur-Prapic fold zone in other words, is the main tectonic boundary between the internal and external domain at the base of the Embrunais-Ubaye nappes, or at the base of the Sub-Briançonnais or even Briançonnais nappes? Another question is the relation of NW and SW-directed deformation to the east of the Pelvoux massif. Is there a major transfer zone, and if yes where is it? Is it the Frontal Pennine Thrust as suggested by Ricou and Siddans (1986)? This brings up the question of the kinematics on the Frontal Pennine Thrust, recent work has highlighted late normal displacements (Tricart *et al.*, 1996) What is their significance and how do they obliterate original kinematic patterns.

Another point is the timing and amount of strike-slip motion in the northern and southern Subalpine chains. This would give further constraints on the validity of the oblique indentation model.

References

- Allen, P. A., Crampton, S. L. and Sinclair, H. D. (1991) The inception and early evolution of the North Alpine Foreland Basin, Switzerland. *Basin Research* **3**, 143-163.
- Allmendinger, E. W., Marret, R. A. and Cladouhos, T. (1989-94) *FaultKin v. 3.8a. Apple Macintosh computer program*, version 3.8a.
- Aprahamian, J. (1974) La cristallinité de l'illite et les minéraux argileux en bordure des massifs cristallins externes de Belledonne et du Pelvoux (variations et relations possibles avec des événements tectoniques et métamorphiques alpins). *Géologie Alpine* **50**, 5-15.
- Arlhac, P. and Rousset, C. (1979) La nappe de Digne près de Gap (Hautes-Alpes): sa place dans les Alpes externes françaises. *Comptes rendus de l'Académie des Sciences; série D* **288**, 47-50.
- Arnaud, H., Barfety, J.-C., Gidon, M. and Pairis, J.-L. (1978) A propos du rhéglissement des zones externes alpines au sud de Grenoble. *Comptes rendus de l'Académie des Sciences; série D* **286**, 1335-1338.
- Arnaud, H., Gidon, M. and Pairis, J.-L. (1977) Précisions sur la structure des chaînes subalpines méridionales dans la région de Faucon-Turriers-Clamensane (Alpes-de-Haute-Provence). *Géologie Alpine* **53**, 5-34.
- Arpin, R., Gratier, J.-P. and Thouvenot, F. (1988) Chevauchements en Vercors-Chartreuse déduits de l'équilibrage des données géologiques et géophysiques. *Comptes rendus de l'Académie des Sciences; série D* **307**, 1779-1786.
- Bale, P. (1986) Tectonique cadomienne en Bretagne nord. Interaction décrochement-chevauchement: champs de déformation et modélisations expérimentales. Unpublished Ph. D. thesis, Université de Rennes.
- Barfety, J.-C., Lemoine, M., Mercier, D., Polino, R., Nievergelt, P., Bertrand, J., Dumont, T., Amaudric du Chaffaut, S., Pêcher, A. and Monjuvent, G. (1995) *Carte géologique de la France (1/50'000). Feuille Briançon (823)*. BRGM, Orléans.
- Barfety, J.-C., Pêcher, A., Debelmas, J., Gidon, M., Mouterde, R., Vernet, J., Le Fort, P., Barbieri, A., Biju-Duval, J., Gillot-Barbieri, C., Bartoli, F. and Ozocak, R. (1984) *Carte géologique de la France (1/50'000). Feuille St.-Christophe-en-Oisans (822)*. BRGM, Orléans.
- Beach, A. (1980) Some observations on the development of thrust faults in the Utradauphinois Zone, French Alps. In *Thrust and nappe tectonics*, eds K. R. McClay and N. J. Price, pp. 335-352. *Geological Society Special Publication* **9**.
- Beach, A. (1981a) Thrust structures in the eastern Dauphinois Zone (French Alps), north of the Pelvoux Massif. *Journal of Structural Geology* **3**, 299-308.
- Beach, A. (1981b) Thrust tectonics and cover-basement relations on the northern margin of the Pelvoux massif, French Alps. *Eclogae geologicae Helveticae* **74**, 471-479.
- Beach, A. (1982) Strain analysis in a cover thrust zone, external French Alps. *Tectonophysics* **88**, 333-346.
- Bergerat, F. (1987) Paléo-champs de contrainte tertiaires dans la plate-forme européenne au front de l'orogène alpin. *Bulletin de la Société Géologique de France; série 8* **3**, 611-620.
- Beuf, S. (1959) Contribution à l'étude géologique du Massif de Soleil Boeuf. Diplôme E.N.S.P.M., Grenoble.
- Beutner, E. C. (1977) Causes and consequences of curvature in the Sevier orogenic belt, Utah to Montana. In: *Wyoming Geological Association 29th annual field conference in conjunction with Montana Geological Society & Utah Geological Society; Rocky Mountain thrust belt, geology and resources* (edited by E. L. Heisey, D. E. Lawson, E. R. Norwood, P. H. Wach and L. A. Hale). Wyoming Geological Association, Teton Village, Wyoming, 353-365.
- Bocquet, J. (1974) Colloque des 19-20 novembre 1973. Séance spécialisée de la Société Géologique de France: Le métamorphisme alpin dans les Alpes occidentales. *Géologie Alpine* **50**, 27-37.
- Borradaile, G. J. (1978) Transected folds: a study illustrated with examples from Canada and Scotland. *Geological Society of America Bulletin* **89**, 481-493.
- Bosworth, W. and Vollmer, F. W. (1981) Structures of the medial Ordovician flysch of eastern New York: deformation of synorogenic deposits in an overthrust environment. *Journal of Geology* **89**, 551-568.
- Bravard, C. (1982) Données nouvelles sur la stratigraphie et la tectonique de la zone des Aiguilles d'Arves au Nord du Lautaret. *Géologie Alpine* **58**, 5-13.
- Bravard, C. (1983) Les structures à vergence Est de la zone des Aiguilles d'Arves (Savoie). *Géologie Alpine* **59**, 33-43.
- Bravard, C. and Gidon, M. (1979) La structure du revers oriental du Massif du Pelvoux: observations et interprétations nouvelles. *Géologie Alpine* **55**, 23-33.
- Bruhn, R. L. (1979) Rock structures formed during back-arc basin deformation in the Andes of Tierra del Fuego. *Geological Society of America Bulletin* **90**, 998-1012.
- Burg, J.-P., Bale, P., Brun, J.-P. and Girardeau, J. (1987) Stretching lineation and transport direction in the Ibero-Armorican arc during the siluro-devonian collision. *Geodinamica Acta* **1**, 71-87.
- Bürgisser, J. and Ford, M. (1998) Overthrust shear deformation of a foreland basin; structural studies south-east of the Pelvoux massif, SE France. *Journal of Structural Geology* **20**, 1455-1475.
- Butler, R. W. H. (1984) Balanced cross-sections and their implications for the deep structure of the north-west Alps: reply. *Journal of Structural Geology* **6**, 607-612.
- Butler, R. W. H. (1985) The restoration of thrust systems and displacement continuity around the Mont Blanc massif, NW external Alpine thrust belt. *Journal of Structural Geology* **7**, 569-582.
- Butler, R. W. H. (1987) Thrust evolution within previously rifted regions: an example from the Vercors, French Subalpine chains. *Memorie della società geologica Italiana* **38**, 5-18.
- Butler, R. W. H. (1989) The influence of pre-existing basin structure on thrust system evolution in the Western Alps. In *Inversion tectonics*, eds M. A. Cooper and G. D. Williams, pp. 105-122. *Geological Society Special Publication* **44**.
- Butler, R. W. H. (1992a) Thrust zone kinematics in a basement-cover imbricate stack: Eastern Pelvoux massif, French Alps. *Journal of Structural Geology* **14**, 29-40.
- Butler, R. W. H. (1992b) Thrusting patterns in the NW French subalpine chains. *Annales Tectonicae* **6**, 150-172.
- Butler, R. W. H., Matthews, S. J. and Parish, M. (1986) The NW external Alpine Thrust Belt and its implications for the geometry of the Western Alpine Orogen. In *Collision Tectonics*, eds M. P. Coward and A. C. Ries, pp. 245-260. *Geological Society Special Publication* **19**.
- Byerlee, J. (1978) Friction of rock. *Pure Appl. Geophys.* **116**, 615-626.
- Casey, M. and Dietrich, D. (1997) Overthrust shear in mountain building. In *Evolution of geological structures in micro- and macro-scales*, eds S. Sengupta, pp. 119-142.
- Casey, M. and Huggenberger, P. (1985) Numerical modelling of finite-amplitude similar folds developing under general deformation histories. *Journal of Structural Geology* **7**, 103-114.
- Chamberlin, R. T. and Shepard, F. P. (1923) Some experiments in folding. *Journal of Geology* **31**, 490-512.
- Choukroune, P., Ballèvre, M., Cobbold, P., Gautier, Y., Merle, O. and Vuichard, J.-P. (1986) Deformation and motion in the Western Alpine Arc. *Tectonics* **5**, 215-226.
- Coward, M. P., Gillcrist, R. and Trudgill, B. (1991) Extensional structures and their tectonic inversion in the Western Alps. In *The geometry of normal faults*, eds A. M. Roberts, G. Yielding and B. Freeman, pp. 93-112. *Geological Society Special Publication* **56**.
- Coward, M. P. and Potts, G. J. (1983) Complex strain patterns developed at the frontal and lateral tips to shear zones and thrust zones. *Journal of Structural Geology* **5**, 383-399.
- Davies, V. M. (1982) Interaction of thrusts and basement faults in the French external Alps. *Tectonophysics* **88**, 325-331.
- Davis, D. M. and Engelder, T. (1985) The role of salt in fold-and-thrust belts. *Tectonophysics* **119**, 67-89.
- Davis, D. M. and Lillie, R. J. (1994) Changing mechanical response during continental collision: active examples from the foreland thrust belts of Pakistan. *Journal of Structural Geology* **16**, 11-20.
- Davy, P. (1986) Modélisation thermo-mécanique de la collision continentale. Unpublished Ph. D. thesis, Université de Paris Sud.
- Davy, P. and Cobbold, P. R. (1988) Indentation tectonics in nature and experiment. 1. Experiments scaled for gravity. *Bull. Geol. Inst. Univ. Uppsala N. S.* **14**, 129-141.
- Davy, P. and Cobbold, P. R. (1991) Experiments on shortening of a 4-layer model of the continental lithosphere. *Tectonophysics* **188**, 1-25.
- Debelmas, J. and Kerckhove, C. (1973) Large gravity nappes in the French-Italian and French-Swiss Alps. In *Gravity and tectonics*, eds K. A. de Jong and R. Scholten, pp. 189-200.
- Debelmas, J. and Kerckhove, C. (1980) Les Alpes franco-italiennes. *Géologie Alpine* **56**, 21-58.
- Debelmas, J., Le Fort, P., Biju-Duval, J., Vernet, J., Monjuvent, G., Beuf, S., Kerckhove, C. and Pêcher, A. (1980) *Carte géologique de la France (1/50'000). Feuille Orcières (846)*. BRGM, Orléans.
- Debelmas, J. and Lemoine, M. (1970) The Western Alps: palaeogeography and structure. *Earth-Science Reviews* **6**, 221-256.
- Debelmas, J., Lemoine, M., Kerckhove, C., Fail, J.-P., Lavergne, M., Leduc, J., Legreneur, J., Ortollan, J., Robert, J.-P., Porié, R. and Gidon, M. (1966) *Carte géologique de la France (1/50'000). Feuille Guillestre (847)*. Service de la Carte Géologique de la France, Paris.

- Debrand-Passard, S., Courbouleix, S. and Lienhardt, M.-J. (1984a) Synthèse géologique du Sud-Est de la France. *Mémoire de Bureau de recherches géologiques et minières* 125.
- Debrand-Passard, S., Courbouleix, S. and Lienhardt, M.-J. (1984b) Synthèse géologique du Sud-Est de la France. *Mémoire de Bureau de recherches géologiques et minières* 126.
- Dewey, J. F., Helman, M. L., Turco, E., Hutton, D. H. W. and Knott, S. D. (1989) Kinematics of the western Mediterranean. In *Alpine Tectonics*, eds M. P. Coward, D. Dietrich and R. G. Park, pp. 265-283. *Geological Society Special Publication* 45.
- Dietrich, D. and Casey, M. (1989) A new tectonic model for the Helvetic nappes. In *Alpine tectonics*, eds M. P. Coward, D. Dietrich and R. G. Park, pp. 47-63. *Geological Society Special Publication* 45.
- Dietrich, D. and Durney, W. D. (1986) Change of direction of overthrust shear in the Helvetic nappes of western Switzerland. *Journal of Structural Geology* 8, 389-398.
- Donath, F. A. and Parker, R. B. (1964) Folds and folding. *Geological Society of America Bulletin* 75, 45-62.
- Durney, D. W. and Ramsay, J. G. (1973) Incremental strains measured by syntectonic crystal growths. In *Gravity and tectonics*, eds K. A. De Jong and R. Scholten, pp. 76-96.
- Elliot, T., Apps, G., Davies, H., Evans, M., Ghibaudo, G. and Graham, R. H. (1985) A structural and sedimentological traverse through the Tertiary foreland basin of the external Alps of South-East France. In *International Symposium on Foreland Basins*, eds P. Allen, P. Homewood and G. Williams, pp. 39-73.
- England, P. and Houseman, G. (1985) Role of lithospheric strength heterogeneities in the tectonics of Tibet and neighbouring regions. *Nature* 315, 297-301.
- Etchecopar, A. (1990-1994) *Faille v. 3.5. Apple Macintosh computer program*.
- Evans, M. J. and Mange-Rajetzky, M. A. (1991) The provenance of sediments in the Barre thrust-top basin, Haute-Provence, France. In *Developments in sedimentary provenance studies*, eds A. C. Morton, S. P. Todd and P. D. W. Haughton, pp. 323-342. *Geological Society Special Publication* 57.
- Fabre, P., Lami, A., Mosser, C., Pairis, J.-L. and Bonhomme, M. G. (1988) Minéralogie, géochimie et datations K-Ar des fractions fines dans le bassin nummulitique, au sud et à l'est du Pelvoux (Alpes externes méridionales, France). In *Le détritisme dans le sud-est de la France*, pp. 265-272. *Géologie alpine; mémoire h.s.* 14.
- Fabre, P., Lami, A., Pairis, J.-L. and Gidon, M. (1985) Influence de la paléomorphologie et de la tectonique synsédimentaire sur les dépôts nummulitiques dans les massifs du Dévoluy et du Pelvoux (Alpes externes méridionales). *Revue de géologie dynamique et de géographie physique* 26, 193-199.
- Fischer, M. P. and Woodward, N. B. (1990) The geometric evolution of foreland thrust systems. In *Thrust tectonics*, eds K. R. McClay, pp. 181-189.
- Flandrin, J. (1966) Sur l'âge des principaux traits structuraux du Diois et des Baronnies. *Bulletin de la Société Géologique de France; série 7* 8, 376-386.
- Fontignie, D., Delaloye, M. and Vuagnat, M. (1987) Age potassium-argon de galets andésitiques des grès du Champsaur (Hautes-Alpes, France). *Schweizerische mineralogisch-petrographische Mitteilungen* 67, 171-184.
- Ford, M. (1996) Kinematics and geometry of early Alpine, basement-involved folds, SW Pelvoux Massif, SE France. *Eclogae geologicae Helveticae* 89, 269-295.
- Ford, M., Lickorish, W. H. and Kusznir, N. (submitted) Evolution of foreland basins around curved orogenic belts: a comparative study of the southwestern and northern sectors of the Alpine foreland basin. *Basin Research*.
- Ford, M., Meckel, L. D. and Bürgisser, J. (1995) Late Alpine kinematics around the Pelvoux massif, SE France: implications for arc geodynamics. *Terra Nova* 7, 274.
- Fry, N. (1989) Southwestward thrusting and tectonics of the western Alps. In *Alpine tectonics*, eds M. P. Coward, D. Dietrich and R. G. Park, pp. 83-109. *Geological Society Special Publication* 45.
- Ghosh, S. K. (1966) Experimental tests of buckling folds in relation to strain ellipsoid in simple shear deformations. *Tectonophysics* 3, 169-185.
- Gibson, R. G. and Gray, D. R. (1985) Ductile-to-brittle transition in shear during thrust sheet emplacement, Southern Appalachian thrust belt. *Journal of Structural Geology* 7, 513-525.
- Gidon, M. (1965) Sur l'interprétation des accidents de la bordure méridionale du massif du Pelvoux. *Travaux du Laboratoire de Géologie de la faculté des sciences de Grenoble* 41, 177-185.
- Gidon, M. (1975) Sur l'allochtonie du "Dôme de Remollon" (Alpes françaises du Sud) et ses conséquences. *Comptes rendus de l'Académie des Sciences; série D* 280, 2829-2832.

- Gidon, M. (1979) Le rôle des étapes successives de déformation dans la tectonique alpine du massif du Pelvoux (Alpes occidentales). *Comptes rendus de l'Académie des Sciences; série D* 288, 803-806.
- Gidon, M. and Pairis, J.-L. (1980-1981) Nouvelles données sur la structure des écaïles de Soleil Boeuf (bordure sud du massif du Pelvoux). *Bulletin du Bureau de Recherches Géologiques et Minières; série 2; section 1* 1, 35-41.
- Gidon, P. (1953) Les rapports des terrains cristallins et de leur couverture sédimentaire dans les régions orientale et méridionale du massif du Pelvoux. *Travaux du Laboratoire de Géologie de la faculté des sciences de Grenoble* 31, 1-202.
- Gignoux, M. and Moret, L. (1937) Description géologique de bassin supérieur de la Durance. *Travaux du Laboratoire de Géologie de la faculté des sciences de Grenoble* 21, 1-295.
- Gignoux, M., Moret, L. and Lory, P. (1932) Révision de la feuille de Gap au 1/80'000. *Bulletin des Services de la Carte Géologique de la France et des Topographies Souterraines* 36, 75-88.
- Gillcrist, R., Coward, M. and Mugnier, J.-L. (1987) Structural inversion and its controls: examples from the Alpine foreland and the French Alps. *Geodinamica Acta* 1, 5-34.
- Goguel, J. (1963) L'interprétation de l'arc des Alpes occidentales. *Bulletin de la Société Géologique de France; série 7* 5, 20-33.
- Gourlay, P. (1986) La déformation du socle et des couvertures delphino-helvétiques dans la région du Mont-Blanc (Alpes occidentales). *Bulletin de la Société Géologique de France; série 8* 2, 159-169.
- Gratier, J.-P., Ménard, G. and Arpin, R. (1989) Strain-displacement compatibility and restoration of the Chaînes Subalpines of the western Alps. In *Alpine tectonics*, eds M. P. Coward, D. Dietrich and R. G. Park, pp. 65-81. *Geological Society Special Publication* 45.
- Gray, D. R. (1995) Thrust kinematics and transposition fabrics from a basal detachment zone, eastern Australia. *Journal of Structural Geology* 17, 1637-1654.
- Guellec, S., Mugnier, J.-L., Tardy, M. and Roure, F. (1990) Neogene evolution of the western Alpine foreland in the light of ECORS data and balanced cross-section. In *Deep structure of the Alps*, eds F. Roure, P. Heitzmann and R. Polino, pp. 165-184. *Société Géologique de France Mémoire* 156, *Société Géologique Suisse Mémoire* 1, *Società Geologica Italiana Volume speciale* 1.
- Gupta, S. (1994) Early development of the south-west Alpine foreland basin: controls on sedimentation and stratigraphy in the Champsaur region, south-east France. Unpublished Ph.D., University of Oxford.
- Gupta, S. (1997) Tectonic control on paleovalley incision at the distal margin of the early Tertiary Alpine foreland basin, southeastern France. *Journal of sedimentary research* 67, 1030-1043.
- Hag, S. S. B. and Davis, D. M. (1997) Oblique convergence and the lobate mountain belts of western Pakistan. *Geology* 25, 23-26.
- Haug, E. (1894) Excursion géologique dans la haute vallée du Drac. *Compte-Rendu des Séances de la Société Géologique de France* 22, CXXXVIII-CLXI.
- Haug, E., Kilian, W., Lory, P., Martin, D. and Termier, P. (1905) *Carte géologique de la France à 1/80'000. Feuille Gap* (200). Ministère des travaux publics. Service géologique des mines.
- Haug, M. E. (1899-1900) Feuille de Gap (la nappe charriée de l'Embrunais). *Bulletin des services de la carte géologique de la France et des topographies souterraines* 11, 194-199.
- Homewood, P. W., Allen, P. A. and Williams, G. D. (1986) Dynamics of the molasse basin in western Switzerland. In *Foreland Basins*, eds P. A. Allen and P. W. Homewood, pp. 119-217. *Special Publication of the International Association of Sedimentologists* 8.
- Hubbert, M. K. (1937) Theory of scale models as applied to the study of geologic structures. *Geological Society of America Bulletin* 48, 14-59.
- Huyghe, P. and Mugnier, J.-L. (1995) A comparison of inverted basins of the Southern North Sea and inverted structures of the external Alps. In *Basin inversion*, eds J. G. Buchanan and P. G. Buchanan, pp. 339-353. *Geological Society Special Publication* 88.
- Johnson, T. E. (1991) Nomenclature and geometric classification of cleavage-transected folds. *Journal of Structural Geology* 13, 261-274.
- Kerckhove, C. (1969) La 'zone du Flysch' dans les nappes de l'Embrunais-Ubaye (Alpes occidentales). *Géologie Alpine* 45, 5-204.
- Kerckhove, C., Debelmas, J. and Cochonat, P. (1978) Tectonique du soubassement parautochtone des nappes de l'Embrunais-Ubaye sur leur bordure occidentale, du Drac au Verdon. *Géologie Alpine* 54, 67-82.

- Laubach, S. E., Reynolds, S. E. and Spencer, J. E. (1989) Progressive deformation and superposed fabrics related to Cretaceous crustal underthrusting in western Arizona, U.S.A. *Journal of Structural Geology* **11**, 735-749.
- Laubscher, H.P. (1969)
- Laubscher, H. P. (1972) Some overall aspects of Jura dynamics. *American Journal of Science* **272**, 293-304.
- Laubscher, H. (1991) The arc of the Western Alps today. *Eclogae geologicae Helveticae* **84**, 631-659.
- Lawson, K. (1987) Thrust geometry and folding in the Alpine structural evolution of Haute Provence. Unpublished Ph.D. thesis, University of Wales, Swansea.
- Lazarre, J., Tricart, P., Courrioux, G. and Ledru, P. (1996) Héritage téthysien et polyphasage alpin: réinterprétation tectonique du "synclinal" de l'Aiguille de Morges (Massif du Pelvoux, Alpes occidentales, France). *Comptes rendus de l'Académie des Sciences; série 2a* **323**, 1051-1058.
- Lemoine, M. (1972) Rythme et modalité des plissements superposés dans les chaînes subalpines méridionales des Alpes occidentales Françaises. *Geologische Rundschau* **61**, 975-1010.
- Lemoine, M., Bas, T., Arnaud-Vanneau, A., Arnaud, H., Dumont, T., Gidon, M., Bourbon, M., de Graciansky, P.-C., Rudkiewicz, J.-L., Megard-Galli, J. and Tricart, P. (1986) The continental margin of the Mesozoic Tethys in the Western Alps. *Marine and Petroleum Geology* **3**, 179-199.
- Lemoine, M., Gidon, M. and Barfety, J. C. (1981) Les massifs cristallins externes des Alpes occidentales: d'anciens blocs basculés nés au Lias lors du rifting téthysien. *Comptes rendus de l'Académie des Sciences; série 2* **292**, 917-920.
- Lemoine, M., Termier, P., Kilian, W., Lugeon, M., Lory, P., Gignoux, M., Moret, L., Raguin, e. and Schneegans, D. (1969) *Carte géologique de la France (1/80'000). Feuille Briançon (189). ed. 3.* BRGM, Orléans.
- Letouzey, J., Colletta, B., Vially, R. and Chermette, J. C. (1995) Evolution of salt-related structures in compressional settings. In *Salt tectonics: a global perspective*, eds M. P. A. Jackson, D. G. Roberts and S. Snelson, pp. 41-60. *AAPG Memoir* **65**.
- Lickorish, H. and Ford, M. (1998) Sequential restoration of the external alpine Digne thrust system, SE France, constrained by kinematic data and synorogenic sediments. In press. In *Cenozoic foreland basins of Western Europe*, eds C. Puidefabrigas and A. Mascle, pp. 189-211. *Geological Society Special Publication* **21**.
- Lory, M. P. (1899-1900) Feuilles de Gap, Vizille et Grenoble. *Bulletin des services de la carte géologique de la France et des topographies souterraines* **11**, 205-208.
- Lory, M. P. (1900-1901) Feuille de Gap (révision de Vizille et de Grenoble). *Bulletin des services de la carte géologique de la France et des topographies souterraines* **12**, 517-524.
- Lory, M. P. (1901-1902) Feuille de Gap; et révision des feuilles de Vizille et de Grenoble. *Bulletin des services de la carte géologique de la France et des topographies souterraines* **13**, 658-664.
- Lory, M. P. (1903-1904) Feuille de Gap et révision des feuilles de Vizille et Grenoble. *Bulletin des services de la carte géologique de la France et des topographies souterraines* **15**, 265-271.
- Lory, P. (1894) Observations sur la coexistence dans le Massif de Chaillol de dislocations appartenant à deux périodes distinctes. *Compte-Rendu des Séances de la Société Géologique de France* **22**, CLXII-CLXIV.
- Malavieille, J., Lacassin, R. and Mattauer, M. (1984) Signification tectonique des linéations d'allongement dans les Alpes occidentales. *Bulletin de la Société Géologique de France; série 7* **26**, 895-906.
- Mancktelow, (1989-1995) *Stereoplot v.3.05. Apple Macintosh computer program.*
- Marshak, S. (1988) Kinematics of orocline and arc formation in thin-skinned orogens. *Tectonics* **7**, 73-86.
- Marshak, S., Wilkerson, M. S. and Hsui, A. T. (1992) Generation of curved fold-thrust belts: Insight from simple physical and analytical models. In *Thrust tectonics*, eds K. R. McClay, pp. 83-92. .
- Martini, J. and Vuagnat, M. (1965) Présence du faciès à zéolites dans la formation des "grès" de Tavéyanne (Alpes franco-suisse). *Schweizerische mineralogische und petrographische Mitteilungen* **45**, 281-293.
- Meckel, L. D. (1997) Sedimentological and structural evolution of the Tertiary Dévoluy Basin, external western Alps, SE France. Unpublished Ph.D., ETH Zürich.
- Meckel, L. D., Ford, M. and Bernoulli, D. (1996) Tectonic and sedimentary evolution of the Dévoluy Basin, a remnant of the Tertiary western Alpine foreland basin, SE France. *Géologie de la France* **2**, 3-26.
- Ménard, G. (1979) Relations entre structures profondes et structures superficielles dans le S.E. de la France. Essai d'utilisation de données géophysiques. Unpublished Ph.D., Grenoble.
- Ménard, G. and Thouvenot, F. (1987) Coupes équilibrées crustales: méthodologie et application aux Alpes

- occidentales. *Geodinamica Acta* **1**, 35-45.
- Ménard, G. (1988) Structure et cinématique d'une chaîne de collision, les Alpes occidentales et centrales. Unpublished thesis, Grenoble, 268 p.
- Merle, O. (1990) *Cinématique des nappes superficielles et profondes dans une chaîne de collision.*
- Merle, O. and Brun, J. P. (1984) The curved translation path of the Parpaillon Nappe (French Alps). *Journal of Structural Geology* **6**, 711-719.
- Mugnier, J.-L., Arpin, R. and Thouvenot, F. (1987) Coupes équilibrées à travers le massif subalpin de la Chartreuse. *Geodinamica Acta* **1**, 125-137.
- Mugnier, J. L. and Gidon, M. (1988) Décrochements en transtension dans la couverture des massifs subalpins septentrionaux: relations avec la tectonique du socle. *Comptes rendus de l'Académie des Sciences; série 2* **307**, 1669-1674.
- Mugnier, J.-L., Guellec, S., Ménard, G., Roure, F., Tardy, M. and Vialon, P. (1990) A crustal scale balanced cross-section through the external Alps deduced from the ECORS profile. *Mém. Soc. géol. suisse* **1**, 203-216.
- Murer, R. (1998) Die tektonische Geschichte der Morges-Region. Diplomarbeit ETH-Zürich.
- Odé. (1968) Review of mechanical properties of salt relating to salt dome genesis. *Geol. Soc. America special paper* **88**, 544-595.
- Odone, F. and Costa, E. (1991) Relationships between strike-slip movement and fold trends in thin-skinned tectonics: analogue models. *Tectonophysics* **228**, 383-391.
- Perriaux, J. and Uselle, J.-P. (1968) Quelques données sur la sédimentologie des Grès du Champsaur (Hautes-Alpes). *Géologie Alpine* **44**, 329-332.
- Pijolat, B., Gay, M., Gratier, J.-P. and Vialon, P. (1981) Les variations des valeurs de la déformation dans un système de plis par cisaillement. *Revue de Géologie Dynamique et de Géographie Physique* **23**, 195-201.
- Platt, J. P. (1986) Dynamics of orogenic wedges and the uplift of high-pressure metamorphic rocks. *Geological Society of America Bulletin* **97**, 1037-1053.
- Platt, J. P., Behrmann, J. H., Cunningham, P. C., Dewey, J. F., Helmann, M., Parish, M., Shepley, M. G., Wallis, S. and Weston, P. J. (1989) Kinematics of the Alpine arc and the motion history of Adria. *Nature* **337**, 158-161.
- Plotto, P. (1977) Structures et déformations des "grès" du Champsaur au SE du massif du Pelvoux. Unpublished Thèse 3e cycle, Université de Grenoble, France.
- Ramberg, H. (1967) *Gravity, deformation and the earth's crust.* Academic Press, London.
- Ramsay, J. G. (1963) Stratigraphy, structure and metamorphism of the western Alps. *Proceedings of the Geological Association* **74**, 357-91.
- Ramsay, J. G. (1989) Fold and fault geometry in the western Helvetic nappes of Switzerland and France and its implications for the evolution of the arc of the western Alps. In *Alpine Tectonics*, eds M. P. Coward, D. Dietrich and R. G. Park, pp. 33-45. *Geological Society Special Publication* **45**.
- Ramsay, J. G., Casey, M. and Kligfield, R. (1983) Role of shear in development of the Helvetic fold-thrust belt of Switzerland. *Geology* **11**, 439-442.
- Rathey, P. R. and Sanderson, D. J. (1982) Patterns of folding within nappes and thrust sheets: examples from the Variscan of southwest England. *Tectonophysics* **88**, 247-267.
- Ravenne, C., Vially, R., Riché, P. and Trémolières, P. (1987) Sédimentation et tectonique dans le bassin marin Éocène supérieure-Oligocène dans des Alpes du Sud. *Revue de l'Institut Français du Pétrole* **42**, 529-553.
- Ray, S. K. (1991) Significance of forelimb folds in the Shumar allochthon, Lesser Himalaya, eastern Bhutan. *Journal of Structural Geology* **13**, 411-418.
- Ricou, L.-E. (1984) Les Alpes Occidentales: chaîne de décrochement. *Bulletin de la Société Géologique de France; série 7* **26**, 861-874.
- Ricou, L. E. and Siddans, A. W. B. (1986) Collision tectonics in the Western Alps. In *Collision Tectonics*, eds M. P. Coward and A. C. Ries, pp. 229-244. *Geological Society Special Publication* **19**.
- Ridley, J. and Casey, M. (1989) Numerical modeling of folding in rotational strain histories: strain regimes expected in thrust belts and shear zones. *Geology* **17**, 875-878.
- Ritz, F. (1991) Evolution du champ de contraintes dans les Alpes du Sud depuis la fin de l'Oligocène. Implications sismotectoniques. Unpublished Ph.D. thesis, Montpellier.
- Roure, F., Heitzmann, P. and Polino, R. (1990) *Deep structure of the Alps.* Zürich.
- Rousset, C. (1978) De l'importance régionale de la faille d'Aix-en-Provence. *Comptes rendus de l'Académie des Sciences; série D* **286**, 189-192.

- Rousset, C. (1986) Le cadre linéamentaire du Sud-Est de la France, à partir d'observations nouvelles sur son rôle dans la sédimentation tardi et post-hercynienne. *Bulletin de la Société Géologique de France; série 8 2*, 487-497.
- Rowan, M. G. and Kligfield, R. (1992) Kinematics of large-scale asymmetric buckle folds in overthrust shear: an example from the Helvetic nappes. In *Thrust tectonics*, eds K. R. McClay, pp. 165-173.
- Sanderson, D. J. (1979) The transition from upright to recumbent folding in the Variscan fold belt of south-west England: a model based on the kinematics of simple shear. *Journal of Structural Geology* **1**, 171-180.
- Sanderson, D. J. (1982) Models of strain variation in nappes and thrust sheets: a review. *Tectonophysics* **88**, 201-233.
- Serre, A., Toury, A., Rampnoux, J.-P., Reyes-Martinez, J. and Tardy, M. (1985) Individualisation de deux unités à flysch nummulitique d'origines paléogéographiques différentes au sein de "l'Écaille ultradauphinoise des Aiguilles d'Arves" (région de Saint-Jean-de-Maurienne, Savoie). *Comptes rendus de l'Académie des Sciences; série 2* **301**, 637-642.
- Seward, D., Ford, M., Bürgisser, J., Lickorish, H., Williams, E. A. and Meckel III, L. D. (submitted) Preliminary results of fission-track analyses in the Southern Pelvoux area, SE France. *Submitted to a special publication of Memorie di Scienze Geologiche (Padova University) on alpine tectonics*.
- Siddans, A. W. B. (1979) Arcuate fold and thrust patterns in the Subalpine Chains of Southeast France. *Journal of Structural Geology* **1**, 117-126.
- Sinclair, H. D. (1996) Plan-view curvature of foreland basins and its implications for the palaeostrength of the lithosphere underlying the western Alps. *Basin Research* **8**, 173-182.
- Sinclair, H. D. (1997) Tectonostratigraphic model for underfilled peripheral foreland basins: an Alpine perspective. *Geological Society of America Bulletin* **109**, 324-346.
- Souriot, T., Ballard, J.-F. and Brun, J.-P. (1991) Influence des "barrières" sur la propagation de la déformation le long des surfaces de décollement: étude expérimentale. *Comptes rendus de l'Académie des Sciences; série 2* **312**, 69-75.
- Spencer, S. (1992) A kinematic analysis incorporating incremental strain data for the Frontal Pennine Zones of the western French Alps. *Tectonophysics* **206**, 285-305.
- Sue, C., Tricart, P., Dumont, T. and Pêcher, A. (1997) Raccourcissement polyphasé dans le massif du Pelvoux (Alpes occidentales): exemple du chevauchement de socle de Villard-Notre-Dame. *Comptes rendus de l'Académie des Sciences; série 2a* **324**, 847-854.
- Suppe, J. and Medwedeff, D. A. (1984) Fault-propagation folding. *Geological Society of America Abstracts with Programs* **16**, 670.
- Suppe, J. and Medwedeff, D. A. (1990) Geometry and kinematics of fault-propagation folding. *Eclogae geologicae Helveticae* **83**, 409-454.
- Talbot, J. L. (1964) Crenulation cleavage in the Hunsrückschiefer of the middle Moselle region. *Geologische Rundschau* **54**, 1026-1043.
- Tanner, P. W. G. and Macdonald, D. I. M. (1982) Models for the deposition and simple shear deformation of a turbidite sequence in the South Georgia portion of the southern Andes back-arc basin. *Journal of the Geological Society, London* **139**, 739-754.
- Tapponnier, P., Peltzer, G. and Armijo, R. (1986) On the mechanics of the collision between India and Asia. In *Collision Tectonics*, eds M. P. Coward and A. C. Ries, pp. 115-157. *Geological Society Special Publication* **19**.
- Tapponnier, P., Peltzer, G., Le Dain, A. Y., Armijo, R. and Cobbold, P. R. (1982) Propagating extrusion tectonics in Asia: new insights from simple experiments with plasticine. *Geology* **10**, 611-616.
- Tommasi, A. and Vauchez, A. (1997) Continental-scale rheological heterogeneities and complex intraplate tectono-metamorphic patterns: insights from a case-study and numerical models. *Tectonophysics* **279**, 327-350.
- Tricart, P. (1980) Tectoniques superposées dans les Alpes occidentales au Sud du Pelvoux; évolution structurale d'une chaîne de collision. Unpublished Ph.D. thesis, Université de Strasbourg, France.
- Tricart, P. (1981) Les marqueurs des mouvements verticaux du socle aux abords du massif du Pelvoux (Alpes occidentales). *Revue de Géologie Dynamique et de Géographie Physique* **23**, 289-300.
- Tricart, P. (1984) From passive margin to continental collision: a tectonic scenario for the Western Alps. *American Journal of Science* **284**, 97-120.

- Tricart, P. (1986) Le chevauchement de la zone briançonnaise au Sud-Est du Pelvoux: clé des rapports zone externe - zones internes dans les Alpes occidentales. *Bulletin de la Société Géologique de France; série 8 2*, 233-244.
- Tricart, P., Bouillin, J. P., Dick, P., Moutier, L. and Xing, C. (1996) Le faisceau de failles de haute-Durance et le jeu distensif du front briançonnais au SE du Pelvoux (Alpes occidentales). *Comptes rendus de l'Académie des Sciences; série 2a* **323**, 251-257.
- Trümpy, R. (1980) *Geology of Switzerland. Part A: an outline of the geology of Switzerland*. Wepf, Basel.
- Vialon, P., Bonnet, J.-L., Gamond, J.-F. and Mugnier, J.-L. (1984) Modélisation des déformations d'une série stratifiée par le déplacement horizontal d'un poinçon. Application au Jura. *Bulletin de la Société Géologique de France; série 7* **26**, 139-150.
- Vialon, P., Rochette, P. and Ménard, G. (1989) Indentation and rotation in the western Alpine arc. In *Alpine Tectonics*, eds M. P. Coward, D. Dietrich and R. G. Park, pp. 329-338. *Geological Society Special Publication* **45**.
- Waibel, A. F. (1990) Sedimentology, petrographic variability, and very-low-grade metamorphism of the Champsaur sandstone (Paleogene, Hautes-Alpes, France). Evolution of volcanoclastic foreland turbidites in the external Western Alps. Unpublished Ph.D. thesis, Université de Genève, Suisse.
- White, S. H., Burrows, S. E., Carreras, J., Shaw, N. D. and Humphreys, F. J. (1980) On mylonites in ductile shear zones. *Journal of Structural Geology* **2**, 175-187.
- Williams, G. and Chapman, T. (1983) Strains developed in the hangingwalls of thrusts due to their slip/propagation rate: a dislocation model. *Journal of Structural Geology* **5**, 563-571.

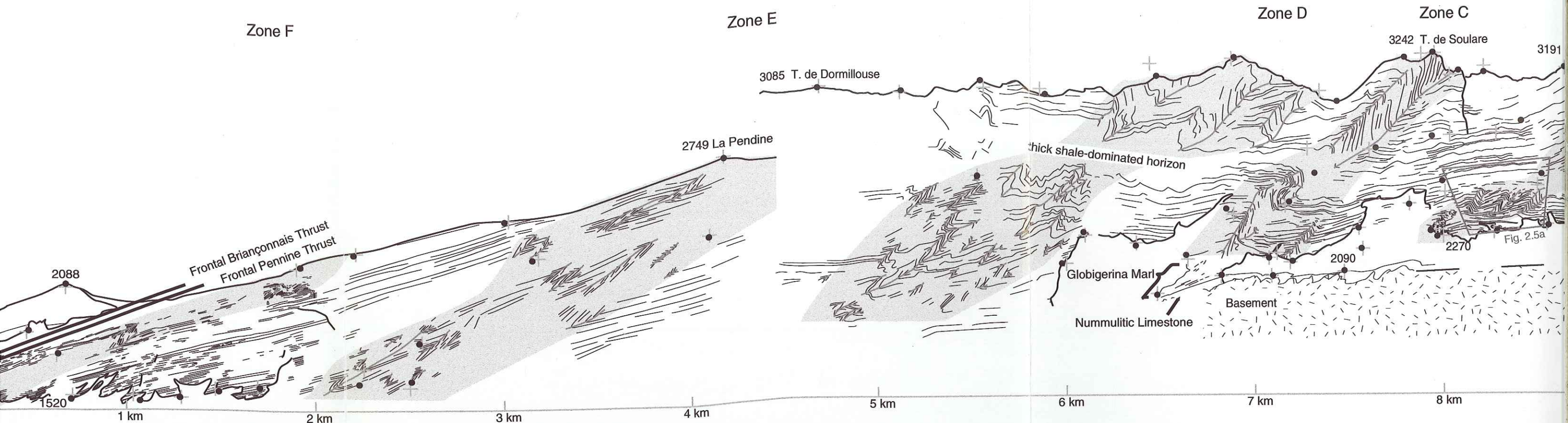
Curriculum vitae

Personal data:

Name:	Bürgisser
First name:	Judith
Date of birth:	11. August 1969
Home town:	Oberlunkhofen AG, Switzerland
Civil status:	single

Education

1994 - 1998	Study of Geology and assistant at Geological Institute Swiss Federal Institute of Technology Zurich (ETH) Ph.D. thesis: "Deformation in foreland basins of the western Alps (Pelvoux massif, SE France); significance for the development of the Alpine arc"
1989 - 1994	Study of Geology at Swiss Federal Institute of Technology Zurich (ETH) Diploma thesis: "Strukturgeologische Untersuchungen in der Sion-Courmayeur-Zone im oberen Val Ferret (Wallis)"
1985 - 1988	High school Real gymnasium, Alte Kantonsschule Aarau, AG Matura type C
1981 - 1985	Secondary school Bezirksschule Brugg, AG
1976 - 1981	Primary school Döttingen and Umiken, AG



ENE-WSW profile (location on Fig. 2.1) along the Fournel valley. Inadequate from field photographs, the exact location of about 7 points was corrected by a digital façade rectification program, used in photogrammetry, ortho-projection on the best fit plane through the 7 identified points. The corrected line was then squeezed (in Adobe Illustrator) in order to correct for the best fit plane, i.e. the inclination of the cliff face. The corrected line was compiled to give the E-W profile. The true fixed-point position (crosses) and point position (dots) give an idea of the error involved. In the last step, the profile was rotated 17° anticlockwise to give a profile plane perpendicular to the P-fold. The part of the final profile is an inverted projection (parallel to the P-fold) of the northern valley wall. Shaded areas are zones of large-scale folding as shown in Figs. 2.5(a & b).

Fig. 2.5: Field photographs (located on Fig. 2.4): a) Isolated asymmetric chevron fold train bordered by shale-dominated shear horizons (fold duplex). View towards the S, width of view ~370 m. b) Upright chevron folds from zone A. View towards the S. Width of view ~1000 m.



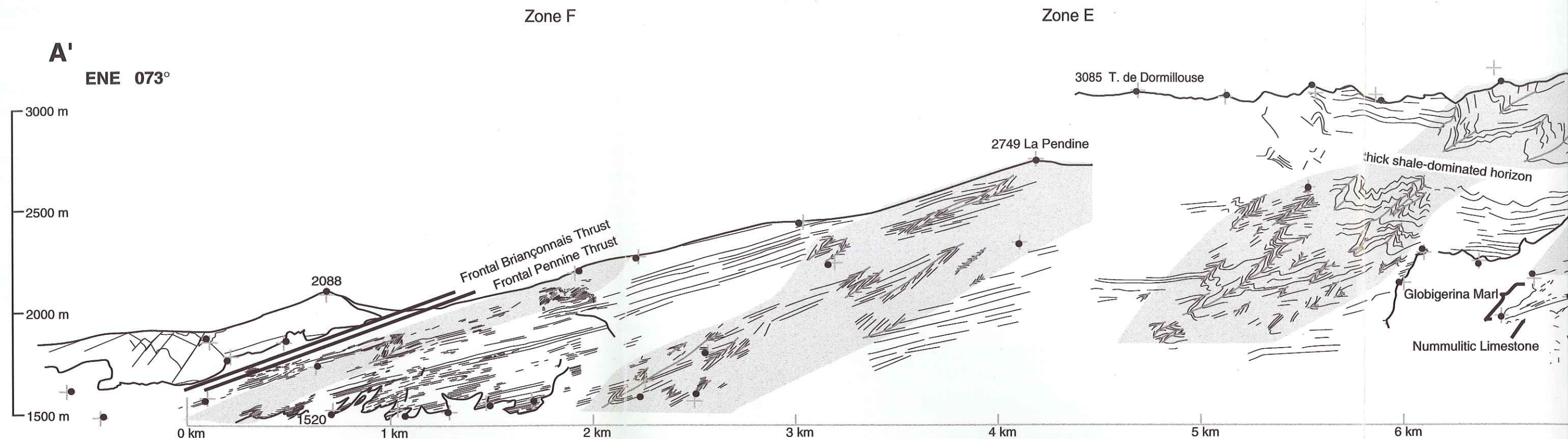
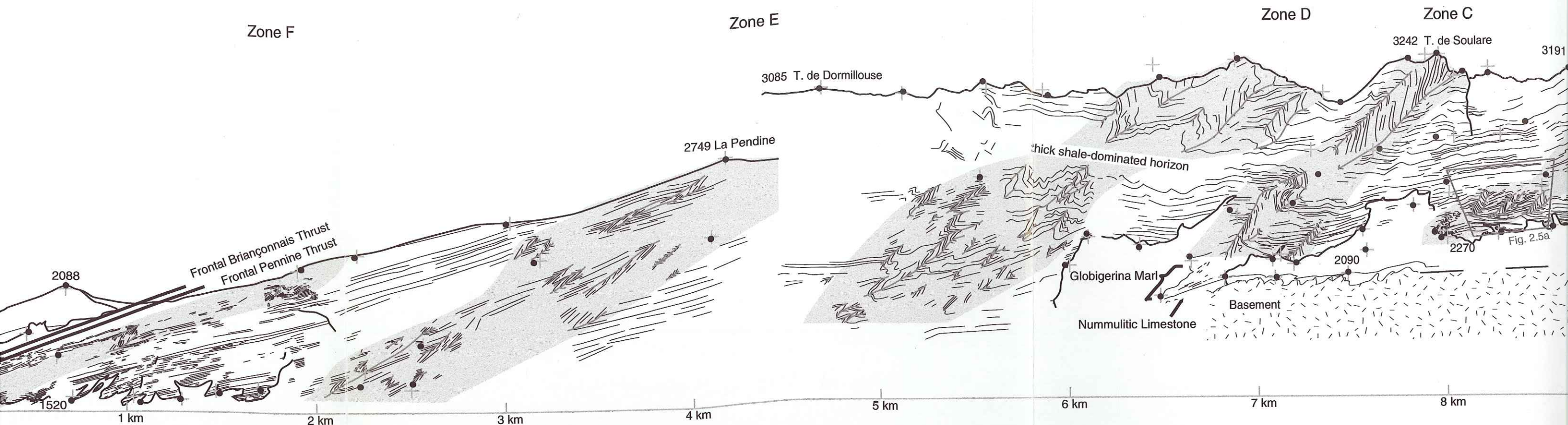


Fig. 2.4: Compiled and rectified ENE-WSW profile (location on Fig. 2.1) along the Fournel valley. In each line drawing, made from field photographs, the exact location of about 7 points was determined. These line drawings were then corrected for obliquity of camera view with respect to the cliff face by a digital façade rectification program, used in photogrammetry, which calculates the ortho-projection on the best fit plane through the 7 identified points. Each ortho-projection was then squeezed (in Adobe Illustrator) in order to correct for the inclination of the best fit plane, i.e. the inclination of the cliff face. The corrected line drawings were then compiled to give the E-W profile. The true fixed-point position (crosses) and the rectified fixed-point position (dots) give an idea of the error involved. In the last step, the E-W profile was rotated 17° anticlockwise to give a profile plane perpendicular to the P-fold axis. The eastern part of the final profile is an inverted projection (parallel to the P-fold axis 343-12), from the northern valley wall. Shaded areas are zones of large-scale folding (labelled A-F). Outlines of Figs. 2.5(a & b) are shown.

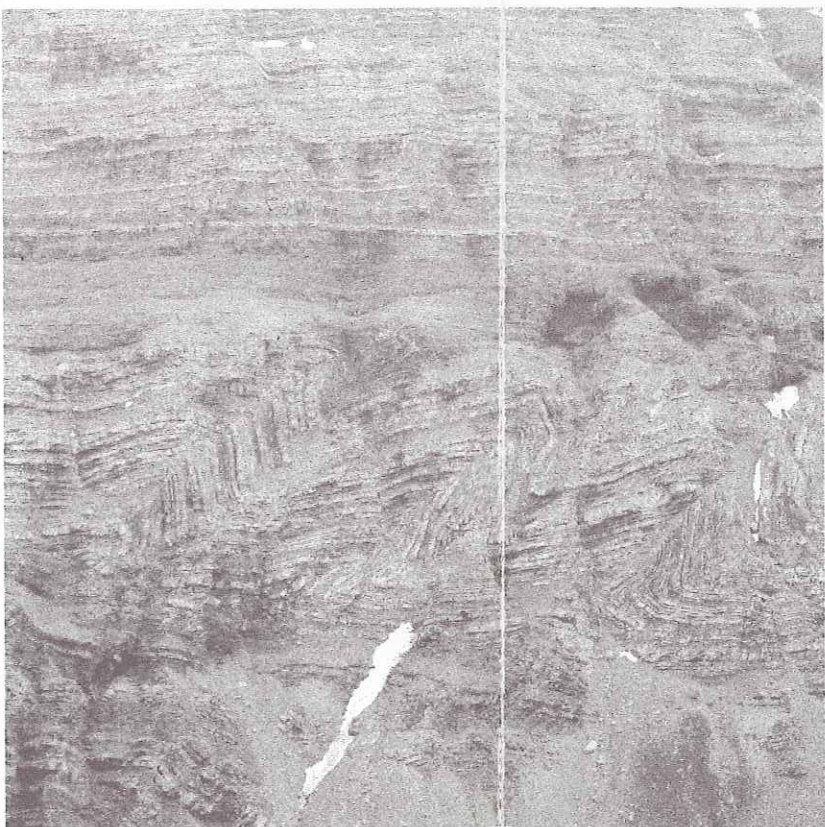
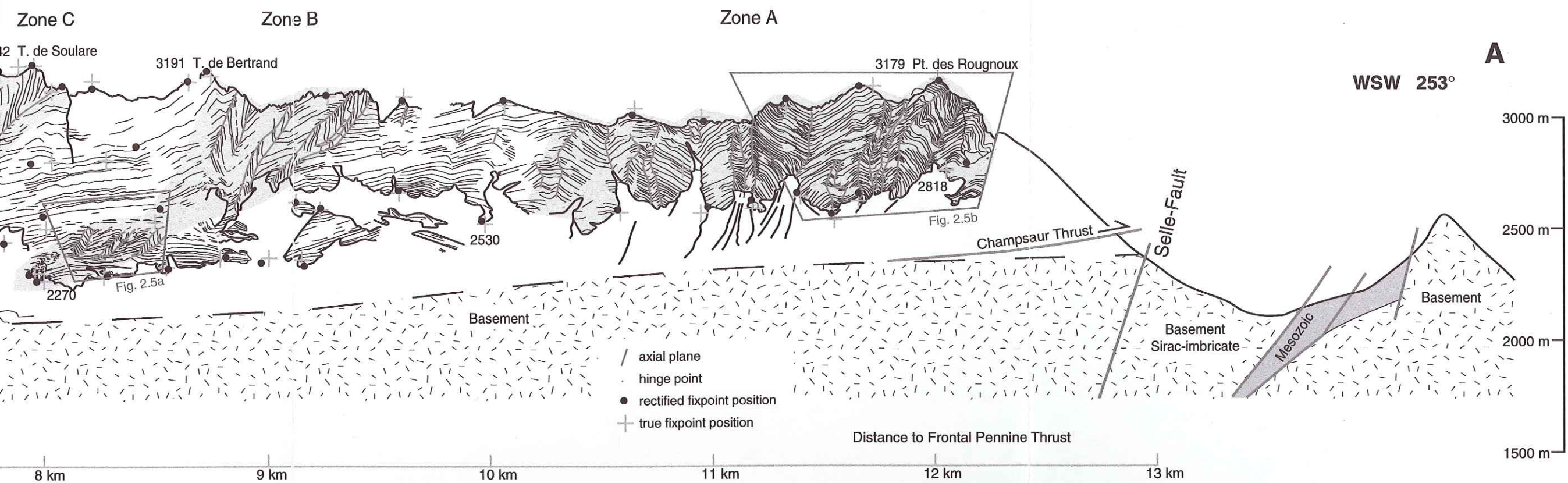
Fig. 2.5: Field photographs (located on Fig. 2.4): a) Isolated asymmetric chevron fold train bordered by shale-dominated shear horizons (fold duplex). View towards the S, width of view ~370 m. b) Upright chevron folds from zone A. View towards the S. Width of view ~1000 m.



ENE-WSW profile (location on Fig. 2.1) along the Fournel valley. Inadequate from field photographs, the exact location of about 7 points was corrected by a digital façade rectification program, used in photogrammetry, ortho-projection on the best fit plane through the 7 identified points. The corrected line was then squeezed (in Adobe Illustrator) in order to correct for the best fit plane, i.e. the inclination of the cliff face. The corrected line compiled to give the E-W profile. The true fixed-point position (crosses) and point position (dots) give an idea of the error involved. In the last step, the profile was rotated 17° anticlockwise to give a profile plane perpendicular to the P-fold. The part of the final profile is an inverted projection (parallel to the P-fold) of the northern valley wall. Shaded areas are zones of large-scale folding as shown in Figs. 2.5(a & b).

Fig. 2.5: Field photographs (located on Fig. 2.4): a) Isolated asymmetric chevron fold train bordered by shale-dominated shear horizons (fold duplex). View towards the S, width of view ~370 m. b) Upright chevron folds from zone A. View towards the S. Width of view ~1000 m.





b)

